

20th International HISWA Symposium on “Yacht Design and Yacht Construction”

Amsterdam, 17 & 18 November 2008

PROCEEDINGS

Edited by Piet W. de Heer

Organizing Committee

Jan Alexander Keuning
Michael Steenhoff

Delft University of Technology
HISWA Vereniging the National Association
of Watersport Industries
Amsterdam RAI Convention Centre

Irene Dros

Scientific Committee

Prof. Jelle Gerritsma
Gerard Dijkstra
Prof. Richard Birmingham
Michael Steenhoff
Hugo van Wieringen
Frans Maas
Jan Alexander Keuning
Geert Kapsenberg

TU Delft
Dijkstra & Partners
University of Newcastle
HISWA Vereniging
Azure Naval Architects
Standfast Yachts
TU Delft
MARIN

November 2008

Organized by HISWA - National Association of Watersport Industries in The Netherlands,
The International Trade Show of Marine Equipment METS 2008
Delft University of Technology

Photo cover: Ed Holt

Delft University of Technology
Ship Hydromechanics Laboratory

Printed by:

CENDRIS CMC DELFT
Leeghwaterstraat 42
2628 CA Delft

Phone: +31 (0)15 3615450
Fax: +31 (0)15 3615451

KONINKLIJKE BIBLIOTHEEK, DEN HAAG
Depot van Nederlandse Publicaties
Postbus 74
2501 AJ Den Haag

20th International Symposium on "Yacht Design and Yacht Construction": Proceedings of the 20th International Symposium on "Yacht Design and Yacht Construction", Amsterdam, 17 & 18 November 2008 – Delft University of Technology, Ship Hydromechanics laboratory, The Netherlands.

ISBN: 978-90-811322-2-0

Subject headings: Yacht Design, Yacht Construction

TABLE OF CONTENTS

Program Monday

Program Tuesday

Introduction

Session 1 – Wubbo Ockels

Session 2 – Ronno Schouten

Session 3 – James Roy and Ben Munro

Session 4 – M.W. Findlay and S.R. Turnock

Session 5 – Suzanne de Vos Efftig and René van Gijlswijk

Session 6 – Evert-Jan Foeth

Session 7 – J. Bokxem

Session 8 – Stephan Brabeck and Tom Schnackenberg

Session 9 – Pepijn de Jong, Michiel Katgert and Lex Keuning

Session 10 – Clay Oliver and John Robinson

Session 11 - Andy Claughton, Fabio Fossati, Sara Muggiasca and Davide Battistin

Session 12 - Bart Verwerft and Lex Keuning

Program Monday November 17, 2008

Moderator: Jack Somer

08:30 – 10:00	Registration
10:00 – 10:15	Opening
10:15 – 10:45	Session 1: Ecolution – Wubbo Ockels
10:45 – 11:15	Session 2: Hybrid propulsion of Feadship's X-stream and F-stream concept designs – Ronno Schouten
11.15 – 11.30	Coffee Break
11:30 – 12:00	Session 3: Longitudinal Vs Transversely Framed Structures For Large Displacement Motor Yachts – James Roy and Ban Munro
12:00 – 12:30	Session 4: Investigation sailing styles and boat set-up on the performance of a hydrofoiling Moth dinghy – M.W. Findlay and S.R. Turnock
12:30 – 13:30	Lunch Break
13:30 – 14:00	Session 5: A life cycle based Eco design consideration for the Rainbow Warrior III – Suzanne de Vos-Effting and René van Gijlswijk
14:00 – 14:30	Session 6: Decreasing frictional resistance by air lubrication – Evert-Jan Foeth
14:30 – 14:45	Coffee Break
14:45 – 15:15	Session 7: Recent developments & future Ideas At Royal Huijsman – J. Bokxem
15:15 – 15:45	Session 8: Vessel propulsion using kites – Stephan Brabeck and Tom Schnackenberg
15:45 – 17:00	Welcome Reception

Program Tuesday November 18, 2008

Moderator: Jack Somer

- | | |
|---------------|--|
| 09:00 – 09:30 | Registration |
| 09:30 – 10:00 | Session 9: Development of a Velocity Prediction Program for Traditional Dutch Sailing Vessels of the type Skûtsje – Pepijn de Jong, Michiel Katgert and Jan Alexander Keuning |
| 10:00 – 10:30 | Session 10: Development of a Vpp based rating for J-Class Yachts – Clay Oliver and John Robinson |
| 10:30 – 10:45 | Coffee Break |
| 10:45 – 11:15 | Session 11: Changes and Development to Sail Aerodynamics in the ORC International Handicap Rule – Andy Cloughton, Fabio Fossati, Sara Muggiasca and Davide Battistin |
| 11:15 – 11:45 | Session 12: The Modification and Application of a Time Dependent Performance Prediction Model on the Dynamic Behaviour of a Sailing Yacht – Bart Verwerft and Jan Alexander Keuning |
| 11:45 – 12:00 | Closing |

INTRODUCTION.

Once again you will find here the Proceedings of the International HISWA Symposium on Yacht Design and Construction to be held in the RAI Congress Centre in Amsterdam on 17th and 18th of November 2008.

This time however it is special.
It is the 20th time that the symposium is being organized!

The first symposium was organized in 1969 almost 40 years ago now. In a joint effort it was put together by the Delft University of Technology and the HISWA Association on an initiative of Prof Jelle Gerritsma. Ever since that time the same organizations have been responsible for the organization of the symposium. Later they were joined by the RAI Exhibition Centre and still later by the METS, when the HISWA Association no longer organized the HISWA boat shows. This is a remarkable fact. And even more remarkable is that still a few of the organizers from the beginning are still active in the present symposium set up. So something to celebrate and during the 20th symposium attention will be paid to this lustrum.

The Organizing Committee again is very content with the work carried out by the Scientific Committee, which put together a very interesting program once again. Between the more usual topics such as issues involved with high performance yachts and new developments, a particular emphasis has been put this time on sustainability. An item, that will influence the design of yachts in the foreseeable future to an ever growing extend.

Also we hope to remain successful to attract a large group of students from all kind of educational programs to the symposium, because the future of the yachting industry is with them and we hope to be able to stimulate their interest through this symposium.

Finally I would like to express my gratitude to our sponsors, without whom the aims of the symposium, i.e. offering a worthwhile and motivating gathering of interested people from the various branches, research institutes and schools, at an affordable price.

I am sure we will meet in the future again during the following 40 years of the symposium!

Jan Alexander Keuning

Session 2

Ronno Schouten

Hybrid propulsion in Feadship's X-Stream and F-Stream concept designs

Ronno Schouten of De Voogt Feadship

Hybrid propulsion sounds complicated and expensive and often is... So why have we chosen for this solution?

Generally, hybrid propulsion is deployed when a single propulsion system cannot offer an optimal performance in various operational conditions. For example, while a hybrid car might run perfectly on an electric motor in the city at low speeds and short range, it requires a combustion engine for higher speeds and longer distances on motorways. This engine is less efficient in the city, however, as it consumes fuel even when standing still, cannot recover brake energy and produces exhaust gases.

The same situation applies for ships. A conventional propulsion set-up with diesel engines and screw propellers performs best between normal cruising speeds of 12 knots and a maximum speed of 20. It is much less suitable at lower or higher speeds.

Let us look first at the low speeds. Normally a yacht will sail a minimum of seven knots when the main engines are running on minimum revolutions. A lower speed can only be achieved by controllable pitch propellers or a trolling gearbox. Although modern engines can sail for longer periods of time at low loads, this is certainly not recommended and will produce smoke and soot.

At high speeds, the load on the propellers becomes unacceptably high or a larger draught needs to be chosen to accommodate a larger propeller. An alternative frequently used for high-speed yachts is the water jet. Although this is a good solution, the efficiency of a water jet decreases to below 40 percent at normal cruising speeds. This means large amounts of fuel are required if a transatlantic range is desired, making it an unattractive solution for fast and lightweight yachts. This is why Feadship has built several yachts with a hybrid combination of propellers for the long range and a booster water jet combined with a gas turbine for high speeds.

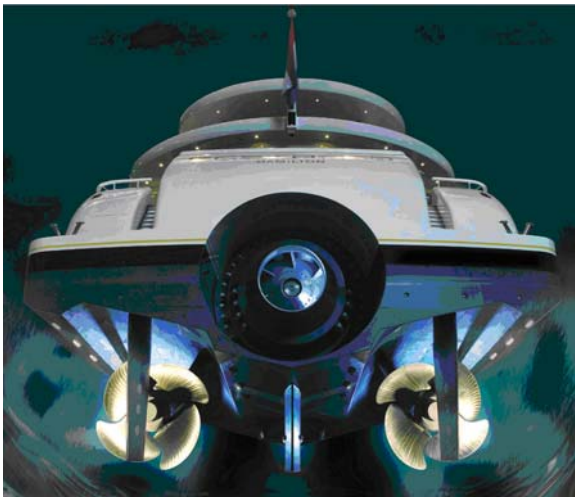


Figure 1 Hybrid propulsion with controllable pitch propellers and water jet on Ecstasea

Diesel electric propulsion

Diesel electric propulsion is seen as a solution when different operating speeds are required and the power demands are widely divergent. The concept is often applied on cruise ships with high hotel loads and offshore support vessels with major dynamic positioning requirements. Several yachts have been built with diesel electric propulsion, including *Air*, *Ambrosia* and *Kogo*.

Diesel electric propulsion does offer clear benefits such as a flexible arrangement, optimal generator loads and subsequent reductions in emissions and fuel consumption. However, there are also disadvantages on yachts that require high speed, notably the enormous discrepancy between the high power demands needed for maximum speed and the low power demands of a yacht in port with only the crew onboard.

A second problem encountered with diesel electric propulsion is the speed-power relationship of a normal displacement yacht: Propulsion power increases exponentially with speed. Small generators are required to have a flexible power supply at low speeds while large generators are needed for maximum power at high speeds. This means making a choice between large generators, a large number of smaller generators or different sizes of generators. All these options have a downside. Large generators will have a low load when the yacht is in port. A large number of generators demands higher investment and maintenance costs. And differing sizes of generators makes the installation less flexible.

In practice, a combination of all three options is needed. For example, a 80m yacht with a speed of 20 knots could require a maximum power of 8MW for top speed but would only use 300kW in port. At a cruising speed of 12 knots, approximately 1.0 MW would be required. The same megawatt will only add an additional knot at the top speed.

To assure an optimum load in port and have some redundancy, this yacht would require two generators with a maximum power of 400 to 500kW. The remaining power of 7MW should be divided over several generators, and a choice made between the maximum flexibility of a large number of small generators and the simplified system of fewer large generators. Although a logical solution would be to install four to six generators with power ranging between 1 and 2 MW, this basically ends up in a normal installation with three to four small generators and four main engines.

Other disadvantages are the additional weight and space requirements and costs. An 85m diesel electric yacht concept designed by De Voogt, for example, had a speed of over 17 knots requiring a power of 4.5 MW. The generator room with six generators was 11m long, equivalent in size to a normal engine room. However, an additional switchboard room with a length of 8m was required for the converters, switchboards and drives needed for the diesel electric propulsion installation. The weight of the equipment in the switchboard room added around 60 tons to the lightship. The additional costs were in the range of three million euros, although that is still a relatively small percentage of the overall building costs.

Another design which required a higher speed of 25 knots - and consequently a higher power of 16 MW - resulted in an even larger system. In this case, the length of the engine room increased to 15m and the additional weight of the installation to 300 tons.

Pods

It is not only the power plant that needs to be flexible enough to cover all operating conditions; the propulsion system also needs to be efficient, quiet and accurately controllable in all operating conditions. One solution that can meet these demands are podded propulsors, which also offer optimal manoeuvrability.

There are disadvantages to pods, including the required weight (far aft) and draught (restricts sailing areas and harbours). Another is the steering in stern quartering seas where strong steering forces are required to keep the yacht on course. Normally this will be done by the rudders, which provide a sideward lift while the propellers provide full thrust forward. As the pods steer by changing the thrust direction, this can reduce the forward thrust and make for lower efficiency in moderate to high sea states.

One of the latest and largest diesel electric yachts is the 90m Lürssen *Air*, launched in 2005 and renamed *Ice*. This yacht has a propulsion power of 5MW and a maximum speed of 18 knots. Although the speed is not spectacular for a yacht of this size, it still requires a draught of 5m to accommodate the Azipods.

These examples show why a diesel electric propulsion installation is not ideal for yachts requiring higher speeds. At De Voogt we consider diesel electric propulsion a good solution so long as normal speeds are required. For higher speeds we prefer a hybrid system with an optimised installation for low and high speeds.

Concept designs

Feadship has used a hybrid solution on our X-stream and F-stream concept designs: A diesel electric system for low speeds and manoeuvring. For cruising and higher speeds an additional diesel-direct propulsion system is added. The benefits are clear: A clean, quiet and efficient system for low speeds with excellent manoeuvring characteristics, and a light and efficient system for high speeds.

X-Stream

X-Stream is our first concept design and was presented at the Monaco and Fort Lauderdale boatshows in 2006. Some 72m in length, it features lots of glass, an X-bow and a new propulsion system. The idea was to design a concept that included new innovations and ideas while remaining realistic. Feadship expects to be able to deliver such a yacht in 2015. As there was such widespread interest in the design, our research is continuing into both the propulsion system as well as the construction.

The propulsion concept suggested for X-stream is known as a CRP-pod - a contra-rotating propeller combined with a pod. It comprises a diesel electric system driving a pod which is used at low speeds up to 12 knots and manoeuvring. Additional diesel-direct propellers are engaged for higher speeds. Together they form a contra rotating propeller system that improves efficiency by approximately 10 percent (Mämäläinen, 2003, Holtrop, 2006).

For X-Stream we have investigated two pod options; the first with an ABB compact Azipod with the electric motor in the pod, the second with a Rolls Royce Azipull which requires an additional drive inside the yacht. As the maximum torque of the electric motor in the compact Azipod is limited, the maximum efficiency gain could not be reached. A higher torque with lower revolutions is possible with the Rolls Royce Azipull. This leads to a higher efficiency as frictional losses are reduced while rotational losses

are recovered with the contra-rotating propeller. In addition, because the body of the Azipull is smaller and more hydrodynamically optimised, it also provides a lifting force when steering.

The CRP-pod solution has already been applied in practice on two ferries built in Japan (Ueda, 2004). These 225m long vessels sail at 30 knots and are powered by a 25MW propeller with an 18MW contra-rotating ABB Azipod. They have been operating since July 2004 and still document a 20 percent saving in fuel consumption (Wheater, 2008). In the above case the CRP-pod system replaces a twin screw installation with one pod and one propeller, therefore offering a even higher efficiency gain.



Figure 2 Hybrid propulsion with controllable pitch propeller and pod on X-stream

F-Stream

Unveiled in 2007, F-Stream is also equipped with a hybrid propulsion system with two new innovations from Voith Turbo. Twin electric Voith Cycloidal Rudders (VCR) are used for manoeuvring, dynamic positioning, zero speed stabilizing and slow speeds up to 10 knots. For speeds of up to 20+ knots, two diesel-driven submerged water jets are engaged and the VCRs (in passive mode) act as rudders.

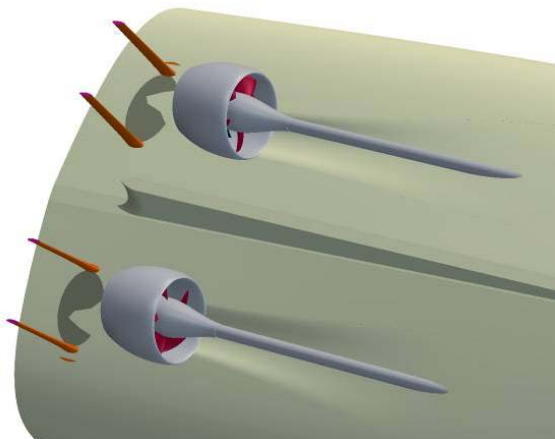


Figure 3 Hybrid propulsion with Voith cycloidal rudder and water jet on F-stream

The new Voith Water Jet (VWJ) has been developed for ships sailing between 20 and 40 knots. The jet consists of a specially shaped nozzle, a rotor and a stator, and can be seen as a combination of a water jet and a ducted propeller.

The jets are submerged and their location under the vessel is comparable to that of conventional propellers. This offers real benefits compared to normal water jets, which

are placed at waterline level and make an aft swimming platform impossible. As the jets are placed beneath the hull, no displacement is lost due to the inlet. The diameter of the jet is smaller than a comparable propeller so larger propulsion powers can be accommodated in the limited space available.

Besides the reduced draught, the clearance can also be reduced. While a conventional propeller requires a clearance of between 30 and 35 percent, the nozzle of the VWJ requires no clearance and may even be partly integrated into the hull. The combination of reduced diameter and clearance results in a 20 percent reduction of the required draught, an important consideration for owners looking to sail in shallow waters or smaller harbours.

The jet's cavitation characteristics are better than conventional, highly loaded propellers. The entrance velocity is lower, which increases the pressure and results in a larger cavitation margin. This virtual absence of cavitation creates more favourable conditions in terms of noise and vibration.

The first operational submerged water jet was built by Rolls Royce several years ago. The US Office of Naval Research funded tests on an Advanced Electric Ship Demonstrator, a quarter-size model of a destroyer used for optimising propulsion technologies. Unfortunately the tests were not considered successful enough to warrant continuing the development.



Figure 4 Advanced Electric Ship Demonstrator with submerged water jet from Rolls Royce

In the early 1990s SVA Potsdam and Voith partnered to develop a submerged water jet (Heinke 1994) and in August 2008 the first model tests were carried out in a mutual research project by Voith, SVA Potsdam and Feadship. Approximately 12MW was deployed on each water jet, which with a rotor diameter of 3m resulted in a specific load of around 1700kW/m². This is about 40 percent higher than what is considered acceptable on a conventional propeller. For example, on the high speed Feadship *Predator*, launched this year, we used 8.6MW on each propeller resulting in a blade load of 1200 kW/m². These first tests have already proven that the efficiencies of the VWJ over the entire speed range are at least comparable to or better than conventional propellers.



Figure 5 Propulsion configuration with VWJ and rudders during model tests at SVA Potsdam

VCR

The Voith Cycloidal Rudder (VCR), on F-stream fitted behind the VWJ, is similar to a Voith Schneider Propeller, although it has only two blades instead of the usual five to seven. The VCR has two operating modes.

In passive mode the rotor casing only performs partial rotations in both directions. The locked blades act therefore as conventional ship's rudders and can be used between cruising and maximum speed.

In active mode the VCR works as a normal Voith Schneider Propeller. Since thrust and thrust direction can be varied at high rates, the VCR is very suitable for manoeuvring, dynamic positioning and slow speed sailing. The noise levels in active mode are low compared to a sternthruster due to the modest blade loads of approximately 50kW/m². At the same time the VCR can be used efficiently for roll stabilisation. To prove the roll damping capabilities, Feadship and Voith performed model tests for a 60m yacht in 2006. The results showed a large roll reduction comparable to or better than zero speed stabilisers.

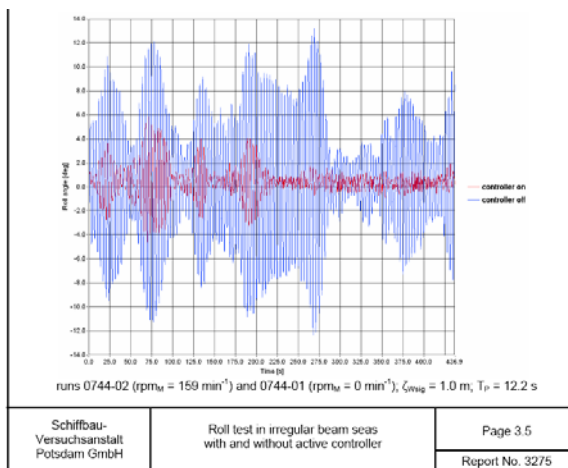


Figure 6 Roll angle with Voith Schneider Propeller on (red line) and off (blue line)

New developments

De Voogt is looking into new developments that might increase the application area of hybrid propulsion and diesel electric propulsion in general. An interesting development is the use of superconductive materials, a presentation on which was given by Rob Rouse from American Superconductor at last year's Global Superyacht Forum. These materials operate at very low temperatures and have near zero resistance, making larger currents possible. As a result, motors and generators can be smaller, lighter and more efficient.

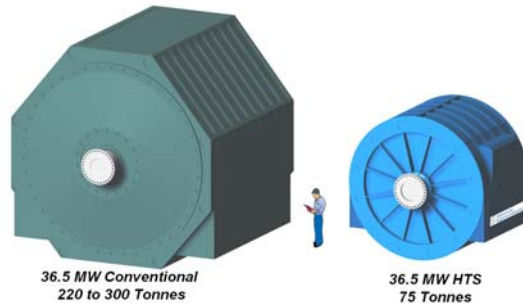


Figure 7 Comparison between conventional and superconducting motor

Conclusion

A hybrid solution offers advantages when optimal performance is required at low as well as high speeds. Although normal screw propellers are an efficient and proven method, manoeuvring and slow speed sailing with the engines working at a minimal load makes for inefficient fuel consumption and increased emissions. Although diesel electric propulsion solves these issues, it requires a heavy, complex and expensive electric system, especially when higher speed (hence propulsion power) is required. While water jets are usually the preferred solution for high speeds, their efficiency decreases at lower speeds. A hybrid installation with different propulsion systems offers the freedom to optimise the system for various operating speeds. It is the best solution when performance at both low and high speeds is required.

References

Wheater, P. "Driving efficient propulsion", *The Naval Architect*, July/August 2008, pp. 47-55.

Ueda, N., A Oshima, T. Unseki, S. Fujita, S. Takeda and T. Kitamura. "The first Hybrid CRP-POD driven fast Ropax Ferry in the world" (Dec 2004) Mitsubishi Heavy Industries Ltd. Technical review Vol 41 No. 6 Nov 2004.

Mämäläinen, R, J. van Heerd, "Wave damping aftbody with hybrid podded propulsors". *Transactions - Society of Naval Architects and Marine Engineers Papers Presented at the 2003 Annual Meeting SNAME 2003 Annual Meeting, San Francisco, CA , 2003, vol. 111 (6 ref.), pp. 33-48.*

Holtrop, J., H Willemsen, "Investigation into hydrodynamic aspects of project X-Stream", Design Advice Report MARIN reference 21278, November 2006.

Hans-Jürgen Heinke. *Hydrodynamische Untersuchungen mit Modell eines LINEARJets*, Bericht Nr. 2023. Schiffbau-Versuchsanstalt Potsdam GmbH, 1994.

Session 3

**James Roy, Ban Munro, Simon Walley
&
Alex Meredith-Hardy**

Longitudinal Vs Transversely Framed Structures For Large Displacement Motor Yachts

James Roy, C.Eng, Yacht Design Manager, BMT Nigel Gee Ltd

Ben Munro, C.Eng, Principal Naval Architect, Devonport Royal Dockyard Ltd

Simon Walley, C.Eng, Chief Structural Engineer, BMT Nigel Gee Ltd

Alex Meredith-Hardy, M.Eng, Naval Architect, BMT Nigel Gee Ltd

1.0 Introduction

The selection of a structural framing system in any vessel must be made from a consideration of weight, production matters, suitability to resist global loads and vibration. Vessels can principally be either transversely or longitudinally framed although hybrid systems are also in use. However the choice of which framing system is best can be the cause of considerable debate between designers and builders with the advantages and disadvantages of each system often being debated but rarely quantified.

This paper explores the structural design of an 80m displacement motor yacht utilising both transversely and longitudinally framed systems, with the aim of quantifying the weight, structural benefits, and production differences between the two. In the development of the basic structural design, rule minimum local scantlings are considered and then suitably increased to account for practical constraints, production aspects and global loads.

Following analysis of the results the Authors have assessed a hybrid framing system which is considered to combine most of the advantages of other systems.

2.0 General Background

The majority of large steel motor yachts are transversely framed featuring heavy shell plate with transverse frames of typically 600 to 800mm pitch. A limited number use longitudinal framing systems with transverse frames typically spaced at 1200mm to 2400mm pitch and closely spaced longitudinal stringers.

Historically, early iron and steel vessels were built with transverse framing as this was the tried and tested configuration used for wooden ship building. The structural design requirements used for wooden ships were copied over to iron ships, featuring very heavy keel structures and relatively light decks. As ships got larger the limitations of thin transversely framed decks were observed and understood, although the industry was slow to adapt. One notable exception to this was the 'Great Eastern' (1858) which was a very early example of a scientifically designed ship. Isambard Kingdom Brunel, a civil engineer, used beam theory in the structural design of this vessel which was based on a cellular system of longitudinal framing. With a tonnage five times greater than any other vessel of the time, this remarkable ship boasted many other innovative features and despite her lack of commercial success, the structure performed well throughout her 31 year life.

Although the technical benefits of longitudinal framing were known in the 19th Century it was not until the British naval architect Joseph Isherwood introduced his longitudinal framing method in 1906, that interest was revived. His system used longitudinal stiffeners and deep transverse web frames in the same way that modern arrangements do. The benefit was primarily a lighter structure, which for commercial vessels equated to increased deadweight for a given displacement, and hence a more profitable ship. This was particularly true for oil tankers where the increased web frame depth did not affect cargo stowage volume. The first ship using this system, the tanker 'Paul Paix', was built in 1908 to Lloyd's Register class. By 1918 over 1000 ships had been built using the Isherwood framing system.^[1]

Early designs had problems with longitudinal end connections. In an effort to reduce collars, which were expensive and problematic in riveted construction, longitudinal stiffeners were terminated and bracketed at every bulkhead. This led to cracking around the rivets on the brackets and the system did not really gain widespread popularity until the advent of all welded construction.

Transverse framing systems feature closely spaced frames, typically at 600mm pitch spanning between tank top and deck. These frames are often Holland Profile [HP] sections bent to the correct moulded line shape. With such a framing system the principal longitudinal material is the shell and deck plating.

Longitudinal framing systems feature widely spaced transverse web frames, typically between 1200mm and 2400mm depending on vessel size, with closely spaced longitudinal stringers. All transverse frames are typically of identical scantlings and longitudinals are spaced to optimise the selected local shell thickness, leading to an effective structure with little structural redundancy.

A graphical example of both systems is presented in Figure 1.

There are advantages and disadvantages to both systems but the fundamental difference from a structural design viewpoint is related to the ability of the stiffened plate to carry in-plane loads. Longitudinal bending of the hull girder, due to the buoyancy and weight distribution of the vessel, as well as the action of the waves, will induce stresses in the fore and aft direction. Thin shell plate is susceptible to buckling, and due to the orientation of the stiffeners, a transversely framed panel will have approximately a quarter of the strength of a longitudinally framed panel of the same size and thickness. As a result, transversely framed vessels tend to have to have thicker plating, particularly on the decks, in order to have adequate buckling capacity to resist hull girder loads.

As the size of a vessel increases the significance of hull girder loads increases dramatically; Lloyd's generally require global strength calculations for all steel hulled yachts over 50m. Currently small vessels are generally transversely framed, and larger vessels, when global loads become significant, are generally longitudinally framed. The transition occurs between 50m and 90m dependent on vessel type and usage.

Hybrid or combination framing employs both transverse and longitudinal framing within the same section. Typically this would entail longitudinally framing for some or all of the decks, with the remainder of the structure being transversely framed.

When selecting a framing system for a new design there is often debate between designers and builders as to the best system, particularly as builders may have historically only used one system or the other. In general the designer is seeking to optimise structural effectiveness and eliminate redundant structure whilst the builder is seeking to minimize construction complexity and time. As steel is relatively cheap the builder may often accept a structure with redundant material if it simplifies the structure and makes it easier and quicker to build.

It is often claimed that a longitudinally framed structure is more time consuming to construct due to (perceived) large amounts of welding of the longitudinals to the shell as well as bracketing or collaring of longitudinals at bulkheads. However this must be offset against the high number of transverse frames found in a transverse system.

Additionally weight is often cited as the reason for selecting one system or the other. Whilst the majority accept that a longitudinally framed structure will be lighter a minority will still argue the reverse. It is of interest to note that the vast majority of high speed light weight vessels, where weight is critical, feature longitudinally framed structures.

Due to the strict noise and vibration limits found in a typical yacht build specification, vibration control is a major issue on these vessels. As a result the structural design can be driven by stiffness requirements rather than strength requirements. This is particularly true for deck structures which will generally exceed class scantlings. The relative merits of different framing systems are analysed and discussed later from a vibration perspective.

It is the aim of the Authors to try and quantify some of these issues in this paper.

3.0 Methodology

A basis design has been adopted. This is a typical 80m monohull and is described in further detail in the following section. It is assumed that the vessel features a steel hull and main deck and aluminium superstructure. In the development of the structure for this paper it is assumed that the aluminium structure does not contribute significantly to the vessel's global strength. This has consequently been ignored and is customary in the experience of the Authors.

Lloyd's Register of Shipping Special Service Craft (SSC) Rules have been used as the design standard because:-

- These rules are based on a first principles approach (albeit with empirically based scantling multipliers) which is useful when comparing designs.
- The SSC Rules are in common use in the large yacht sector. At the time of writing it was reported that Lloyd's Register's market share of new yacht build projects greater than 50m in length is 86%^[2].

The methodology adopted for the development of structure is presented in Figure 2. The design approach is based on the derivation of scantlings to meet local design loads which are then increased as necessary to comply firstly with a set of defined practical constraints and secondly, failure modes control based on global loads and buckling criteria. Additionally, vibration aspects concerned with deck response to excitation at propeller blade passing frequencies have been considered and are discussed.

A transverse framing system with a frame spacing of 600mm has been developed. For the longitudinal framing system a pitch of both 1800mm and 2400mm has been considered. Under the SSC Rules the frame pitch must be 'generally' limited to 2000mm or less. The higher value of 2400mm was investigated in order to explore the benefits that would be offered from a pitch more reflective of larger vessels (>85m & 3000 GRT). All frame pitches investigated are multiples of 600mm for practical reasons.

Comparative results are presented for structural weight, length of welding and number of structural parts within a length of parallel mid body between bulkheads.

4.0 Basis of Design

The work presented is based on a typical 80m displacement motor yacht of normal proportion and form. This size of modern, high volume yacht (circa 80 – 85m LOA) typically represents the length associated with the 3000 GRT limit applicable to the MCA Large Commercial Yacht Code (LY2) and consequently is (generally) the limit for the application of SSC Rules. Above 3000 GRT the LY2 Code is no longer applicable and a popular option is to build the vessel as a SOLAS passenger ship. This usually dictates a change in class society rules. Continuing with the Lloyd's example this would mean using the LR Passenger Ship Rules rather than the SSC Rules – the implications of doing so are discussed later in the paper. Additionally in this size regime global loads will have more influence on the scantlings.

The principal characteristics and mid ship section geometry are presented in Figure 3. The candidate geometry has a double bottom with a tank top height of 1700mm above base, an inner deck (5350mm AB), and main deck (8350mm AB). Primary girders are spaced at 2.4m and 4.8m off centreline with a span of 9.6m between bulkheads.

Mild steel has been considered throughout with the use of HP and fabricated steel sections.

5.0 Local Scantling Design & Practical Constraints

Minimum scantlings were calculated using local loads and minimum plate thicknesses. The scantlings of a section based purely on this approach produce a very light structure. However, the level of complexity and lack of robustness of the structure make it impractical for yacht applications. As a result, some practical constraints based on achievable construction practices have then been applied. These constraints are summarised as follows;

- To limit weld distortion a minimum practical plate thickness of 6mm on decks was applied.
- Plate thickness kept to a full mm, i.e. no half thickness plates.
- Maximum girth distance of 2.8 m between plate seams.
- Construction unit seams typically 100 mm above tank top, deck etc; plate thickness changes occur here if applicable.
- Minimum girder depth of 450mm to allow penetrations for HVAC; The routing of services, particularly the large diameter HVAC ducting in deck heads, can be very challenging on large yachts. In reality there will not be enough 'tween deck height to be able to run HVAC services under the girders, so the girders must be deep enough to accommodate penetrations of around 250 – 300 mm. A practical solution is to make the girder structure as deep as the general arrangement allows, leaving enough space under girder structure for linings, shallow cable trays and minor pipe work. This suggests that a girder depth of 450-500 mm is the minimum practical depth.
- For a practically laid out structure all stiffener pitch values were generally a function of 600mm.
- For fairness and robustness a minimum shell thickness of 8mm on hull sides and 11mm on hull bottom.

With the application of the above constraints the scantlings increased somewhat over the design for pure rule minimum scantlings.

6.0 Application of Global Loads

Wave bending moments were derived from the SSC Rules. An estimate of still water bending moment was made based on statistical data from a number of similarly sized yachts. Values utilised are presented below.

			Max (Hog)	Min (Sag)
Still Water Bending Moment	M_s	=	31950 kNm	26550 kNm
Wave Bending Moment	M_w	=	52607 kNm	-65990 kNm
Rule Bending Moment	M_R	=	84557 kNm	-39440 kNm

Section modulus calculations were performed on each of the sections with the practical constraints applied so that an assessment of the global strength for each could be made.

In reality there would not generally be a fully intact section in the midships region. Openings for stairwells, atriums, large hull side windows, shell doors and bilge wells would normally be removed from the section calculation - the remaining effective material is often slightly sobering. These vessels should pass global strength requirements using intact section properties with ease, and it is recommended that a good reserve on global strength is maintained in any design to account for late changes to openings and still water bending moment. Often the hull openings and structural discontinuities are so extensive that hull girder strength can only be verified using FEA.

In the case of this study, having a non-fully-intact section is true for both the longitudinally and transversely framed sections so from a comparative view would appear not to matter. However it would mask the true effect and influence of the global loads if ignored. Therefore the average stresses that were derived from the global bending moment/section modulus calculations were factored by 25% to account for loss of effective structure.

Once the global average stresses were derived, each section was assessed for buckling. Failure mode calculations were carried out on all critical parts of each section in accordance with the SSC Rules. Several areas required an increase in scantlings to pass the requirements. These are summarised in the tables below.

Longitudinally Framed Sections

Structure Component	Cause of increase	Before	After
Main Deck Stiffeners	Stiffener buckling (global loads)	60x6 OBP	80x5 OBP
Main Deck Frames	Consequence of stiffener depth change	140x7 OBP	180x6/60x6 T
Lower Deck Stiffeners	Stiffener buckling (global loads)	60x4 OBP	80x5 OBP
Lower Deck Frames	Consequence of stiffener depth change	140x7 OBP	180x6/60x6 T
Double Bottom Side Girders	Plate buckling (global loads)	8mm Plate	9mm Plate

Transverse Framed Section

Structure Component	Cause of increase	Before	After
Main Deck Plate	Plate buckling (global loads)	6mm Plate	8mm Plate
Upper Topside Shell Plate	Plate buckling (global loads)	8mm Plate	9mm Plate
Main Deck Frames	Stiffener buckling (global loads)	80x5 OBP	120x6 OBP
Lower Deck Frames	Stiffener buckling (global loads)	60x4 OBP	80x5 OBP
Double Bottom Side Girders	Plate buckling (global loads)	8mm Plate	9mm Plate

It can be seen that the transversely framed structure generally requires greater scantling increases in the shell than the longitudinally framed structure. This is due to its inferior ability to resist globally induced buckling loads.

The designs of the final midship sections are presented in Figure 4 (transversely framed), 5 (longitudinally framed at 1800mm) and 6 (longitudinally framed at 2400m). It should be noted that decks are designed to local load criteria only and do not include the increases in scantlings required to meet vibration criteria.

7.0 Results

Results are presented to compare the following factors;

- Weight
- Number of structural parts, joint length and length of welding

Additionally a number of secondary factors are discussed in general terms which may influence the choice of framing system.

7.1 Weight

The weight of each framing system has been calculated from the midship sections that have been produced. Calculations are for a 9.6m length of parallel mid-body containing one watertight bulkhead. Weights are presented at all 3 stages of the section development process to demonstrate the differences in weight between rule minimum structure, addition of practical constraints and influence of global loads. The results are presented in the table below;

Frame System	Longitudinal	Longitudinal	Transverse
Frame Spacing	1800mm	2400mm	600mm
Weight - Minimum Scantlings	6.732 t/m	6.903 t/m	7.686 t/m
Weight - Design Constraints Applied	8.149 t/m	8.345 t/m	8.492 t/m
Weight - Global Strength Requirements	8.256 t/m	8.457 t/m	8.846 t/m

The results illustrate that the lightest structure is produced by the longitudinally framed structures, in particular the 1800mm frame pitch. The transversely framed structure is some 7% heavier.

It can be seen that in general the application of practical constraints to the rule minimum structure adds around 10% to the transversely framed structure and 20% to the longitudinally framed system. This difference is due mainly to the fact that the longitudinally framed structures can be optimised to rule minimum scantlings by adjustment of the stiffener pitch. This is not possible on the transversely framed structure where the frame spacing drives the shell thickness. Consequently, the selection of 8mm and 11mm minimum (practical) shell thicknesses limits the extent to which the longitudinally framed system can be optimised.

Additionally the influence of the global loads can be seen to be more significant on the transversely framed structure. The longitudinally framed structures require a 1% increase in weight to meet global strength requirements whilst the transversely framed structure requires a 4% increase in weight. This is due to the large increase in the deck and shell scantlings required to resist buckling.

Yachts unusually represent very high value tonnage and this will need to be considered when assessing the significance of saving weight as a cost saving measure. In order to put this into perspective, for a yacht typical of the design used in this paper, the hull structure is probably 40% of the final weight of the vessel, but only represents around 12% of the cost.

7.2 Number of Parts, Joint & Weld Length

The cost of steelwork fabrication is often compared by using the measure 'man-hours per tonne'. Although useful in cost estimating for similar ships it can be misleading when comparing construction methods. A longitudinally framed vessel might take a little longer to build, but because it is lighter will appear costly in terms of man-hours per tonne relative to the transversely framed system.

In an attempt to make a relative comparison and quantify the labour involved in the assembly of all the framing systems, an estimate of the number of structural parts, joint lengths and weld lengths have been made.

Additionally, it is generally perceived that transversely framed vessels are easier to build. This is due to:

- Less welding.
- Fewer orthogonal welded connections (i.e. longitudinal to transverse web frame connection).
- Fewer cut parts.
- Weld shrinkage is easier to predict as welds are predominately in one plane.

In quantifying the number of parts and weld length the Authors have attempted to make an objective assessment of the above perceptions. This has required some simplifying assumptions to be made. For example it should be noted that no detailed optimised welding schedule has been undertaken. Consequently weld specifications have been made based on past projects of similar size and type.

The table below illustrates the results;

Frame System	Longitudinal	Longitudinal	Transverse
Frame Spacing	1.8m	2.4m	0.6m
Length of joint per 9.6m span	2938m	2724m	2704m
Length of weld per 9.6m span	4527m	4199m	4662m
Number of Parts per 9.6m of ship	817	761	931

It can be seen that the length of welding required for each system is approximately the same but marginally higher for the transversely framed system whilst the number of parts is significantly lower for the longitudinally framed system.

7.3 Secondary Factors to Consider

A comparison between midship sections cannot be limited to a weight comparison and quantified production aspects, and so the Authors have addressed a number of secondary factors below. Whilst those discussed are not exhaustive they highlight areas where further consideration may be required before selecting a framing system.

7.3.1 Hull-form Geometry

In commercial ships with a parallel mid-body it is relatively easy to fabricate a longitudinally framed mid-body section, since the longitudinals have an easy run in areas of equal girth. The flat of side and flat of bottom areas can be fabricated in a panel hall on a flat floor using semi-automated welding of the stiffeners to the plate. In the bow and stern areas, where the girth measurement decreases rapidly, the longitudinals will tend to run out and require more complex bending to get them to take the form required. Hence it is usual practice to adopt the transverse framing system in the fore and aft regions.

Yachts typically have relatively low block hulls, and their fine form and lack of parallel mid-body makes longitudinal framing appear less attractive, although it is by no means impossible to achieve.

7.3.2 Minimum Plate thickness

The practical limits for minimum plate thickness are dependent on the skill and welding processes of the yard, the need to have a surface robust enough to hold filler and to generally be stiff enough to avoid vibration problems in service. All of these factors tend to drive minimum plate thicknesses beyond the rule minimums.

It is suggested that for most yards, using plate thicknesses less than 5-6 mm will start to be problematic. The ability to optimise longitudinally framed structure can therefore be somewhat limited as the large shell and deck areas are where the most significant weight savings can be made.

7.3.3 Fairness of Form

Yacht builders seek to achieve very high levels of fairness and finish in both transverse and longitudinally framed hulls. Weld shrinkage and distortion will be different for the two arrangements and consequently the amount of fairing compound needing to be applied will be different. However in the Authors experience neither method shows a clear advantage in this area.

7.3.4 Routing of services

As previously discussed [ref. Section 5] the routing of services, particularly large diameter horizontal HVAC ducting in deck heads, can be very challenging on these vessels. This can drive the scantlings of the structure, particularly on longitudinally framed decks, well above those required from a pure strength perspective.

Vertical service routing is also often problematic and one advantage of a transversely framed side shell is the ability to route larger services vertically within the hull side linings which are unhindered by longitudinal stiffeners and consequently offer more room.

7.3.5 Vibration Considerations

Large yachts generally have strict noise and vibration limits; usually in excess of ISO 6954 and Class Notation requirements. In order to keep below these vibration limits it is important that deck structures do not resonate at frequencies close to major excitation frequencies. Since this problem will only emerge during measurement trials of the finished vessel, it is necessary to design the deck structures with these requirements in mind.

The major low frequency source is the propeller at blade rate passing frequency (BPF). This is dependent on number of blades and shaft rate, but a cruise speed blade passing frequency of 10-15 Hz is not uncommon. In order to ensure that the decks do not resonate at any point in the speed range, the design approach with least risk is to ensure that the first mode frequency of every deck panel is in excess of BPF. Generally this will not dictate the plate thickness required, but will dictate the selection of deck secondary and primary structure to ensure natural frequencies in excess of BPF are achieved.

A frequency analysis of the lower deck panel with both framing configurations was undertaken, including a typical outfit weight. The analysis was limited to a single deck field rather than an entire deck, and as such, the boundary conditions are not wholly representative but are sufficient for comparative purposes. The table below presents the natural frequencies of the two framing systems.

Mode Shape	Resonant Natural Frequency (Hz)	
	Longitudinal	Transverse
1	13.891	12.644
2	14.240	12.653
3	15.540	12.798
4	18.123	12.843
5	21.636	13.177
6	23.984	13.500
7	24.040	14.386
8	24.054	14.457
9	24.200	15.357
10	24.386	15.373
11	24.405	15.856
12	24.496	16.118

For the model analysed the comparative deck mass was 9.94 tonnes for the longitudinally framed deck and 9.39 tonnes for the transversely framed deck. Plots of the first mode shape of excitation are presented in Figures 7 & 8.

The results can be summarised as follows:

- The longitudinal framing example has a higher natural frequency despite its increased mass, and so is a stiffer structure.
- Both examples fall below the typical frequency required for risk adverse vibration design on this size of vessel. The frequency could be increased by using internal pillars and partitions to reduce span lengths or by considerably increasing scantlings in large pillar free areas. This reflects current practice.
- There are a greater number of modes below 15 Hz on the transverse framing example, suggesting raising the natural frequency of this deck would be more problematic.

It can be concluded that longitudinally framed decks are advantageous with respect to vibration control.

7.3.6 Side Shell Framing

The side shell is one area where transverse framing can offer advantages. The deep web frames required for longitudinal framing can impact on the accommodation, reducing internal space, and increasing recess depths in way of hull windows etc. In addition, since the transverse hull side frames

only have to support a modest plate area, it is easier to incorporate and manage late design changes in window and port light positions which seems an inevitable part of the stylist's GA development.

7.3.7 Risk management

All builders will have their favoured methods of construction, including the selection of a framing system. Weight estimation, costing and yard standard details will all be based around their normal construction methods. As steel cutting is often an early contract milestone there is usually little time to develop alternative structural arrangements. Consequently changing current practice is frequently viewed as increasing commercial risk without significant technical benefit.

7.3.8 Progressive Failure

There is one hidden benefit of longitudinal framing which should be borne in mind, and that is the reserve factor over progressive failure. With transversely framed decks the only longitudinally effective material is the deck plate and girders. Should the upper deck exceed its buckling stress only the girders are left to carry the in-plane loads. With longitudinally framed decks the longitudinally effective material also includes the secondary stiffeners. The stiffeners have a buckling capacity far higher than the plating (which is in any case improved over the transversely orientated plate by a factor of 4) and so should the deck plate exceed its buckling stress the longitudinals and girders will generally be able to carry the in-plane load and prevent progressive failure. Although this is not usually considered in design, this additional reserve makes it easier for the structural designer to accommodate some of the more extreme whims of the stylist knowing that should the design loads be exceeded, the section will still remain intact.

8.0 Hybrid Section Development

Giving due consideration to the results achieved, a hybrid framing system is often adopted by the Authors (and others). This combines longitudinally framed decks with a transversely framed side shell and double bottom. At vessel lengths much beyond 85m a longitudinally framed double bottom will also be required.

The geometry of the Hybrid System is presented in Figure 9. The hybrid section weight is 8.648 t/m (for comparative purposes with Section 7.1).

9.0 Impact of Length & Class Society

Current market trends are for ever larger yacht structures and the debate on framing systems changes as size increases. Global loads on the hull girder will increase proportional to the beam, and to the square of the length of the vessel.

$$\text{Bending Moment} \propto L^2 B$$

As a yacht gets longer it will increase in beam but not significantly in depth, and hull section modulus will increase roughly proportionally to the beam. Hence hull girder stress will increase approximately in proportion to L^2 . This would result in a 100 m vessel seeing a 50% stress increase over its 80 m cousin. Hull girder strength issues rapidly dominate the design of the 100 m + size range, and there clearly comes a size of vessel where transverse framing is no longer a viable option.

As discussed in section 4.0 the regulatory framework changes above 3000 GRT which generally drives the design towards the use of more empirically based 'traditional' ship rules. When faced with this option it is useful to realise the impact that this will make to the structural design of the yacht.

The fundamental differences between the SSC Rules and (LR) Passenger Ship Rules can be summarised as follows:

- Corrosion margins. SSC Rules are net scantling rules (no corrosion margin). Ship Rules include a corrosion margin, which is not generally required for highly maintained yacht structures. The exact value is not transparent, but generally scantlings will be heavier for that reason.
- Minimum plate thicknesses are increased.

- Standard frame spacing. Ship Rules provide a standard frame spacing based on vessel length, which there is no benefit in reducing. This will dictate shell thickness.
- Global Loads are increased. Pt 4 Ch 2 increases the sagging wave bending moment on ships with large bow and stern flare, probably by 20% on a typical yacht hull form.
- Minimum Hull Section Modulus requirement. Regardless of still water bending moment, the vessel needs to satisfy this additional global strength requirement.
- Bow and stern strengthening. Ship Rules have specific requirements to strengthen against slamming, which are in considerable excess of the SSC Rules.
- Ship Rules require a minimum plate buckling capacity of 40 N/mm^2 , which effectively means 8mm minimum deck thickness for transversely framed vessels.
- Ship Rules do not permit the critical buckling stress of plates to be exceeded, regardless of the stability of the structure as a whole. This further increases global strength requirements on the design.
- Ship Rules on aluminium structures is based on a steel equivalence and requires special consideration to apply sensibly to a yacht superstructure.

It is suggested that these differences could add approximately 20% to the steel weight of an 80-90 m vessel, although a detailed comparison is beyond the scope of this paper.

10.0 Conclusions

A comparative analysis of both longitudinally and transversely framed structures has been made with specific reference to large yacht yachts.

It has been illustrated that longitudinally framed structures will be lighter, have fewer parts and involve less welding than a transversely framed structure. The longitudinal framing system is easier to optimise for weight and the vibration characteristics of longitudinally framed decks have been shown to be superior.

From consideration of practical construction constraints as well noise and vibration considerations it has been illustrated that, for large yachts, achieving a structure which is close to rule minimum scantlings, is difficult to achieve. Consequently the adoption of a longitudinal framing system can be of limited benefit for yacht sizes which are not dominated by global load considerations, as surface fairness, robustness and noise and vibration requirements penalise the ability to build a very light longitudinally framed structure.

A hybrid framing system has been presented which employs a transversely framed side and bottom structure in conjunction with longitudinally framed decks, and is shown to be a good compromise between weight and practical limitations on these types of vessel.

The influence of increasing the vessel length has been discussed both from a perspective of applicable classification society rules and it has been suggested that the application of more traditionally based ship rules could add approximately 20% to structural weight. Additionally the influence of size on global load requirements has been illustrated and it is suggested that for vessels of 100m and above the use of longitudinally framed bottom structures becomes mandatory to efficiently meet buckling criteria.

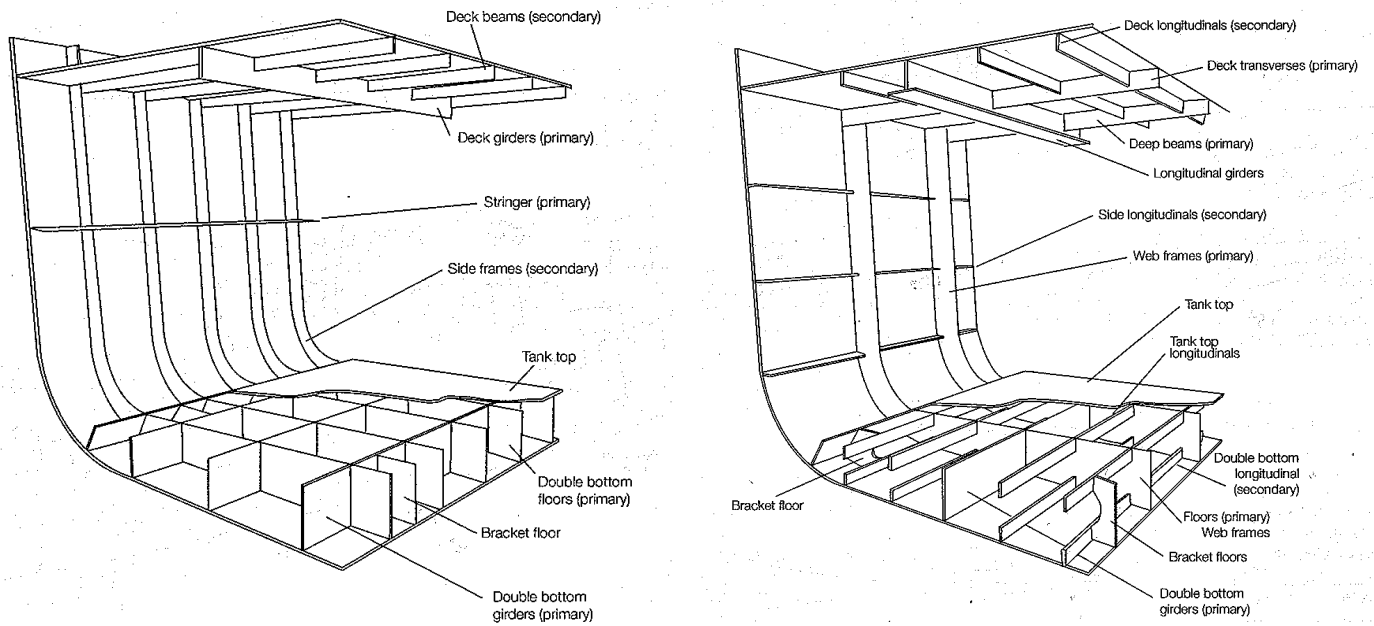


Figure 1 – Transverse (Left) and Longitudinal (Right) Framing
 (Images supplied courtesy of the Lloyd's Register Group)

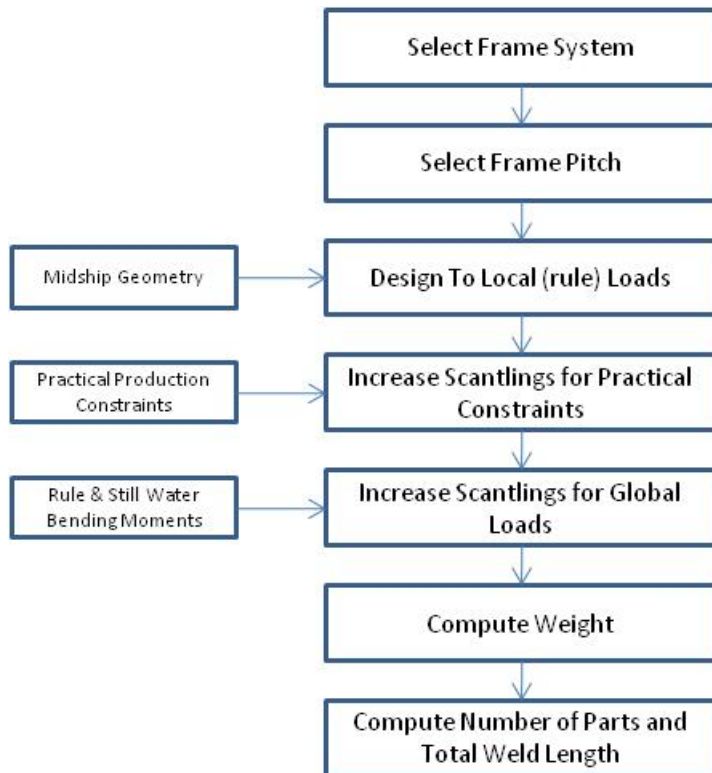
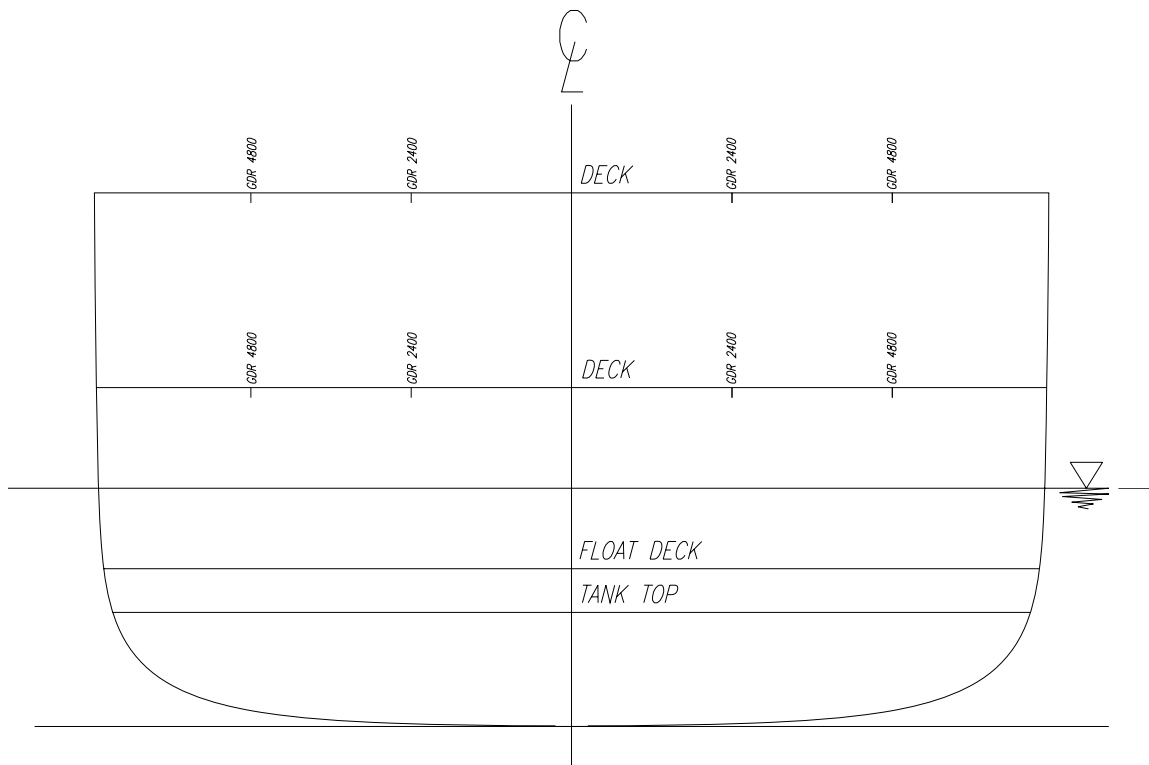


Figure 2 – Design Methodology



Principal Dimensions	
Length Overall	80.00 m
Length Waterline (Design)	71.40 m
Length between Perps	71.40 m
Waterline Beam	14.00 m
Displacement (Design Draught)	2000 tonnes
Design Draught	3.55 m
Service Speed	14 knots
Max Speed	16 knots

Figure 3 – Midship Geometry and Principal Characteristics

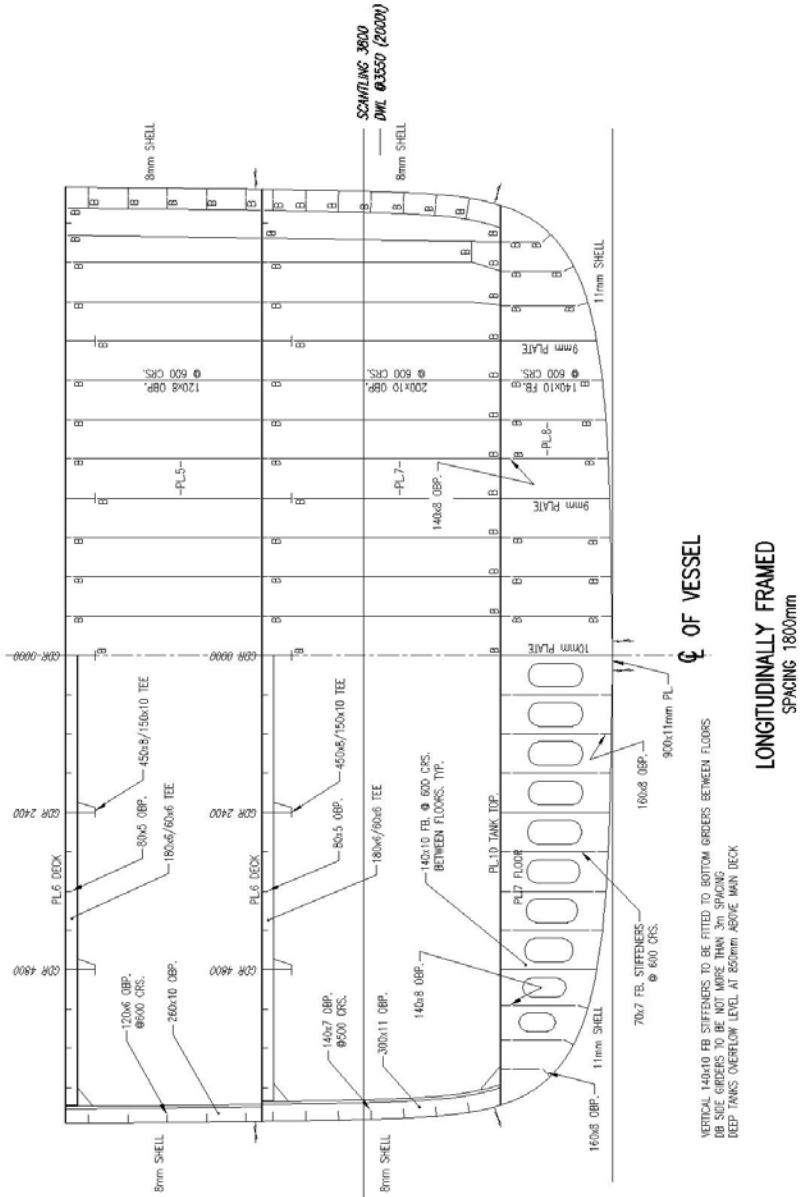


Figure 5 – Longitudinally (1.8m Pitch) Framed Structure

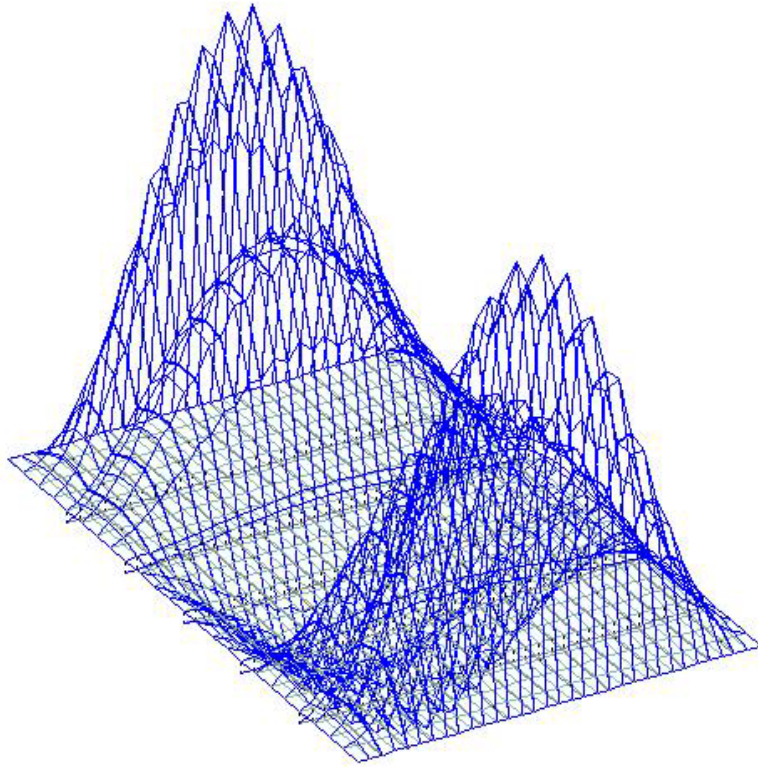


Figure 7 - Transverse Framing Mode Shape 1: 12.64 Hz

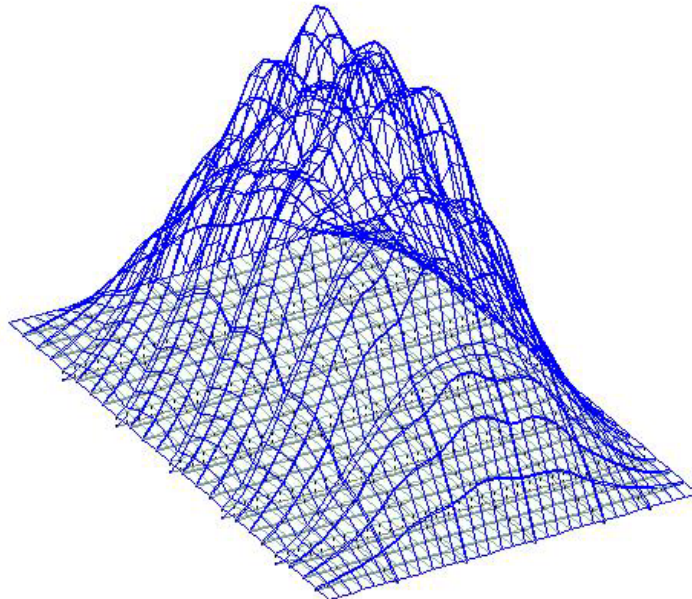


Figure 8 - Longitudinal Framing Mode Shape 1: 13.89 Hz

Session 4

M.W. Findlay & S.R. Turnock

Investigating sailing styles and boat set-up on the performance of a hydrofoiling Moth dinghy

M W Findlay, S R Turnock

Fluid-Structure Interactions Research Group, School of Engineering Sciences,
University of Southampton, UK

Email: matt.findlay@soton.ac.uk, srt@soton.ac.uk

Abstract

The adoption of hydrofoils in the International Moth class of dinghy has posed new challenges to sailors both in terms of the set-up of the boat and hydrofoils, and their sailing techniques and styles. The experience of sailors in the class indicates that the height above the water surface at which the boat is flown (ride height) and the amount of windward heel (heel angle) are critical factors affecting performance, particularly in upwind sailing. The fore-aft position of the helm affects the stability of the craft and, in conjunction with the aft foil settings, alters the pitch orientation of the craft and offers potential for significant gains in performance. A four degree of freedom velocity prediction programme (VPP) with the capability to investigate these factors is presented and used to demonstrate how the fore-aft position of the helm and the aft foil may be used in conjunction to maximise speed.

Nomenclature

α	Incident flow angle	[rad]	c	Chord of foil	[m]
∂CB^x	Movement of centre of buoyancy in X-direction	[m]	D	Drag	[N]
$\frac{\partial C_L}{\partial \alpha}$	Lift-curve slope of foil	[rad ⁻¹]	D_{Spray}	Spray drag	[N]
$\Delta_i^{x,y,z}$	Distance along X, Y, or Z-axis, between centre of effort of i^{th} component of force and centre of mass of craft	[m]	D_W	Drag due to windage	[N]
ρ_{air}	Density of air	[kgm ⁻³]	e	Oswald efficiency factor	[-]
ρ	Density of water	[kgm ⁻³]	$F_i^{x,y,z}$	Force in X, Y, or Z-direction, acting on i^{th} component	[N]
θ_H	Heel angle	[deg]	I	Moment of Inertia of craft about centre of mass	[kg m ²]
θ_P	Pitch angle	[deg]	L	Length	[m]
AR	Geometric Aspect ratio	[-]	L	Lift	[N]
C_D	Coefficient of drag	[-]	M	Total mass	[kg]
C_{D_i}	Coefficient of induced drag	[-]	S	Area of foil	[m ²]
C_{D_p}	Coefficient of profile drag	[-]	t	Thickness of foil	[m]
$C_{D_{spray}}$	Coefficient of spray drag	[-]	v_a	Apparent wind speed	[m/s]
C_L	Coefficient of lift	[-]	$v_{x,y,z}$	Craft speed in X, Y, or Z-direction	[m/s]
C_{WP}	Coefficient of waterplane area	[-]	W	Total weight of craft and crew	[N]
			z	Vertical distance between craft centre of mass and water surface	[m]

1 Introduction

Hydrofoils are lifting surfaces fitted to marine craft that act at speed to partially or fully lift the main body of the craft clear of the water with the aim of reducing total drag at speed and therefore offers potential for an increased top speed. The practical application of hydrofoils to sailing craft is difficult for two main reasons [1]. Firstly, the power to weight ratio of most sailing boats is relatively low because of the need to carry ballast in order to provide righting moment against the heeling moment from the sails. This generally limits the application of hydrofoils to catamarans and dinghies which can extend the crew weight on racks or trapezes to provide the necessary righting moment. Secondly, the operating speed of sailing craft is highly variable, being a function of apparent wind speed and direction, and so the use of hydrofoils is also largely a problem of developing suitable control systems to account for these fluctuations.

Nevertheless, since 2005, hydrofoil-equipped International Moth dinghies have won every major championship [2] demonstrating that in this class hydrofoils can be used successfully in a large enough range of conditions to consistently win regattas against non hydrofoil-equipped craft from the same class. The impressive speed of these craft (top recorded speed close to 30 knots [3]) has caused an explosion in interest from both sailors and the sailing media and development has taken place at a rapid pace – posing many interesting challenges to both designers and sailors.

The major aims of this paper are to give an overview of the International Moth dinghy (section 2), present a new velocity prediction program (VPP) for the Moth (section 3) and use the VPP to look specifically at the influence of aft foil setting and helm longitudinal centre of gravity (LCG) on performance (section 4.)

2 The International Moth Dinghy

The International Moth dinghy is a 3.355m long, single handed, una-rigged monohull dinghy. The class rules do not limit hull shape, materials or weight, but limitations are placed on length, beam and sail area. As a result the craft have evolved to be lightweight (<30kg fully rigged), have a narrow waterline beam (~0.3m), and large wings (*beam overall* = 2.25m) from which the helm hikes. This is a craft that has a large power to weight ratio, low drag and is therefore a great platform for the use and development of hydrofoils.



Figure 1. International moth. Showing narrow hull and wide beam overall due to ‘wings’. Appendages (daggerboard and rudder) can be seen piercing the surface and have lifting hydrofoils mounted on the submerged ends. Photo by Hannah Kemlo.

The class rules prohibit surface piercing hydrofoils, forcing designers to adopt a bi-foil airplane configuration utilising daggerboard and rudder mounted, fully submerged T-foils, with a mechanical control system using a bow-mounted sensor arm (‘wand’).

2.1 The control system

An active control mechanism is required to control ride height over a range of speeds and this is achieved through the use of a bow-mounted wand sensor (figure 3a) controlling a trailing edge flap on the forward (daggerboard-mounted) foil (figure 2a) via a cam and push-rod system (figure 3b). Screw fittings in the system allow the sailor to set the wand angle which gives a neutral flap position but the ratio of wand angle to flap angle is governed by the cam system and therefore effectively fixed. The wand length can be varied (though not *currently* whilst sailing) for the conditions. It is possible to adjust the aft (rudder-mounted) foil (figure 2b) angle manually whilst sailing using a worm gear system which in some cases alters the entire angle of incidence of the foil relative to the boat, and in others adjusts the angle of a trailing edge flap on the aft foil.



(a) Daggerboard and lifting hydrofoil ('T-foil'), showing trailing edge flap that is controlled by bow mounted wand sensor.

(b) Rudder mounted on gantry and showing lifting hydrofoil ('T-foil') at depth. Photo from [4]

Figure 2 Views of typical Int. Moth appendages and foils



(a) Bow mounted wand sensor that tracks water surface and controls flap angle on forward hydrofoil. Photo by Hannah Kemlo.

(b) The linkage between the wand sensor and the push rod which leads back to the daggerboard and mechanically controls flap angle. Photo from [5]

Figure 3 Views of Wand sensor

There are a number of variables relating to foil size, shape and position that must be fixed by the designer to achieve the aim of creating a 'fast' craft, and other variables that may be controlled by the sailor relating to the set-up of the craft in order to maximise speed (or stability) in a given wind condition on any given leg of the course. In the field of yacht design these variables are chosen based on (in approximately increasing order of cost and time) empirical evidence, understanding of isolated components, modelling of the complete system using a velocity prediction program (VPP), tank testing, use of computational fluid dynamics and two boat testing. Most tuning decisions are made based on empirical evidence, full scale testing, two boat tuning and, less frequently, through the use of a VPP.

In [1] approaches to foil design and configuration for the International Moth were discussed and a VPP presented and used to predict the performance of International Moth dinghies in context of the decisions faced by designers, particularly with regard to foil selection. It was noted however, that limitations of that VPP meant it was not suitable for examining in detail techniques for sailing the craft, or set-up and tuning of the foil control systems.

2.2 Sailing styles

The international moth utilises an 8m² sail which, in combination with the high apparent wind speeds, generates a large amount of force. This force is directed approximately perpendicular to the sail surface and its sideways component must be balanced by the side-force from the appendages to prevent sideways acceleration. The roll moment from the sail and appendage forces must be balanced by the righting moment from the action of the helm hiking to prevent the craft rolling over. These forces are illustrated in figure 4.

When sailing to windward, the sail force is large enough that, with the mast vertical, the sailor is unable to develop sufficient roll moment to counter it. This problem is solved by heeling the craft to windward (see figure 4), which increases the perpendicular lever arm of the helm's weight and utilises a component of the weight of the craft and rig to increase the righting moment. This is similar to the common style used by windsurfers.



Figure 4. Demonstrating the windward heel angle and the showing the lift and weight forces. Note that drag and windage forces are not represented. Photo from [4]

A consequence of this windward heel is that a component of the weight now acts to oppose the sideways sail-force, thus reducing the force required from the appendages and thereby reducing leeway angle and induced drag, with the consequence that the craft may track

higher (to windward) and have greater speed. However, as the efficiency of the sail is reduced with increasing heel angle [6], there is likely to be an optimum angle of windward heel; dependent on the wind conditions, boat set-up and helm weight, and it is of interest to investigate this computationally to examine the trade-offs and search for an optimum.

In setting up the boat the sailor also controls whether the craft flies higher ('riding high') or lower on the foils. Combined with windward heel, 'riding high' may have a positive effect by increasing the lever arm over which the weight of the craft acts to provide righting moment, yet there is also an increase in the lever arm by which the sail force acts to oppose righting moment, and the payoff between the two must depend at least partially on the windward heel angle. Increased ride height also decreases stability, making the craft harder to sail, and increases the risk of foil ventilation – which may be catastrophic. Again a trade-off must be made and it is of interest to examine the behaviour of the system.

Affecting the forces on the lifting foils, rather than the sail force and righting moment, the fore-aft position of the helm, in conjunction with aft foil settings, are known to affect the stability, pitch orientation and speed of the craft. At the 2008 International Moth world championships in Weymouth, the Australian sailors demonstrated superior upwind speed in the stronger winds by flying high and with a bow down orientation. Another area of great interest is therefore in investigating why this orientation was faster than the traditional set-up used by the European competitors who used essentially the same equipment.

3 Development of the VPP

There are many questions regarding the set-up of the International Moth, and those associated with the optimal foil settings and sailing styles are motivating factors towards developing a computational simulation of the craft. In this paper a new VPP is presented in which the craft is free in four degrees of freedom and may be used to examine the influence of hydrofoil set-up and sailing styles on performance. The VPP is used to specifically investigate the relationship between fore-aft position of the helm and aft-foil angle and their impact on ride height, pitch orientation (bow-down, bow-up), speed and stability. The results give insight into the progress in boat set-up and sailing styles (particularly for stronger winds) made by Australian sailors, using essentially the same equipment as their European counterparts, demonstrated at the 2008 World Championships [7].

3.1 Overview

The VPP replicates the geometry of the International Moth (crucially the wand-foil system) and aims to find the stable ride-height, velocity and pitch orientation at which the craft converges for a given boat set-up and true wind condition. This is achieved by quasi-steady calculation of fluid and weight forces to accelerate the craft from rest through displacement sailing, take-off and ultimately stable flight. The result of interest is the steady motion of the craft and the design of the VPP reflects this by adopting rudimentary but sufficient models of hull-related forces (which are zero when foil-borne) and using a damping factor approach to account for added mass. This does not affect the final solution but may affect the acceleration of the craft. Nevertheless the time-related motion of the boat is predicted and is of interest because it indicates the stability of the set-up. Comparison of the predicted motion with video footage of a Moth accelerating from rest shows that the time-scales of the acceleration (onto the foils and up to full speed) are similar.

The VPP constrains the craft's yaw and roll motions but leaves it free to move in all other dimensions (surge, sway, heave and pitch.) Any heel angle can be specified in order to look at the effects of windward heel and other model inputs include aft foil setting and helm LCG. The dimensions of the Moth dinghy used in the simulation are those of the 'Flying Lime' (figure 1), a Fastacraft built 'Prowler' design of International Moth, which is available for measurement and future validation trials. Foil settings are determined from the geometry of the wand system and its position relative to the water surface, as in the real craft. Sail drive force is maximised under the constraint that heeling moment may not exceed the maximum righting moment and standard aerodynamic empirical formulae are used to find the lift and drag forces acting on the craft, which are resolved into the body axis system and govern its behaviour. The simulation is coded in Matlab™ and uses a one step solver based on an explicit Runge-Kutta formula using a variable step size based on derivatives and error

tolerance criteria. One 60s simulation can take between 20s and 2 hours to run on a modern desktop PC depending on the number of iterations to achieve convergence at each step.

3.2 Computational Process

The computational process is illustrated by the flow chart of figure 5.

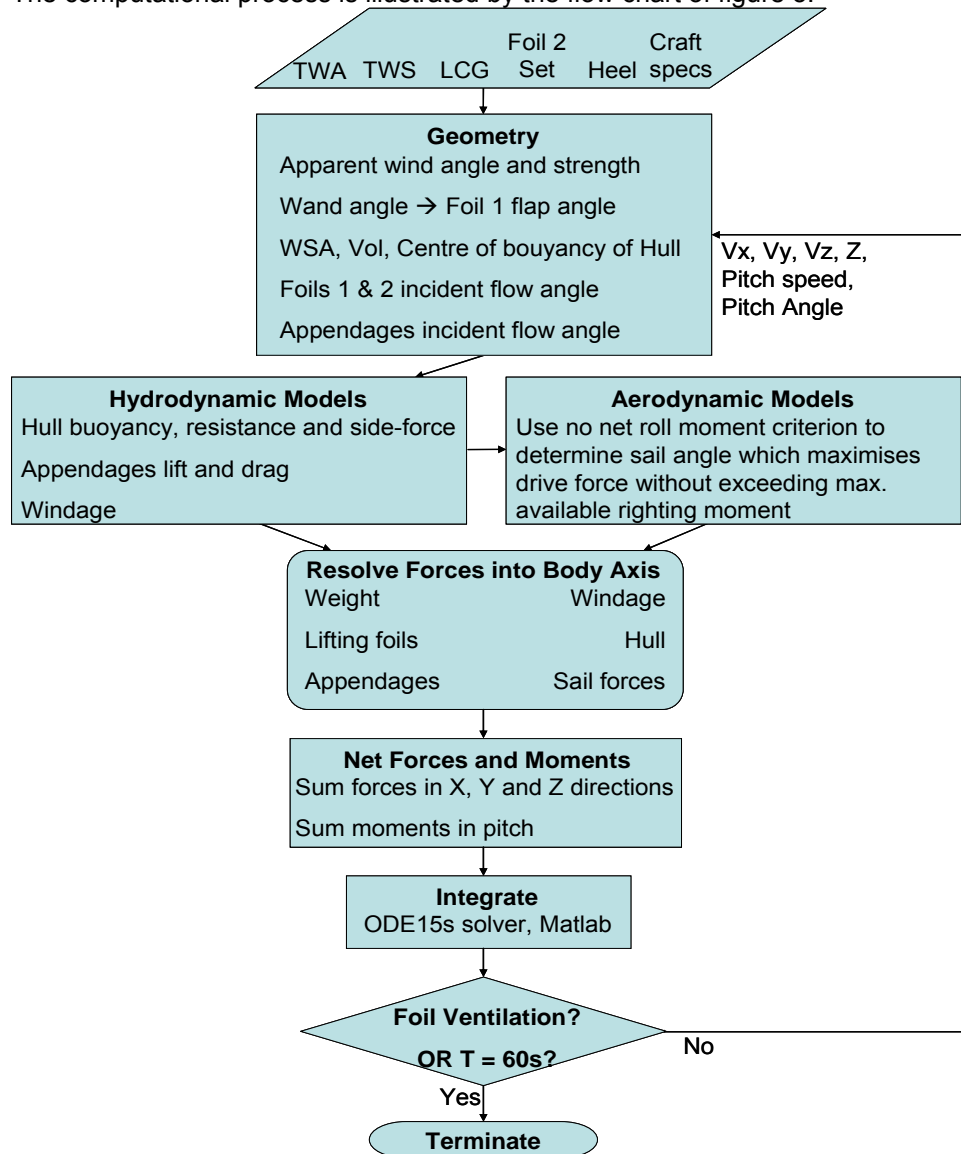


Figure 5. Computational process for simulation of International Moth

3.3 Governing Equations

The forces acting on the craft and included in the VPP are attributable to the following sources: hull side-force, hull buoyancy and hull resistance, appendage (daggerboard and rudder) lift and drag, lifting foil (forward, 'foil 1', and aft, 'foil2') lift and drag, sail lift and drag, windage and weight.

Forces are calculated in the appropriate fluid axis and then resolved into the body axis for X (*longitudinal axis of boat, +ve at bow*), Y (*lateral axis of boat, +ve to windward*) and Z (*orthogonal to X and Y, +ve towards mast tip*) components. The motion of the craft is determined in a quasi-steady approach by summing forces (or moments) in each axis using the appropriate components (1), and in the pitch direction using appropriate moments (3). All motions are calculated about the centre of mass of the craft.

$$\frac{\partial v_x}{\partial t} = \frac{1}{M} \sum_i F_i^x \quad \frac{\partial v_y}{\partial t} = \frac{1}{M} \sum_i F_i^y \quad \frac{\partial v_z}{\partial t} = \frac{1}{M} \sum_i F_i^z \quad (1)$$

$$\frac{\partial z}{\partial t} = v_z \quad (2)$$

$$\frac{\partial^2 \theta_p}{\partial t^2} = \frac{1}{I} \sum_i (F_i^z \Delta_i^x + F_i^x \Delta_i^z) \quad (3)$$

$$I = \frac{ML^2}{5} \quad (4)$$

$$\sum_i (F_i^y \Delta_i^z + F_i^z \Delta_i^y) = 0 \quad (5)$$

The constraint that heel angle must remain constant allows the roll moment equation (5) to be used to determine the sail forces. First the maximum available righting moment is calculated based on the action of the helm and craft weights, and accounting for the appendage and windage forces contributing to roll moment, then the sail is effectively trimmed from maximum in to maximum out and the sail lift and drag are evaluated at each trim point. The sail forces are resolved into the body axis and the trim angle is chosen that maximises the drive force without the moment due to side-force exceeding the maximum righting moment.

3.4 Component Force Models

The individual forces attributable to each component of the craft are calculated using the models and assumptions described next. These are based on standard aerodynamic or ship-theory and a 'sufficient approximation' approach. The most difficult aspect of creating the simulator is not the implementation of the models but establishing the correct geometrical relationships within and across the various fluid axis systems as the craft experiences changes in heave, pitch, surge and sway in the boat axis system.

Geometric calculations are made at every time step to establish:

- Wand angle (the wand rotates in the body axis x-z plane and is assumed to track the surface at all times.)
- Apparent wind strength and angle.
- Foil flow incidence angle (including foil setting, pitch angle, flow due to vertical and rotational velocity, and (forward foil only) wand-flap system.)
- Appendage incident flow (leeway angle due to sway speed.)
- Foil tip distance from the surface.
- Wetted length and areas of appendages.
- Location and amount of submerged volume of hull.

The following section details the ways in which forces have been modelled in the VPP, starting with the lift and drag forces on the sail, foils and appendages, then the windage forces and finally the hull resistive and buoyancy forces.

3.4.1 Foil lift

The approach taken to model lift is consistently applied to appendages, foils, sail and the hull. The approach used is based on lifting line theory to determine the lift coefficient, C_L , from the angle of attack, α , based on the effective aspect ratio, AR . [8]

$$C_L = \frac{\partial C_L}{\partial \alpha} \frac{AR}{(AR + 2)} \alpha \quad (6)$$

In all cases, aspect ratios are large, ≥ 8 , and the hydrofoils are approximately elliptical. $\frac{\partial C_L}{\partial \alpha}$

is the 2D foil lift curve slope, which can be determined from empirical data or a program such as X-Foil. The lifting foils use a NACA63412 section and the daggerboard and rudder are NACA0012 sections.

Equation 6 holds for small angles of attack but fails when the foil begins to stall. Incident flow angles can be shown to be small but for the lifting foils, the lift coefficient, C_L , is limited to 1.5, and in the case of the sail the onset flow is limited to 35 degrees (a stalled sail condition can sometimes be desirable due to the high drag, for example when running downwind.)

The centre of effort of the daggerboard is assumed to be located at its centre, or midway between the free surface and the tip of the daggerboard if foiling. The centre of effort of the sail is assumed to coincide with the geometric centre of area; at approximately 1/3 the luff length above the gooseneck. The centre of effort of the lifting foils is assumed to be in the centre of the foil.

3.4.2 Foil drag

For all lifting surfaces, the same basic approach is taken to calculate drag. The constituent components are skin-friction, pressure form, induced drag and, for surface piercing foils, spray drag. Profile drag is calculated using a skin friction coefficient (from the ITTC '57 skin friction correlation line) and a form factor (based on thickness – chord ratio) as in [9]. Induced drag is calculated using lifting line theory based on geometric aspect ratio and including Oswald's efficiency factor, e , to account for the influence of shape on efficiency [8].

$$C_D = C_{D_i} + C_{D_p} \quad (7)$$

$$C_{D_i} = \frac{C_L^2}{e\pi AR} \quad (8)$$

In the case of the sail, e is related to heel angle to account for the decrease in efficiency of the sail as the craft heels [6]:

$$e = 0.8\cos(\theta_H) \quad (9)$$

$$AR = \frac{L^2}{S} \quad (10)$$

Spray drag is a drag force attributable to the formation of spray, which is always present on the rudder as it is hung from a gantry behind the boat and therefore at all times a surface piercing strut (figure 2b). Spray drag is included for the daggerboard only when the top of the board pierces the surface. Spray drag is calculated using a formula due to Chapman [10] that modifies a formula of Hoerner and is based on the thickness – chord ratio.

$$C_{D_{spray}} = 0.009 + 0.013\left(\frac{t}{c}\right) \quad (11)$$

$$D_{Spray} = \frac{1}{2}tcv_s^2\rho C_{D_{spray}} \quad (12)$$

Tip loss drag, associated with the acceleration of flow across the tip of a foil, junction drag, associated with the interaction of boundary layers at intersecting sections, and foil wavemaking drag, associated with the generation of waves when the foils are operating very close to the free surface, are considered negligible [11], [12].

3.4.3 Windage

The components of windage are helms-person, wings, hull, foredeck and rigging. Mast and boom are assumed implicit in the sail model and foils above water (aerodynamic) drag and wand drag are neglected. No blanketing effects are accounted for and the projected area (in the plane perpendicular to the apparent wind) of each component is used as the dimensionalising area, S . Drag coefficients are approximated based on the shape of the components and using data from Hoerner [13] and are given in table 1.

$$D_w = 0.5\rho_{air}v_a^2\left(\sum_i S_i C_{D_i}\right) \quad (13)$$

3.4.4 Hull Forces

The main purpose of the hull within the VPP (and indeed in real life) is to support the craft prior to it becoming fully foiling, and therefore the models are rudimentary. In this investigation the hull has no bearing other than at the beginning of a run when the craft initially accelerates. Hull sections are assumed to be rectangular with vertical sides and flat bottom. The hull is assumed to have no rocker and be symmetrical about mid-ships (so that the bow and stern are identical.) The hull is assumed to have a coefficient of waterplane area, C_{WP} , of 0.75. The wetted surface area and volume are estimated using the average draft; calculated geometrically according to the ride height and pitch angle of the craft. The centre of buoyancy is assumed to move with pitch angle according to:

$$\partial CB^x = \frac{L}{2}(1 - e^{-5\theta_p}) \quad (14)$$

So that as pitch angle changes the buoyancy forces “moves quickly towards the ends of the hull, but never quite gets there”. This is a ‘sufficient approximation’. The model accounts for no lateral (sideways) movement of the centre of buoyancy as the craft are very narrow. This simplifies the calculation of maximum available righting moment – which is therefore solely due to the action of weight. Physically the boat cannot be heeled much when the hull is in the water as the wings will make contact with the water surface.

Forces due to the hull are buoyancy, side-force and resistance. Vertical force due to the action of the hull as a planing surface and associated drag forces are neglected. Buoyancy force acts in the opposite direction to gravity and with magnitude equal to the displaced weight of water.

The hull is assumed to act as a very low aspect ratio foil, based on geometrical calculation of wetted length and average draft, and thereby generates side-force and induced drag in accordance with (6) and (8). Hull resistance is calculated using skin friction and a form factor, as in [9], with Reynolds number based on wetted length. Residuary resistance is neglected on the basis that the craft are very slender ($L/B \sim 10$) and only operate at low F_n (the craft are fully foil-borne at higher speeds). Added resistance in waves is also neglected on similar basis – that the craft is fully foil-borne when there is enough wind to generate waves.

3.4.5 Other assumptions

The centre of effort of windage is assumed to be on the fore-aft centreline of the boat. As a consequence there is no moment due to the Z- (upward) component of the windage force. Similarly, to simplify the geometrical calculations, the centre of effort of the sail is assumed to be on the fore-aft centreline. The Moth, being a high speed craft, usually sails with the boom closely sheeted to the centreline so this assumption probably also has a low impact. The centre of mass of the boat (excluding helm) is assumed to be on the centreline implying that the moment due to the weight of boom and sail (the only components not symmetrical about the centreline) is negligible.

Pitching is neglected from the aerodynamic model for sail force calculations; being relatively insignificant in comparison to forward speed, wind speed and heel angle. Leeway (as a result of sway velocity) is neglected from the model of hydrofoil lift as it is relatively insignificant in magnitude and affects the effective sweep angle of the foils rather than the angle of attack. Similarly pitch angle is neglected from the appendage models for exactly the same reason.

3.5 Implementation

Measured and estimated values for overall dimensions and coefficients used in the simulation are given in Table 1. Centres of mass were estimated by lifting the fully rigged craft to find the balance point in each axis. The centre of windage of the craft is assumed to be positioned at the boat centre of mass. The centre of windage of the helm is assumed to act at

the centre of mass of the helm. All positions are defined within the VPP relative to the centre of rotation of the wand which was arbitrarily chosen as the origin for measurements on the boat.

Table 1. Design Parameters of Modelled Moth

Hull	3.35		Foil2		
Length	5	m	Length	0.8	m
BWL	0.3	m	Chord - root	0.12	m
	1.12		Chord - tip	0.07	m
wing half beam	5	m	Thickness	0.008	m
hiking distance max	0.3	m	E	0.7	
mass helm	65	kg	Sail		
mass boat	45	kg	form factor	1.05	
C_{WP}	0.75		luff length	5.585	m
form factor	1.06		Area	8	m ²
Daggerboard			Other		
Length	1	m	Craft Mol	247.63	
Chord	0.12	m	helmCD	3	kgm ²
	0.00		foredeckCD	1.2	
Thickness	8	m	shroudDiam	0.8	
e	0.7		shroud length perp	0.003	m
Rudder			shroudCD	5	m
Length	0.9	m	wandNeutralAngle	1.2	
Chord	0.12	m	wandFoilRatio	70	deg
	0.00			0.15	
Thickness	8	m			
e	0.7				
Foil1					
Length	1	m			
Chord - root	0.12	m			
Chord - tip	0.07	m			
	0.00				
Thickness	8	m			
e	0.7				
set	2	deg			

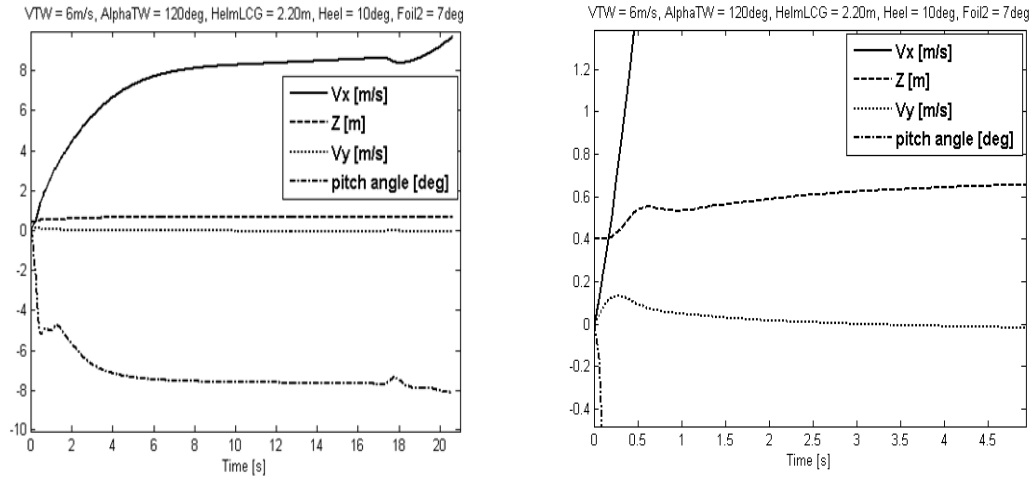
3.6 Validation

It has not been possible so far to conduct trials of an instrumented hydrofoil Moth in order to verify the predictions of the VPP. However, the results of the VPP regarding upwind sailing speeds (of approximately 12 knots in 15 knots of true wind) and high end speeds (approximately 25 knots downwind in 22 knots of true wind) are similar to those observed on the water. In addition, video records of the craft sailing and accelerating from standstill show that the time-scale over which the craft transition to foil-borne mode and approach top speed is comparable with that given by the VPP (eg. <4 s onto foil).

4 Results

Figure 6a gives an example of the predicted motion of the craft from the VPP. The first five seconds of this run are shown in detail in figure 6b to help identify the surge and sway motions. The craft can be seen to accelerate quickly from rest, adopting a small sway velocity as a result of the sail side force. The sway velocity decreases as the forward speed increases. Initially the craft pitches bow-down due to the moment generated by the sail drive force and the hydrodynamic resistive forces. This pitching moment is opposed by the shift in hull centre of buoyancy at about -5 degrees but this effect diminishes as the craft increases ride height to become fully foil-borne after about 5 seconds. In this example the craft continues to accelerate for about 20s, reaching a top speed in the region of 8.5 m/s before

apparently coming so close to the surface that the sway velocity increases significantly to account for the reduced wetted surface of the appendages. This ultimately leads to one of the foil tips encroaching the critical distance within the surface and the simulation is ended (the VPP equivalent of catastrophic foil ventilation.) In other simulations (figures 10 and 11) the craft can be seen to converge at a steady speed, in which case this is the speed taken as representative of that run.



(a) Simulation lasting approx 20s
Figure 6. Example of VPP Output

(b) Enlarged view of first 5 seconds

The particular variables under investigation are the aft foil setting (alpha) and longitudinal position of the weight of the helm (LCG). The range of values for LCG are from 1.6m, which represents the helm sitting as far forward as possible (by the mast), to 3.1m which represents the helm sitting as far back as possible (at the transom.) Aft foil angle is adjustable by a few degrees while sailing but can be set at any particular region by adjustment of the gantry. Initially results were gathered for aft foil angles in the region -9 to +10 degrees, and this showed that the region in which the aft foil is most effective is 6-10 degrees, which is where subsequent efforts were focussed.

In order to manage the case study, all variations of alpha and LCG were applied to just one arbitrary wind condition and heel angle: true wind speed of 6 m/s, true wind angle of 120 degrees, and a windward heel angle of 10 degrees. The results of this test matrix are given in table 2.

Table 2. Results matrix of simulations. Values are speed in m/s.

		Alpha											
		-9	-6	-3	0	3	4	5	6	7	8	9	10
LCG	1.6	3.81	4.29	4.80	5.75	7.10	7.55	7.96	8.28	8.34	8.37	0	0
	1.9	3.69	4.07	4.71	5.51	6.92	7.40	7.84	8.20	8.40	8.45	0	0
	2.2	3.56	3.88	4.37	5.19	8.32	7.21	7.69	8.09	0	0	0	0
	2.5	3.47	3.73	4.11	4.75	0	7.00	7.40	7.95	8.09	0	8.35	0
	2.8	3.37	3.58	3.86	4.34	0	0	7.24	8.01	8.18	0	8.34	0
	3.1	3.27	3.43	3.62	3.92	0	0	7.13	8.40	8.50	8.68	8.33	8.00

It can be seen from the table that there are four distinct regions. On the left the configurations which failed to achieve full foiling because the aft foil angle is simply too low. Here the speed is limited to 3 or 4 m/s and an example ($LCG = 2.5$, $aft\ foil = 0$) can be seen in figure 7. The craft initially pitches bow down due to the moments from sail force and resistive forces but this pitch angle is opposed by the longitudinal movement of the centre of buoyancy of the hull (which remains in the water) and the craft settles at a pitch angle of about -0.5 degrees.

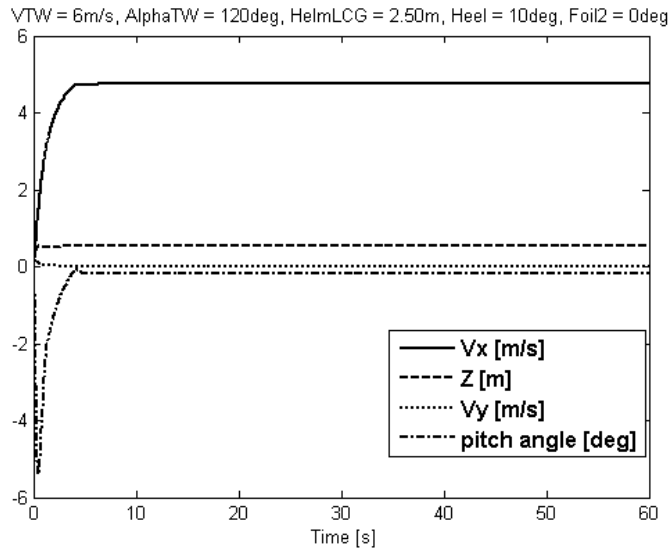


Figure 7. Not enough lift from aft foil to promote foiling and consequent low speed.

The next region of the test matrix is highlighted by the '0' entries in the bottom left. These signify that the craft was unstable and did not converge to a steady motion without 'crashing'. In the bottom left region are low aft foil angles and high LCG values, which forces a relatively bow up condition. The craft is able to attain a fully foiling state but the wand is not able to remove enough lift from the forward foil and this ultimately breaks the surface. This is a common occurrence for novice 'foilers' who sit too far back in the boat. Figure 8 shows an example.

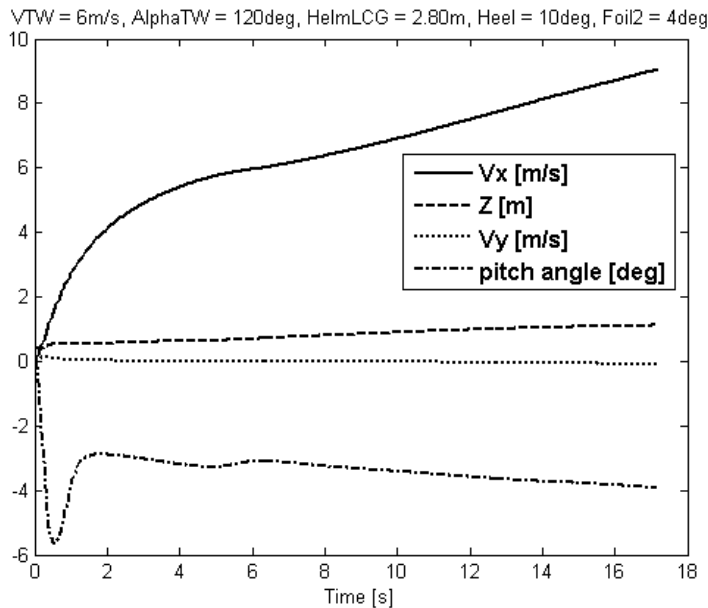


Figure 8. Helm too far aft or not enough lift from aft foil.

In the opposite corner of the test matrix, again highlighted by the '0' entries, the opposite occurs. In this region (high aft foil angles and low LCG values) the craft is forced to adopt a bow-down orientation as the excessive lift from the aft foil produces a trimming moment that is not sufficiently balanced by the helm's weight. The aft foil ultimately breaks the surface. Figure 9 shows an example where the craft accelerates over about 4 seconds into a catastrophic pitch pole – a frustrating and tedious experience!

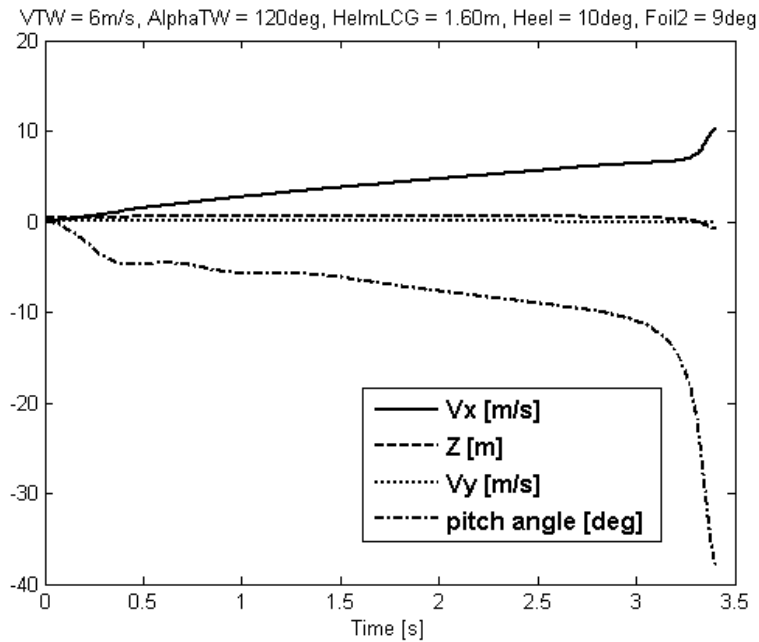


Figure 9. Helm too far forward or too much lift from aft foil.

The middle region of the table is of greatest interest because it indicates where the set-up is both fast and stable. A typical example of this is shown in figure 10 where the craft attains a top speed of just over 8m/s. Significantly this region of the table shows that for lower aft foil angles the craft speed increases as the helm moves forward (reducing LCG), and for higher aft foil angles the craft speed increases as the helm moves aft (increasing LCG.) The limit can be seen by the '0' entry at LCG = 2.2m, alpha = 7 deg, when the system achieves such a high speed that it simply generates too much lift. This is the case of figure 6a.

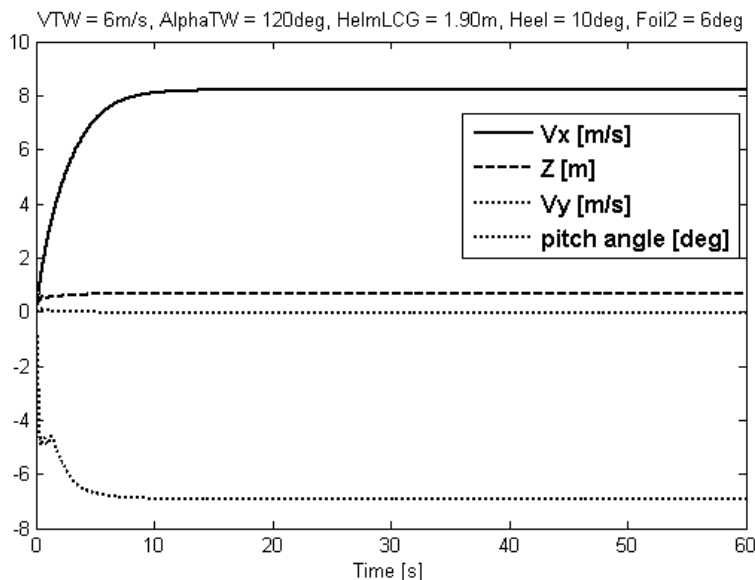


Figure 10. Fast and stable foiling.

4.1 Analysis

The data clearly indicates that the highest speeds are attained when the weight of the helm and craft is supported by the combination of aft foil and forward foil, and that positioning the weight solely over one of them is less efficient. This is due to the reduction in total induced drag when the weight is supported by lift from both foils rather than just one of them, due to the squared power relationship between lift and induced drag (8). In the particular case examined it appears that higher speeds could have been achieved had less total lift been

generated (the case of figure 6) which suggests that an optimum set-up for the conditions would use less built in angle of attack on foil 1 (currently 2 degrees), a shorter wand or smaller 'wand neutral angle.'

5 Discussion

In addition to the reduction in total induced drag observed making more use of the aft foil, there are secondary benefits to this set-up. With increasing aft foil angle to support the moment due to increasing helm LCG, the craft adopts an increasingly bow-down orientation which is interpreted by the wand sensor in the same way as an increase in ride-height (since the wand rotates relative to the craft), and the action of the control system is to reduce the lift on the forward foil. This cycle results in decreased angle of attack on the foils and means that the control system can be set more aggressively relative to a bow-up condition. This in turn is beneficial because for the same change in ride-height, the wand moves through a larger angle the closer it is to vertical. This gives a tighter control at the foils by effectively increasing the ratio of change in foil angle with change in ride-height. In turn this reduces the impact of pitch variations on flap control relative to height variations.

The feature of the control system of decreasing lift with decreasing pitch angle, and vice versa, is destabilising in pitch, and therefore reducing the impact of pitch variations on flap control is favourable. Tighter control could also be achieved by reducing the wand length, which with the correct systems, should be possible to implement whilst sailing.

The aft-wards movement of LCG directly reduces the pitch-stability of the craft by decreasing the moment arm over which the aft foil can exert restoring moment for small changes in pitch (against positive feedback from the forward foil.) This effect was not observed in these simulations (though it may be partly responsible for the consequences of figure 9) and a calculation suggests that the helm needs to be positioned virtually over the aft foil for it to become significant.

6 Conclusions

A new Velocity Prediction Program has been developed to examine the impact of set-up and sailing styles on the performance of hydrofoil-equipped dinghies. The VPP gives a more realistic simulation of the craft than previous work by including windward heel angle, the wand-foil control system, positioning of the helm and aft foil settings, which are all critical elements of sailing the International Moth. The VPP predicts the motion of the craft and is therefore useful for identifying unstable set-ups as well as stable configurations.

A case study for the Moth shows that utilising the aft foil to generate a proportion of the lift rather than just as a control surface minimises the total induced drag and therefore increases top speed. This requires that the sailor sits further back in the craft and the craft adopts a bow down orientation. The boat set-up for the case study appears not to be optimal because it is possible for the craft to generate too much total lift at the highest speeds, despite being stable and well balanced indicating that a set-up adjustment is required.

6.1 Future work

A common use for VPPs is to allow the generation of polar diagrams that indicate the maximum speed of a yacht for any given true wind strength and angle. It is possible to use the new Moth VPP, in conjunction with an optimisation procedure over variables including windward heel angle, aft foil setting, LCG, and wand settings, to produce a polar diagram for the Moth and associated optimum settings for each wind condition as predicted by the VPP. The large number of variables involved and function calls makes this a computationally intensive task but could give sailors not only target boat speeds for upwind and downwind legs, but also indicate the set-ups required to achieve those boat speeds and give an understanding of how variations to the set-up affects boat speeds. Most useful would be an analysis of the conditions for maximum velocity made good (VMG) in upwind and downwind sailing as the usual race course comprises only upwind and downwind legs.

Specific case studies of interest are the relationships between windward heel angle, and ride height (due to wand settings) on boat speed (at or near optimal angles for maximum upwind and downwind VMG) and the VPP can be used to undertake this.

At times there are differing requirements for sailing style between take-off and steady speed sailing such as moving body weight aft to assist take off before returning to the steady LCG condition. This option is incorporated in the VPP, although it was not used for these results and it would be of interest to sailors to understand how movement of body weight can be used to maximise the acceleration to top speed. The VPP could therefore be used to look at the dynamic performance of the craft as they accelerate at starts or out of tacks and gybes although it would be desirable to adopt a more comprehensive added mass approach. Extension of the VPP for this purpose would also include the effects of small course changes ('heating it up') and pumping of the sail for temporary larger sail force to overcome the drag hump near take-off.

Finally the VPP also offers great potential for examining the control system – particularly in waves, where the water surface could be represented by any function rather than a flat surface and the resulting craft behaviour, based on the wand tracking the surface and the foils proximity to it could be examined.

References

1. Findlay, M.W. and S.R. Turnock, *Investigation of the effects of hydrofoil set-up on the performance of an international moth dinghy using a dynamic VPP*, in *Innovation in High Performance Sailing Yachts*, 2008, London, UK, Royal Institution of Naval Architects, Lorient, France. p. 43-56.
2. <http://www.moth-sailing.org/imca/faces/WorldChampions.jsp>. *World Champions*. [webpage] 2008 [cited 2008 01-10].
3. <http://www.int-moth.org.uk/NewPages/Vavavoom2.htm>. *Speed Matters*. [webpage] 2008 31-8-08 [cited 2008 01-10].
4. <http://www.int-moth.org.uk/NewPages/Design2.htm> and A. May. *Foil ventilation*. 2008 16-03-08 [cited 2008 01-10].
5. http://www.fastacraft.com/moth_hulls_prowler.html and J. Illet. *Fastacraft International Moth Hydrofoils*. [cited 2008 01-10].
6. Wellicome, J.F., *Aerodynamics of Sails*, in *Sailing yacht design: theory*, A. Claughton, J. Wellicome, and R. Sheno, Editors. 1998, Addison Wesley Longman Limited.
7. http://www.moth-sailing.org/worlds/2008_uk.xml. *2008 World Championships Results*. 2008 [cited 2008 01-10].
8. Abbott, I. and A. Von Doenhoff, *Theory of Wing Sections*. 1959: Dover Publications.
9. Keuning, J.A., *The hydrodynamics of hull, keel and rudder*, in *Sailing yacht design: theory*, A. Claughton, J. Wellicome, and R. Sheno, Editors. 1998, Addison Wesley Longman Limited.
10. Chapman, R.B., *Spray Drag of Surface Piercing Struts*, in *AIAA/SNAME/USN Advanced Marine Vehicles Meeting*: . 1972: Annapolis, MD.
11. Chen, 1960. *Optimum Wing-Strut Systems for High Speed Operation Near a Free Surface*.
12. Martin, M., *The Stability Derivatives of a Hydrofoil Boat*, in *Hydronautics Incorporated, Technical Report 001-10*. 1963.
13. Hoerner, S., *Fluid-dynamic drag*. 1958: Hoerner.

Session 5

Suzanne de Vos-Effting & René van Gijlswijk

A life cycle based Eco design consideration for the Rainbow Warrior III

Suzanne de Vos-Effting. René van Gijlswijk. TNO Built Environment and Geosciences

1 Introduction

Greenpeace has asked Gerard Dijkstra & Partners (hereafter 'GDNP') to design a new ship for Greenpeace. During the design of the new Greenpeace ship TNO is to provide advice on the best choice of options from an environmental point of view. This advice is based on the results of environmental life cycle assessment calculations.

The environmental impact of options is compared over the full life cycle of the ship:

- influence on **production** of raw materials, production processes, including upstream processes (the production processes up to mining of raw materials)
- influence on the **use phase**: energy consumption (diesel) and maintenance (antifouling, epoxy coating, etc.)
- influence on **end-of-life**: at the end of the life of the ship it will be dismantled and some materials will be reused

The impact on the environment has been calculated using EcoScan¹ software and the results are expressed in Eco-indicator 99 points². The Eco-indicators have been developed for designers by commission of the Dutch Ministry of VROM (Housing, Spatial Planning and the Environment) and in cooperation with European scientists. This method is recommended and used by designers all over the world (for example at Philips, BiC, the furniture industry) and supported by governmental organisations (for example in the Netherlands, the Ministry of VROM, SenterNovem), Universities, Universities of Professional Education etc. The Eco-indicator 99 method and life cycle assessment calculation is described in Annex A.

This report discusses several topics in relation to the environment that have been considered during the project. These topics are:

- comparison of a steel versus an aluminium hull
- comparison of a ship with sail propulsion or engine propulsion
- use of anti-fouling paint (details not included in this paper)
- measures for emission reductions (details not included in this paper)

¹ www.ecoscan.nl Quickscan tool for Eco-design developed by TNO

² The Eco-indicator 99. A damage-oriented method for Life Cycle Impact Assessment. Manual for Designers. Ministry of Housing, Spatial Planning and the Environment, October 2000.

2 Summary of results

2.1 Steel hull versus aluminium hull

Compared to a steel hull, an aluminium hull has a lower environmental impact over the life cycle of the vessel. This is the net result of a small increased impact in the production/disposal phase, and a slightly reduced impact in the use phase (due to a lower weight of the ship and resulting reductions in fuel consumption when sailing with engine assistance).

Looking at the full life cycle of the ship, including all impacts for production, use and end-of-life, the difference caused by choosing aluminium instead of steel is small: 1.21% less impact for a ship with an aluminium hull over the full life cycle compared to a ship with a steel hull. The hull contributes little to the environmental impact of the ship. Most impact comes from using the engine in the use phase, with limited influence from the hull weight on fuel consumption.

Considering global warming only, a steel hull is preferred. A ship with an aluminium hull causes more CO₂ emissions over the full life cycle of the ship compared to a ship with a steel hull.

2.2 Sail propulsion versus engine propulsion

The new build has been designed as a sailing ship. A comparison has been made in order to get an idea of the reduction of the environmental impact by selecting a sailing ship instead of a ship with an engine. This shows that a ship with an engine of the same dimensions, same engine installation and operational profile, would have a 61% higher environmental impact compared to the sailing ship.

The environmental impact of the production and maintenance of sails is very small compared to the environmental impact of the (saved) fuel.

2.3 Antifouling

Under the pressure of stricter legislation progress has been made in the development of anti-fouling coatings that do not leach toxic substances, such as fouling release coatings. This type of coating has been applied for some time on Greenpeace ships. The new generation Fouling Release Coating (Intersleek 900) will be applied to the new build Greenpeace ship. Compared to toxic containing anti-fouling coatings, fouling release coatings have the following environmental advantages:

- no release to water of toxic substances
- as a result of a longer lifetime the coating needs to be applied less frequently. The frequency of coating application does also depend on the maintenance requirements of the ship owner. Claims made by the manufacturer that the disadvantages of silicone fouling release coatings have been overcome are promising³, but these new paints need to prove themselves in practice.

In the use phase attention needs to be paid to repair (as a result of mechanical damage) and to cleaning of the underwater hull - by high-speed sailing, or by diver or robot cleaning. The

³ According to the manufacturer, this new generation Fouling Release Coating has less overspray and less abrasion resistance, and can be used on vessels that have a lower speed (10 knots) and are inactive for longer periods of time. Source: http://www.international-marine.com/include/Intersleek900_Brochure.pdf

cleaning frequency and method are related strongly to the desired use pattern (weeks without sailing). TNO recommends that a cleaning protocol for the new build should be prepared.

In the future, when other fouling release coatings may be selected, attention needs to be paid to additives such as silicon oil, as these may leach out of the coating. Leaching is undesirable as the components may cause environmental damage.

2.4 Measures for emission reduction

The new build will be equipped with a wet scrubber (Ecosilencer). This emission reduction measure will result in the reduction of sulphur dioxide, particulate matter (dust) and a small amount of NO_x. As far as particulate matter is concerned, independent studies show that wet scrubbers are not as effective at reducing small particles - mainly larger particles are removed from air emissions. As a result, due to the increased fuel consumption (2.5%) the net environmental effect of the wet scrubber, as calculated using Eco-indicator 99, is a small increase in environmental impact. The increased fuel production and consumption causes more environmental damage compared to the benefit gained from decreased emissions.

Other emission reduction measures can be taken to improve the impact of emission reduction. Soot filters in combination with a de-NO_x installation will reduce the environmental impact by 32% over the life cycle of the ship, if all engines are equipped with this reduction technology.

Soot filters dedicated to the reduction of small particles are not yet fully developed for marine application. The technology has not yet been demonstrated to be robust over a period of several years. However, it can be expected that possible problems will be tackled in the next few years as a result of coming legislation, and besides this, cost reduction and efficiency improvements might be achieved. It is recommended to wait until soot filters are fully developed and to facilitate the new build for retrofit, e.g. by reserving space required for soot filters and/or buying engines with an engine-management system that is already designed for soot filtration.

3 Steel hull versus an Aluminium hull

3.1 Differences over the life cycle

The hull of the ship can be made out of steel or out of aluminium. The steel hull is taken as reference for the comparison. The differences resulting from choosing aluminium instead of steel are shown in Table 1. Aluminium is produced in a different way to steel, and also has a different impact in the end-of life phase. When the ship is no longer used, it will be dismantled and valuable materials, such as metal, will be recycled. Recycling reduces the need for the production of new material (i.e. mining is not necessary) and the saved environmental impact is expressed as a bonus. As the production of aluminium gives more impact compared to the production of steel, the bonus for recycling aluminium will be higher compared to the bonus for recycling steel. The aluminium hull weighs less and needs more insulation and less paint. Due to the lower weight, less diesel fuel is consumed for propulsion by diesel engine (see GDNP report on Hull Material study⁴).

Table 1 Differences resulting from material choice for hull

		Steel hull	Aluminium hull	Difference of aluminium compared to steel
Production and end-of-life	Hull	236,520 kg	191,250 kg	-19%
	Insulation	18,000 kg	22,000 kg	+22%
	Paint	6,750 kg	4,725 kg	-30%
Use phase: fuel consumption	Economic sailing	63 tons fuel /year	61 tons fuel /year	-3.2%
	Max. speed sailing	120 tons fuel /year	116 tons fuel /year	-3.2%

3.2 Results

Figure 1 shows the environmental impact of the ship. More Eco-indicator points [Pt] mean more environmental impact (indicated in red). 'Negative' points represent an environmental bonus (in green). As a reference, 1000 Eco-indicator points represent the environmental impact of 1 European citizen during one year. More references of the environmental impact expressed in Eco-indicator points can be found in the Annex (Table 5).

⁴ Gerard Dijkstra & Partners. Hull Material Study. Amsterdam, December 2006. By commission of Stichting Marine Services / Greenpeace International

Environmental impact for production, 30 years use, and disposal in 1000 Eco-indicator 99 Points

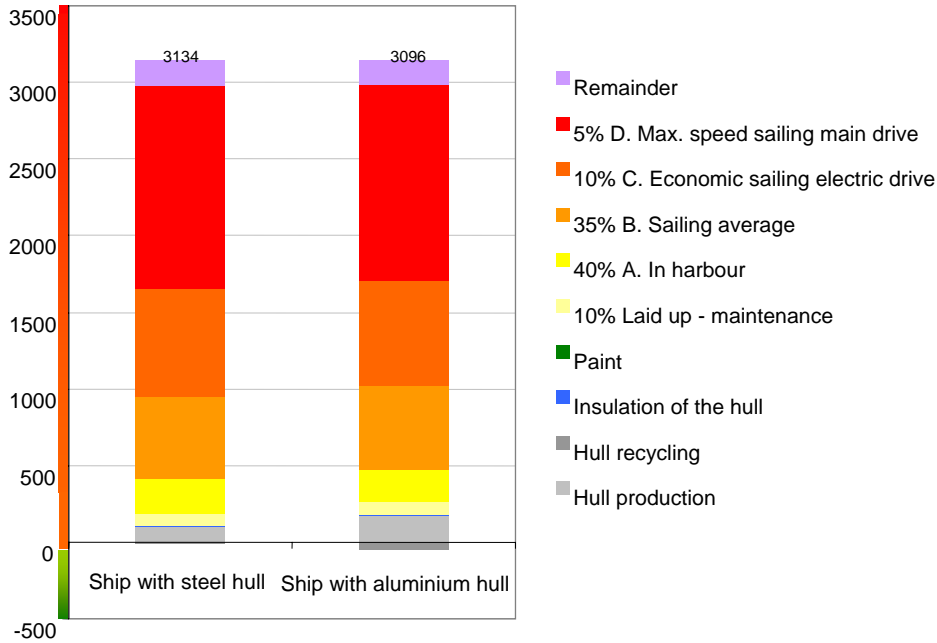


Figure 1 Environmental impact for the production, 30 years use and disposal expressed in Eco-indicator 99 points of a ship with a steel hull and a ship with an aluminium hull

Table 2 Environmental impact for the production, 30 years use and disposal expressed in 1000 Eco-indicator 99 points of a ship with a steel hull and a ship with an aluminium hull

	Ship with steel hull [1000 Eco-indicator Pt]	Ship with aluminium hull [1000 Eco-indicator Pt]	Difference of aluminium compared to steel	
			[1000 Eco-indicator Pt]	Compared to total of steel ship [%]
Hull production	104	171	67	2.14%
Hull recycling	-8	-48	-40	-1.28%
Insulation of the hull	6	7	1	0.04%
Paint	3	2	-1	-0.03%
10% Laid up - maintenance	78	78	0	0.00%
40% A. In harbour ⁵	218	218	0	0.00%
35% B. Sailing average	545	545	0	0.00%
10% C. Economic sailing electric drive	700	678	-22	-0.72%
5% D. Max. speed sailing main drive	1327	1285	-42	-1.34%
Remainder	161	160	-1	-0.02%
Total	3134	3096	-38	-1.21%

⁵ Electricity is needed when the ship is in harbour. The environmental impact is calculated for the scenario where shore power is used 80% of the time, and electricity is generated with the engines on board the ship 20% of the time. The environmental impact increases if the ship is producing more of its own electricity in harbour (as the environmental profile of shore power is more favourable).

As the hull contributes relatively little to the overall environmental impact of the ship, a closer look will be taken at the differences resulting from the hull material choice, leaving out all impacts that are the same for a ship with a steel or aluminium hull. The results focussing on the differences are displayed in Figure 2 and in Table 2.

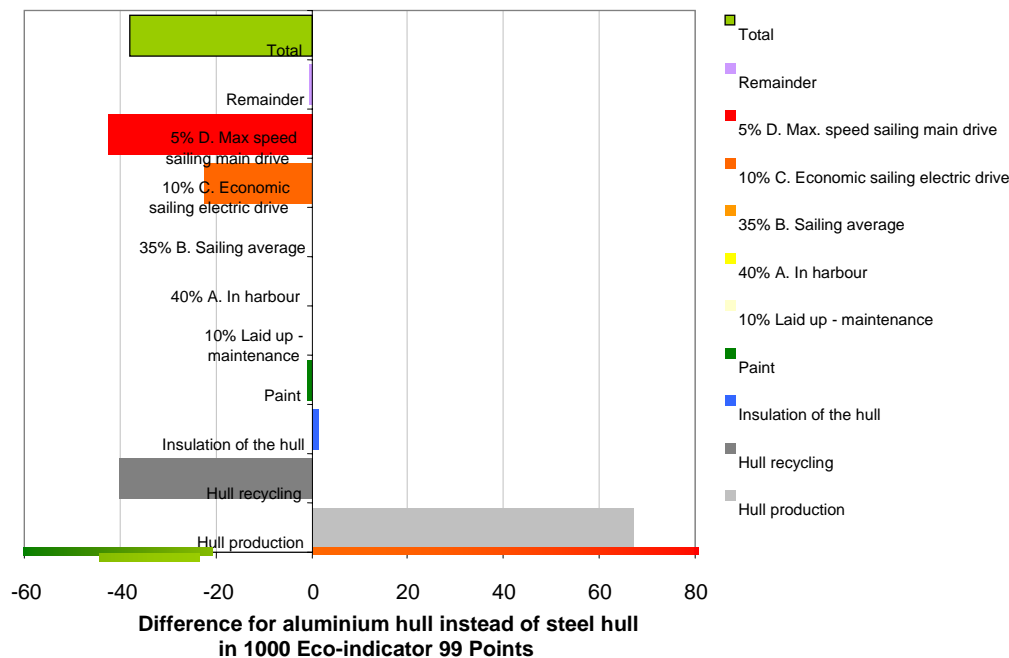


Figure 2 Difference in environmental impact as a result of choosing an aluminium hull instead of a steel hull, expressed in Eco-indicator points

3.3 Discussion of results

Compared to the steel hull an aluminium hull has a lower impact over the life cycle. There is only a small difference between the environmental impact of a ship with a steel hull and a ship with an aluminium hull: over the life cycle there is only a difference of 1.2% (3,134,000 Pt for the life cycle of a ship with a steel hull versus 3,096,000 Pt for a ship with an aluminium hull). This conclusion holds for other use patterns of the ship: more sailing increases the advantage of an aluminium hull. If the ship was sailing using the engine all the time (never on sail, never in the harbour) the advantage of aluminium increases up to 3% compared to a ship with a steel hull. The steel hull would only have an advantage compared to aluminium when the sailing time using the engine is reduced by a factor of 2 (2.5% max. speed and 5% economic sailing).

The hull production and recycling, and the other differences resulting from choosing aluminium instead of steel, contribute little compared to the other impacts that are not affected by the material choice for the hull. The impact of the ship is dominated by the fuel consumption for sailing and other fuel consumption. The fuel consumption in the use phase contributes 91.5% (2,868,000 Eco-indicator 99 Pt) to the total life cycle impact of the steel ship (3,134,000 Pt) and for aluminium the fuel consumption in the use phase contributes 90.5%.

The reduction in the environmental impact when choosing an aluminium hull instead of a steel hull is a result of:

- **Increased impact of production/disposal.** This difference is caused by an increase of 67,000 Pt for production (see the light grey bar for hull production in Figure 2). Although

the hull weighs 19% less compared to steel, the environmental impact of the production of aluminium is a lot higher per kg compared to steel. On the other hand, recycling of aluminium gives a larger bonus (– 40,000 Pt, see Figure 2) compared to steel. Recycling saves metal production and thus saves more impact for aluminium. The net difference resulting from production and disposal is $(67,000 - 40,000) = 27,000$ more Eco-indicator 99 points for aluminium compared to steel; i.e. producing an aluminium hull has more environmental impact.

- **Decreased impact in the use phase** due to saving of 3.2% fuel when sailing on the engine as a result of reduced weight of an aluminium hull compared to a steel hull. In the use phase 63,000 Eco-indicator Pt are saved (-22,000 Pt for economic sailing and -41,000 Pt for maximum speed) compared to the fuel consumption for the heavier steel hull.

A ship with an aluminium hull needs 40% less paint over the full life cycle of the ship as the function of the paint on an aluminium hull is mainly decoration (instead of protection). The decrease in environmental impact is more or less compensated by the increased impact related to more insulation, but both impacts are very small.

Beside a calculation using Eco-indicator 99, covering many environmental aspects, an analysis has also been made for the global warming potential. Looking at global warming only, a steel hull is preferred. A ship with an aluminium hull contributes more to CO₂ emissions over the full life cycle compared to a ship with a steel hull.

4 Sail propulsion versus motor propulsion

In an early stage it was decided that the new build Greenpeace ship had to be a sailing ship. Using sails saves a lot of fuel as the energy for transport is provided by the wind. An environmental comparison of the new build with a similar ship with motor propulsion is made in this chapter. For this comparison, the production of the sails⁶ has been subtracted, and the time of economic sailing has been increased (see Table 3). The results of the environmental impact are shown in Figure 3 and Table 4.

Table 3 Use pattern of ship with sails and fictive use pattern for ship without sails.

Activity	Ship with sail propulsion		Ship with motor propulsion	
	Hours /year	Percentage	Hours /year	Percentage
Laid up maintenance	876	10%	876	10%
A. In harbour	3504	40%	3.504	40%
D. Sailing	3066	35%	0	0%
C. Economic sailing	876	10%	3942	45%
D. Max. speed	438	5%	438	5%
Total	8760	100%	8760	100%

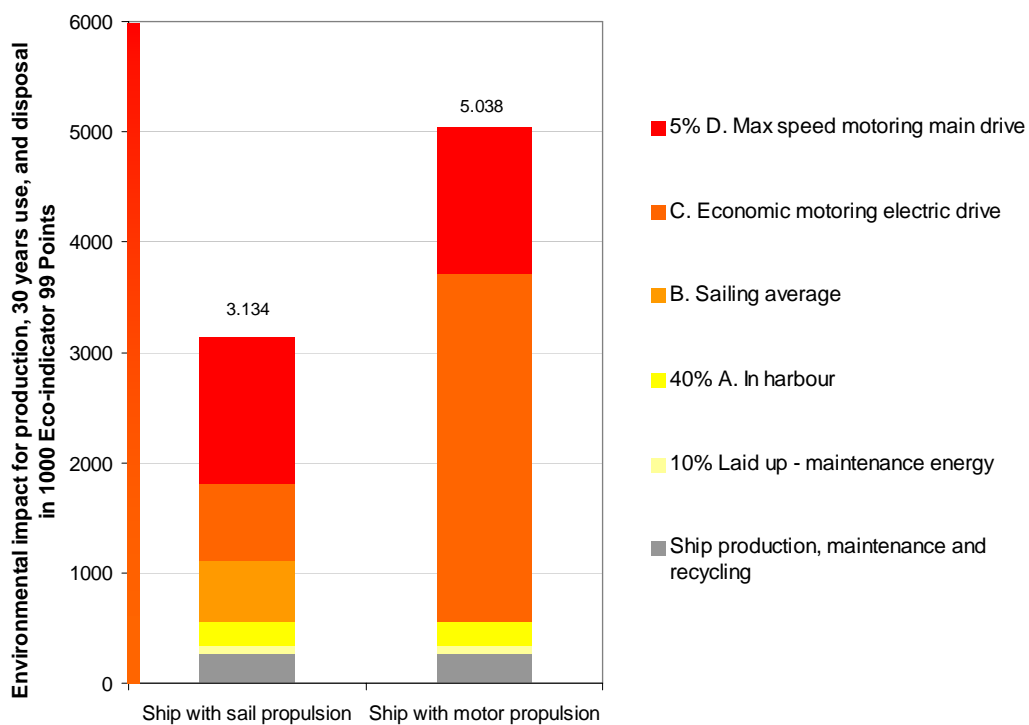


Figure 3 Environmental impact of the production, 30 years use and disposal expressed in Eco-indicator 99 points of a ship with sail propulsion, and a ship with motor propulsion

⁶ Production of the sails includes the sails for replacement during the use of the ship (maintenance)

Table 4 Environmental impact of the production, 30 years use and disposal expressed in 1000 Eco-indicator 99 points of a ship with sail propulsion and a ship with motor propulsion

	Ship with sail propulsion [1000 Eco-indicator Pt]	Ship with motor propulsion [1000 Eco-indicator Pt]	Difference between sail and motor propulsion	
			[1000 Eco-indicator Pt]	Compared to ship with sail propulsion [% of Total]
Ship production, maintenance and recycling	266	263	-3	0%
10% Laid up - maintenance energy	78	78	0	0%
40% A. In harbour	218	218	0	0%
35% B. Sailing average	545	0	-545	-17%
10% C. Economic sailing electric drive	700	3152	2452	78%
5% D. Max. speed sailing main drive	1327	1327	0	0%
Total	3134	5038	1904	61%

4.1 Discussion of the results

A comparable ship with motor propulsion instead of sail propulsion will have 61% more environmental impact. The environmental impact of production and maintenance of sails is very small (three thousand Eco-indicator points) compared to the environmental impact of the (saved) fuel).

The same conclusion can be drawn when looking at the global warming potential only: a ship without sails would have caused 61% more CO₂ emissions over the full life cycle compared to a ship with sails.

A Annex: Eco-indicator 99

The environmental impact of the life cycle of a ship is calculated in two steps.

Data is collected on resource consumptions, emissions to air, water and soil, and waste (including processing of waste) for the ship production, use and end-of life. A large database is used for production of materials, energy etc. for this first step.

The pressure on the environment is calculated in the second step, using the Eco-indicator 99 impact assessment method⁷. For example, how each toxic emission moves through the environment, and what the uptake is by humans, is calculated in Eco-indicator 99. The uptake results in a health effect.

⁷ The Eco-indicator 99. A damage-oriented method for Life Cycle Impact Assessment. Manual for Designers. Ministry of Housing, Spatial Planning and the Environment, October 2000.

Environment is defined by three types of damages in Eco-indicator 99:

- damage to human health expressed as the number of life years lost and the number of years lived disabled due to environmental causes. The effects included here are climate change, ozone layer depletion, carcinogenic effects, respiratory effects and ionising (nuclear) radiation
- ecosystem quality: effects on the diversity of species, especially on vascular plants and lower organisms. The effects included are ecotoxicity, land-use, acidification and eutrophication
- resources: the surplus energy needed in the future to extract lower quality mineral and fossil resources

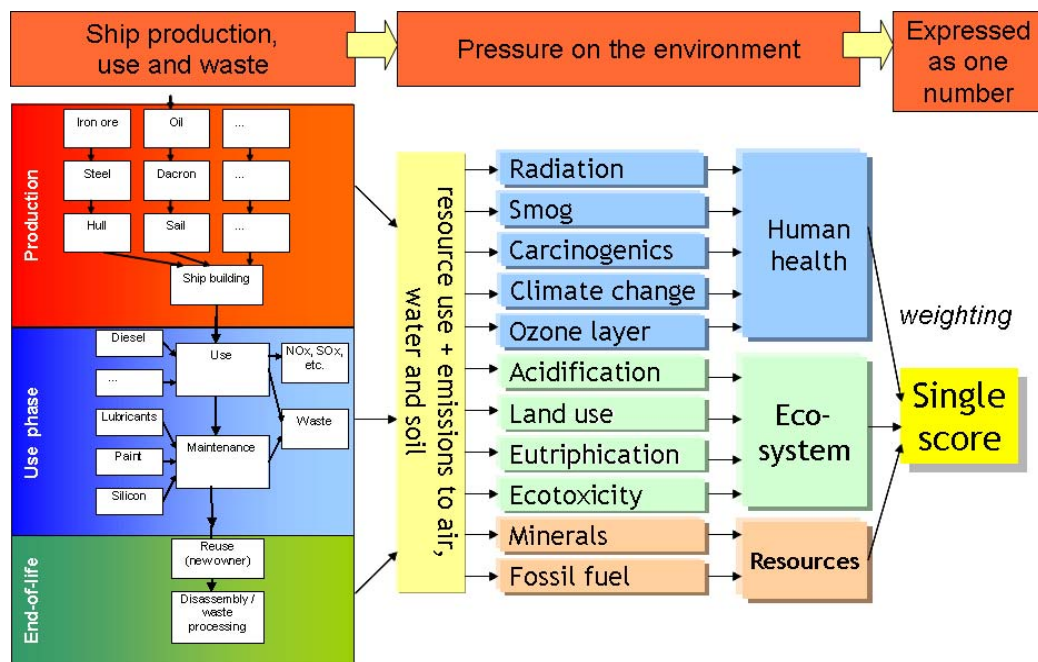


Figure 4 Schematic overview of calculation of Eco-indicator points

Four steps are needed for the calculation of the damage (pressure on the environment):

1. **Fate analysis:** when a chemical substance is released, it finds its way through the environmental compartments of the air, water and soil. Where the substances will go and how long they will stay depends on the properties of the substance and of the compartments. A soluble substance will be collected in the water compartment while a substance that will easily bind to organic particles may end up in specific types of soil. Another aspect is the degradability as most organic substances have a limited lifetime. The transfer between compartments and the degradation of substances is modelled in fate-analysis models. The concentrations in the air, water and soil is calculated as a result.
2. **Exposure:** based on calculated concentrations it is determined how much of a substance is taken in by humans, plants and other life forms.
3. **Effect analysis:** once the exposure is known, diseases (frequency and duration) and other effects are predicted.
4. **Damage analysis:** the predicted disease is expressed in damage units. For instance, if a certain exposure results in additional cases of cancer, the average age that people will get this type of cancer, the duration of the illness and the life years lost are determined.

Other damage models are used for land use and resource depletion. The effects of land use are based on field observations on the diversity of species for different uses of land. For resource depletion the energy needed for extraction is related to ore grade (for mineral resources) and to the quality of the fossil resources. Models for declining resource quality in the future are linked to the energy for extraction, to calculate the additional energy required in future to extract the same amount of resource.

The damage analysis results in three scores: one for human health, one for ecosystem quality and one for resources. The three scores are totalled to give one value, using weightings determined by a panel of environmental specialists:

- 40% to human health
- 40% to ecosystem quality
- 20% to depletion of resources

The result is a dimensionless score: Eco-indicator Points. Of course, the chosen weighting is subjective. The most used, and therefore accepted, weighting set has been applied here.

It is important to pay attention to the uncertainties in the methodology that is used to calculate Eco-indicators. There are two types of uncertainties.

1. Uncertainties about the **correctness of the models** used. This includes value choices such as the time horizon in the damage model, and the question whether an effect should be included even if the scientific evidence is incomplete. Eco-indicator 99 is available in three different conceptual models regarding the time horizon, the inclusion of effects, and the weighting of the three types of damage. The default (and most used) method in which there is a balance between the short term and the long term, and in which effects are included based on consensus among scientists, has been selected here.
2. **Data uncertainties**. These uncertainties refer to difficulties in measuring or predicting the environmental effects. These uncertainties are expressed in ranges and can be included in the calculation of results by applying a statistical Monte Carlo analysis. This uncertainty analysis will not be carried out in this project as resources are limited. The focus is on design options instead of LCA methodology.

The life cycle calculation results in Eco-indicator 99 points. More points represent a higher environmental impact. As points are a rather abstract result Table 5 shows the environmental impact of several activities expressed in Eco-indicator 99 points which can be used to form an idea about the magnitude of Eco-indicator 99 points. These references can also be used to compare the environmental impact of activities: for example, a household's annual laundry causes the same environmental impact as driving 2100 km in a car.

Table 5 Environmental impact of activities expressed in Eco-indicator 99 points

Activity	Environmental impact expressed in Eco-indicator points [Pt]
Annual environmental impact of one European citizen during one year	1000 Pt
Electricity consumption (for all household activities) per household per year (3350 kWh)	94 Pt
Electricity consumption for laundry (washing and drying) per household per year (736 kWh)	21 Pt
1000 km driving in a private car	10 Pt
Production and use of 1 barrel of oil as fuel, including emissions (159 litres of oil)	35 Pt

Session 6

Evert –Jan Foeth

Decreasing frictional resistance by air lubrication

E.J. Foeth

Maritime Research Institute of the Netherlands (MARIN)

Abstract

The decrease of ship resistance is one of the most effective way to reduce operating costs and CO₂ production. The wave making resistance and form drag can be reduced by optimizing the hull form, but the frictional drag remains proportional to the wetted surface. The use of air as a lubricant in order to reduce that frictional drag is an active research topic and three techniques are identified: injecting air bubbles in the boundary layer, the use of air films along the bottom plating, and using air cavities in the ship's bottom. These approaches are the research topic for the Dutch joint-research project PELS and the EU project SMOOTH, both of which have the goal of not only predicting energy savings using numerical models and model tests, but proving it using full-scale demonstrator ships adapted for air lubrication. Although decreases in frictional resistance of nearly 20% have been obtained on model-scale ships, experience shows that the implementation of air lubrication can also easily increase the resistance of a ship.

Introduction

The increase in fuel costs and looming restrictions on carbon dioxide emissions are driving the ship owner into reducing the ship resistance and required installed power. The propulsive efficiency using the propeller is often good and it is difficult to gain a few percent. Thrust augmenting devices such as high-efficiency rudders and kites will undoubtedly be prevalent in the future. Reducing the required propulsive thrust is a more direct means to lower operating costs and can even be used in conjunction with thrust augmenters to further sharpen the competitive edge of the ship owner. The main components of ship resistance consist of resistance due to wave drag, pressure drag, and frictional drag. The wave and pressure (form) drag can be optimized by carefully manipulating the lines of the vessel, but frictional resistance remains proportional to the wetted surface and the square of the ship speed. As this resistance drag is by far the largest resistance component in normal operating speed ranges, any reduction of this component will have an immediate and favorable influence on the performance of the vessel. Such reductions can be achieved by compliant coatings, ribblets, polishing the surface, or polymer injection; measures that are not very practical for ships. A promising technique to obtain lower frictional resistance is using air as a lubricant to reduce the wetted surface of the ship.

Three distinct approaches are identified: the injection of bubbles, air films, and air cavity ships. The first technique, bubble injection, is a direct means to reduce the friction of the ship by positive interaction with the boundary layer. When the bubbles are within 300 viscous wall units—defined as $l = \nu/u_0^*$ and u_0^* the friction velocity of the fully-wetted flow $u_0^* = \sqrt{\tau/\rho}$ —the effect of air lubrication can be measured in laboratory tests, indicating a strong dependence on the

boundary layer (Sanders et al., 2006). When the bubbles are farther away from the wall, no effect is measured. The use of air films is self-explanatory; the air film separates the water from the hull thus reducing friction. Air cavity ships are vessels that have a series of openings in the bottom where a free surface is formed. The downside of all three techniques is that it is surprisingly easy to increase, rather than to decrease, the resistance and that many aspects of the behavior of air in water are poorly understood. For example, the full-scale demonstrator vessel *Seiun Maru* showed a 2% decrease at only a limited speed range with an increase in required power over most of its speed range, notwithstanding huge resistance decreases tested at model scale.

The three approaches are the subject of two of MARIN's research projects, PELS (Project Energy-saving air-Lubricated Ships) and SMOOTH (Sustainable Methods for Optimal design and Operation of ships with air lubricated Hulls). PELS is a Dutch research consortium and SMOOTH is an EU-funded consortium both consisting of ship owners, ship yards, paint manufacturers, model basins, and universities. The main goal is not only to perform model experiments, but also to demonstrate the effect on full-scale ships. Simultaneously, MARIN is a partner in a PhD research project focusing on understanding the fundamental mechanisms of air lubrication together with the Laboratory of Hydro and Aerodynamics at the University of Delft and the Physics of Fluids department at the University of Twente.

Micro Bubbles

The application of micro bubbles is an often-named candidate for resistance reduction, as it ideally requires a small conversion of an existing ship hull and no resistance increase is experienced when the pump system fails. But there is some uncertainty on the size of what can be defined as a micro bubble. As the bubble increases in size, so does its tendency to deform in the shear and turbulent fluctuations of the flow (typically when their Weber numbers exceed unity) and it is no longer a micro-bubble. A distinction between bubble drag reduction and micro-bubble drag reduction is required. For the micro-bubbles, experiments with flat plates show a spectacular resistance decrease as large as 80%. This resistance decrease is thought to originate by favorable interaction with the boundary layer and not through the reduction of viscosity. In fact, viscosity increases by the injection of micro-bubbles. The production of these small and undeformable on a ship-wide scale is difficult and major scale effects are present.

The mechanisms by which friction is reduced is unclear. It can be simply a reduction in density, modifying turbulence or perhaps even by bubbles merging and splitting. At very low speeds, around 1m/s, bubbles with a diameter of only a few viscous length scales of the flow can generate a 10% decrease in resistance at only 1 volume percent of air in the boundary layer (Olivieri et al., 2005, Park & Sung, 2005). At more realistic flow speeds of 5m/s to 15m/s, this viscous length scale drops rapidly enforcing a small bubble that is difficult to produce in large quantities. Moriguchi & Kato (2002) used bubbles between 0.5mm and 2.5mm and measured up to a 40% decrease in resistance, but for air contents over 10%. Shen et al. (2005), using smaller bubbles between 0.03mm and 0.5mm, found a 20% drag reduction at an air content of 20%. No appreciable influence of bubble size was found.

Sanders et al. (2006) performed experiments with a very large flat plate over 10m in length with speeds up to 20m/s. This experiment allowed for tests at Reynolds numbers that were hitherto not obtainable at model scale with bubbles ranging from 0.1mm to 1.0mm. The experiments showed that the bubbles were pushed out of the boundary layer a few meters behind the air injectors, even when the bubbles were injected at the lower side of the plate. A nearly bubble-free liquid layer was formed near the wall and the effect of air lubrication almost vanished. It is hypothesized that the lift force experienced by a bubble in the boundary layer is more than sufficient to overcome the buoyancy of the bubble. This experiment indicates that a strong Reynolds-scale effect is present for model testing with bubble injection.

In order to increase our understanding of the behavior of bubbles in air layers, an extensive research program with Technical Universities of Delft and Twente has started. At the University of Twente, test will be performed with a Taylor-Couette setup, consisting of a thin water channel between two counter-rotating cylinders. This setup has the advantage that it allows for statistically stationary flow and accurate resistance measurements by means of the applied torque on the rotating drum. Moreover, the bubble distribution in this stationary case will be measured, and its effect on the overall torque will be theoretically analyzed. Research by van den Berg et al. (2005) showed that the resistance decreased only after exceeding a Reynolds number of nearly 1 million. At this point, the bubbles can no longer be considered undeformable. Kitagawa et al. (2005) found that bubbles deformed with a favorable orientation with respect to the flow, reducing turbulent stress as the flow field around the bubble is more isotropic. However, other mechanisms are possible, such as compression (Lo et al. 2006) or bubble splitting (Meng & Uhlman 1998). At the University of Delft, the drag reduction will be studied in a non-stationary flow over a flat plate. The stability of the air film, the breaking up in bubbles and the injection of bubbles will be visualized with high-speed cameras and measured by means of Particle Imaging Velocimetry. The drag reduction itself will be measured with existing and experimental shear stress sensors.

The advanced inland shipping concept of the Futura carrier is the topic of research on the EU-funded program SMOOTH, displayed in Figure 1. This vessel, christened the *Till Deymann*, is fitted with an air injection system. It is propelled by four thrusters, two at the stern and one in a tunnel in each of the two bows of this semi twin-hull bow. These forward thrusters give the *Till Deymann* exceptional maneuvering characteristics, but an increase in skin friction at the tunnel due to the high speeds induced by the propeller. Local air injection is therefore a viable option to improve performance,



Figure 1 The Futura carrier *Till-Deymann*, a full-scale test ship for bubble injection, showing its typical semi twin-hull bow.

Air layers

The air layer concept can be seen as a combination of micro bubbles techniques and air cavity ships. An air stream is injected into the bottom region of a ship and an air film forms. This air layer is subjected to influences as turbulence and the natural instabilities that occur on any fluid-liquid interface. Fukada et al. (2000) compared the effect of air injection for a series of objects with a water repellent paint applied to the test objects. With an air film of half a millimeter thick, a drag reduction of 90% was obtained although no Reynolds effects were taken into account. Shimoyama carried out experiments with air film lubrication on a flat plate and for model ships, all without a water-repellent coating (His results are described by Kato & Kodama, 2003). They managed to obtain drag reduction, but had difficulties in obtaining a stable air film, especially at higher flow Reynolds numbers. They noted that the air layer can increase the frictional drag when the liquid-gas interface become unstable, resulting in breaking up the layer in larger sized bubbles that also may reduce frictional drag. On the other hand air injection of bubbles may also lead to patches of air films and therefore the two techniques are closely related with the properties of the surface treatment (coating) as a main parameter influencing the results. The application of such so-called hydrophobic coating explains the participation of paint manufacturers in many research programs for drag reduction by air.

Air cavity ships

The air cavity ship or ACS, is a vessel with several recesses in its bottom that need to be filled with air, see Figure 2. Of course, these cavities can only be fitted to a flat horizontal surface. For the length of the air cavity no wetted surface is present whatsoever, leading to a local but effective drag reduction. However, a standing wave is created in the air cavity and the fluid-air interface must re-attach smoothly at the end of the cavity. A simplified model of a two-dimensional cavity is given by Matveev (1999) and MARIN calculated the wave pattern in a barge with many air cavities with RAPID, a fully non-linearized potential flow code. Obtaining correlation with model experiments, however, proved to be less straight forward than expected.

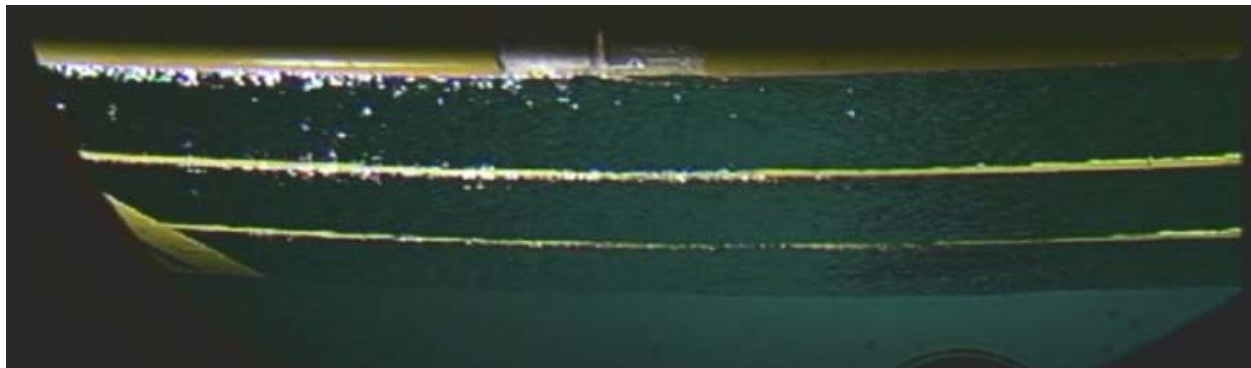


Figure 2 Side-view of an ACS tested for SMOOTH at SSPA, Sweden, with three large air cavities per section. Flow direction from left to right.

A distinct disadvantage of the ACS is that air can escape from the cavities when the ship is pitching and rolling in seaway and that its stability is negatively affected by the creation of additional free surfaces. This means that the ACS is a technique that can be ideally suited for inland ships, a sector where exhaust and carbon dioxide emissions restriction regulations are expected to be imposed in the near future. The ACS has the added advantage that it can actively improve its stopping behavior by releasing air from the cavities, a feature relevant for the busy inland traffic.

The project PELS and its successor PELS II focus on the application of air cavities on a full-scale ship, in this case a barge. The vessel from the project PELS-I is presented in Figure 3 with a good view of its bottom in Figure 4. But from an initial series of model tests it became readily apparent that it is far easier to increase the resistance, even after an optimization of the air cavities using computational fluid dynamics. Several configurations were tested, changing the number and size of the cavities along both the length and width of the vessel, but none reduced the resistance of the model. A careful appraisal of the results led to the conclusion that the flow over the bow of the vessel distorted the flow over the bottom to such an extent that no good configuration of air cavities was possible at all.



Figure 3 The segmented ACS vessel for the project PELS-I

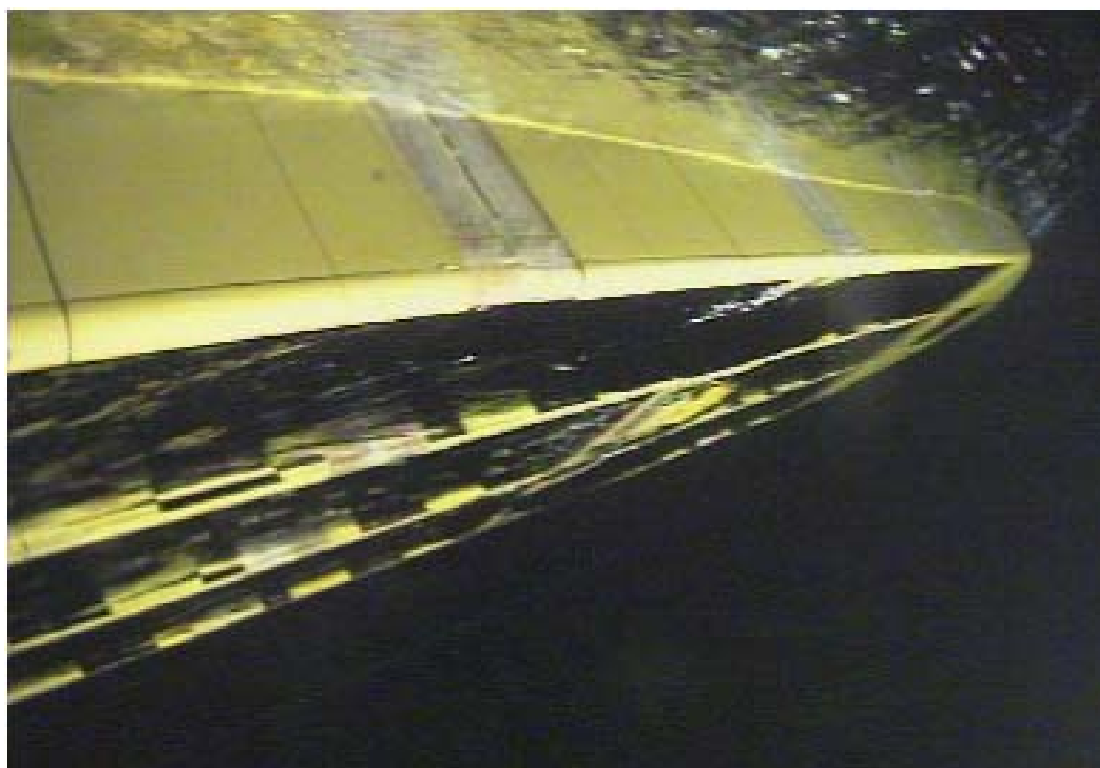


Figure 4 A submerged view the PELS-I vessel at speed, clearly showing the air layer trapped in the bottom.

To test this hypothesis, the barge was fitted with a new bow and the tests were repeated. This time the frictional resistance dropped 20% leading to an overall drag reduction well over 10%. This leads to the important conclusion that the application of air cavities to just any hull form without consideration and understanding of the local dynamics of the flow can have counterproductive results. It also underscores the ongoing need for verification, be it on model or full scale.

Extrapolation

The extrapolation of model-scale data to full-scale data for ships is a well-known procedure. The measured total resistance C_T —made dimensionless by dividing by $\frac{1}{2}\rho V^2 S$ with S the wetted area of the ship—is the sum of friction drag, form drag, and wave drag whereby the form drag is expressed as a fraction k of the frictional drag, so that the wave resistance is determined by

$$C_W^{\text{REF}} = C_T^{\text{REF}} - (1+k)C_F^{\text{REF}}$$

Customary with Froude-identity tests, the wave resistance coefficient remains the same at all scales and the frictional resistance is estimated by friction lines (e.g., ITTC '57). For an air-lubricated ship, the reduction in resistance can be found by comparing the air-lubricated ship with the fully-wetted ship. For the ACS, this means that the air cavities during the model test must be fully closed off. Assuming for a moment that form drag and wave drag do not change for the air lubricated ship, then a new frictional resistance with air lubrication can be determined as

$$C_F^{\text{AIR}} = C_T^{\text{AIR}} - kC_F^{\text{REF}} - C_W^{\text{REF}}$$

From the combination of the reference and air lubricated test, a new frictional resistance curve can be determined. The change in frictional resistance is expressed in a second coefficient k_2 so that

$$k_2 = \frac{C_F^{\text{AIR}}}{C_F^{\text{REF}}}$$

It is noted that any effect of waves in the air cavities is fully considered an effect on frictional resistance at this point. The wave length in the air cavity is known to be Froude-dependent but the effect of both the reduction in drag in the change in wave resistance cannot be determined simultaneously for a resistance test. However, an example of the maximum spread in k_2 of one ACS configuration is plotted in Figure 5. Some variation is visible in k_2 , which is not surprising considering the velocity-dependent drag of the waves in the air cavities, variations in wetted surface (i.e., degree of filling in the air cavity), or variations in model heel angle. The optimum configuration showed a value of $k_2 = 0.82$. The total resistance is now extrapolated to full scale as

$$C_T^{\text{FS}} = (k + k_2)C_F^{\text{FS}} + C_W^{\text{REF}} + C_A$$

FRICTIONAL RESISTANCE DECREASE PARAMETER k_2
MARIN TEST 9808127 / 9808128

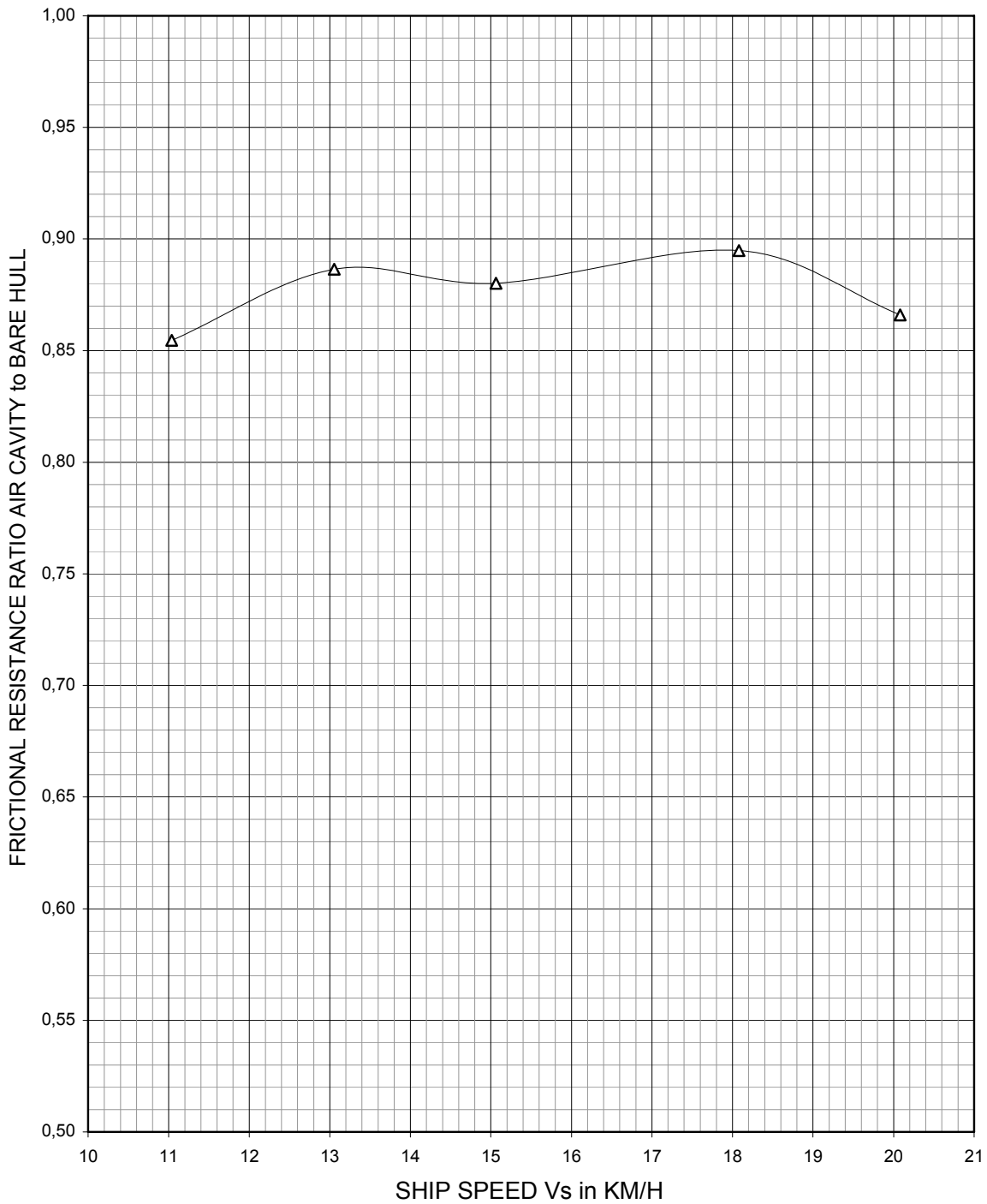


Figure 5 Ratio of frictional of an air cavity ship versus full hull, showing a 10.5% to 14.5% decrease in frictional resistance. Values up to 18% have been measured.

The correlation C_A can be estimated using an empirical function or regression analysis on the database of a model basin. From the constant value of k_2 , an important conclusion can be drawn. The wave resistance is known to increase exponentially as the velocity of the ship increases, but the waves in the air cavity prefer a high ship speed to obtain a long wave length. This means that the application of air cavities results in a minimum ship velocity whereby the wave pattern is still favorable and a maximum ship velocity whereby the improvement in frictional resistance is still significant compared to the total resistance. This means that application of air cavities is only viable for a restricted speed range. For the optimum air cavity configuration of the model, the total resistance decreases 3% at model scale from a 11.5% to 12.5% range during extrapolation. Nevertheless, a total full-scale resistance decrease of a 8.5% to 9.5% range is an impressive reduction. This figure does not yet include the power losses required by the air compressors and ideally no or little air is lost with the ACS. Both air cavities and micro bubbles should be configured such that no air should enter the propeller as the reduction in density results in a reduction of thrust or increase in required power.

But uncertainties remain. Does the friction scale with plate-friction line formulae and to what extent is the correlation coefficient C_A valid for an air-lubricated vessel? This coefficient can easily comprise of 20% of the vessel resistance, more than able to negate any favorable resistance reduction by air lubrication. Without a full understanding of the mechanisms of air lubrication and its scaling mechanisms, tests with full-scale ships are required. From these tests it can be determined how effective the various approaches in air lubrication are and how much air and pumping power is required in service conditions

Future outlook

Drag reduction by air lubrication is a very active and actual research topic. MARIN is participating with universities to investigate the interaction between bubbles, turbulence, and boundary layers to form an understanding of the mechanisms of bubble drag reduction. Model scale tests for both resistance and propulsion, and maneuvering and sea keeping are being performed with all types of air lubrication. Full-scale trials are planned for both an air cavity ship and a vessel with bubble-injection.

For sailing yachts, air cavities and air films do not seem readily applicable considering the large heeling angle during sailing and the absence of any flat bottom. But the application of special paints and bubble-injection of a ship is a promising application. The Reynolds effects of yachts are several order of magnitude less than for a bulk carrier or container ship. For larger ships, unknowns remain on both ends of the scale ladder, ranging from uncertainties in bubble-boundary layer interaction to the extrapolation to high Reynolds numbers.

References

Berg, T. H. v.d., Luther, S., Latrhop, D. P. and Lohse, D., 2005, "Drag Reduction in Bubbly Taylor-Couette Turbulence", *Physical Review Letters*, 94.

Fukada, K., Tokunaga, J., Nobunaga, T., Nakatani, T. and Isawaki, T., 2000, "Frictional drag reduction with air lubricant over a super-repellent surface", *J. of Marine Sc. And Techn.* Vol 5, pp 123-130

Lo, T.S., L'vov, V.S. and Procaccia, I., 2006, "Drag reduction by compressible bubbles", *Phys. Rev.*, vol 72, 036408

Kato, H., 2003, "Microbubbles as a skin friction reduction device", 4th symposium on smart control of turbulence, Tokyo.

Kitagawa, A., Hishida, A. and Kodama, Y., 2005, "Flow structure of microbubble-laden turbulent channel flow measured by PIV combined with the shadow image technique", *Experiments in Fluids*, vol 38, pp 466-475

Meng, J.C. and Uhlman, J.S., 1998, "Microbubble formation and splitting in a turbulent boundary layer for turbulence reduction", *Intl. Symp. N Seawater drag reduction*, Newport, RI, USA, ONR, Arlington, VA, pp 341-355

Matveev, K.I., 1999, "Modeling of vertical plane motion of an air cavity ship in waves", *Fifth International Conference on Fast Sea Transportation, FAST*, Seattle, USA

Session 8

Stephan Brabeck & Tom Schnackenberg

VESSEL PROPULSION USING KITES

STEPHAN BRABECK AND TOM SCHNACKENBERG

1. INTRODUCTION

Maritime shipping is entirely dependent on oil. The latest price increases have placed tremendous cost pressures on the industry: today, marine fuel costs from US-\$500 to US-\$1200 or more per ton depending on the grade and quality – a price that seemed inconceivable just a few years ago. And there is no end in sight to this trend: The respected investment bank Goldman Sachs considers an increase in the price of oil to US\$ 200 a barrel to be possible in the near future.

Cargo shipping is the most efficient transportation of the world. However cargo shipping is now considered one of the primary causes of climate-damaging emissions and as such contributes significantly to the pollution of our environment.

Maritime shipping, with its output of 813 million tons of CO₂ per year, is responsible for almost 3% of worldwide CO₂ emissions (ca. 30 billion tons in 2005). Meanwhile, other studies consider the figure to be more like up to 5% (The Guardian).

The use of cheap and highly sulphurous fuel oil places cargo shipping among the main global producers of climate-damaging gases. Experts estimate that shipping is responsible for 10 million tons of sulphur dioxide emissions per year, which corresponds to more than 7% of the worldwide emissions. == Lloyd's Register Quality Assurance (London)

Sulphur oxides can exacerbate respiratory disorders and are considered one of the contributing causes of acid rain.

In addition, the burning of heavy fuel produces mostly nitrogen oxides. Nitrogen oxides react with hydrocarbons (HC) in sunlight to form ozone, and can lead to smog. Ozone itself is toxic, causes respiratory problems in humans and damages plant life.

In April 2008 the International Maritime Organization (IMO) - the UN agency responsible for maritime safety and protecting the seas - approved a reduction in sulphur emissions for the shipping industry.

From the year 2020 shipping companies either have to use distillate fuels with a limited sulphur content of 0.5% instead of heavy fuel oil or have to use scrubbing technology to clean their exhaust gases. For shipping companies using distillate fuels means a doubling of fuel costs in the future, since refined products such as MGO and MDO are considerably more expensive than highly sulphurous bunker oil.

In addition to the regulations already passed, the IMO is currently preparing a regulation on the reduction of CO₂ emissions from shipping in the form of a CO₂ indexing scheme. Experts assume that corresponding regulations will be implemented in a timely manner. Thus, shipping companies will also be burdened with emissions-based levies in the future. CO₂ emissions can only be effectively reduced by burning less fuel.

The only way out of this subjection to the oil price is to open up alternative energy sources for ships.

This makes the use of wind power especially attractive.

USING WIND POWER PROFITABLY

Wind is cheaper than oil and is the most economic and environmentally sound source of energy on the high seas. And yet, shipping companies are not taking advantage of this attractive savings potential at

present - for a simple reason: So far no sail system has been able to meet the requirements of today's maritime shipping industry.

However SkySails, a company based in Hamburg, is offering a wind propulsion system based on large towing kites, which has the potential to meet all these requirements.

Depending on the prevailing wind conditions, a ship's average annual fuel consumption – and emissions - can be reduced by 10 to 35% by using the SkySails-System. Under optimal wind conditions, fuel consumption has been lowered by as much as 50%.

These figures are based on test results with ocean going vessels and current kite sizes. As the technology advances, relative kite sizes can be increased and fuel savings will grow.

Virtually all existing cargo vessels and new builds can be retro- or outfitted with the auxiliary wind propulsion system. The kite system is used for relief of the main engine, which remains fully available if required. This dual propulsion solution offers the flexibility required to minimise operating costs.

Economical acquisition and operating costs for the SkySails-System lead to short amortization periods of between 3 and 6 years, depending on the routes sailed.

The ship's regular crew is adequate for operating the system and no additional personnel costs should arise.

The business case for an 88m ship burning 5.7 tonnes per day runs as follows:

Fuel costs (210 days) ==	1200 tonnes MGO fuel at €750 per tonne	€900,000
Annual savings on route:	Rotterdam to Reykjavik (est. 29%)	€261,000
Annual saving on route	Rotterdam to Marseille (est. 15%)	€135,000
Acquisition plus installation cost		€465,000
Annual maintenance and servicing		€45,000

2. SKYSAILS TECHNOLOGY SUMMARY

The SkySails-System consists of three simple main components: A towing kite with rope, a launch and recovery system, and a control system for automatic operation.

Instead of a traditional sail fitted to a mast, SkySails uses large towing kites for the propulsion of the ship. Their shape is comparable to that of a paraglider.

The towing kite is made of high-strength and weatherproof textiles.

The tethered flying kite can operate at altitudes between 100 and 300 m where stronger and more stable winds prevail.

By means of dynamic flight manoeuvres, e.g. the figure of "8", the kites generate five times more power per square meter sail area than conventional sails.

The traction forces are transmitted to the ship via a highly tear-proof, synthetic cable.

The launch and recovery system manages the deployment and lowering of the towing kite and is installed on the forecastle. During launch a telescopic mast lifts the towing kite, which is reefed like an accordion, from its storage compartment. At sufficient height the towing kite then unfurls to its full size

and can be launched. A winch releases the towing rope until operating altitude has been reached. The recovery process is performed in reverse order.

The entire launch and recovery procedure is carried out largely automatically and lasts approx. 10 - 20 minutes in each case.

The ship's crew can operate the system from the bridge. Emergency actions can be initiated at the push of a button. The automatic control system performs the tasks of steering the towing kite and adjusting its flight path. All information on the operation status of the system is displayed in real-time on the monitor of the workstation and thus easily accessible for the crew.

The kite system supplements the existing propulsion of a vessel and is used offshore, outside the 3-mile zone and traffic separation areas.

The system is designed predominantly for operation in prevailing wind forces of 3 to 8 Beaufort at sea. The system can be recovered, but not launched at wind forces below 3 Beaufort.

With regard to classification society regulations, the kite system is categorized and treated as an auxiliary propulsion. The operation of the system is not limited by any regulations at present.

Their double-wall profile gives the towing kites aerodynamic properties similar to the wing of an aircraft. Thus, the system can operate not just downwind, but at courses of up to 50° to the wind as well.

The kite is easy to stow when folded and requires very little space on board ship. A folded 160m² kite for example is only the size of a telephone booth.

In contrast to conventional sail propulsions the kite system requires no superstructures to obstruct loading and unloading at harbours or navigating under bridges, since the towing kite is recovered as soon as the 3-mile zone is reached.

Unlike conventional forms of wind propulsion, the heeling caused by the kite is minimal and virtually negligible in terms of ship safety and operation.

Depending on the operator's preferences, the main engine can either be throttled back to save fuel, or kept running at constant power and using the kite tow forces to increase the ship's speed.

3. HISTORY & MILESTONES

SkySails started with the development of the world's first practicable towing kite propulsion system for commercial shipping in 2001. Having successfully completed the basic research and engineering in 2005, the system's towing kite area was scaled up to 160m² and thoroughly tested on the 55m-long former buoy tender MV "Beaufort" in the years 2006 and 2007.

Currently the SkySails-System is being pilot tested on board the pilot customer vessels MV "Michael A." (WESSELS Reederei; first retrofit system) and MV "Beluga SkySails" (Beluga Shipping; first installation on new build) during regular shipping operations. Within the framework of this pilot phase, all system components are being durability tested and the results immediately flow into the process of improving and optimizing the product for series production.

The following pictures document the development process of the SkySails-System:

2001/02: Testing platform I "Da Vinci"

The basic physics underlying the technology were examined with the modified catamaran "Da Vinci" that served as a SkySails testing platform. The catamaran was easy to operate and had the desired hydrodynamic properties. The ship and the towing kite were controlled manually. The series of tests demonstrated that it is physically possible to propel a ship with a towing kite.

2003/04: Testing platform II "Galileo"

As Testing Platform II SkySails used the "Galileo" an 8-meter, 2-ton scale model of an existing container ship from the Hamburg Ship Model Basin (HSVA). The first step was to conduct scientific tests in the towing tank at the Hamburg Ship Model Basin to examine a kite's traction behaviour on conventional cargo ships. Practical tests on the Baltic Sea that used this very same model propelled by a small towing kite proved that the SkySails technology is suitable for cargo shipping. The data collected in the test allowed the first back calculation to be made on the system in original scale. Already at that time the ship and towing kite were remotely controlled.

2004/05: Testing platform III MY "Jan Luiken"

The outfitting of systems components for towing kites having a surface area of up to 40 square meters onto the 15-meter, 18-ton "MY Jan Luiken" as Testing Platform III began in November 2004. All key system components, such as the launch and recovery system, were successfully tested in practice first-hand over the course of 2005. The system operated in a semiautomatic mode and the alpha version of the autopilot was already implemented at that time.

The "MY Jan Luiken" still serves the company today as a development platform. New engineering and technology concepts are tested aboard her in small scale before being implemented in full scale on the experimental ship "MS Beaufort." This approach helps reduce development costs. The "MS Jan Luiken" was named after Jan Luiken Oltmann, the founder of the Oltmann Group, the renowned ship financing company based in Leer.

2006/2007: Further development SkySails-System for cargo ships

Work to equip the almost 55-meter and 800-ton former buoy tender "MS Beaufort" (formerly the "MS Buk") began in January 2006. After completion of the installation, test operations with system sizes of 80m² commenced.

By the end of 2006 the towing kite's area of the SkySails-System on this ship had been scaled all the way up to 160 square meters and thoroughly tested on the North and Baltic Sea in the year 2007. This marked the first time that the SkySails-System aboard the "Beaufort" had reached full-scale size. Small cargo ships, fish trawlers and super yachts can already be equipped with systems of this size.

The SkySails staff reported: *"We used a 160m² kite on the Beaufort for the first time, which was during the last period of tests on this vessel, the kite generated so much thrust at a wind of force 6, (25 knots) that the ship was going faster just with the kite than with its engine (1,260kW). At a speed of 11 knots, compared to the normal 9 knots the captain told us to stop because he got frightened by the power of the kite and the abnormal speed of his ship. This made it clear to us that we had to put this kite on bigger vessels, which we did.*

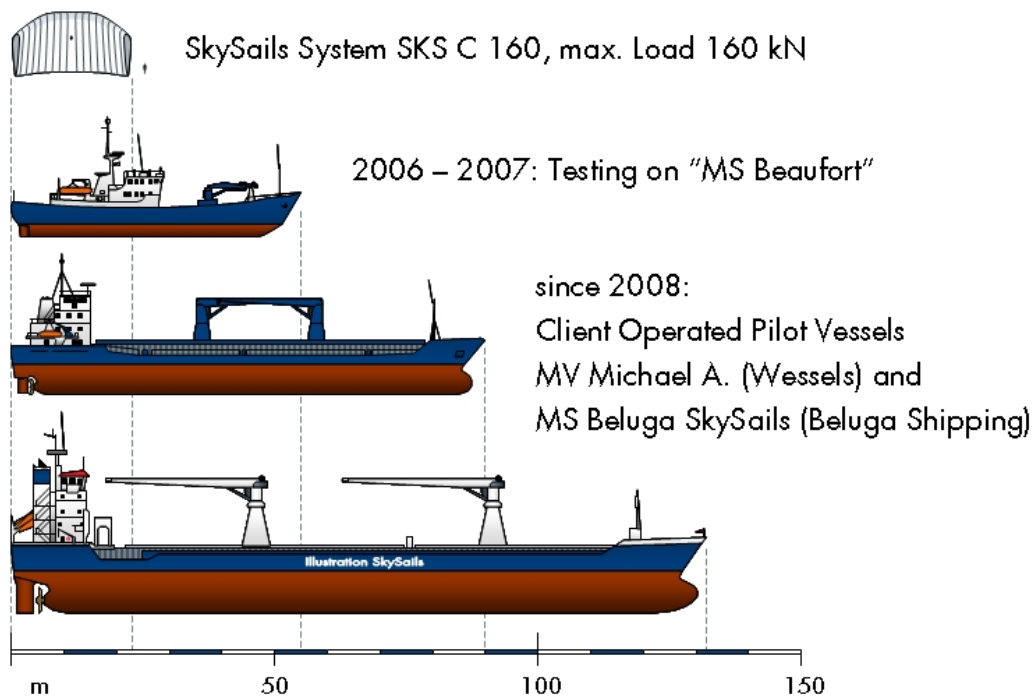
2007/2008: Pilot Series Cargo Ship

Since the end of 2007 / beginning 2008, the SkySails-System is being pilot tested on board the cargo vessels MS "Michael A." (WESSELS Reederei; retrofit system) and MS "Beluga SkySails" (Beluga Shipping; installation on new build) during regular shipping operations.

In the first half of the pilot phase system robustness and reliability is developed to industry standard. In the second half of the pilot phase system performance will be evaluated extensively and optimized.

The customer vessels remain in regular commercial operation throughout the pilot phase. Initially, three SkySails engineers will be aboard of each ship. All components are being durability tested while the SkySails-Systems are deployed on board. The results immediately flow into the process of improving and optimizing the product.

Once this pilot testing is completed, series production of the SkySails-System for cargo ships will begin in 2009.



Above: Comparison of SkySails kite and vessel sizes

4. CONSULTANTS AND SUPPLIERS

Stefan Müller from Aerolabs AG, Munich, has been responsible for the design of the kites since early times. Development has concentrated on stability, control, and the desire for low control forces to save on energy and to minimize the size of the motors in the gondola.

North Sails New Zealand has been actively involved in kite making for SkySails since the beginning of the development programme and the sailing tests with the Galileo on the Baltic in 2003. The designs have been supplied by Stefan Müller, and SkySails engineers have worked with North Sails staff to improve aspects of construction and material development.

Fortunately for the development programme, sailcloth fabrics as used in racing and cruising spinnakers and gennakers has been excellent adequate for the SkySails kites up to quite large sizes, with appropriate construction techniques.

One feature that will be rewarded as we scale up to larger and larger sizes and loads is to recognise that the main loads run across the kite in a span-wise direction and propagate both span-wise and through the thickness of the section.

Cloth is laid chord-wise for manufacturing ease, and spinnaker fabrics are designed to have the strongest direction along the “warp”, which is the chord-wise direction for these kites.

Kite manufacturers will need to work with the fabric manufacturers to develop fabrics which have the main axis of strength in the “weft” or “fill” direction (across the cloth). Fortunately this is not new to cloth manufacturers and there are many existing styles of fabric which are designed this way.

As kites get larger, specialist fibres will increasingly become important, but at present nylon and polyester are perfectly adequate for kite manufacture, further contributing to the economic viability of the system

5. KEY AREAS OF DEVELOPMENT

Autopilot.

Autopilot development is one of the systems unique to the SkySails development programme and has required a large portion of the in-house development attention.

Kite flying is a skill not quickly learned and mistakes would lead to kite crashes and put the system out of action. For these reasons it was recognised from the start that the viability of SkySails depended on developing an automatic kite flying system so that ship crew need not be at all skilled in manoeuvring the kites.

This has progressed enormously over the years. SkySails staff include skilled kite fliers and for a long time the kites were always flown by a SkySails engineer, albeit by remote control and radio signals from the beginning of the programme.

As the autopilot program has developed, not only has the safety improved, but in fact the autopilot software now flies the kite more efficiently than the skilled pilots so that kite performance has increased far behind our earlier standards.

A higher average apparent wind speed at the kite, (from the autopilot skill) and improvements in the kite design have meant that we are achieving line loads well in excess of those forecast and achieved in our early test program

The autopilot resides in the control pod, while overall control of the system is maintained at the bridge station

Routing system & route optimization.

The weather routing system, which SkySails has also developed, provides shipping companies with a means to guide their ships to their destinations on the most cost-effective routes and according to schedule. SkySails meteorologists do the weather routing in four steps:

The first task is to develop the weather forecast. Modern meteorological methods make precise three to five-day weather forecasting possible. Major weather systems and weather trends can be forecast for even longer periods. A decisions model includes requirements of the shipping company. A balance of fuel saving, and the importance of arrival times are important for the decisions on routing and kite deployment.

Critical to these decisions are the performance calculations. The weather forecast data and the decision model flow into the performance calculation which can then calculate optimal routes based on the projected performance

This route is converted into a series of waypoints, and these, along with the supporting data, are sent to the shipmaster. The solution can of course be re-visited during the actual voyage.

Launch and recovery system

Anyone who has watched kite-surfers operating on a beach can appreciate how much can go wrong during the launch and landing of kites!

The key advantage of kites – the enormous power they can develop for a given kite area due largely to the freedom to fly over a wide surface unlimited by masts and rigging, can become a serious liability in this phase of the operation.

The development of a reliable and simple launch and recovery system lies at the heart of the viability of the SkySails system and, along with the autopilot, has taken much of the development time to date.

As well as demanding system reliability, the company has been at pains to minimize the “intrusion” that any part of the SkySails system makes on the layout of a vessel.

This has resulted in a single integrated unit which can handle all the physical operations of the kite system in one compact location.

The launch and recovery system manages the deployment and lowering of the towing kite. It is installed on the forecastle and consists of a telescopic mast with reefing system which unfurls and reefs the kite respectively during the launch and recovery process.

A coupling mechanism connects the towing kite with the mast adapter attached to the launch and recovery mast. The towing kite is stored in the kite storage on the forecastle.

During the launch, the telescopic mast raises the towing kite - which arrives folded like an accordion - from the kite storage. Subsequently, the telescopic mast extends to its maximum height. The towing kite then unfolds to its full size under natural air flow from the apparent wind, and once it has achieved a flying shape, it can be launched and set flying.

The winch releases the towing rope slowly, and the kite is flown by the autopilot at the “zenith” of its scope, until operating altitude has been reached.

The recovery process is performed in the reverse order of the launch. The winch retracts the towing rope and when fully retracted, the nose of the towing kite is captured at the top of the mast. The towing kite is then reefed. The telescopic mast retracts and the towing kite is stowed in the kite storage unit along with the control pod.

Each of these procedures (launch procedure and recovery procedure) is carried out largely automatically and each requires approximately 10-20 minutes

6. PERFORMANCE

The technical possibilities resulting from the spatial separation of the ship and the “sail” or towing kite give SkySails an entirely new performance spectrum.

The towing kite of the SkySails propulsion can be navigated “dynamically”. This means that the autopilot can perform flight manoeuvres with the towing kite such as the figure of eight in front of the ship.

The high airspeed of the towing kite is particularly relevant since the airflow velocity at the kite’s aerodynamic profile is the key to performance. For the calculation of the traction force of towing kites the airflow velocity is squared:

$$F_{\text{line}} = V_{\text{Kite}}^2 * \text{Rho} / 2 * A * C_R$$

where

$$V_{\text{Kite}} = a * (V_{\text{AWS}} * \cos(\theta) * \cos(\zeta))^b$$

F_{line} := line force

V_{Kite} := air flow velocity seen by the kite

Rho := air density

A =: kite area

C_R := aerodynamic reaction coefficient

a,b: coefficients for kite characteristics (depending on profile and trim)

V_{AWS} : apparent wind speed as seen by the ship at kite flight level

theta and zeta are the azimuth and elevation angle of kite line to the apparent wind vector

The kite speed in the air can be many times the apparent wind speed as seen by a static kite. The limit is defined by the overall L/D ratio which defines the “slipperiness” of the kite as flown dynamically

The average sustained force of the kite is proportional to the root-mean square of V_{Kite} and to calculate this exactly requires an integral over the range of theta and zeta prevailing in each situation.

The equation above is semi empirical, and was adapted to suit the theory (in which the velocity would depend on the L/D only), and the flying data which includes the reality of manoeuvring throughout the range of angles. This is what leads to the power term in “b”

If $b = 1$, then “a” is equivalent to the L/D-ratio.

If the airflow velocity is doubled, the traction force of the kite quadruples. In practice, the towing kite easily reaches speeds three times that of the true wind and often more.

It is for this reason that you will see kite-surfers planing back and forth while the windsurfers are sitting on the beach, and its for this reason that SkySails has observed a factor of more then 5 in the increase of the wind loading (force / sq m) developed by kites as opposed to conventional sails

This efficiency also leads to increased safety as the kite can develop a much larger range of forces for a given sailing situation than conventional sails.

When underpowered, heading downwind, the autopilot can generate an effective force coefficient of 5 through dynamic flying, yet the same kite can be flown at the zenith and de-powered so that its force coefficient is only 0.5 and that force directed essentially vertically.

A further significant technological advantage of the SkySails propulsion is that the towing kites can operate at altitudes between 100 and 300 m where stronger and more stable winds prevail.

At an altitude of 150m the average wind speed can be 25% higher than at a height of 10m.

For all of these reasons, it is possible to gain significant tow force and fuel savings by using surprisingly small kite areas.

For comparison: The 109m long four-mast barque “Sea Cloud” has a sail area of 3,000m² in total. A cargo ship of the same length would be fitted optimally with a towing kite of about 300m² in size.

During the enduring pilot phase the calculated performance of the SkySails-System has been proven true:

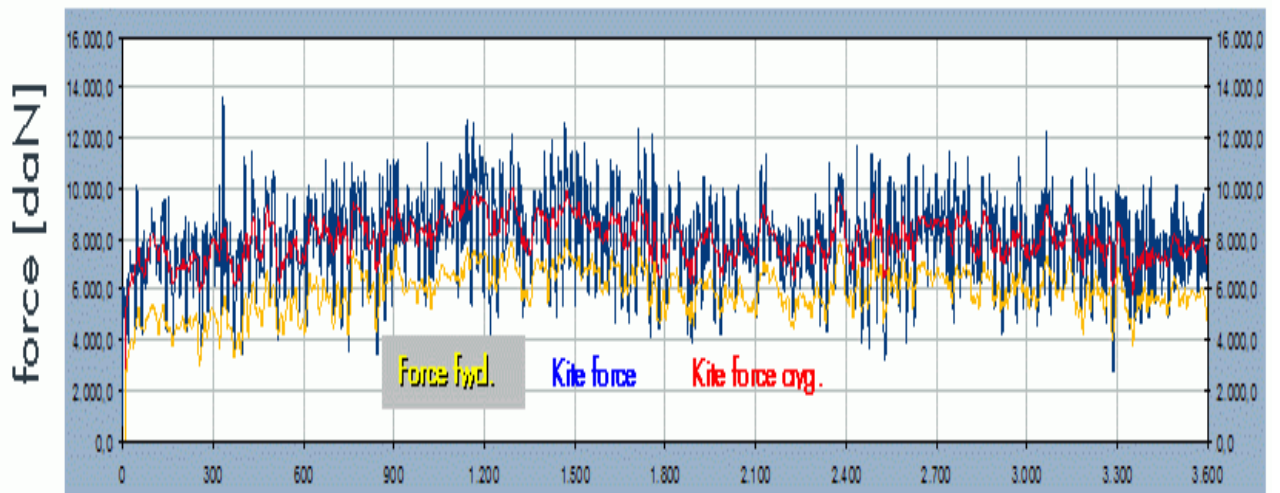
MS “Beluga SkySails”:

Savings of 20% at low wind speeds (160m² Kite)
Savings of up to 40% possible (with 320m² Kite)

MS “Michael A.”:

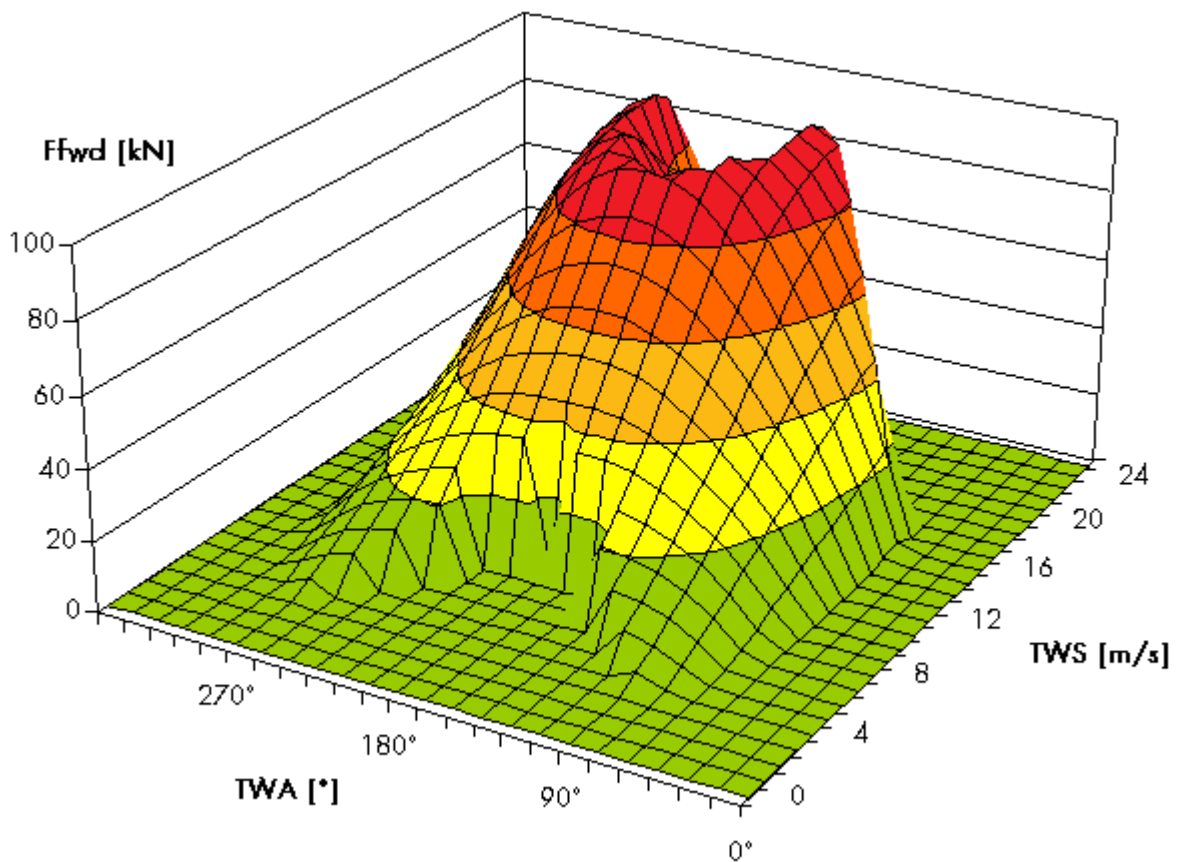
Savings of 70% under optimal conditions (160m² Kite)

Average annual savings of between 10% and 35% (depending on the route) are quite realistic.



Above: Extract from operational results

It can be seen that the forward force (yellow trace) averaged 6000 daN (6 tonnes) in this sample



Above: Force mapping of SkySails propulsion for the SK160 kite system

7. SUCCESSES

The latest measurements made aboard the cargo ship “Michael A.” of the Wessels Shipping Company demonstrate how the towing kite propulsion system delivers far more than five times the performance per square meter of sail than traditional wind propulsion systems. With the help of the wind, the 160 square meter kite generates up to 8 metric tons of traction force – this approximately corresponds to the thrust of an Airbus A318 turbine engine.

“Our own measurements show that we were able to temporarily save far more than half the fuel by deploying SkySails in favourable wind conditions,” reports Gerd Wessels (37), managing director of the Wessels shipping company based in Haren/Ems, adding that “alternatively we were able to increase the ship’s cruising speed from 10 to 11.6 knots with the help of this towing kite propulsion.”

Each of the shipping company’s next three new 88-meter, multipurpose sister ships with a deadweight capacity of some 3,700 metric tons and nearly 1,500 kW of power will be fitted with a 160 m² kite. With favourable wind conditions, a kite of this size can generate up to 8 tons of traction power. For comparison: in order to reach a cruising speed of 11 knots, these ships require approx. 11 tons of thrust.

8. RETROFITTING, ADAPTING VESSEL DESIGN FOR SKYSAILS

Supply Interfaces

Most of the components are installed on the foredeck on mounts welded to the ship’s hull. The system requires a connection to the ship’s electronics and/or hydraulics on the foredeck. The workstation for operating the system is installed on the bridge. In addition to a power supply, an appropriate interface to the ship’s computer is needed in order to supply the system with the ship’s data.

Installation & Commissioning

Virtually all existing cargo vessels and new builds can be retro- or outfitted with this auxiliary wind propulsion system. Installation can be made in the shipyard of choice or in any port that has an adequate crane system. The ship can remain in the water during installation.

In line with the installation process, the client first provides the company with all the needed information and records pertaining to the ship onto which the system is to be installed. The company project manager also inspects the ship together with the client to examine the installation options on board.

On the basis of this examination, SkySails provides all background information necessary for the customer to compile and submit the relevant records to the insurance company, the classification society and the installing shipyard. The system is then installed on the vessel at the shipyard designated by the client and under supervision of service staff from the company.

The components are installed in three steps:

1. Preparation of the mounts and foundations for winch and launch system; Cutting of openings for the wiring and hydraulic lines. Reinforcement of the foredeck may be required. Typically, however, the ship’s structure in this area is designed with adequate strength due to the reinforcement requirements for the anchor windlass.
2. Installation of the components winch and launch system on the foredeck mounts. Installation of the workstation on the bridge.
3. Laying of the electrical and hydraulic lines and connection of the system components. Winding of the towing rope onto the winch. Stowing the towing kite and control pod in the kite storage.

Normally, a total of 3 pairs of consecutive workdays are required for installing the SkySails-System. If necessary, a few more days may be required for work on the electric system, which however can

usually be completed while the ship is at sea.

As desired or needed, each of the individual installation steps can be performed independently, at different times and at different locations. This, for example, allows using extended docking times for loading and offloading to install the SkySails-System.

The costs of the installation work are handled directly between the shipyard and the client.

Once the installation is complete, a function check of the components fitted on the ship is conducted in port. The function of the entire system is tested during subsequent sea trials. Following that the seller then provides the buyer with a record of delivery verifying that the system is in proper working order.

Operating conditions

The SkySails-System supplements the existing propulsion of a vessel and is used offshore, outside the 3-mile zone and traffic separation areas. The system is designed for operation in predominantly prevailing wind forces of 3 to 8 Beaufort at sea. The system can be recovered, (but not launched), at wind forces below 3 Beaufort. The kites will provide a net forward force at all angles deeper than 50 degrees to the true wind.

9. FUTURE PLANS

The company is continuing to scale up its towing kite technology. In 2009 towing kites with an effective load of 16 tons will be available, in 2010 32 tons, in 2012 64 tons. The goal is to develop a system able to generate an effective load of 130 tons under standard conditions.

Its universal design opens up an attractive market for the system: Some 60,000 of the worldwide approximately 100,000 ships listed in Lloyd's Register and about 1,100 of the 1,900 newly built vessels joining the world's merchant fleet each year would be logical ships to be outfitted with kites.

SkySails plans to equip 1,500 cargo ships and fish trawlers, as well as numerous super yachts, with its systems by the year 2015.

Thanks to its broad applicability in the shipping sector, the kite system can make a major contribution to curbing climate change. The systematic and worldwide use of this technology would make it possible to save over 150 million tons of CO₂ a year, an amount equivalent to about 15% of Germany's CO₂ emissions.

10. CONCLUSION

Flying kites to propel ships is a fairly obvious idea in its broad scope, but has many technical issues.

The SkySails concept has explored a novel way in which to propel vessels using kites and by dint of painstaking development over the past 8 years, the company has made progress in solving many of the technical problems. The areas of development that remain are concerned with improving reliability, particularly in the "launch and recover" phases, and scaling the systems to larger and larger sizes.

This will take time and a good deal of hard work remains, but the prognosis is an optimistic one. Since the system was envisaged, oil costs have soared and the potential market for SkySails has grown.

On the supply side, technology advances, both within and outside the company have improved potential performance of the SkySails and the range of application.

The future for this technology looks promising indeed.

Session 9

**Pepijn de Jong, Michiel Katgert
&
Jan Alexander Keuning**

THE DEVELOPMENT OF A VELOCITY PREDICTION PROGRAM FOR TRADITIONAL DUTCH SAILING VESSELS OF THE TYPE SKÛTSJE

Pepijn de Jong¹

Michiel Katgert²

Lex Keuning³

ABSTRACT

A Velocity Prediction Program has been developed for the verification of the handicap rule used for sailing races with traditional Dutch sailing vessels of the type skûtsjes. To make this VPP suitable for this type of vessels model experiments in the towing tank and the wind tunnel have been performed and the resulting formulations for the hydromechanic and aerodynamics are integrated into a specially tailored VPP.

The paper presents the background of the hydromechanic and aerodynamic models and the inner workings of the resulting VPP. Results are shown for the comparison of performance of the competing vessels on pre-defined racing course for a number of wind velocities.

The paper concludes that the newly developed VPP is found to be suitable to quantify the performance differences between the boats it is aimed for and in such way can be used as a tool to verify and when necessary improve the handicap rule currently used.

1. INTRODUCTION

A frequently returning theme in sail racing with yachts that are not part of a one design class is the creation of a handicap system that is deemed fair by all competitors. The idea behind such a system is that in the race results the capabilities of the crews are only accounted for and not, as is the case with the plain race results, the technical capabilities of the yachts. For such a system basically two main solutions exist:

1. The correction of the racing time for technical differences between the competing yachts;
2. The technical adaptation of the yachts, such that their theoretical performance, without the influence of the crew, is equivalent.



Figure 1 Skûtsje

¹ Assistant Professor, Ship Hydromechanics Laboratory, Delft University of Technology

² Researcher, Ship Hydromechanics Laboratory, Delft University of Technology

³ Associate Professor, Ship Hydromechanics Laboratory, Delft University of Technology

Of both methods, the latter can be much harder to achieve when there are large differences between the competing sailing yachts. Both solutions require adequate knowledge of the theoretical performance of the participating yachts. One way of obtaining this information is by using a so called Velocity Prediction Program or VPP. A VPP is a computer program that can calculate the sailing performance of a sailing yacht by linking an aerodynamics model for the sailing forces with a hydromechanics model for the resistance, stability and lifting forces on the yacht's hull. Both computational models usually are obtained by model experiments, in wind tunnel for the sailing forces and in the towing tank for the resistance. Usually these experiments are generic and by using systematical parameter variations (of the geometry, the weight, and the weight distribution) it is possible to describe the characteristics of all yachts involved.

In the north of the Netherlands the SKS (Sintrale Kommissje Skûtsjesilen) sail races are held yearly. In these races 14 syndicates, using *skûtsjes*, compete in a yearly organized race series, each syndicate often representing a city or a village. *Skûtsjes* are traditional Frisian sailing vessels from the start of the 20th century, and form a subtype of the Dutch *tjalk*. These vessels were originally used for cargo transport in the inland waters of Frisia. They are flat-bottomed and carry shallow rounded leeboards on their sides that are used as a substitute for the keel. Their length is about 15 to 20 meters; they are 3.5 to 4 meters wide and have a draft of only around 0.4 meter. Their rig is of the sloop type, with a short curved gaff of about a third of the boom length and a stay sail. Figure 1 shows a skûtsje as used in the SKS races.

To keep the SKS races attractive for the public a fairly basic handicap system is used. This system attempts to equalize the sailing performance of the 14 different skûtsjes, by limiting the amount of sail that can be used for each vessel. The result is that the actual finish equals the race result. The maximum allowed sailing area is prescribed by a simple formula, based on the main dimensions of the vessels:

$$SA = 2.15 \cdot L_{wl} \cdot [B_{wl} + 2T] \quad (1)$$

The formula has most recently been revised in 2000; hence it is referred to as Formula 2000. At the time of this revision an evaluation was foreseen several years later. During this evaluation the SKS felt the need to perform an in depth study to verify the formula. For this reason the SKS contracted the Kenniscentrum Jachtbouw (a knowledge center for the yachting industry of the Noordelijke Hogeschool Leeuwarden - NHL). The NHL subcontracted the Ship Hydromechanics Laboratory of Delft University of Technology to devise a Velocity Prediction Program specifically tailored for skûtsjes. This VPP is created to enable the NHL to study the effectiveness of the Formula 2000, and to provide theoretical support when devising a new formula in case this is deemed necessary. Besides the TUDelft, the Maritime Research Institute Netherlands was subcontracted for performing full scale resistance tests and Anmar Engineering for measurement of the hulls to obtain lines plans of each boat and for performing stability tests.

The current paper describes the development of this VPP specifically tailored for skûtsjes. In the next section the general approach of the research project is laid out. The following sections detail respectively the resistance model, the stability, the aerodynamic model, and the VPP solver and optimizations. Finally results are presented for the comparison between the 14 skûtsjes. The final section summarizes the conclusion.

2. APPROACH

To set up the VPP three aspects of the vessels are combined:

1. The resistance and side force production (resistance model, described in section 3)
2. The stability and volume of displacement (section 4)
3. The sail forces (aerodynamic model, described in section 5)

The first aspect is covered by the resistance model as detailed in section 3. In this case model experiments in the towing tank are used to obtain resistance data at a number of forward speeds and geometrical variations (trim, drift, heeling, leeboard angle and rudder angle). Due to budgetary restrictions only four boats were selected to carry out the towing tank tests. These models were selected to cover the most important parameter variations in the group of 14 boats. With one of the four a full set of measurements were carried out to obtain polynomial expressions for the influence of the geometric variations due to trim,

heeling and drift. With the other three a more limited test program was carried out to obtain polynomial expressions for the influence of the hull form on the upright and heeled resistance.

This approach enabled obtaining a resistance model at limited cost, while providing as much information as possible for the range of 14 boats. The approach was deemed justifiable, especially due to the fact that the VPP was aimed at quantifying the differences in performance between 14 relatively similar boats, and not at obtaining an absolute performance indication nor at addressing performance differences between very dissimilar designs.

For the water depth 2.5 m full scale was chosen. This value deemed to be representative of the water depth in which the races are performed. Due to the restricted water depth, the resistance of the boats is highly influenced and will steeply increase when the boat speed increases. The model experiments were setup with limiting value of the Froude number over the depth of 0.8, as beyond this velocity the resistance will steeply increase due to shallow water effects.

The second aspect, the stability, is determined by the hull shape and the height of the center of gravity. Both were unknown and therefore all vessels have been measured to construct a digital lines plan and stability tests have been performed to obtain the position of the center of gravity. This is detailed in section 4.

The third aspect, the sail forces or the aerodynamic model, has been dealt with in two ways. Within the original budget, there was no room for additional wind tunnel testing. Therefore, the sail force model was initially based on wind tunnel tests previously carried out and published. In particular use was made of the sail coefficients obtained in the so-called Indosail project. In the 80s of the last century numerous wind tunnel tests were carried out with different sail types by HSVA. The results have been partially reproduced by Indesteege (1989).

At a later stage, due to fortunate circumstances the possibility arose to perform wind tunnel tests with a model of one of the 14 skûtsjes. Although no geometric variations were possible in these limited tests, a much more realistic sail model was obtained, which was used to significantly enhance the VPP. This latter model is presented in the current paper. The sail force model will be detailed in section 5.

Finally, these three aspects were combined with a solver routine to form the VPP. The results of this VPP can be used to obtain the time per sailed mile on a predefined track to compare the results of 14 boats, as well as to evaluate possible measures to equalize the sailing performance.

As the model is setup with limited budget and as a means to compare the relative performance of the boats the effort has been directed at adequately describing the differences between the skûtsjes and not so much at achieving absolute performance predictions. The latter would require a much higher level of detail and in turn much more extensive and costly model experiments.

3. RESISTANCE MODEL

3.1. Model selection

As stated, due to budgetary restrictions only four boats could be selected for the towing tank tests. To get an idea which parameters of these boats mostly determine the residuary resistance characteristics of this type of ships, regression analysis was carried out on the resistance results of similar traditional vessels, tested earlier at the Ship Hydromechanics Laboratory. It was found that the following parameters and the relation them were most important for the specific residuary resistance:

- Length waterline
- Width waterline
- Draft
- Waterline area
- Lengthwise position of the center of buoyancy

While studying the main particulars of the 14 skûtsjes, no. 10 (widest and shallow), no. 2 (most narrow, almost shortest and deepest), no. 14 (longest and wide), and no. 12 (waterline area) were selected to perform towing tank measurements with.

	Lwl	Bwl	T	D	∇	S	SA	ZCE	GM
	m	m	m	m	m ³	m ²	m ²	m	m
1	17.29	3.51	0.43	0.79	17.42	62.80	163.7	6.88	1.68
2	17.30	3.36	0.45	0.68	17.45	62.39	156.1	6.77	1.69
3	17.43	3.78	0.42	0.81	19.83	68.11	168.4	7.18	2.01
4	17.44	3.59	0.41	0.75	18.32	65.81	168.4	7.14	2.00
5	17.46	3.58	0.45	0.79	18.63	64.56	165.8	6.99	1.89
6	17.48	3.57	0.38	0.81	16.98	63.68	165.0	6.99	1.93
7	17.51	3.47	0.43	0.75	17.71	63.10	162.0	6.79	1.76
8	17.55	3.48	0.43	0.76	17.87	63.68	162.6	6.70	1.75
9	17.57	3.48	0.41	0.69	16.38	61.48	160.2	6.55	1.87
10	17.69	3.92	0.38	0.75	18.61	68.49	177.9	7.45	2.46
11	17.70	3.46	0.45	0.8	18.13	63.80	161.3	7.02	1.61
12	17.75	3.68	0.40	0.85	18.63	68.04	168.8	7.15	2.17
13	17.79	3.61	0.40	0.71	17.26	64.12	168.0	6.92	2.01
14	17.89	3.72	0.40	0.83	17.91	68.39	170.4	7.42	2.39

Table 1 Main particulars of the SKS fleet

3.2. Test setup

The experiments were performed in towing tank #2 of the Ship Hydromechanics Laboratory of the TUDelft. This tank measures 75 m in length and 2.75 m in width. The testing was performed at a model scale of 1:9. The reason to choose the smaller towing tank was the limited water depth of 2.5 m full scale, equivalent to 0.278 m on model scale.

The models were tested accordingly the standard testing procedure of the Ship Hydromechanics Laboratory of the TUDelft. The models were free to heel, sink and trim by using two vertical balance arms. The trimming moment was applied by transferring a weight over longitudinal rails on the model. The heeling angle was applied by moving this same weight transversely on an electrical driven worm drive and using an accurate spirit level. The drift angle was applied by transversely moving the forward balance leg. The resistance force was measured by attaching the tow-string to a force transducer and on both balance arms force transducers were mounted to measure the side force and the yaw moment. Trim and sinkage were determined with two potentiometers in the balance arms.

Turbulence stimulation was achieved by using strips of carborundum particles attached to the model at three stations. The additional resistance of these strips was corrected for by first performing test with single width carborundum strips and subsequently with double width strips and recording the difference in resistance.

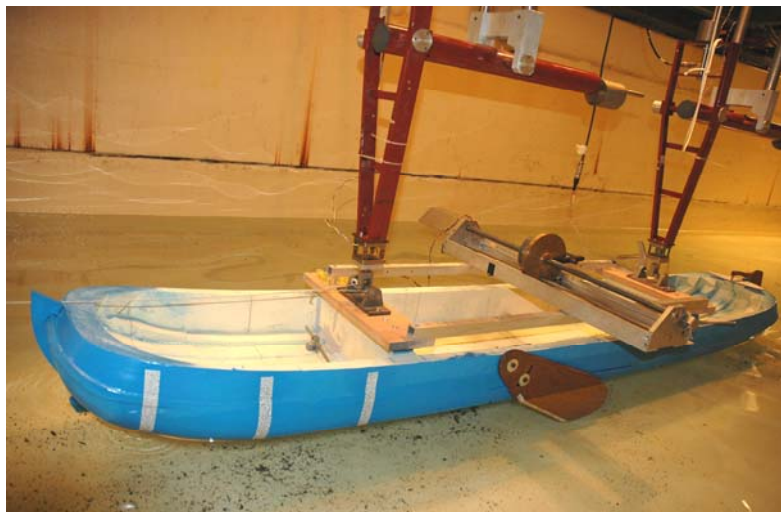


Figure 2 Test setup, three single width carborundum strips are visible near the bow

All measured signals were amplified and filtered with a low-pass filter with a cut-off frequency of 5 Hz. The signal was passed via an A/D-converter to the data recording PC. The signals were zeroed. The runs were about 20 seconds in length. Figure 2 shows the test setup.

3.3. Test program

All four models were subjected to a limited test program, while model 14 was more extensively tested.

The limited testing program consisted of tests for the upright resistance for a Froude number range from 0.1 to 0.3 at three different trimming moments. These trimming moments were applied to correct for the difference in height of the attachment point of the tow string and the height of the center of effort of the sail forces. Besides the upright resistance also the resistance at 15 degrees heeling angle for the same speed range was measured. No leeboard was mounted during these tests and the rudder was fixed at 0 degrees rudder angle.

The upright resistance was measured twice for each forward speed; once with single width carborundum strips and once with double width strips to account for the increased resistance due to the strips.

Model 14 was subjected to a more extensive program, according to the standard testing method of sailing yachts of the Ship Hydromechanics Laboratory. Three forward speeds (Fn 0.1, 0.2, and 0.3), four heeling angles (0, 10, 15, and 20 degrees), three leeway angles (0, 6, and 9 degrees), and two rudder angles (0 and 10 degrees) were tested. The leeboard was mounted and fixed in the maximum submerged orientation. This orientation was limited by the relatively small water depth to 0.27 m.

3.4. Data processing

The measured resistance was corrected for the influence of the carborundum strips and subsequently extrapolated using Froude's method. The resistance was split into a viscous part and a residuary part. The viscous part was determined by applying the ITTC-57 friction line for both model scale and full scale and using a form factor of 1.20 obtained with the method of Prohaska. The residuary part was extrapolated by applying the scale factor α^3 , where α is the linear geometric scale factor.

3.5. Hydromechanic model

The hydromechanic model has been setup in accordance with work carried out in the Ship Hydromechanics Laboratory in conjunction with the Delft Systematic Yacht Hull Series as published by Gerritsma et al. (1981) and (1988) and Keuning et al. (1996), (1997) and (1998).

Resistance of bare hull with rudder

The viscous resistance can be calculated using the ITTC-57 friction line and the form factor found from the model experiments:

$$R_v = \frac{1}{2} \rho V^2 S C_{f \text{ ITTC-57}} (1+k)$$

$$C_{f \text{ ITTC-57}} = \frac{0.075}{(\log(Rn) - 2)^2} \quad (2)$$

$$Rn = \frac{VL}{\nu}$$

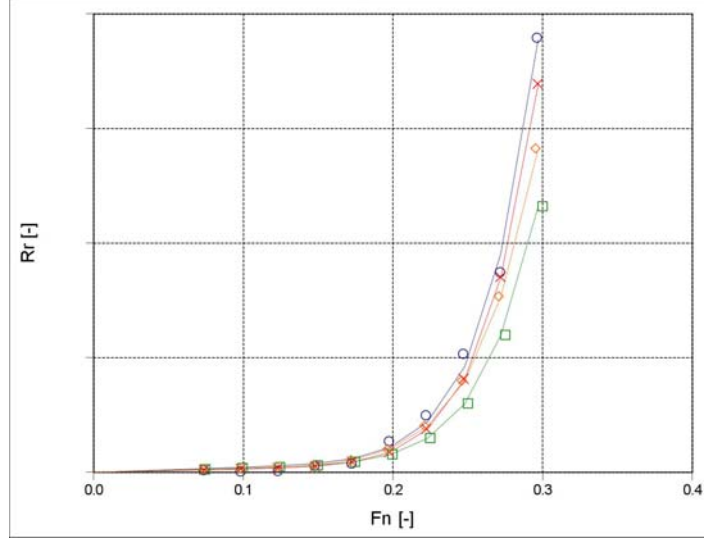


Figure 3 Residuary resistance measured (points) and modeled (solid lines)

For the upright residuary resistance of the bare hull with rudder a polynomial expression has been determined using the upright resistance experiments of the four models. The coefficients a_0 to a_3 are dependent on the Froude number.

$$\frac{R_r}{\nabla \rho g} = a_0 + a_1 \frac{B_{wl}}{L_{wl}} + a_2 \frac{B_{wl}}{T} + a_3 \frac{L_{wl}}{\nabla^{1/3}} \quad (3)$$

Figure 3 shows a comparison of the measured residuary resistance for these four models and the residuary resistance calculated with equation(3).

Extra resistance due to trim

The residuary resistance of the bare hull has been determined for trimming moments of 51 kNm and 115 kNm. The resistance force at 115 kNm can be described with a similar polynomial expression, with a different set of coefficients b_0 to b_3 :

$$\frac{R_{r\theta 115}}{\nabla \rho g} = b_0 + b_1 \frac{B_{wl}}{L_{wl}} + b_2 \frac{B_{wl}}{T} + b_3 \frac{L_{wl}}{\nabla^{1/3}} \quad (4)$$

Moreover, it has been found that the extra residuary resistance at 51 kNm is 25% of that of 115 kNm. Now the extra resistance due to a trimming moment can be found with:

$$\Delta R_{r\theta} = factor \cdot (R_{r\theta 115} - R_r) \quad (5)$$

Where factor is a quadratic interpolation function that is 0 for $M_{trim} = 0$, 0.25 for $M_{trim} = 51$ kNm, and 1 for $M_{trim} = 115$ kNm.

Extra resistance due to heel

The change of resistance due to heel consists of a change in frictional resistance due to the changed wetted surface (6) and a change of residuary resistance determined during the experiments at 15 degrees heeling angle (7). The latter can again be described with a similar expression as previously found, now with coefficient set c_0 to c_3 .

$$\Delta R_{f\theta} = \frac{1}{2} \rho V^2 C_f (S_\phi - S) \quad (6)$$

$$\frac{\Delta R_{r\phi 15^\circ}}{\nabla \rho g} = c_0 + c_1 \frac{B_{wl}}{L_{wl}} + c_2 \frac{B_{wl}}{T} + c_3 \frac{L_{wl}}{\nabla^{1/3}} \quad (7)$$

The residuary resistance due to heel at the correct heeling angle is found by linear interpolation:

$$\Delta R_{r\phi} = \frac{\phi}{15} \Delta R_{r\phi 15^\circ} \quad (8)$$

Induced resistance

The induced resistance has been determined with the extensive measurements performed with model 14. The induced resistance, the resistance associated with the side force production generated by bare hull, rudder, and leeboard traveling at a leeway angle. The induced resistance is determined adopting the method of the Delft Systematic Yacht Hull Series, using the so-called effective draft T_e . This method has been detailed by Keuning and Sonnenberg (1998).

$$R_i = \frac{F_h^2}{\pi T_e^2 \frac{1}{2} \rho V^2} \quad (9)$$

The effective draft was determined for from the measurements for two situations:

1. Maximum leeboard submergence, limited by the water depth (set at 2.5 m). This is used when sailing close hauled to beam reaching, when significant side force is generated by the sails.
2. Minimum leeboard submergence. The leeboard is covered by the hull and does not contribute to the side force production. This case occurs when broad reaching to dead running.

For both cases the effective draft has been determined and tabulated dependent on heeling angle and forward speed. The dependence on forward speed is weak; however, the effective draft is strongly dependent on the heeling angle and becomes larger when the heeling angle increases. This can be attributed to end plate effects due to the proximity of the floor, that become stronger when the heeling angle increases, decreasing the distance between the leeboard tip and the floor.

Leeboard resistance

The total leeboard resistance does not equal zero when it is not producing side force. The remaining resistance consists of frictional, form, and residuary components. Due to its small waterline area the residuary component of the leeboard resistance was assumed negligible. Then the leeboard resistance was assumed equal to the frictional resistance determined with the ITTC-57 friction line. Any deviation from this friction line and the actual measured leeboard resistance (measured with the presence of the hull) is discounted in the form factor. It should be noted that this approach is very coarse. Interaction effects are ignored and the wave making resistance is, although very small, scaled incorrectly with the viscous resistance.

$$R_{leeboard} = \frac{1}{2} \rho V^2 C_{f \text{ ITTC-57}} S_{leeboard} (1+k) \quad (10)$$

Total resistance

The total resistance is found by addition of the previously detailed components:

$$R_t = R_r + R_v + \Delta R_{r\theta} + \Delta R_{r\phi} + \Delta R_{f\phi} + R_i + R_{leeboard} \quad (11)$$

4. STABILITY

The stability, volume of displacement and along with that the centers of gravity and buoyancy were acquired by measuring the lines plans of all 14 skûtsjes and performing stability tests. All boats have been built around 1900 and over the years have undergone numerous changes, damages and repairs, making any

available lines drawing obsolete. Especially over the last years most of the boats have been extended to the maximum length possible within the originality regulations.

Each boat has been taken out of the water and measured by using a semi automatic technique to obtain the frames and center vertical by Annmar Engineering, as published by Wagenaar (2008). Even then it took significant effort with 3D modeling software to obtain reasonable 3D lines drawings of each boat. Still then numerous irregularities and asymmetries were present, often due to damages and repairs. The lines drawings used for the models have been averaged over port and starboard side. All this leads to a difficult to quantify geometrical uncertainty.

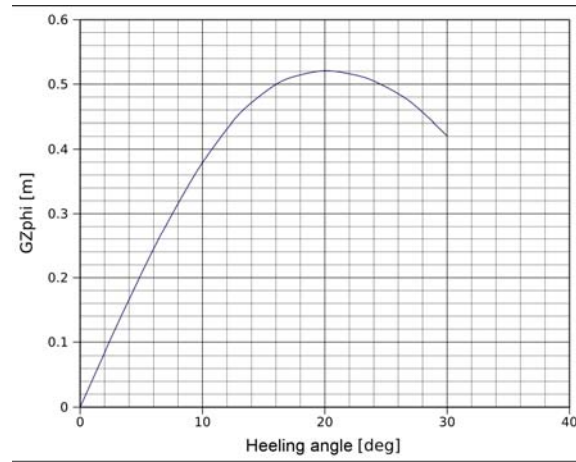


Figure 4 Arms of stability

With the resulting lines drawings and the heights of the center of gravity the curves of arms of stability can be constructed. These curves are used in the VPP to calculate the heeling moment at a given heeling angle. Figure 4 shows a typical curve of arms of stability. The relative small angle of maximum stability is apparent and is due to the fact that the stability of these vessels is for the largest part based on the form stability and not due to a low center of gravity. This stems from the absence of a ballasted keel.

5. AERODYNAMIC MODEL

5.1. Wind model

A wind gradient is assumed based on the wind velocity given at 10 meters above the water level. To calculate the wind velocity at the height of the center of effort ZCE equation (12) is used.

Figure 5 Arms of stability

$$wndgrad = \left(\frac{ZCE \cdot \cos(\varphi)}{10} \right)^{0.1} \quad (12)$$

The sine and cosine components of the true wind velocity become, where α_{tw} is the true wind angle, φ the heeling angle and V_{tw} the true wind velocity:

$$\begin{aligned} V_{tw\sin} &= V_{tw} \sin(\alpha_{tw}) \cdot wndgrad \cdot \cos(\varphi) \\ V_{tw\cos} &= V_{tw} \cos(\alpha_{tw}) \cdot wndgrad \end{aligned} \quad (13)$$

In this equation the cosine of the heeling angle is assumed to include the influence of the heeling angle on apparent velocity and the sailing forces. Finally the apparent wind velocity and angle can found as:

$$V_{aw} = \sqrt{(V_s + V_{tw\cos})^2 + V_{tw\sin}^2}$$

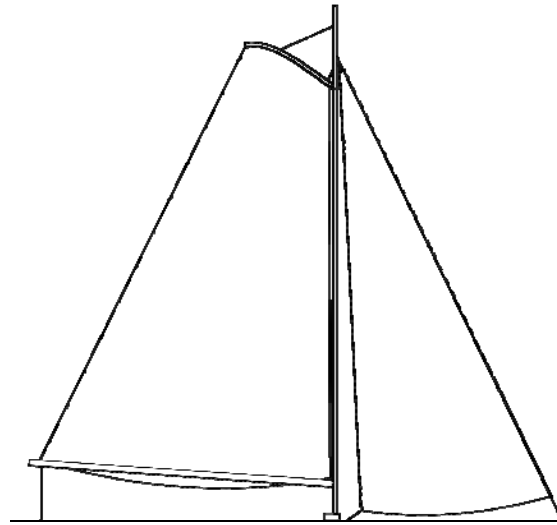
$$\alpha_{aw} = \arctan\left(\frac{V_{tw\sin}}{V_s + V_{tw\cos}}\right) \quad (14)$$

5.2. Sail model

Test setup

For the wind tunnel measurements the Low-Speed Low-Turbulence Wind Tunnel of the Faculty of Aerospace Engineering of the Delft University of Technology was used. This tunnel is an atmospheric tunnel of the closed throat single return type, with a contraction ratio of 17.8. This tunnel is capable of test section velocities up to 120 m/s. The free stream turbulence level in the test section varies from 0.015% at 20 m/s to 0.07% at 75 m/s. The 10 interchangeable octagonal test sections are 1.80 m wide, 1.25 m high and 2.60 meters long.

The model used was again model 14. A polyurethane foam model was made of the above water part of the hull. The boom, gaff and mast were made of wood and the sails of spinnaker rip-stop nylon. Figure 6 shows a typical rig of a skûtsjes. The scale factor was 1:25, resulting in a model of about 80 cm length and a mast height of 73 cm. The total sail area became 0.273 m², resulting in a maximum blockage of the test section of about 16%.



main sail AR = 2.1 and jib AR = 4.4
Combined AR = 2.9

Figure 6 Typical rig skûtsje

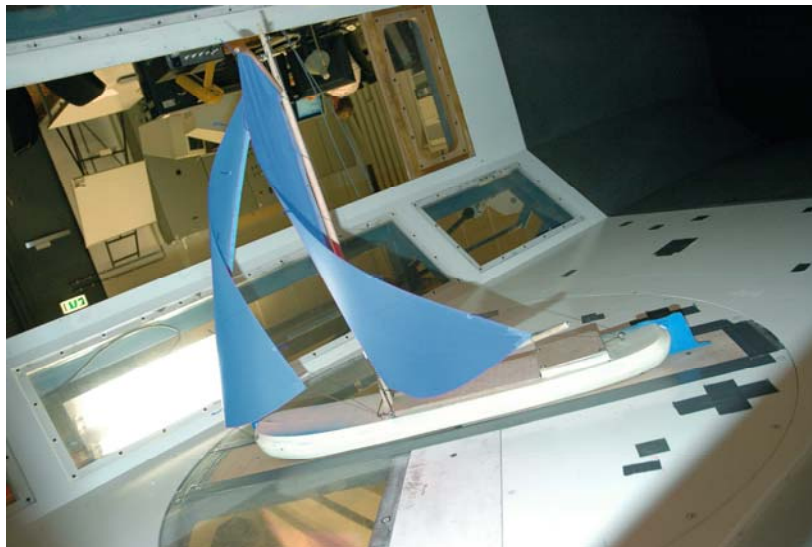


Figure 7 Test setup wind tunnel

The model was attached to a mechanically actuated turn table flush with the tunnel wall allowing the model to be rotated around its vertical axis. The model itself was attached to a force balance system, allowing the accurate measurement of forces and moments on the model in six degrees of freedom. The test setup is depicted in Figure 7.

The data acquisition system recorded the forces and moments on the model, the orientation of the model (the angle of attack), and the flow velocity.

For correct scaling the Reynolds number should be kept constant for model and full scale, resulting in very high flow velocities (full scale wind velocity times the scale factor). Nevertheless, the flow velocity in the wind tunnel is limited by the power of the sheet winches and by the structural strength of the model. Additionally, it would be very hard to find materials for mast and sails that would have similar deformation compared to the full scale materials within the limits of the model geometry.

For that reason, the velocity for sail testing in wind tunnels usually is kept much lower and the inaccuracies due to the incorrect scaling are taken for granted. The only way of restricting dissimilarity between model and full scale is using larger models. A flow velocity of 7 m/s was found to be feasible for the test setup. At larger flow velocities the deformation of mast and sails became unrealistically large.

A boundary layer profile of the flow on the model was achieved by mounting the model flush on the tunnel wall. Generally for wind tunnel experiments a very thin boundary layer is required. For this reason most facilities are designed to minimize the boundary layer thickness. For the wind tunnel tests presented here the boundary layer profile was assumed to have the same shape and relative thickness as its full scale equivalent. The velocity gradient has not been verified.

In real life a ship sailing at forward speed will encounter a different apparent wind velocity and apparent wind angle at different heights above the water level, due to the velocity gradient. This is known as twist. No twist stimulation has been performed for the wind tunnel experiments.

The wind tunnel boundaries have additional effects on the flow about the model. Rea and Pope (1984) separate three distinct effects:

1. Lateral constraint to the flow pattern around the body, solid blockage, leading to an increase of the flow velocity around the body.
2. Lateral constraint to the flow pattern around the wake, wake blockage, again leading to an increase of the flow velocity around the body.
3. Alteration to the curvature of the flow due to lifting devices due the tunnel walls, leading to an increase in angle of attack.

These three influences are discounted in the measured data.

Testing procedure

As stated, a flow velocity of 7 m/s was chosen. The driving force, heeling force, and heeling moment were measured for a range of apparent wind angles of 10 (close hauled) to 180 (running ahead) degrees at intervals of 2 degrees upwind and of 5 and 10 degrees downwind. At each apparent wind angle the sheeting of jib and main sail was adjusted to yield the maximum driving force. With this sail setting fixed the apparent wind angle was adjust to +4, +2, -2, and -4 degrees. At all 5 points the forces and moments were measured, along with the flow velocity and air density to obtain the force and moment coefficients.

Additionally, the bare poles forces at the same range of apparent wind angles were measured.

Data processing and results

The bare pole forces were subtracted from the full sail set forces. Subsequently, the force and moment coefficients were corrected for the three blockage effects and the enveloping curve was found for the maximum driving force for each apparent wind

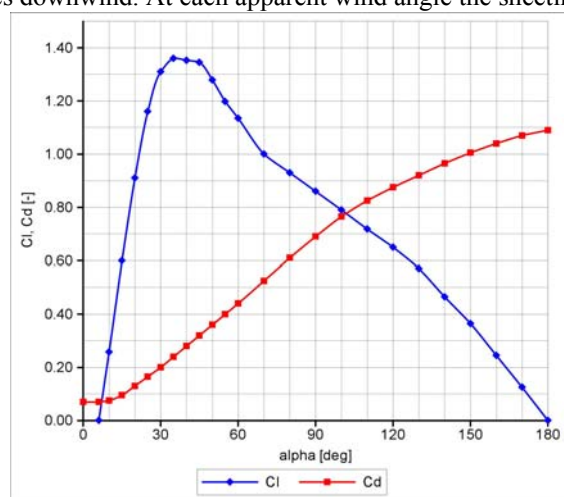


Figure 8 Aerodynamic lift and drag coefficients

angle.

The lift and drag curves were constructed by selecting the corresponding points on the heeling force curve and conversion of each driving force-heeling force pair to lift and drag. The resulting curves were slightly faired. The faired data is depicted in Figure 8. At large apparent wind angles (larger than 150 degrees) deviations were visible between the raw and faired data. These were caused by the irregular behavior of the jib that was partially covered by the main sail. In the faired data this effect has been removed.

Sail model

The faired lift coefficient determined above has been used directly in the sail model and is designated C_{l0} . The drag has been further processed, in order to implement dependence of the rig on the rig dimensions. In particular dependence on the aspect ratio has been added. Therefore, the drag has been separated in several components:

$$C_d = C_{d0} + C_{ds} + C_{di} + C_{dhull} + C_{drigging} \quad (15)$$

The induced drag is determined by:

$$C_{di} = \frac{C_l^2}{\pi AR_e} \quad (16)$$

With AR_e the effective aspect ratio of the rig, equaling the geometric aspect ratio times a efficiency factor e . This factor has been found by fitting the slope of the $C_l^2 - C_d$ -graph (refer to Figure 9) for small angles of attack. Using this approach, a value of 2 has been found for the efficiency factor e .

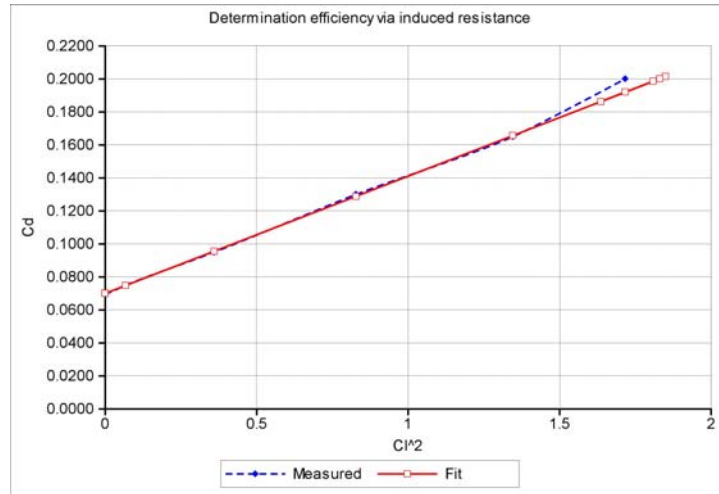


Figure 9 Determination of effective aspect ratio

The quadratic separation drag is given by:

$$C_{ds} = 0.016C_l^2 \quad (17)$$

And finally the remaining part of the drag C_{d0} can be found by subtracting the induced drag and the quadratic separation drag from the measured drag that in turn was already corrected with the bare poles measured data. The values for C_{l0} and C_{d0} are tabulated for a range of apparent wind angles. In the VPP use is made of interpolation to find the correct values. After this the other drag components are computed and added to the interpolated aerodynamic drag.

5.3. Windage

The windage has been subtracted from the measured data. In general due to scale effects (mostly Reynolds effects) the windage measured in the wind tunnel is too high and is therefore discounted from the measured data.

In the VPP the drag due to hull and rigging is determined as follows:

$$\begin{aligned} C_{dhull} &= 0.764 fva^2 (B_{oa} [0.5 \cos(\alpha') + 0.5] + L_{oa} \sin(\alpha')) \cdot (EHH \cos(\varphi) + B_{oa} / 2 \sin(\varphi)) / A_{ref} \\ C_{drigging} &= 1.1 \cdot A_{rigging} / A_{ref} \end{aligned} \quad (18)$$

The first equation is adapted from Hansen et al. (2002). In this equation fva is the speed reduction from the center of effort height to the half hull height due to the assumed wind gradient and α' the apparent wind angle at the hull. EHH is the effective height of the hull and B_{oa} and L_{oa} are the overall width and length of the hull. $A_{rigging}$ is the combined area of all rigging. In this case only the mast has been included, as it was assumed that the bare sail coefficients already took most of the other drag components into account.

The effect of heeling is for these relatively wide and shallow boats very large and has been included in the windage.

Center of effort height

The height of the center of effort is determined in a simplified manner, taking into account the geometric dimensions of the sails, the windage and the relative loading of the various windage components.

6. VELOCITY PREDICTION PROGRAM

6.1. General approach

The velocity prediction program integrates the resistance model, the stability, and the aerodynamic model. The VPP presented here is built along the lines of the VPP as described by Kerwin (1975) and by Claughton et al. (1998).

In synthesis it works as follows:

1. A true wind velocity and true wind angle are assumed. Based on an assumed boat speed the apparent wind velocity and direction can be found.
2. The aerodynamic model (section 5) is used to find the heeling force and driving force due to the combined sail forces and influence of the hull and rigging.
3. The heeling force causes a heeling moment that is balanced by the stability. Using the curve of arms of stability (section 4) the resulting heeling angle can be found.
4. The heeling angle influences the center of effort height and thus the apparent wind velocity and angle and moreover has an influence on the profile of the sails. Steps #2-#4 are repeated until a consistent heeling force and heeling angle are found.
5. Now the resistance is calculated at the assumed boat speed. The resistance is found using the resistance model (section 3) and is composed of:
 - a. Upright viscous and residuary hull resistance, both dependent on the boat speed.
 - b. The change of hull resistance due to heel; again split in a residuary and a viscous part. These components are dependent on the boat speed and heeling angle.
 - c. The change of hull resistance due to trim, dependent on the trimming moment and the boat speed.
 - d. Induced resistance, dependent on boat speed, heeling angle, leeboard position, and magnitude of the side force.
 - e. The appendage resistance. The rudder resistance is included in the upright hull resistance. Remaining is the part of leeboard resistance that is not included in the induced resistance.

This part consists for the most part of viscous resistance and dependent on the boat speed and the leeboard position.

6. The resistance is compared to the driving force. The boat speed is adjusted until the driving force equals the resistance. Generally this velocity will divert from the assumed velocity in step #1 and the whole process is continued until the velocity calculated in step #6 equals the velocity used in step #2.

6.2. Optimizations

For the velocity iteration a bisection method has been employed to enhance the stability of the iteration.

Moreover a scheme has been implemented to control the heeling angle. A so-called reefing angle is preset. When the heeling angle increases beyond this reefing angle a depowering scheme is invoked, using reef and flat parameters to reduce the sailing forces until the heeling angle is below the threshold set by the reefing angle. When the iteration results in the boat speed, the reefing angle is increased and the procedure is repeated until the boat speed starts decreasing or when the reef and flat parameters become unity. Now it is assumed that the optimum boat speed and heeling angle at this wind angle and speed has been found. This scheme is in accordance with the work of Kerwin (1975).

The reef and flat parameters have been incorporated as follows:

$$C_{d0} = reef^2 C_{d0} + reef^2 flat^2 C_{ds} + reef^2 flat^2 C_{di} + C_{dw} \quad (19)$$

$$C_{l0} = C_{l0} reef^2 flat$$

In the VPP it has been assumed that the reefing is preset in the input by specifying a sail set for each wind speed. For this reason the reef parameter is only allowed to operate in narrow band from 0.9 to 1.0. The flat parameter is allowed to operate in a much broader band. In practice flat was never found to be smaller than 0.85.

Figure 10 shows the influence of the reef and flat parameters along with the preset reefing on the lift and drag coefficients of the sails. The continuous line represents the original sailing model. The circles represent the sail model as used for low wind velocities (4 m/s). Clearly no reef and flat is used in this case. The crosses show the sail model as used for higher wind velocities (9 m/s). In this case the reefing is preset and shows as a reduction of both the lift and drag for all apparent wind angles. The flat parameter is used for apparent wind angles below 50 degrees and shows as a clear reduction of the lift and a slight reduction of the drag.

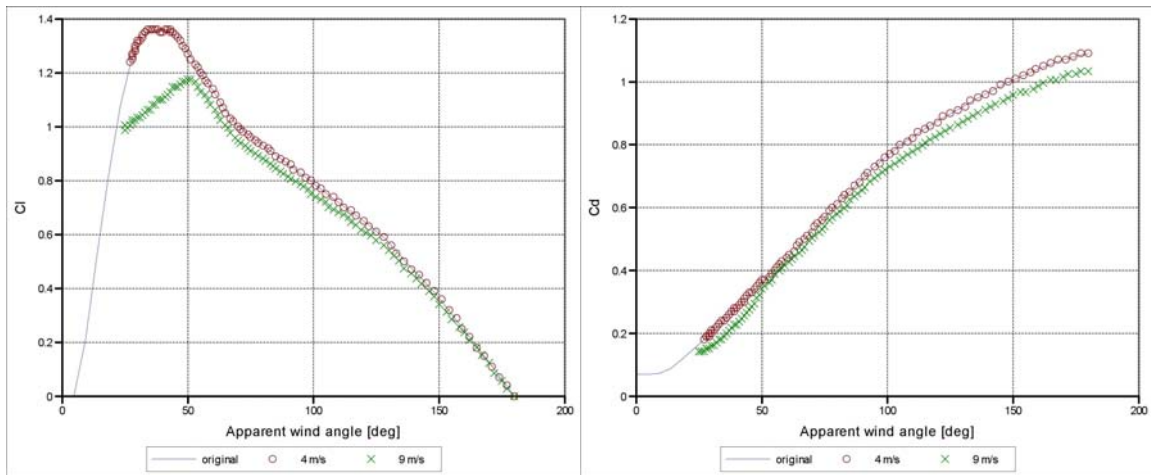


Figure 10 Influence of reefing and flat on the lift (left) and drag (right) coefficients of the sails

Additionally, the VPP calculates the optimum speed made good.

6.3. Input and output

The input to the VPP consists of the true wind velocities and angles, the main dimensions of the ship and sails and of control parameters for the VPP.

The output consists of polar plots and hydromechanic and aerodynamic force tables. Besides that, the VPP is capable of producing the results of the boat on a predefined race course in terms of sailing time and velocity on each leg of the course. The latter data can be used to compare the performance of different boats.

Figure 11 shows a typical polar plot

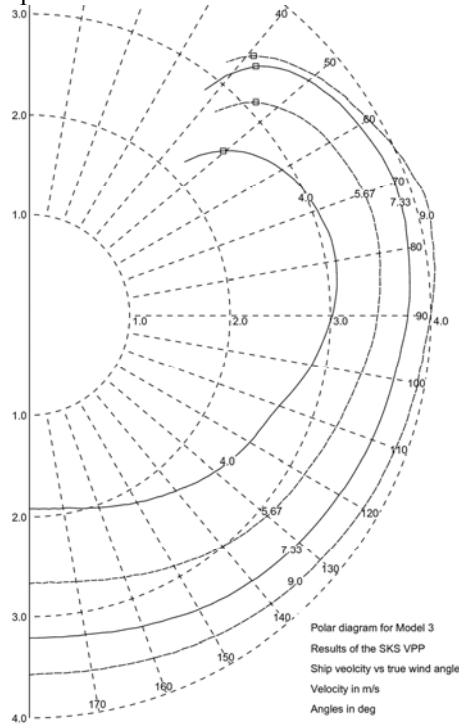


Figure 11 Polar plot Model 14 based on true wind velocity and angle

7. RESULTS

7.1. Comparison of the sailing performance

To compare the performance of the 14 skütsjes the results of the VPP have been used to calculate the sailed time on racing course at four different wind velocities, ranging from 4 m/s (3 Bft) to 9 m/s (5-6 Bft). The course selected was the course of the race at Terherne in the Sneekermeer as used in the 2007 season. The course depicted in Figure 12 had an hourglass shape. The top and bottom legs of the course were aligned with the wind, requiring the boats to tack; both diagonal legs were running courses. Table 2 shows more detailed data of the course.

Wind direction	229	Deg	
leg	course	true wind angle	Length
1	tacking	0.7 deg	1363 m
2	running	156 deg	1315 m
3	tacking	0.6 deg	1318 m
4	running	160 deg	1570 m
total			5567 m

Table 2 Data of the racing course

The performance on the adverse wind courses was calculated by using the speed made good, while the performance on the running courses was calculated using the polar data at the true wind angle of the course. The performance over the complete course was expressed in terms of sailing time per nautical mile. Table 3 shows the averaged values for each wind velocity.



Figure 12 Construction of the racing course

Wind velocity	sec/n.m.
[m/s]	[1/kts]
4.0	1003
5.7	754
7.3	642
9.0	597

Table 3 Seconds per nautical mile for four true wind velocities

Clear is the relative slower reduction of sailed time per mile when the wind speed increases. Two effects play a role here. First, due to the reduced water depth the ship resistance increases greatly when the boat speed increases. At the highest wind velocity the boat speed is around 4 m/s, which means a Froude number over the water depth of 0.80. At this Froude number shallow water effects will play an important part in the resistance. Secondly, due to relatively low stability the boats will need to use a reduction of sailing area at the higher wind velocities to avoid excessive heeling or capsizing, having consequences for the boat speed.

Figure 13 shows the deviations of the time per nautical mile from the average time per nautical over all boats per ship in percentages. The top figure shows the values averaged over the four wind velocities. The middle figure shows the values for the lowest wind velocity and the bottom figure for the highest wind velocity. The order of the boats is arbitrary and not equal to Table 1. A positive deviation means a slower ship. Clear is that the maximum difference between the ships is around 4% in terms of seconds per mile. This equals around 40 seconds per mile for the lowest wind velocity and around 25 seconds for the highest wind velocity. Both equal around 4 boat lengths per sailed mile.

Figure 14 shows the deviations of the average speed made good on the left hand side and the deviations of the average boat speed for the running courses on the right hand side. The top figures represent low wind velocity and the bottom figures the high wind velocity. A positive deviation means a faster ship.

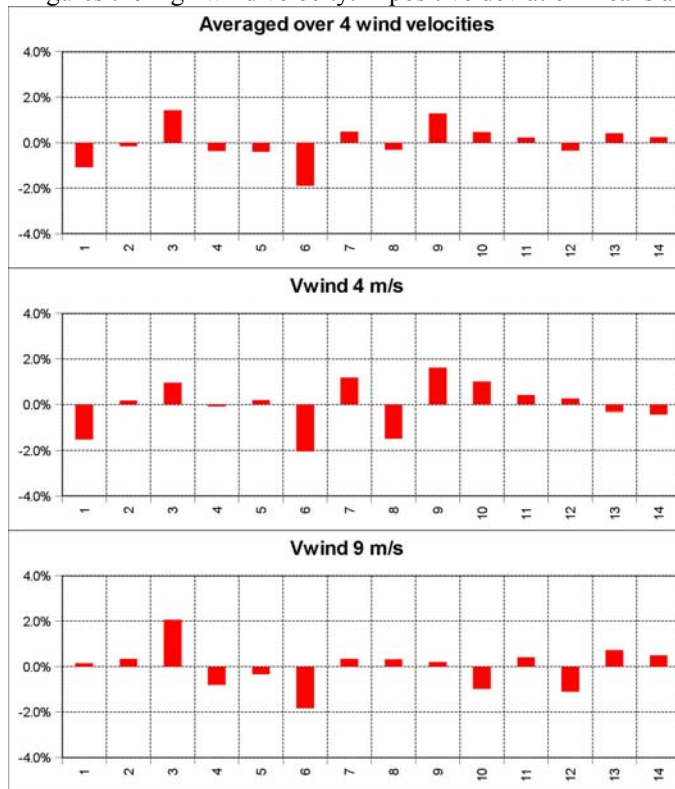


Figure 13 Comparison of deviations of sailed time per mile (positive: slower ship)

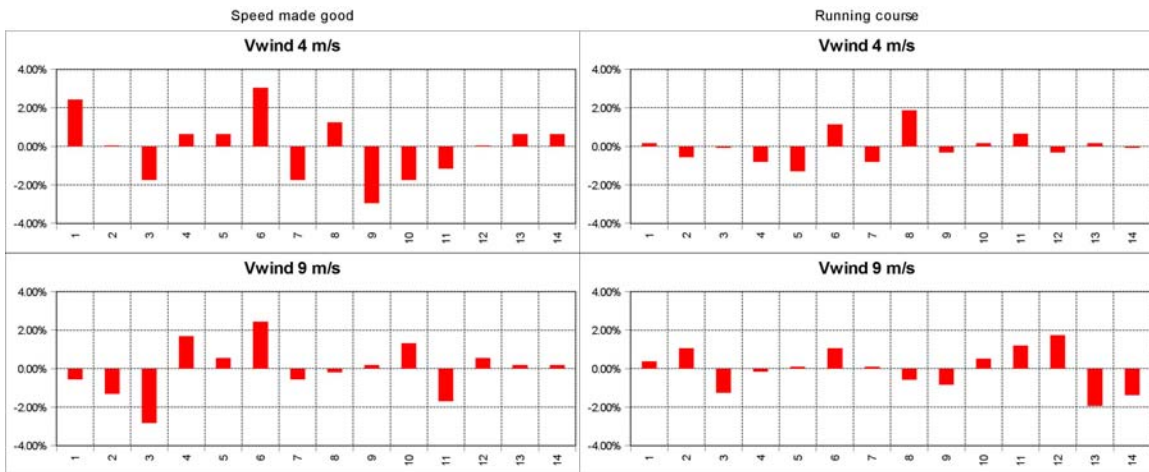


Figure 14 Comparison of deviations of the speed made good and the running speed (positive: faster ship)

It is apparent that the most important differences, up to 6 %, in boat performance are found in the speed made good, while the differences in performance for running courses are limited to maximum 3.5%. Clearly, the highest gains are made when tacking and the differences between the ships are less critical for the performance on running courses.

When studying Figure 13 and Figure 14 it stands out that there are ships that perform better at low wind velocities and have a degrading performance when the wind velocity increases, for instance numbers 1 and 2, and the other way around, like number 7 and 9. Boat numbers 1 and 2 have a relatively low stability,

while numbers 7 and 9 have a much higher stability. This could partly explain the differences found between these boats. For when the wind velocity increases the stability becomes increasingly important to counteract the increasingly higher heeling moment. Boats with relatively low stability have more difficulties in counteracting the heeling moment and need to reduce the sailing forces much earlier, leading to a reduced performance at higher wind velocities.

7.2. Comparison sailing time difference in real life and according to the VPP

When observing the data from real sailing races a typical difference between the fastest and the slowest ship is 10 to 15 minutes for a race that lasts typically 2 hours. The VPP predicts in similar circumstances maximum 4% difference between fastest and slowest ship, which comes down to around 5 minutes. Disregarding the simplifications made in the model and the fact that the model is not aimed at predicting the absolute performance, this would mean that around a third to a half of the performance differences between the ships can be explained with the technical differences between the ships, while the remaining part can be attributed to differences in skill of the teams and the fact that the VPP neglects interaction effects between the boats and maneuvering.

8. CONCLUSIONS

The setup of a velocity prediction program for traditional Dutch sailing vessels of the type skûtsje has been detailed in this paper. The aim of this VPP is to verify the handicap rule currently employed by the race organizer (the SKS) and when necessary to provide a means to setup a new handicap system. The background of the three main parts of the VPP, the resistance model, the aerodynamic model, and the stability, has been detailed and the inner workings and optimizations of the VPP have been described.

Results have been shown for the performance comparison of the 14 skûtsjes of the SKS fleet. A maximum performance difference between slowest and fastest boat has been found of around 4% in terms of seconds per nautical mile. This means about 4 ship lengths difference per sailed mile. The predicted differences are compared to the differences occurring in real life sailing races with the same boats and are found to be of the same order of magnitude, being around a third to a half of these differences. The remaining difference can be attributed to crew skill and the fact that interaction effects between the boats and maneuvering are neglected.

In conclusion it can be stated that the newly developed VPP is found to be suitable to quantify the performance differences between the boats it is aimed for and in such way can be used as a tool to verify and when necessary improve the handicap rule used by the SKS. It is emphasized that the VPP is specifically aimed at quantifying performance differences between the skûtsjes and not at providing an absolute estimate of the performance of individual boats. For such estimated would require a much higher level of attention to the details of each boat, outside of the scope of this research.

It should be noted that this VPP contains force models especially tailored and suited for the 14 SKS skûtsjes and care should be taken when the VPP is applied to ships of different hull form and sail plan and outside of the parameter range of the 14 SKS skûtsjes.

ACKNOWLEDGEMENT

This research has been commissioned by the Kenniscentrum Jachtbouw of the Noordelijke Hogeschool Leeuwarden with support of the Sintrale Kommisje Skûtsjesilen, the Province of Fryslan and the Samenwerkingsverband Noord-Nederland (the Northern Netherlands Provinces).

REFERENCES

1. Cloughton, R.A. Sheno, and J.F. Wellicom. *Sailing Yacht Design - Theory*. Addison Wesley Longman, WEGEMT, 1998.
2. Larsson, L. and R.E. Eliasson. *Yacht Design*. Adlard Coles Nautical, London, 1994.
3. Indesteege, R.M.L. *Prestatieberekningen van zeilschepen*, Afstudeerwerk TUDelft, Rapportnr. 833-S, 1989.

4. Kerwin, J.E., *A Velocity Prediction Program for Ocean Racing Yachts*, Report 78-11, Department of Ocean Engineering, Massachusetts Institute of Technology, 1975.
5. Gerritsma, J., Onnink, R. and Versluis, A., "Geometry, resistance and stability of the Delft Systematic Yacht Hull Series" *7-th HISWA Symposium*, 1981, Amsterdam
6. Gerritsma, J. and Keuning, J.A., "Performance of Light- and Heavy-displacement Sailing Yachts in Waves", *The 2nd Tampa Bay Sailing Yacht Symposium*, St. Petersburg, 1988.
7. Keuning, J.A., Onnink, R., Versluis, A. and Van Gulik, A., "The Bare Hull Resistance of the Delft Systematic Yacht Hull Series", *International HISWA Symposium on Yacht Design and Construction*, Amsterdam RAI, 1996
8. Keuning, J.A. and Binkhorst, B.J., "Appendage Resistance of a Sailing Yacht Hull", *13th Chesapeake Sailing Yacht Symposium*, 1997
9. Keuning, J.A. and Sonnenberg, U.B., "Approximation of the Hydrodynamic Forces on a Sailing Yacht based on the Delft Systematic Yacht Hull Series", *International HISWA Symposium on Yacht Design and Construction*, Amsterdam RAI, 1998.
10. Rae, W.H. and Pope, A., *Low-Speed Wind Tunnel Testing*, Second Edition, John Wiley and Sons, New York, 1984.
11. Wagenaar, M. *Rompvorm en stabiliteitsmeting veertien SKS skûtsjes*. Rapportnr. 07.216, Annmar Engineering, Kraggenburg, 2008.

Session 10

Clay Oliver & John Robinson

'Development of a Vpp based rating for J-Class Yachts'

Clay Oliver, Yacht Research International, and John Robinson, Wolfson Unit MTIA.

Abstract

The J-Class was originally one of a number of level rating classes, developed under the 'Universal Rule', rating at 76 feet. The class was designated for each of the three America's Cup series from 1930 to 1937. Most of the yachts were either scrapped or laid up at the end of the 1930's, but more recently interest in the class has revived. Following refits and restorations, and one complete rebuild, there is now a class association and interest in further builds is strong, with two new boats already well into construction and fit out.

For several years, the J-Class Association has run regattas based upon a Time Correction Factor (TCF) calculated using the standard WinDesign Velocity Prediction Program (Vpp). In 2007, the Association transferred the operation of this rating system to the Wolfson Unit both as a measure of independence and further to refine the process.

The form and proportion of the J-Class contrast dramatically with those of the modern yachts which have largely driven developments in VPP hydrodynamic formulations in recent years. This paper describes the some new formulations geared specifically to the J-Class yacht, and generally applicable to the traditional yacht. The fact that the keel and hull of the traditional yacht cannot be rationally delineated is an issue and an approach to obviate this problem is described. Data from 1936 towing tank experiments of 1/24th and 1/8th-scale J-Class models are reanalyzed for new J-Class Vpp formulations. These include a specific wave resistance formulation and extensions to the heel drag model that treat vertical volume distribution and the relatively long overhangs of the J yacht.

The overall approach to rating J yachts is described, along with a summary description of the existing fleet. The final TCF ratings are presented and compared with previous years' ratings, as well as the Time Allowance calculated under the 'Universal Rule' itself, and a comparison is made of these different ratings for the existing J-Class competitors in their modern configurations.

Introduction

The J-Class has its roots in the evolution of sailing yacht design on both sides of the Atlantic. Driven by different measurement systems in the late 19th century, the trend in Europe was narrow and deep, and in America, wide and shallow. Neither system produced particularly satisfactory results. Interestingly, the much criticized plank-on-edge designs of that period had lower ballast ratios than the America's Cup Class (ACC) yachts of today.

Both traditions were clearly in need of better regulation, both to improve design and also to make racing more equitable. Around the turn of the 20th century two new rating rules were introduced that have stood a reasonable test of time: the International Rule in Europe, still with us in the form of the metre yachts, 6, 8 and 12; and the Universal Rule in America, developed by Herreshoff and adopted in 1902 by the New York Yacht Club.

The rule itself was a simple formulation relating an effective rating in units of length, to the length, sail area and displacement of a yacht.

$$Rating = \frac{0.2 \times L \times \sqrt{S}}{\sqrt[3]{D}}$$

This rating could be used in two ways, either to provide handicapping data on a time allowance in seconds per mile, again worked out by Herreshoff, or as a means of grouping yachts by level rating, which is where the alphabetic I, J, K, L down to S classes arose. The I class yachts had a rating of 88 feet, J's of 76 feet, and so on to the S class with a rating of 17 feet. Like all rules, the 'Universal' gradually became hedged about with particular restrictions as designers worked out how to adapt designs to achieve a favourable rating, but its fame today rests on its role in the history of the America's Cup, and the legacy of the 'Big Boats' still sailing today.

In 1928, the rule was adopted for future America's Cup racing, and more specifically the J-Class rating length, but it was not until 1930 that the first of three Cups was raced under it, pitting Sir Thomas Lipton's last Shamrock V, against Enterprise. Two further sets of races were held in J's, in 1934 Endeavour against Rainbow, and 1937 Endeavour II against Ranger. It was this era that still quintessentially defines opulence in yachting, even now in a time where sailing super yachts of 60 – 70 metres in length have become almost unremarkable. That era did not last, and of the ten J-Class yachts built in the period, all except Shamrock were scrapped or laid up by the end of the 1940's.

But they were not forgotten, and as large yacht sailing prospered again in the late 20th century interest in the boats revived. Velsheda and Endeavour were rescued from their mud berths, and rebuilt. Shamrock was restored closer to her original rig, and when they reappeared on the classic racing circuit a new J-Class Association was formed to preserve the tradition and promote the class. The success of the association means that new boats have been, and are being, built to the class rules, the most important of which is that a yacht can only call itself a J if it is built to lines of those either built or proposed in the 1930's.

Where the original boats were seen only as day racers, the restored and newly built vessels are true super yachts. They have interiors, and engines, and tanks of fuel and water. All of this means that none complies with the original J rating under the Universal rule, so, if they were to compete equitably, a new method of rating needed to be determined.

Initial use of the existing WinDesign Vpp for J-Class rating

Providing a rating for a modern J-class is not so simple. They can be measured under IRC, and indeed often race under that rule, but like all modern rules it is more suited to a modern design where keels and rudders are separate from the hulls. So when the Dijkstra office was asked to propose a method of handicap that could be used for J-Class only regattas, they turned to the modern Velocity Prediction Program, that can match aerodynamic and hydrodynamic performance with inherent stability, and predict times around courses. Dijkstra & Partners were already using the WinDesign Vpp in their project work, so it was natural for them to select it for working on the J ratings as well. As

consultants to all of the existing vessels and prime movers in the formation of the J-Class association, they were particularly well endowed with data on the yachts.

As with the modern rating formulations, the existing Vpp contains information more akin to the modern yacht forms than long keel J boats. So it was necessary to try and break the yacht up into a hull and separate keel. Methods to do this were devised, and, using a particular version of the program in order to maintain stability of the resulting speed predictions, TCF values were calculated by comparing the predicted times around windward-leeward and random courses against a base boat, Velsheda in her 2001 configuration was chosen as the base boat.

The resulting TCF values were used successfully for several seasons, as the data matched the perceived performance on the race course sufficiently well, particularly as racing was restricted to the three existing boats, and more often to Endeavour and Velsheda alone.

As interest grew, and with the advent of a new boat with the 2004 rebuild of Ranger, it became clear that the existing Vpp-based system had its limitations. Alongside this, the interest of other designers in J-Class projects meant that Dijkstra and Partners needed to stand back from direct control of the ratings. At this point, the J-Class Association asked the Wolfson Unit to undertake the required calculation in order to provide rating certificates, and also to examine the methods used and suggest improvements.

The first phase of work undertook to examine the sensitivity of the Vpp formulations to various hull parameters typical of a J-Class yacht, and in particular to the nature of the separation of the natural hull form into a canoe body hull and separate keel.

Although previously a more complex separation had been used to achieve this, it had already been proposed to base separation upon the concept of a horizontal cut at the level of the inflection of the midship section as shown in Figure 1. A new keel was then added below the horizontal cut, with the required volume and wetted area such that, when combined with the hull, it matched the full hull.

A study was undertaken by progressively moving the horizontal cut above and below the inflection point and calculating TCF values for each variant hull, as compared with the original cut position.

The resulting data are shown in Figures 2 and 3, and immediately highlight a significant problem with the use of this forced separation method within the Vpp. Different hull forms, even within the restricted range of J-Class shapes, reacted differently to the height of cut.

For Velsheda, there is a relatively simple variation in the TCF both with increasing wind speed and also as the horizontal cutting plane moves up and down.

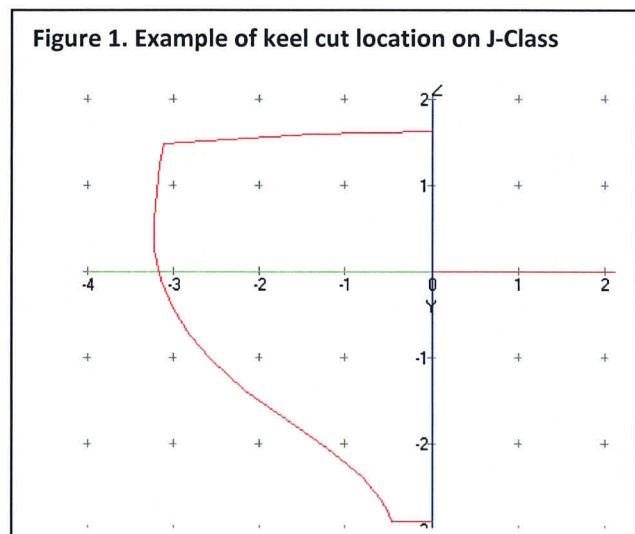
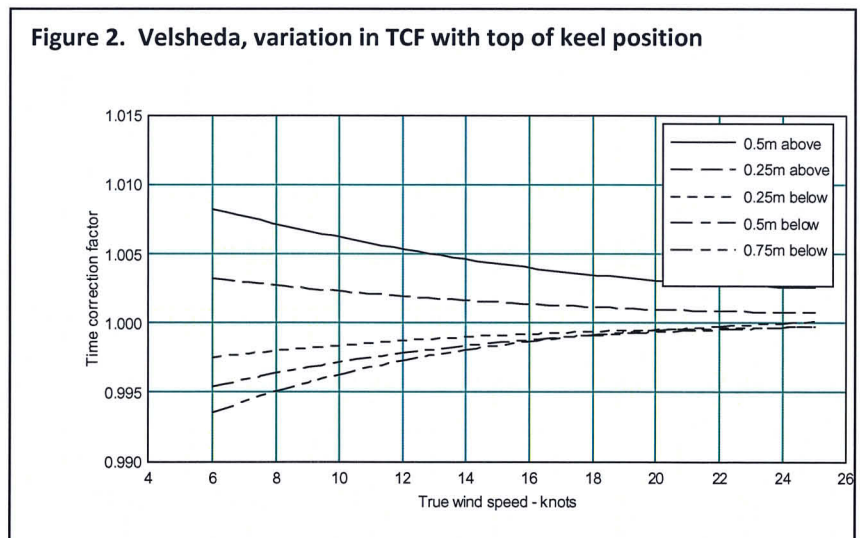


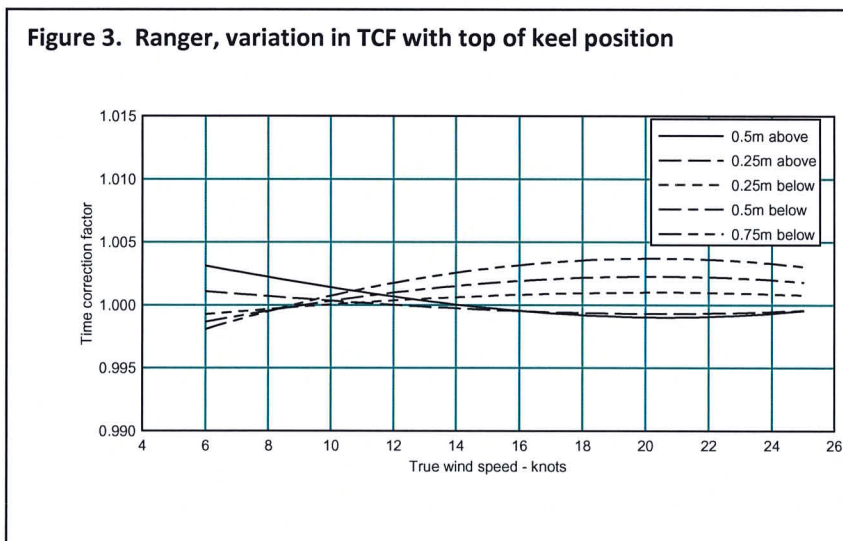
Figure 2. Velsheda, variation in TCF with top of keel position



However, for Ranger, in Figure 3, the situation is significantly different. Not only do the TCF data vary in a more complex manner with wind speed, but also there is a different relationship with the height of the cutting plane that separates hull and keel.

These differences imply sensitivity to cutting height that differs between yachts, and therefore means that the final ratings would depend upon the choice of position of the top of the keel. Clearly this is not an acceptable option, and so on this basis, the concept of separation into hull and keel was discarded.

However, the Vpp's hydrodynamic force calculations are based on upon such a separation, and so new methods had to be found in order to characterize the performance of classic long keel yachts in general, and J-Class in particular.



Existing Vpp methods

The modern yacht is characterized by a canoe body with clearly-defined appendages. This separation of parts has made the calculation of hydrodynamic forces relatively straightforward, inasmuch as we use one set of methods for the canoe body and then another set for the appendages.

For example, the canoe body viscous drag calculation typically uses ITTC frictional formulation, the Reynolds number based on *full* wetted length. A form factor derived by various means is applied to the frictional drag. By contrast, the appendage viscous drag estimate for fins and rudders works with 2D airfoil sections and associated data or methods. Bulb drag calculations assume streamline symmetric bodies with associated data and methods. For the calculation of upright wave drag, the effect of the appendages on the canoe body wave making drag is implicit in the canoe body wave drag formulations. The difference in upright wave drag due to the appendage variations between wide varieties of modern racing yachts is included assuming a standard modern yacht hull-keel configuration.

Traditional yachts with long integrated keels and attached rudders such as the J-Class do not easily divide into canoe body and appendage. In essence there is just the yacht, and the rudder, keel and hull are all melded into one elegant form. Nevertheless, various approaches have been used to try to apply to the classic yacht the "modern" canoe body/appendage procedures of LPP and VPP. One approach is to place a horizontal cut at some water plane, as described above, with the consequences shown, others rely on direct use of the hull parameters in order to determine resistance in the normal characterization as a combination of elements due to upright, heeled and induced parts, but little data had previously been used to check these.

Original towing tank data

Background

Happy with the performance of his new J-Class Endeavour II, T.O.M Sopwith in August 1936 issued an America's Cup challenge. Set for the end of July 1937 rather than the traditional month of September, he hoped there may be more wind in Newport at that time of year. In America the feeling was that no existing American J-Class was up to the task of defending against the Endeavour II. Harold Vanderbilt asked Starling Burgess and Olin Stephens (Sparkman & Stephens) to start on new designs.

The designers embarked on a model testing program at Stevens Institute of Technology (SIT) in New Jersey. A new 100-ft tank had been installed in 1935 and an era of testing very small yacht models

had begun, largely due to methods and efforts by Professor Kenneth S.M. Davidson, instructor of mathematics and Director of the tank, as described in the first reference [1]. The original tank test reports were kindly made available by Sparkman & Stevens for this project.

Each designer drew two new models designated 77A through 77D. A wider model 77F was tested, as well as some rudder and counter modifications to 77D and 77C, respectively. Models of several existing yachts were to be tested as well, including competitors in the 1934 Cup: Endeavour and Rainbow. A model of 1930 J-Class Weetamoe, previously tested [SIT Rept. 12] was included in the analysis. Table 1 lists the model particulars. Model 77C would become the basis for the yacht Ranger.

The new models followed the direction from Vanderbilt for the new design to go to the maximum of 87' waterline, longer than earlier J-Class yachts. There had been concerns about longer waterlines and heavier displacement in light airs, but these had been allayed after Vanderbilt had tried ballasting down Rainbow to 87' and found her light air performance to be surprisingly good.

Table 1. Full Scale Particulars of 1:24 Scale Models tested at SIT – 1936

Name	Particulars				Wetted Surfaces			Remarks
	SIT #	Lwl m	Bwl m	Dspl kg	No board m ²	Board m ²	Total w/b m ²	
Weetamoe #3	97	25.756		153460	194.17	---	194.170	<i>Previously tested - SIT R12</i>
Endeavour I	120	25.604	6.490	148844	196.12	7.804	203.927	<i>with estimated centreboard</i>
Rainbow	130	25.604	6.276	150064	191.57	6.736	198.306	<i>with 1936 keel</i>
77A	134	26.518	6.608	166028	206.71	8.919	215.633	<i>new 87' design</i>
77B	133	26.518	6.416	167189	205.79	8.919	214.704	<i>new 87' design</i>
77C	131	26.518	6.279	169163	203.46	8.919	212.382	<i>new 87' design(Ranger)</i>
77D	132	26.518	6.206	167479	201.79	8.919	210.709	<i>new 87' design</i>
77C2	131	26.518	6.279	169163	213.22	8.919	222.137	<i>77C rud profile ext. Not Tested</i>
77D2	132	26.518	6.206	167479	211.82	8.919	220.743	<i>77D rud profile extended</i>
77E	138	26.518	6.279	167682	203.65	8.919	212.567	<i>77C counter lower, f'body mod</i>
77F	139	26.518		167334	205.32	8.919	214.240	<i>new wide model</i>
77CE	140	26.518	6.279	169163	203.46	8.919	212.382	<i>lower aft profile of 77C</i>

A wide range of tests and analyses were conducted, including upright, heel-yaw, sea keeping and balance. SIT Report 34 presents the results of a "J-Boat Investigation for H.S. Vanderbilt, Esq. relating to the design of Ranger" [2]. The model scale was 1:24.

The typical size for tank models up to this point was at least 10 feet. A larger model of Ranger (77C) was tested at 1/8-scale at the Experimental Model Basin at the Navy Yard in Washington, D.C on November 4, 1936. At that time there may have been some concern about inadequate turbulence stimulation on the small models. In April 1937 a supplemental report [3] describes an investigation into the accuracy of the sand strip corrections, comparing to the drag of bare model behind a separately towed strut. The original comparison between Ranger and Endeavour was reworked and the report concluded with the statement, "Differences between the two boats are, of course, smaller than in Report 34, but an advantage for Ranger is still indicated."

Basis for new formulations

In the development of new formulations for the J-Class, we wanted to use as much of these data as possible. This effort required various approaches to "back-out" useful information from SIT Report 34. Of the tested models we only have hydrostatic information for Ranger (77C) and Endeavour I. Note

that the J-Class yachts now race in heavier conditions than these. The particulars used for the test data analysis for Ranger and Endeavour are shown in Table 2.

Table 2. VPP Particulars, Endeavour I and Ranger (77C) corresponding to SIT 1/24 Tank Tests

	Endeavour	Ranger 77C	Wetted Surface		
Dspl	148500	169162	Heel	End	77C
Dsplc	148500	169162	0	192.593	202.111
Lwl	25.606	26.657	2	192.587	202.097
Lsunk	31.883	34.334	10	192.211	202.139
Bwl	6.49	6.275	25	191.356	203.380
Bmax	6.748	6.411	40	197.961	209.569
Tc	4.648	4.583	LWL		
Tmax	4.648	4.583	Heel	End	77C
Ax	11.573	12.693	0	25.606	26.657
Cp	0.496	0.488	2	25.598	26.651
Awp	116.17	118.15	10	25.419	26.497
LCB	-3.02	-2.91	25	25.275	26.424
LCF	-3.03	-3.02	40	25.930	27.301
GYR	0.25	0.25			
PIPA	0.083	0.083			
VCB	-0.928	-1.387			
ProjA	67.389	73.402			

The main task was to come up with the wave making drag for 77C. Knowing that the SIT procedure used the Schoenherr frictional formulation based on a 70% waterline Reynolds number, the so-called run-in procedure with a Prohaska plot yields a viscous correction factor that includes an aggregate sand strip drag and any bona-fide form factor. Thus the viscous drag and sand strip drag is subtracted from the SIT total full scale drag to give an estimate for wave resistance. This method actually allowed for very consistent curves of wave resistance when plotted against Froude number, irrespective of the original sand coefficients.

Using these data, a new base wave resistance curve was developed for the J-Class formulations. The parameters in the WinDesign wave resistance formulations include length-displacement ratio, beam-to-draft ratio, prismatic coefficient and longitudinal centre of buoyancy. Some small adjustments were made to other coefficients in the VPP, but at this point there is insufficient data from two tests carried out at 1:24 scale to suggest making any significant changes, other than to recast the base curve to fit these upright data. There is an indication from the 1:8 scale tests conducted at EMB that the small models had dropped out of turbulent flow at the lower speeds ($Fn < 0.275$).

Revised Vpp formulations

Formulations for the calculation of wave drag, heel drag, induced drag and viscous drag all include the Bwl/Tc ratio. Bwl is clear enough, but for a long keeled yacht the canoe body draft Tc is not. The

approach we use here defines a substitute non-dimensional $\frac{B}{Tc'}$ ratio as:

$$\frac{B}{Tc'} = \frac{Bwl^2}{0.9 Amax}$$

Modifications of various formulations for new J-Class data use this substitute B/T to achieve fits to various data. One can back out a substitute canoe body draft:

$$Tc' = \frac{0.9 A_{max}}{Bwl}$$

In the following sections we discuss how the Vpp computes various hydrodynamic forces. The principal focus is on those areas where the formulations have been modified or extended for the J-Class. More details on the formulations contained in the Vpp can be found in various papers and reports listed in the references [4] through [8].

Wave drag

Wave resistance is a function of the following four parameters:

Vol/Lwl^3	<i>Displacement-length ratio - total volume over length cubed.</i>
Bwl/Tc	<i>For J-Class, this becomes the effective B/Tc'</i>
LCB	<i>longitudinal location of centre of buoyancy</i>
Cp	<i>canoe body prismatic coefficient $\forall/(Lwl Ax)$ where Ax is maximum canoe body sectional area.</i>

These parameters are based on the physical characteristics of the boat in a given condition of flotation. An upright wave resistance C_w is evaluated as the sum of a Fn-dependent base coefficient and products of the above parameters with Fn dependent coefficients $A_0 - A_6$.

$$C_w = A_0 + A_1 \forall/Lwl^3 + A_2 Bwl/T' + A_3 LCB + A_4 LCB^2 + A_5 Cp + A_6 Cp^2$$

These coefficients were developed over the years for various types of boats and do not follow IMS or DELFT formulations. For the J-Class the base coefficient has been set to match the wave resistance curve from the 1:24 scale tank tests of Ranger. Thus model 77C from tank tests reported in SIT Report 34 is used as the base boat for the revised wave resistance formulations. The displacement-length ratio coefficients have been modified to be more applicable to these heavier traditional boats.

Heel drag

For the upright yacht with no side forces, wave drag and viscous drag comprise our estimate of total drag. We generally assume the hydrodynamic interaction between these two components is small enough to ignore. As it heels the yacht presents an asymmetric immersed form and generates side force, sinkage and trim typically vary as well. These heel-related changes and the asymmetric distribution of hydrodynamic pressure on the hull and its appendages produce a different wave system, creates induced drag, and affects the viscous drag.

The category of heel drag is in fact the collection of these various interrelated heel effects. For convenience, some of these effects are reasonably included in other categories:

- The variation in canoe body wetted surface with heel is accounted for in the canoe body drag calculations, and thus shows up as part of hull viscous drag.
- The effects of heel on induced drag are accounted for in the induced drag calculations.

The remaining effects relate mostly to wave drag changes and include:

- Change in effective length as the boat heels and trims.
- Asymmetry of hull as measured by upright Bwl/Tc ratio. Whilst the hull's wave system is modified by the asymmetric immersed shape, generally it is the appendages that produce

additional wave systems which are typically deleterious. The waves related to the appendages coming closer to the surface often make up the majority of the heel drag.

- Asymmetry due to a “flare” as parameterized by the ratio of B_{max}/B_{wl}

In addition to wave drag changes, heel-related form drag is added. Whilst the change in the boundary layer thickness and wake as the boat heels is not easily evaluated – with modern, beamier boats a pattern has often emerged in which increasing B_{wl}/T_c results in an increase in form factor. Certain yachts with full after bodies and high aft prismatic coefficients, e.g. International Metre Class will have high form factor upright, but this varies little with heel. So the basic heel model in the VPP will have a small component of form drag change as a function of B_{wl}/T_c , but not to C_p .

These components are shown in Table 3 below. The development of successful heel drag formulations requires a mixture of theory, experimentation and common sense. Because we have access to the LPP data for Ranger and Endeavour at this point, we have worked with their rather limited 1:24 scale heeled-and-yawed data. Determining the relative importance of various components requires some juggling with the limited data.

Table 3. Various components of heel drag formulations, noting the J-Class extensions.

Nom.	Physical	Description	Function Parameters	
			Std WinDesign	J-Class Model
R _{h1}	Wave	Change in effective length at sailing flotation	$Le(\varphi)$	$Le(\varphi)$
R _{h2}	Wave	Effect of overhangs with heel	not included	L _{sunk} – overhang effect
R _{h3}	Wave	Asymmetry of Hull	B/T	B/T
R _{h4}	Wave	Appendages volume & lift depth change heel	not included	VCB
R _{h5}	Wave	Additional mid-hull asymmetry due to flare	B_{max}/B_{wl}	B_{max}/B_{wl} – less important
R _{h6}	Viscous	Form drag change	B/T	B/T – less important

For the J-Class yachts under consideration, there is not a wide range of B/T ratio. There would be little “flare drag” and in cases where there is tumblehome one might say there is a negative flare effect – and it would be very small component. Also there will be negligible effect of the change of form factor with heel between the various yachts presently under consideration. Thus many of the functions that exist in the standard monohull Vpp formulations will have little effect on relative J-Class performance.

However, there are two areas for which extensions to the standard formulations are developed. The first area treats the fact that the J-Class has very long overhangs compared with the modern yacht. The overhangs on modern yachts have less of an influence on the change of effective length with heel than might be the case with the J-Class. Consequently a modification is included that will add a fraction of the “sunken length” to the heeled length $Le(\varphi)$ as a function of heel. The second extension is due to the fact that the long keels of the J-Class effectively spread out the concentrated keel and rudder wave that are significant constituents of the modern yacht heeled wave pattern. Both these extensions to the standard WinDesign formulations are described below.

Inclusion of long overhang in heel drag

As the boat heels over the effective waterline length changes and this is evaluated by the LPP for five heel angles. In the VPP the heeled length is used to evaluate the heeled Froude number, which is then used as the argument in the wave resistance formulation. In the VPP we actually evaluate the difference in the wave drag with this modified Fn compared to wave drag with upright Fn . This gets thrown in as heel drag and can be negative or positive:

$$R_{h1} = R_w (Fn_{upr}) - R_w (Fn_{\theta})$$

As the J-Class yacht heels, the effect of the overhangs as measured in the LPP as the sunken length $L_{sun k}$ comes into play. Additionally it should be pointed out that $L_{sun k}$ does enter the picture at low speeds, but as the bow and stern wave effectively extend the length of the boat $L_{sun k}$ becomes influential. Because we presently calculate $L_{sun k}$ only for the upright condition, we will apply a function to introduce a portion of the additional length as the boat begins to heel. R_{h2} is the component of heel drag we have introduced for the J-Class, but for convenience we calculate the sum $R_{h1} + R_{h2}$ by using the revised heeled-overhang length L_{h2} for the Fn_{θ} in the above equation. This heel-overhang length is:

$$L_{h2} = (1 - t)L(\theta) + t k_{h2} L_{sun k} f(\theta)$$

where

$$k_{h2} \sim 0.25$$

$$f(\theta) = \frac{\sin^{2.5}\theta}{\sin^{2.5}25}$$

$$t = \sin^4[\pi(Fn - 0.025)] \dots Fn < 0.525$$

$$t = 1 \dots Fn \geq 0.525$$

Effect of vertical centre of buoyancy on heel drag

In the standard Vpp wave resistance model, a component of heel drag is tied to B/T ratio. For the modern yacht a higher B/T will generally result in higher heel drag, partly due to adverse affect on the yacht's wave system from greater asymmetry, and more so from the keel wave. A linear function of B/T ratio has seemed work reasonably well in the past.

$$R_{h3} = k_{h3} \frac{B}{T_c} R_w$$

where

$$k_{h3} \sim 0.015$$

For the J-Class, the coefficient k_{h3} in the above equation is less than what is used in the standard monohull formulation because of the lack of the concentrated keel wave. For the long keel yachts, more of the total volume is placed further down in the long keel. Thus for the J-Class yacht it seems more appropriate to consider how wave making drag is modified as the yacht heels due to vertical movement of volume towards the free surface. The characteristic parameter to which we will tie this movement will be the vertical center of buoyancy vcb of the yacht. Our approximation will broadly derive from hydrodynamic theory from J-Class era, part of which is presented in 1936 by Havelock [9].

The approximation is derived from the fact that the Kelvin wave spectra can be written as an integral over a Havelock distribution defining the hull surface. We assume this distribution is not a strong function of depth and also where the primary wavelength ($2\pi v^2/g$) is large compared to the maximum draft.

Wave resistance is proportional to the integrated square of the magnitude of the spectra function, and in that function we approximate the depth dependence as $(T_c e^{kz_b})^2$ where $k = g/v^2$ and z_b is the vertical centre of buoyancy ($z_b < 0$). We will remove the T_c from the relationship because it is not an

explicitly defined parameter for the J-Class, and its effect is treated through the B/T ratio term used in drag component R_{h2} .

We can write the following approximation for one component of heel-related wave resistance:

$$R_{h4} = k_{h4} r^2 R_w$$

where

$$r = \frac{e^{k z_b} - e^{k \cos \theta z_b}}{e^{k z_{b0}} - e^{k \cos \theta z_{b0}}}$$

$$k_{h4} \sim 0.05$$

$$z_{b0} = \text{reference vertical center of buoyancy} = -0.9284$$

$$R_w = \text{upright wave drag}$$

Imagine a hypothetical J-Class, call it Yacht 1 (Y1), that has a vertical volume distribution yielding a deeper vcb than Yacht 2 (Y2). As a yacht heels, its relative movement of vcb from its upright position is $vcb (1 - \cos \phi)$. As both yachts heel, the Y1 vcb moves a greater distance toward the free surface than Y2 vcb. The result will be an increase in this component of wave drag for Y1 relative to Y2. The effect of this relative shift depends on the speed, through the wave number. It should be emphasised this is but one factor of upright wave drag, and the wave drag would be different for Y1 and Y2 -- the J-Class with a lower vcb would probably have smaller Bwl , as in the case of Ranger vs. Endeavour.

Viscous Drag

The usual approach in WinDesign for the calculation of canoe body viscous drag uses the ITTC frictional formulation line with a canoe body form factor. A typical form factor for a modern yacht is about 1.10 ± 0.02 . Big bustles featured in International Twelve-Metre class, for example, may be in excess of 1.14.

$$R_{vc} = q k_{form} C_f S_c(\phi)$$

In which:

k_{form} canoe body form factor, typically ranging from 0.10 - 0.15 (use .125 as a typical value)

C_f $0.075/(\log(Rn)-2)^2$ friction coefficient from the ITTC formulation and Reynolds number Rn is evaluated using full wetted length.

$S_c(\phi)$ canoe body wetted surface at heel ϕ in still water

On top of the canoe body drag is added the appendage drag. There are various methods for this in WinDesign which generally use 2D airfoil section drag coefficients as a function of Reynolds Number, or alternately ITTC formulation with widely-used form factor fits as presented by Hoerner.

Because of sensitivity of results to the cut line approach previously used shown, the normal method needs to be modified. Other methods were considered such as slicing up the whole yacht into

longitudinal strips and then applying some blend of 2D airfoil sections and ITTC frictional formulation, but this just introduced one more layer of arbitrariness.

Like many others, we have carried out numerous approaches over many years of tank testing and research to calculate hydrodynamic viscous drag. As a gesture to traditional methods with a traditional yacht, we employ the procedure of calculating a single effective Reynolds Number for the whole yacht. The reference length for the Rn is 70% of waterline length (in racing flotation.) The form factor is set to 1.00 and there are no separate appendage calculations. The total wetted surface calculated is calculated as a function of heel angle.

Induced Drag

The induced drag is calculated using the convenient concept of effective span Te according to:

$$Di = L^2 / (2\pi q Te^2),$$

The effective span Te is calculated by

$$Te = k_1 f(Vol/L^3) f(Fn) f(B/T) f(\phi) Tr$$

The reduced draft Tr is evaluated according to slender body theory assuming a semicircular cross section and trailing edge of keel near the position of maximum sectional area:

$$T_r^2 = T_{max}^2 - 2 A_x / \pi$$

Comparison with the original test tank data

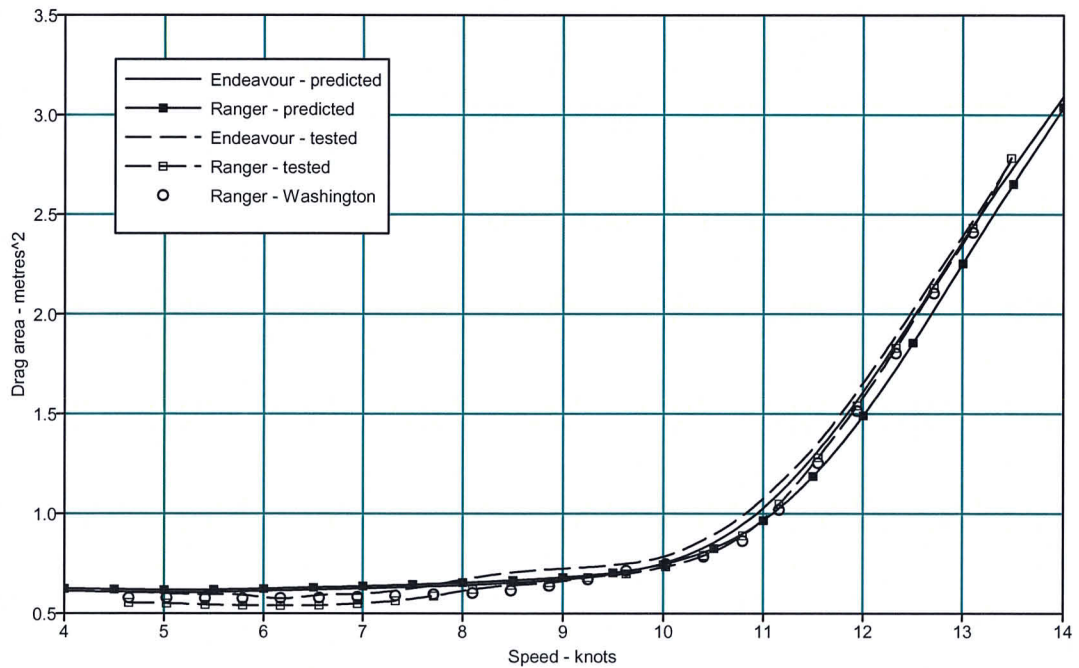
Using the new formulations in the Vpp allows a comparison of the predicted resistance data with those determined in the original test programme for both Endeavour and Ranger.

The upright resistance comparisons are shown in Figure 4 in terms of Drag Area, where:

$$D.a = \frac{R}{0.5\rho V^2}$$

Data are presented for both vessels, as predicted by the Vpp and as tested at Stevens, with the larger scale tests on Ranger, at Washington, included.

Figure 4. Upright Drag comparisons



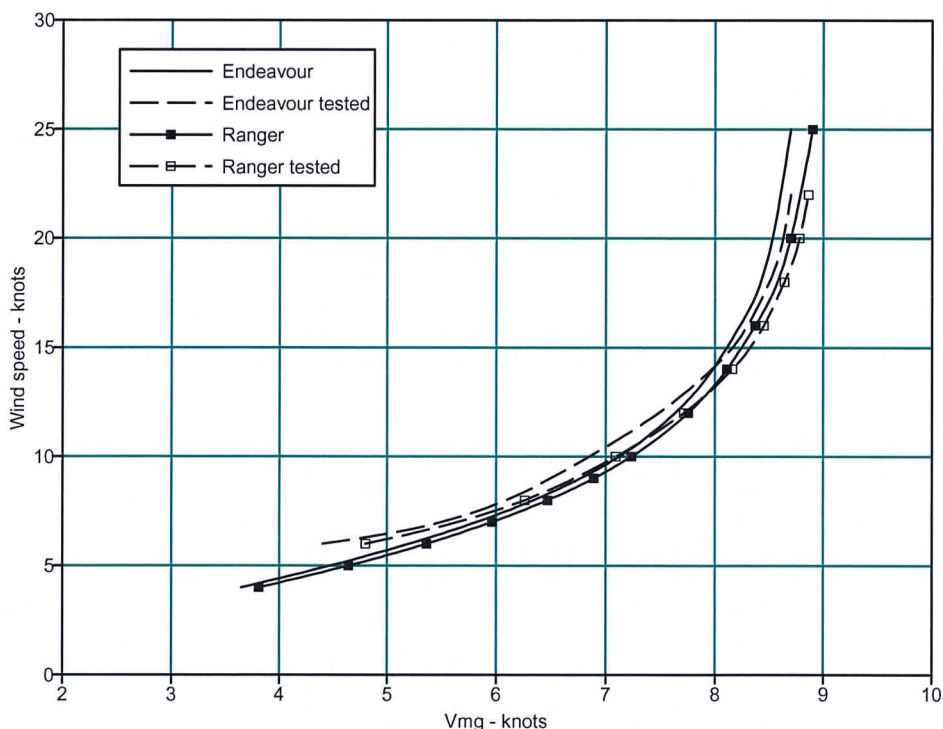
The data predicted from model testing shows that Ranger has less resistance over the speed range from 5 to 13.5 knots, with a reasonably consistent difference at speeds less than 12 knots. The Washington data are similar to the Stevens Institute values, although with less evidence of a hump between 6 and 10 knots, and an indication that the resistance is slightly lower at speeds above 11 knots.

The differences between the two Vpp predictions are smaller than those found in the tank at speeds up to 11 knots, with little indication of a hump. The data indicate that Ranger may fare a little better under the Vpp rule than she should in lighter winds. At speeds above 11 knots the Vpp predictions differ a little more than the tank results, but with Ranger always predicted to have less resistance than Endeavour.

Figure 5 presents the predictions of velocity made good to windward from both the tank and Vpp, as all of the heeled tank work was done with a centerboard, this has been replicated in the comparison, although the modern J's do not use them.

There is broad agreement between the predictions and tank results, both in absolute and relative terms although the Vpp predicts better performance for both boats at wind speeds less than 8 knots than the tank analysis.

Figure 5. Windward comparisons



Final formulation

The final version of the Vpp formulations allow J-Class vessels to be entered into the Vpp in the normal way, by specifying their hydrostatic and stability qualities within the associated Lines Processing Program (Lpp), and adding specific rig and sail wardrobe data. This latter point is of note, as the lack of an extensive wardrobe can be accounted for in the final rating and should not prove to be a disadvantage.

The J-Class Association rules call for ratings in terms of Time Correction Factors. These are calculated in three wind bands to cover light medium and heavy air racing.

The TCF values are calculated by using the Vpp's inbuilt Race Committee function with its standard Windward-Leeward, and Circular Random courses. By comparing the performance of the yacht in question against the standard Velsheda 2001 data file, TCF are calculated at a number of specific wind speeds by dividing the time for Velsheda 2001 by the time achieved for the test yacht. The Light wind TCF is the average value between 6 and 9 knots wind speed, the Medium wind TCF the average of 9 and 14 knots, and the Heavy wind TCF the average of 14 and 20 knots.

Finally, in order to maintain close racing, a maximum rating is calculated, and existing or new yachts cannot exceed this if they are to be eligible to race.

Comparison with the original Universal Rule

Although the success of the Vpp rating method can only be measured in its acceptance on the race course, it is instructive to compare its recommended time corrections with those of the original Universal Rule.

The three J Class boats currently racing have moved away from their level rating of 76 feet, as shown in Table 4. Under the original time allowance tables determined by Herreshoff, vessels of different rating receive or give a single time on distance on the races course.

Table 4. Current rating under the Universal Rule

	Universal rating		Time allowance
	metres	feet	seconds
Velsheda	23.9	78.31	0
Endeavour	23.7	77.66	1.02
Ranger	24.9	81.54	-4.87

Running the Vpp on the boats' current configurations leads to predictions of time around one mile courses, either pure windward-leeward or in all directions denoted as a circular random course. These times can be compared, and corrected both by use of the original time allowance, and also the TCF values calculated in each wind band. The results are shown in Table 5, and show significant differences between the boats. The Universal Rule deltas shown in the table are constructed by subtracting the course time for Velsheda from that of Endeavour and Ranger, and then subtracting the Time Allowance of Table 4. The Vpp deltas are arrived at by application of the rated TCF, calculated itself by the Vpp in each wind band, to the course time of Endeavour or Ranger, and subtracting Velsheda's time.

For racing between Ranger and Velsheda, both systems produce close racing as indicated by the small predicted time differences (deltas) under either method. However, the situation when racing Endeavour against Velsheda is different. In light and medium winds Endeavour is at a significant disadvantage if racing under the Universal rating, this is partially due to her lack of an asymmetric sail, but, even if one is added to her wardrobe the Vpp based rating provides much closer results.

Table 5 Comparison of Vpp and Universal Rule results

Course Times and deltas in seconds for one nautical mile

TWS knots	Velsheda		Endeavour					
	WL	CR	WL	CR	Universal deltas	Vpp deltas		
6	710	522	734	539	23.0	16.0	2.8	1.8
7	627	466	645	479	17.0	12.0	-0.6	-0.5
8	568	429	581	438	12.0	8.0	-3.8	-3.3
9	525	402	534	409	8.0	6.0	-6.4	-4.5
10	491	383	499	388	7.0	4.0	1.5	0.0
12	447	357	452	361	4.0	3.0	-0.9	-0.7
14	419	340	423	343	3.0	2.0	-1.5	-1.4
16	400	329	403	331	2.0	1.0	0.7	-0.3
20	375	313	376	315	0.0	1.0	-1.1	-0.2
25	357	301	359	303	1.0	1.0	0.0	-0.1

Ranger					
WL	CR	Universal deltas		Vpp deltas	
706	518	0.9	0.9	0.5	1.1
623	462	0.9	0.9	0.0	0.6
563	424	-0.1	-0.1	-1.4	-0.8
520	397	-0.1	-0.1	-1.7	-1.1
487	377	0.9	-1.1	1.9	0.7
442	350	-0.1	-2.1	0.3	-0.8
413	333	-1.1	-2.1	-1.0	-1.1
393	321	-2.1	-3.1	1.1	0.1
366	305	-4.1	-3.1	-1.4	-0.3
348	292	-4.1	-4.1	-1.8	-1.6

Endeavour - assymmetric					
WL	CR	Universal deltas		Vpp deltas	
726	533	15.0	10.0	0.3	0.1
639	474	11.0	7.0	-1.9	-1.7
577	435	8.0	5.0	-3.5	-2.9
532	408	6.0	5.0	-4.5	-2.4
499	388	7.0	4.0	2.4	1.2
452	360	4.0	2.0	0.0	-0.5
423	343	3.0	2.0	-0.7	-0.4
403	331	2.0	1.0	0.7	0.2
376	314	0.0	0.0	-1.1	-0.7
359	302	1.0	0.0	0.0	-0.7

Conclusions

The Vpp model of J-Class yachts appears to perform well in comparing the upwind performance, both in terms of absolute and relative performance between Endeavour and Ranger, when compared with the results from the tank testing.

There is slightly greater divergence of data when comparing the upright resistance between the Vpp model and the tank tests on the basis of Drag Area, which might tend to favour Ranger's rating in light winds, and penalise her in heavy winds, but these differences are small, and, well within the expected uncertainty of any prediction method based solely upon hull parameters, such as a Vpp.

The method currently proposed within the J-Class Vpp version, is as good as can reasonably be expected from such a tool. Although alternative Vpp models could be created, the variation in performance prediction between the different boats may be altered, but is not likely to be improved.

Should the J-Class Association wish better to predict the true potential performance differences between the existing and future fleet, a set of model tests could be undertaken, under its auspices, that would provide detailed hydrodynamic performance data for each design, and thus overcome the inevitable assumptions that underlie a parameter based prediction.

References

1. Davidson, K.S.M. (1936) "Some Experimental Studies of the Sailing Yacht," TRANS. SNAME, Vol. 44, 1936, pp. 288-334.
2. "J-Boat Investigation for H.S. Vanderbilt, Esq. relating to the Design of Ranger", Stevens Institute of Technology, Report No. 34, 1936.
3. "Supplemental Report to Report No. 34", Stevens Institute of Technology, Report No. 35, 1937.
4. Oliver, J.C., Letcher, J.S., and Salvesen, N. (1987) "Performance Predictions for Stars & Stripes", TRANS SNAME, Vol 95, 1987.
5. Oliver, J.C. (1994) "VPP Model and Methods", Chap. 6, WinDesign Users Manual.
6. Oliver, J.C. and Cloughton, A.R., (1995) "Development of a Multifunctional Velocity Prediction Program (VPP) for Sailing Yachts" CADAP '95, Southampton, U.K.
7. Cloughton, A.R. and Oliver J.C., "Developments in Hydrodynamic Force Models for Velocity Prediction Programs", The Modern Yacht Symposium, RINA, 2003.
8. Robinson, J., As the battle rages (or VPPs, what are they and what are they good for ?) ,Seahorse International Sailing Magazine, Issue 306, pp37-39 August 2005
9. Havelock, T.H. The Theory of Wave Resistance. Proceedings of the Royal Society of London. Series A, Containing Papers of a Mathematical and Physical Character, Vol. 138, No. 835 pp. 339- 349, 1932.

Session 11

**Andy Cloughton, Fabio Fossati,
Sara Muggiasca & Davide Battistin**

CHANGES AND DEVELOPMENT TO SAIL AERODYNAMICS IN THE ORC INTERNATIONAL HANDICAP RULE

Andy Cloughton¹, Fabio Fossati², Davide Battistin³, Sara Muggiasca⁴

***Abstract.** Aim of this paper is to describe changes and developments in the ORC International Rule (including work in progress) with particular reference to sail aerodynamics. After a brief introduction of the most important modifications between IMS and ORC International adopted in order to give a response to some of perceived rating inequities under the International Measurement System (IMS), an updated treatment of sails aerodynamics is discussed in detail. In particular Code 0 sails and the effects of jib overlap, rig fractionality and mainsail roach profile on induced drag and centre of pressure have been introduced in the ORC International VPP using an experimental database available from wind tunnel tests. Experimental data and new de-powering scheme which has been included in the VPP are finally presented.*

1 INTRODUCTION

In 2008 the Offshore Racing Congress introduced a new handicap rule – ORC International – replacing the former IMS. [1] and [2].

The Velocity Prediction Program underlying the new handicap system introduced some fundamental changes in order to overcome some perceived unfairness of the old system, yet retaining the fundamentals of the old IMS VPP.

Since the main argument against IMS handicaps was that it penalized fast, light and stiff boats, the new ORC International features addressed (or at least tried to!) the above criticisms. The key points that modify the VPP prediction are the adoption of a new procedure for the stability calculation, and a modification of the residuary resistance curve. A new evaluation of the Righting Moment is used, based on both the RM measured during the floatation test and on a standard RM (RM) derived by boat characteristics (Sail Area, Length, Beam, Displacement, Draft). The final RM is the average of these two values. This procedure allows stiff boats, which are likely to have a measured RM greater than the "standard" RM, to be less penalized than before. The new corrected Residuary Resistance (RR) curve is based on a LVR (length/volume ratio) function that takes into account light boats characteristics that old IMS RR was not properly assessing, probably because of the effect of the many heavy models included in the data set used to derive the RR polynomial.

Besides the changes to the underlying VPP, some other important facts distinguished the ORC International introduction on the race courses in 2008: the managing of boat certificates was completely renewed, through a new "ORC Manager" program, a modern "point and

¹ University of Southampton - ORC ITC Member

² CIRIVE Wind Tunnel - Politecnico di Milano - ORC ITC Research Associate

³ ORC Programmer

⁴ Department of Mechanical Engineering, Politecnico di Milano

click” program with a friendly graphical interface. The ORC Manager contains all relevant features for managing files, printing certificates, looking at the output, and sending data to the ORC server. Indeed, a web database was installed, giving Rating Offices the facility to upload and download data files. This database is currently under further development, and it will become the source from where one will be able to “trace” the history of a boat, looking at its certificates and data year after year.

There is an important legacy of the International Measurement System, which has been retained on the newborn rule: it’s the overall concept of “fair handicapping”, trying to predict faithfully the performance of a yacht in all conditions and around any course, by means of the VPP. Moreover, the evolution of modern calculus means allows it to be, step by step, closer to the reality each year. An example of this trend is the new procedure adopted for inputting headsails, the so called “sail inventory”: each single sail is taken into account and its data recorded in the input file, leaving the VPP choosing the fastest one.

A key factor for continuously updating the VPP is the experimental activity. Experimental data presented in this paper gave the fundamental insight for modifying the aerodynamic model. On one side the new “Code0” sail has been modelled and adopted since the release in 2008, and on the other side a new de-powering scheme and new formulations for the centre of effort height and effective height have been proposed for the 2009 version of ORC Int.

2 EXPERIMENTAL ACTIVITIES

In [1] research activities carried out at Politecnico di Milano Twisted Flow Wind Tunnel with the aim of better addressing the performance of different rig designs in upwind conditions have been presented. These activities started in 2005 in order to overcome some perceived inequities in the ratings of boats of various rig design racing under the International Measurement System (IMS).

In particular a series of rig planform variations in mainsail roach and jib overlap have been tested and some preliminary results relevant to upwind aerodynamic behaviour of tested sailplans have been reported.

The above mentioned research program has been further extended, considering also variation in fractionality ($I/(P+BAS)$) and wider apparent wind angle range has been tested in order to have a more comprehensive database. In the following a summary of the test results including more recently performed tests will be reported. Moreover the need to address new sail configurations, in particular the Code0, lead to wind tunnel tests using two different Code 0 sails with respectively 58% and 67% mid girths. Experimental obtained results have been used in order to define aero-characteristics in the VPP and the relevant yacht performance for rating purposes. A brief summary of Codes 0 results will be outlined in the following.

A series of sails was designed to investigate a series of rig planform variations in mainsail girth, jib overlap and rig fractionality.

In particular 3 different main sails (with the same actual and IMS area but 3 different roach) named Mims, Mhr, and Mtri) and 3 different jibs with different overlap (named G100, G135 and G150) have been combined in a 92% fractionality configuration..

Note that the Mims mainsail has the IMS rule maximum allowed roach without any penalty applied.

A new mainsail with smaller area and IMS maximum allowed roach (named Mstd) has been manufactured and tested with the same 3 jibs with the same overlap but arranged in masthead configuration (100% fractionality).

Mainsail roach level has been defined according to:

$$Roach = \frac{Area_{Main}^{IMS}}{P * E / 2} - 1 \quad (1)$$

Mainsails code roach and main dimensions are defined as follows:

	Roach	P	E
Mims	0.193	1.94	0.637
Mhr	0.335	1.94	0.571
Mtri	0.096	1.94	0.695
Mstd	0.193	1.76	0.568

Then 3 new jibs were manufactured with the same previous overlap (named G100sh, G135sh and G150sh) but different dimensions in order to obtain an 85% fractionality configuration.

Jib codes are defined as follows:

	Overlap
G100	100%
G135	135%
G150	150%
G100sh	100%
G1350sh	135%
G150sh	150%

The 85% fractionality jibs have been tested with the medium roach mainsail (Mims).

In the following some pictures of different tested sail combination are presented. *Please note that some pictures show the model with non zero heel but all the results presented in this paper refer to upright condition.*

Apparent wind angles (AWA) were chosen within the 20°-60° range.

Pictures of figure 2.1 show sailplans tested with 92% fractionality.

Two CODE 0 sails have been manufactured and tested with the medium roach mainsail Mims. Code 0's are defined as follows:

	LPG	Mid Girth
Code 58	165%	58%
Code 68	165%	68%

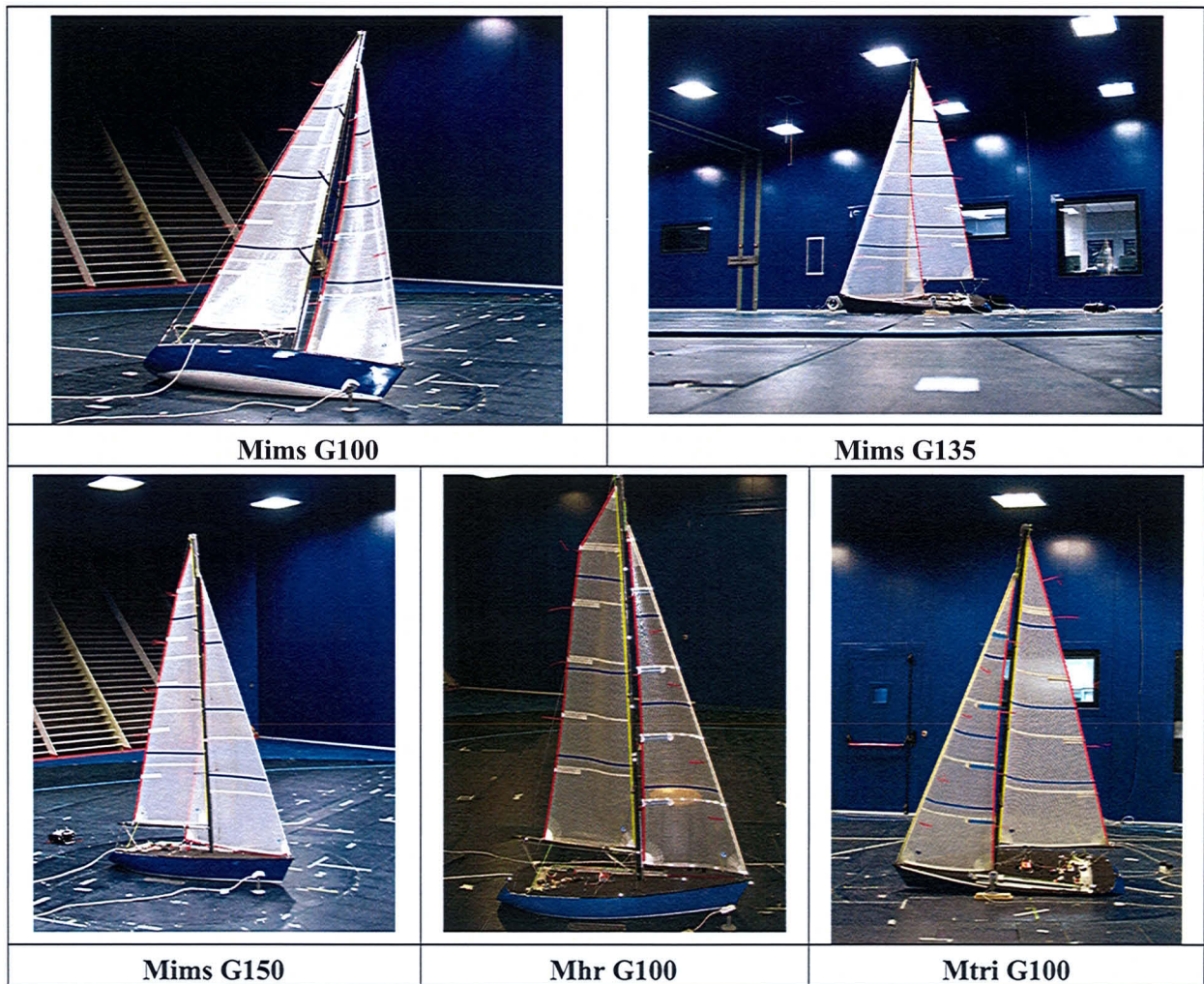


Figure 2.1 – 92% fractionality sail plans with different main roach and jib overlap

Figure 2.2 show respectively 85% fractionality and masthead configurations.

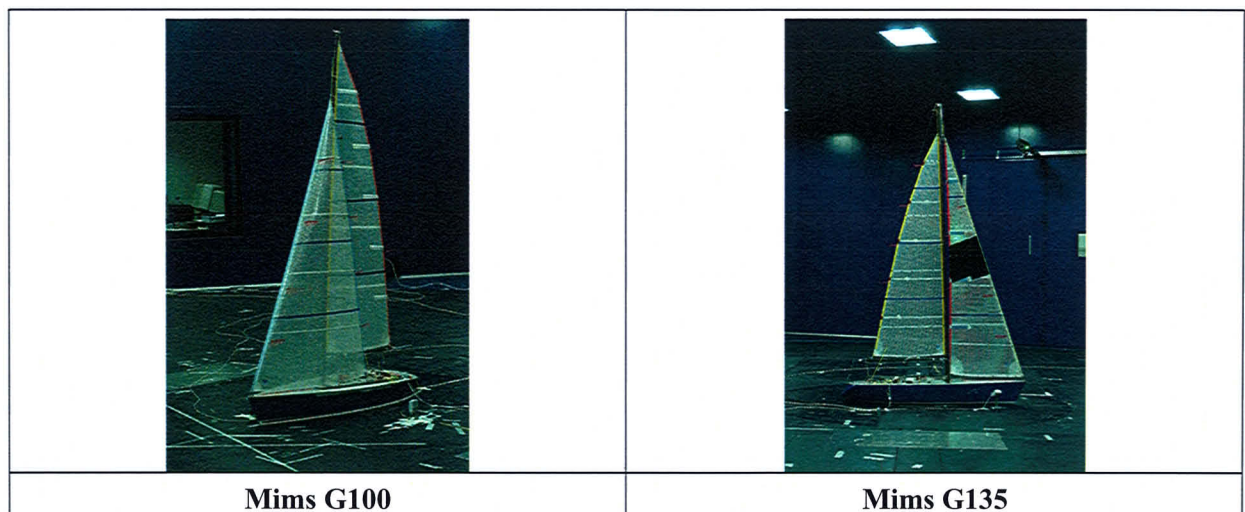


Figure 2.2 – 85% fractionality and masthead rigs

In particular both CODE 0 sails have been tested with the medium roach mainsail Mims. All tests were performed in the upright condition. An apparent wind angle range 32° - 60° has been explored. The CODE 0 with 58% mid girth length has been tested also at AWA 24.5° and AWA 29.5° .

Figure 2.3 shows CODE ZERO wind tunnel experiments.

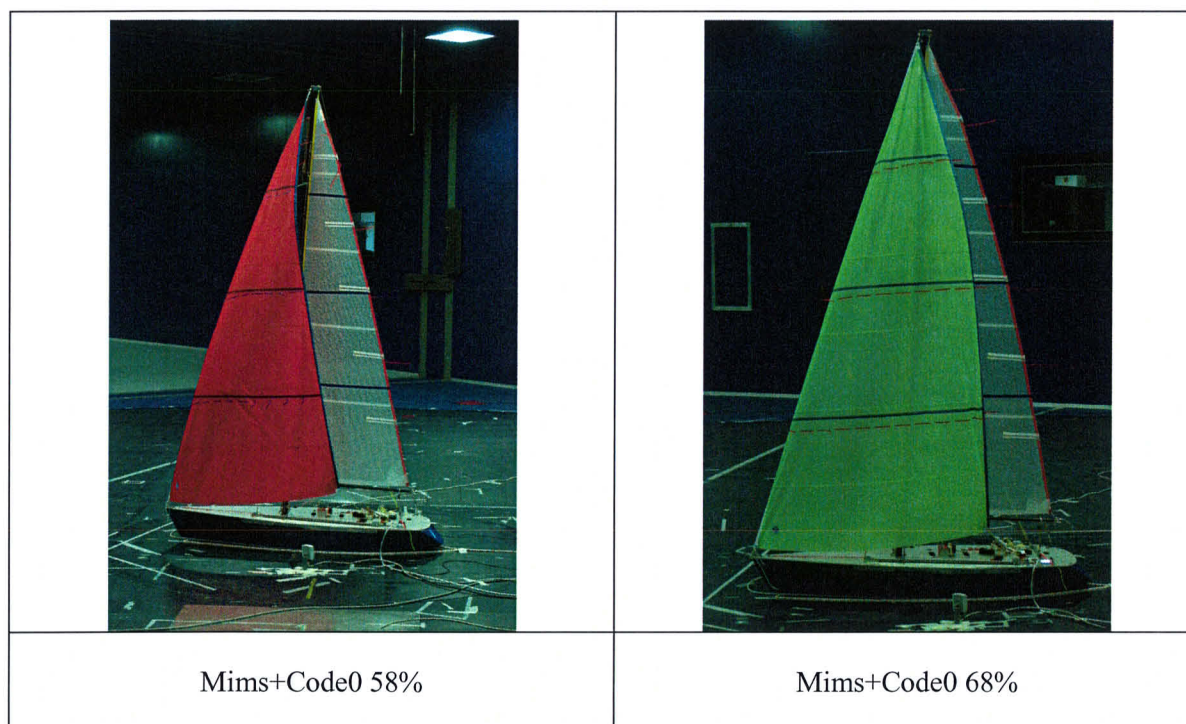


Figure 2.3 – CODE ZERO wind tunnel test

A total of 17 different sails combinations were tested at various apparent wind angles. The main aim of each test was to measure aerodynamic forces and moments: sail trimming during the wind tunnel tests was performed according to the procedure described in details in [1]. Basically for each apparent wind angle tested the first task was to reach the maximum driving force potentially achievable. At the same time the influence of the sail trimming changes was observed using the data acquisition program that presents the forces acting on yacht model in real time.

Trimming the sails to obtain optimum sailing points proved to be the most challenging task of the testing process. Attempts were made to carry out the job as systematically as possible. Firstly, the maximum drive point was found by trimming the sails to the best using the cameras views, the tufts on the sails and the force measurements output data.

From there, the heeling force would be reduced to simulate the trim of the sails for windier conditions. In fact in real life windy conditions, to keep the optimum heeling angle, heeling force has to be reduced by the crew. The sail trimming routine adopted was to choose the mainsail traveller position (initially quite high up to windward) and then to vary the incidence and the twist of the mainsail to power or de-power it, by over-trimming or easing the main traveller and main sheet. The genoa was initially trimmed in order to have the maximum driving force condition and was fixed varying the mainsail shape.

Once a specific trimming condition has been obtained using the real time force and moments values displayed by the data acquisition system, a 30 second data acquisition was made, and both time histories and mean values of each measured quantity have been stored in a file.

Some runs have been performed on the bare hull and rigging only (without sails) at different apparent wind angles to be able to evaluate windage. This has been subtracted from the measured data points in order to study the effect of the sail plan only.

Regarding data analysis procedure and main interesting aerodynamic data which can be extracted from experimental database readers can refer to [3], [4] and [5].

In the following some results concerning CODE 0 sails and systematic sailplan variations for upwind conditions are reported.

2.1 Code Zero Results

In figure 2.4 the driving force coefficient C_x versus heeling moment coefficient C_{Mx} is reported for each sail at each of the apparent wind angle tested.

Different symbols used refer to different sailplan according to the legend.

These plots show the relative performance of different sail configurations: in particular for light wind conditions by comparing the maximum values of driving force at particular apparent wind angle.

With reference to the light wind conditions at wider apparent wind angles CODE ZERO with 68% mid girth gives the higher driving force.

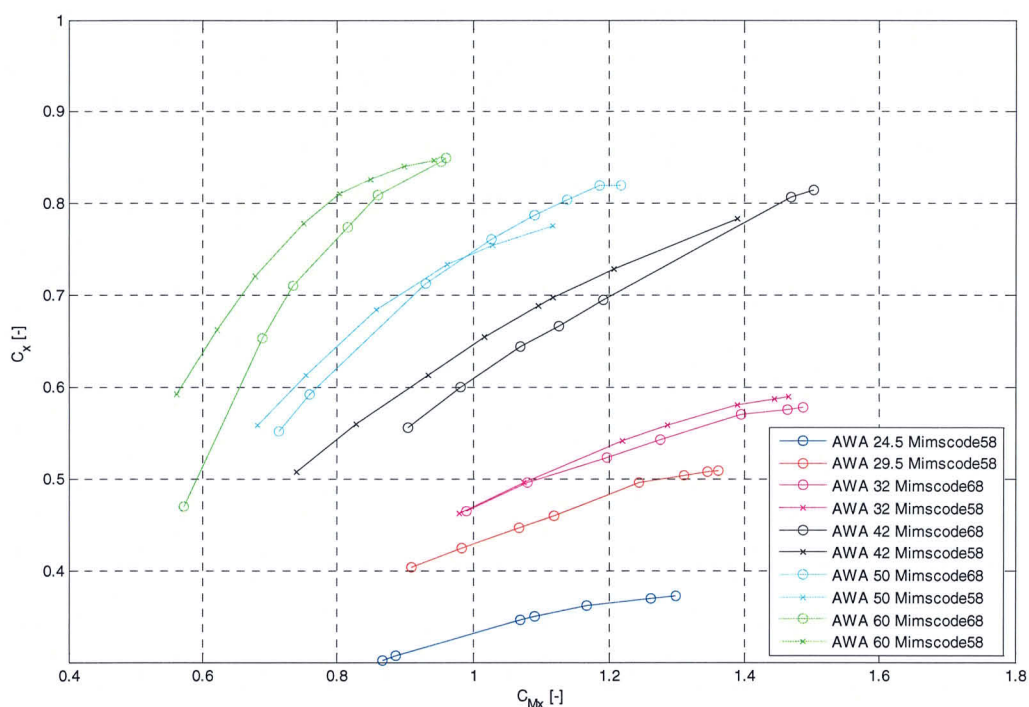


Figure 2.4

It's also interesting to make a comparison between CODE ZERO and the largest genoa tested with the same mainsail (Mims) as reported in figure 2.5.

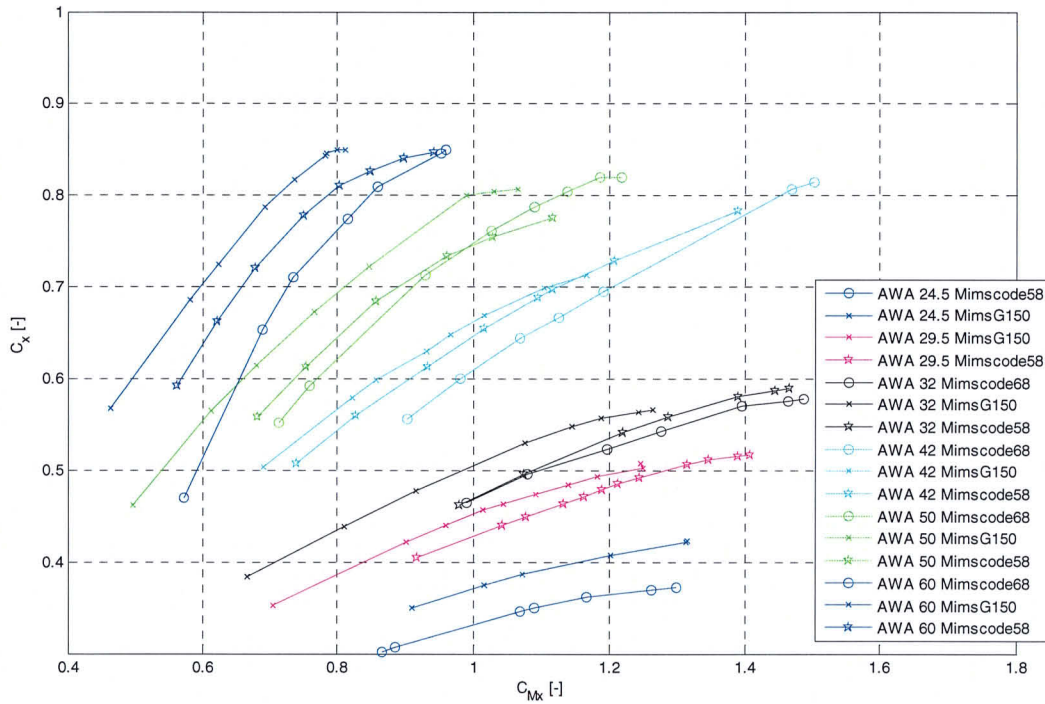


Figure 2.5 – Comparison between Code Zeros and genoa performance

With reference to the closer apparent wind angle tested (24.5°) the mainsail+genoa sailset is more effective than the main+code0 sailset: as can be seen with the same heeling moment the obtained driving force is higher.

Considering larger angles, at the lower heeling moments generally the genoa combination has higher driving force coefficients, but maximum achievable driving force is greater for the code0 sailset.

From these data drag and lift coefficients have been extracted in order to provide VPP aerodynamic input according to procedure described in paragraph 3.1.

2.2 Upwind Sail Plan Systematic Series Investigation Results

According to the procedure described in [1] for each tested sail plan the variation of driving force with heeling force coefficient and aerodynamic centre of effort position can be easily evaluated from wind tunnel tests.

Then more information can be obtained from lift and drag coefficients because both the induced drag and quadratic profile drag vary with the square of lift. In particular from plots of drag coefficients against lift coefficient squared for each run performed at different AWA the effective height can be evaluated considering the linear regression between points that at low values of C_L^2 collapse to a straight line according to the following equation:

$$H_{eff} = \sqrt{\frac{SailArea}{\pi Slope}} \quad (2)$$

where “Slope” is the slope of the abovementioned straight line. (C_L^2 vs C_d)

Finally the intercept of the straight line with the zero lift axis directly represent the parasitic drag coefficient C_{D0} . Then for each C_L value the corresponding total drag coefficient can be evaluated superimposing the parasitic drag C_{D0} to the induced drag according to the following relationship:

$$Cd = Cd_0 + \frac{C_L^2 \text{SailArea}}{\pi H_{eff}^2} \quad (3)$$

2.2.1 Centre Of Effort Height

Figure 2.6 shows the centre of effort height above deck non-dimensionalised with respect to the mast height evaluated for different sail plans. In particular for each sail plan the relevant mean value at different AWA of the measured values corresponding to the maximum driving force is presented.

In figure 2.7 Centre of Effort Height (mean value with respect to the AWA) of medium roach sail plans versus jib overlapping is presented for each tested fractionality configuration.

In figure 2.8 Centre of Effort Height (mean value with respect to the AWA) of medium fractionality sail plans versus jib overlapping is presented for different roach configuration.

In figure 2.9 Centre of Effort Height trend of medium roach versus sail plan fractionality is presented for different jib overlap.

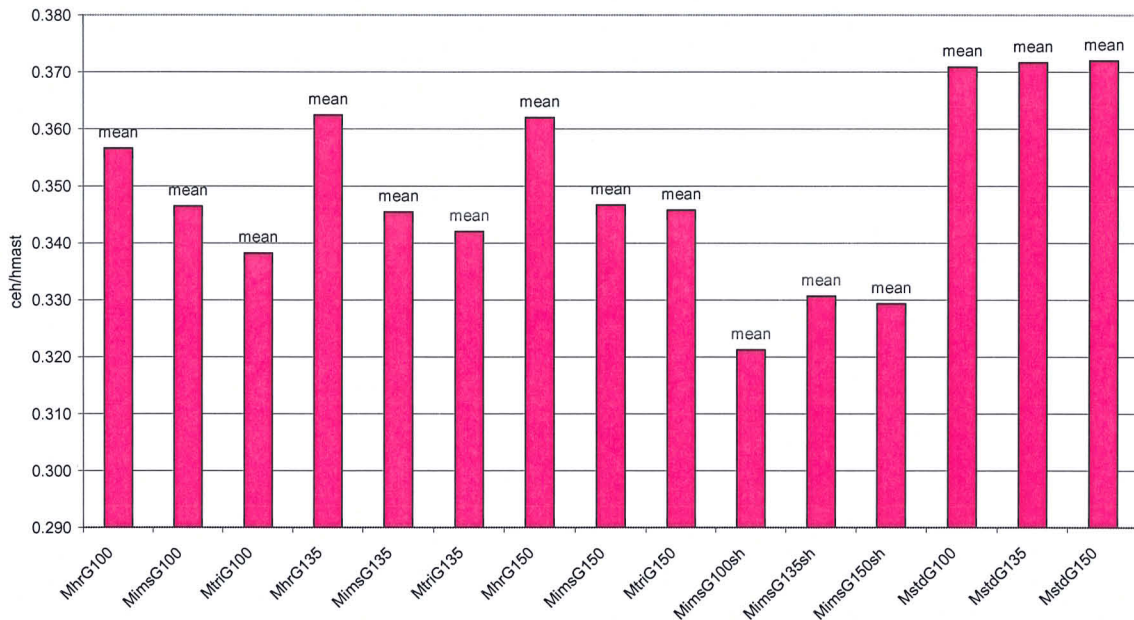


Figure 2.6 – Centre of effort height

ceh vs overlap Roach Med

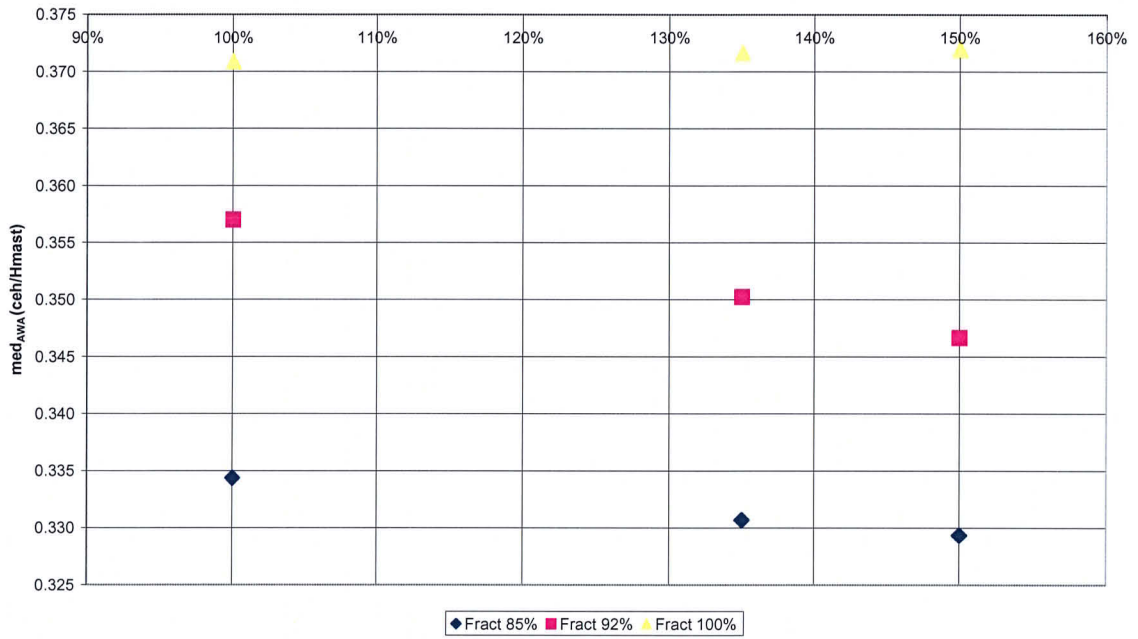


Figure 2.7

ceh vs overlap Fract 92%



Figure 2.8

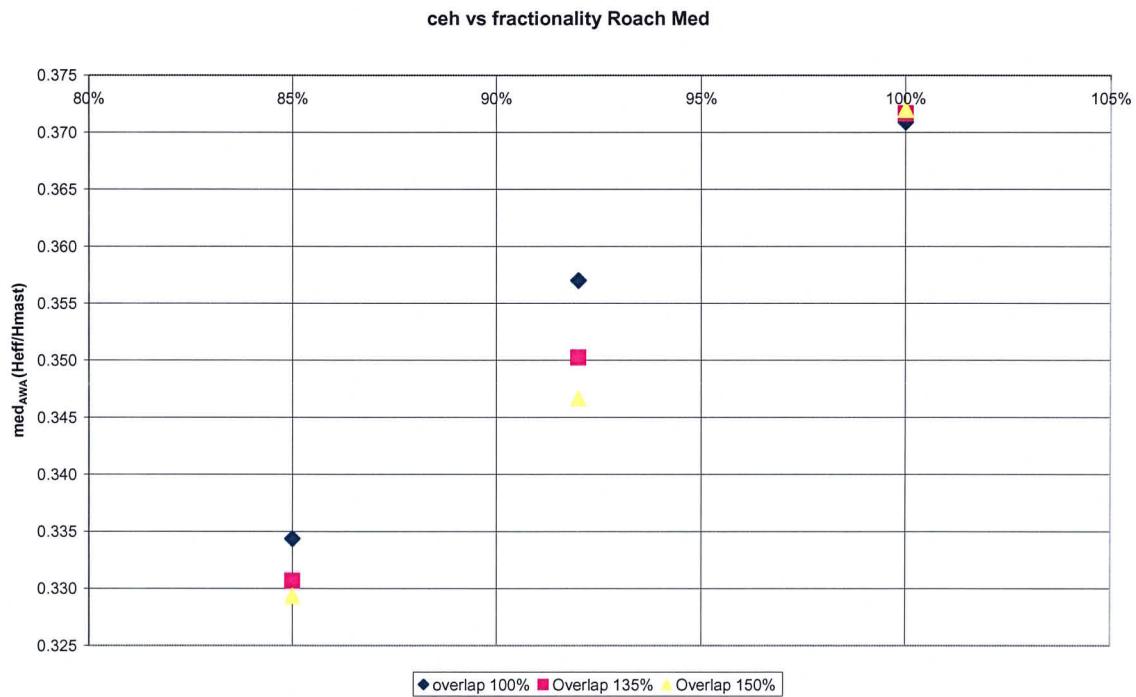


Figure 2.9

A number of comments can be made on the information given by that plot:

- Increasing mainsail roach with the same overlap and same fractionality the Centre of Effort becomes higher.
- At the same mainsail roach, the smaller the overlap, the higher Centre of Effort is. This is explained by the fact that increasing overlap more sail area is added in the lower part of the sail plan.
- Increasing fractionality obviously CEH rises.

2.2.2 Rig Effective Height

As previously said for each sail plan, at each apparent wind angle, effective height has been evaluated considering the slope of the linear regression between points that seem to be on a straight line in the C_D versus C_L^2 plot.

Considering the mean value at different AWA's, figure 2.10 shows Effective height ratio over the mast height for each tested sail plan. In particular for each sail plan the relevant measured mean value corresponding to the maximum driving force at different AWA is reported.

Figure 2.11 shows effective rig height trend (mean value of different AWA results) with varying overlap for each fractionality at medium roach.

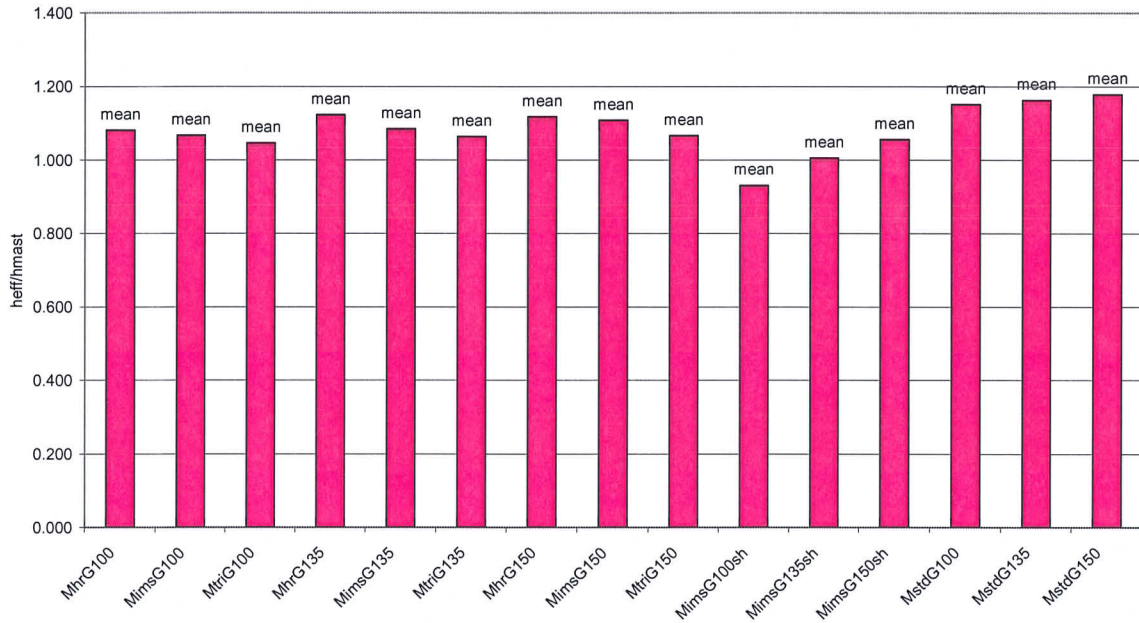


Figure 2.10

Heff vs overlap Roach Med

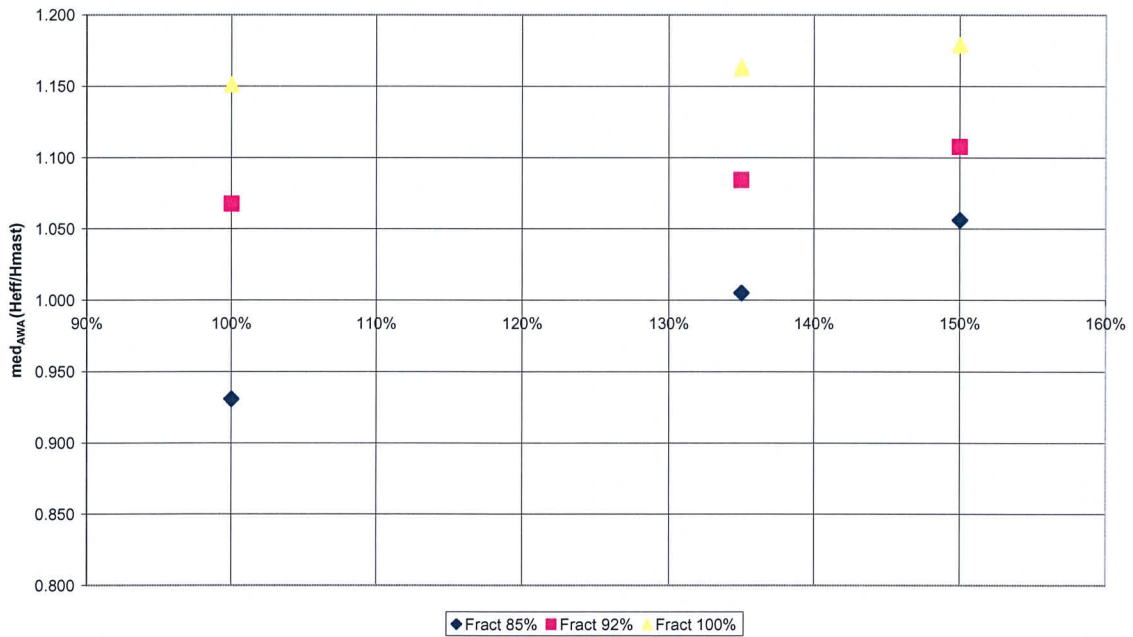


Figure 2.11

Figure 2.12 shows the change in effective rig height (mean value of different AWA results) versus fractionality for different job overlapping at medium roach.

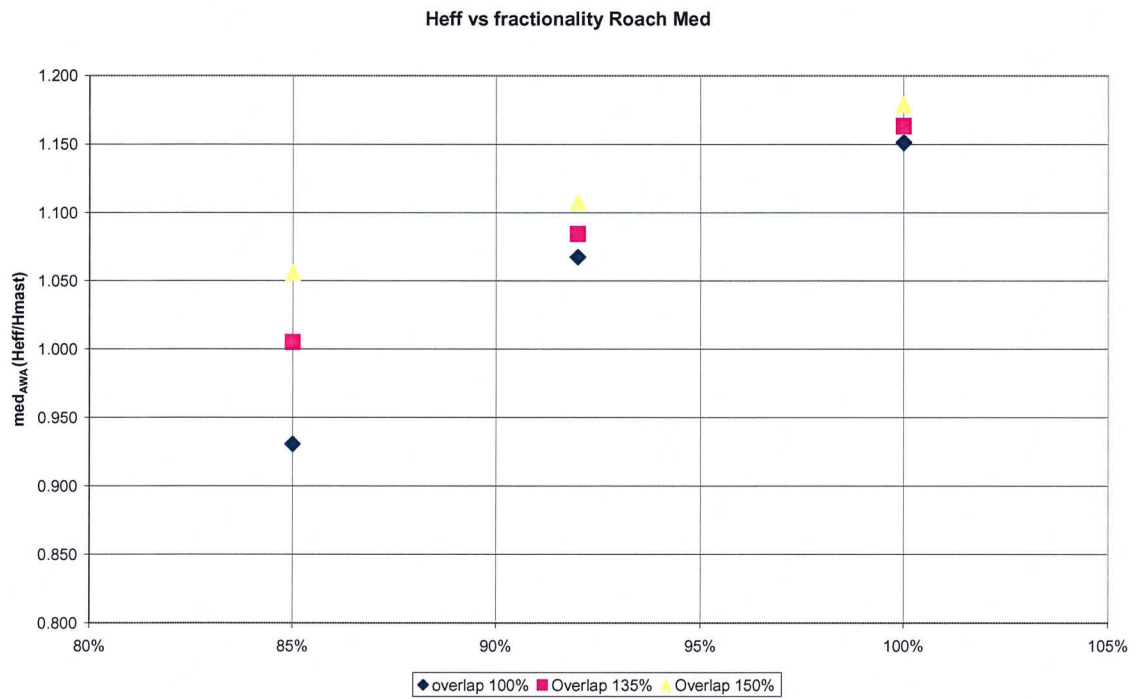


Figure 2.12

Following figure 2.13 shows the change in effective rig height (mean value of different AWA results) versus overlap for different mainsail roach at medium fractionality.

The results show that effective height increases with both overlap and fractionality. Moreover it grows increasing main roach.

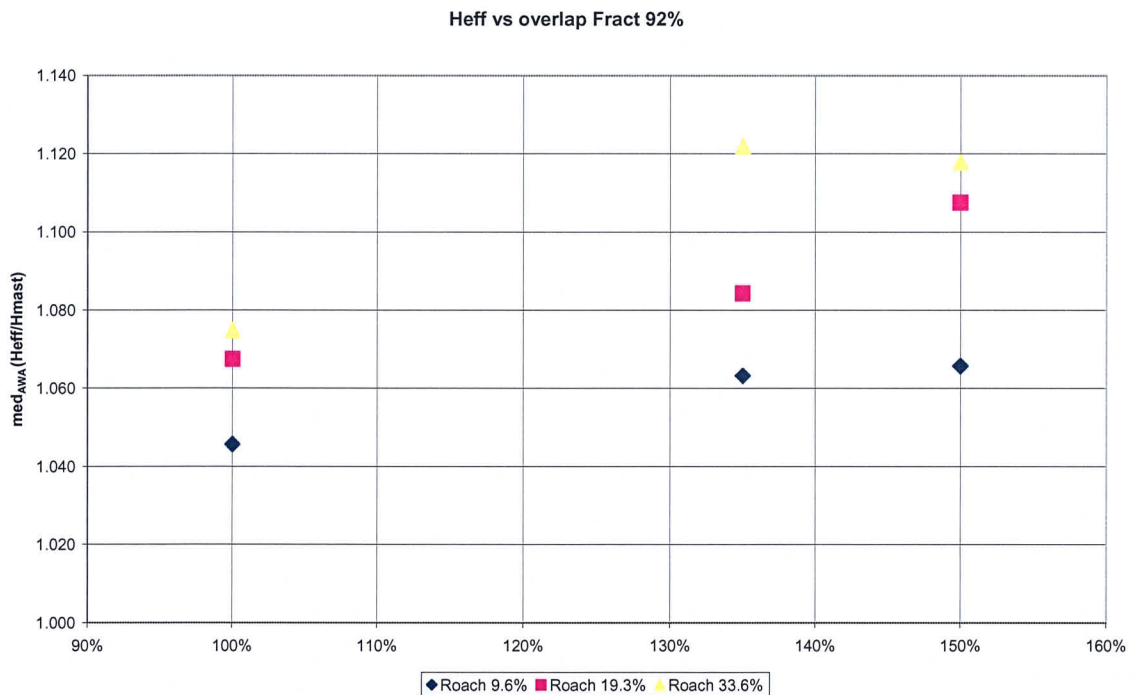


Figure 2.13

3 VPP AERO-MODEL CHANGES

In this paragraph the ORC International VPP aerodynamic model changes will be outlined with particular reference to the new assessment of CODE ZEROS sails (introduced in 2008 VPP release) and new de-powering scheme proposed for the 2009 release (still under discussion at the present moment).

The fundamental aggregation of a set of sail force coefficients for each sail set (combination of main and jib or main and spinnaker) has been retained. The values of the individual curves of Lift coefficient against parasitic drag coefficient have been retained as these embody the fundamentals of handicapping different rigging arrangements and off wind sails. In the rig analysis program the individual sail force coefficients are summed. The aggregate maximum lift and linear parasite drag coefficients are the sum of each sail components contribution normalized by reference area, and modified by a blanketing function B_i :

$$Cl_{max} = \sum Cl_{max_i} \times B_i \times A_i / A_{ref} \quad (4)$$

$$Cdp = \sum Cdp_i \times B_i \times A_i / A_{ref}$$

A typical form of the collective sail force coefficients is shown in Figure 3.1. The “Drag” Curve is the parasitic drag contribution, and the Total Drag curve includes the induced drag contribution.

Also the complete windage drag package has been retained.

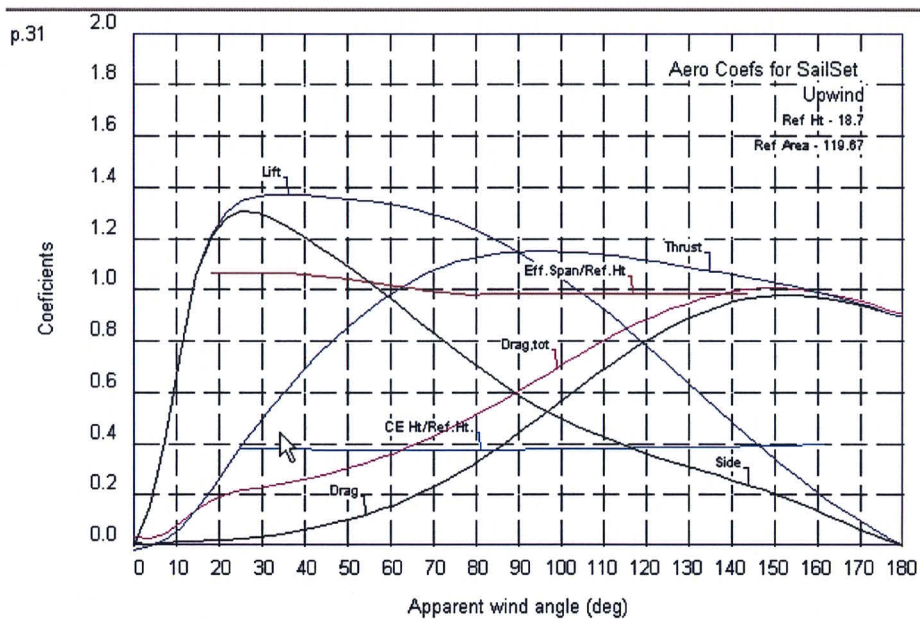


Figure 3.1: Typical Form of “Collective” Upwind Sail Force Coefficients.

3.1 Code 0 treatment

Following the evolution of modern racing yachts, ORC promoted the experimental tests on the Code0 sails, with the aim of modeling it inside the VPP, thus reproducing reliable results. The Code0 is considered an asymmetric spinnaker with its own aero coefficients. The VPP

runs the boat with this set of aero coefficients, and compares at each TWA the performances with those of other sails, like genoa and spinnaker, in order to select the sailset that gives the best performance.

The aero model used for the Code0 is the same as for other sails: curves of C_{d0} (parasitic drag) and C_l (maximum lift) are prescribed, varying along the all range of apparent wind angles. Then the thrust and side force are calculated combining the total lift and drag force coming out from the complete sail plan. The induced drag coefficient due to the lift generation is determined according to equation (3) in such a way that effective height (H_{eff}) takes into account the effective span of the sailplan.

In developing the coefficients for the Code0, the aim was that of reproducing closely wind tunnel results, always monitoring that the results were consistent with those of the other sails used in the same range, i.e. big genoas and asymmetric spinnakers tacked on the centerline. To do this, three “trial horses” were chosen, a Comet45, a TP52 and a Maxi, and each boat was tested with a genoa, with a Code0, and with an asymmetric on centreline of the same area.

Secondly, another set of sails was tested for the same boats, including a “real” genoa, Code0 and spinnaker, which have clearly different areas in the real world. The results were analyzed in terms of lift and drag forces, and in terms of boat speed, heeling angle and handi-cap.

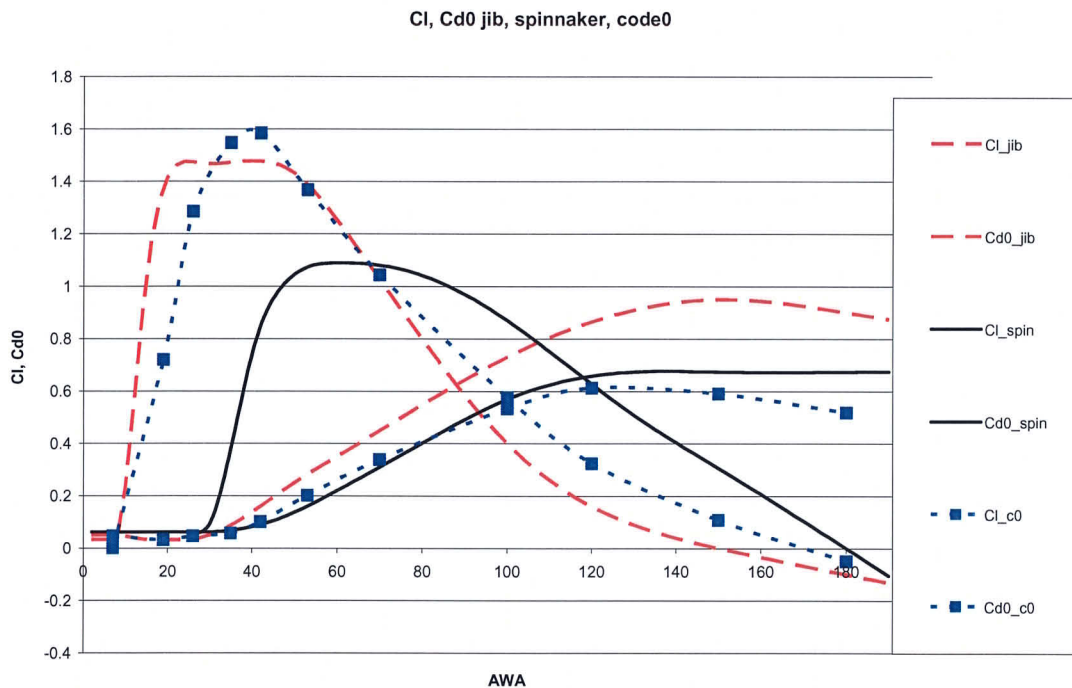


Figure 3.2

Figure 3.2 shows the aero coefficients C_{d0} and C_l versus AWA respectively for a jib, an asymmetric spinnaker and a code0.

It can be noted that there is a distinct spike of the code0 lift in a restricted region of AWA. This indicates a sail with high performance, although usable in quite a narrow range. In modeling the sail within the VPP frame, the C_l curve adopted is slightly damped compared to the experiments: this is due to the fact that the final comparison was made on the total aero lift and drag forces of the complete sailset (mainsail+headsail), including the induced drag. They are shown in figure 3.3 in terms of drag and lift areas. Looking at the total drag of the sailset

with the 68% code0, it can be noted a drag “bubble” in the range between 20 and 60 degrees, due to the induced drag created by the high lift values. To avoid an even worse behaviour in this region, the lift coefficient had to be kept lower compared to the experiments.

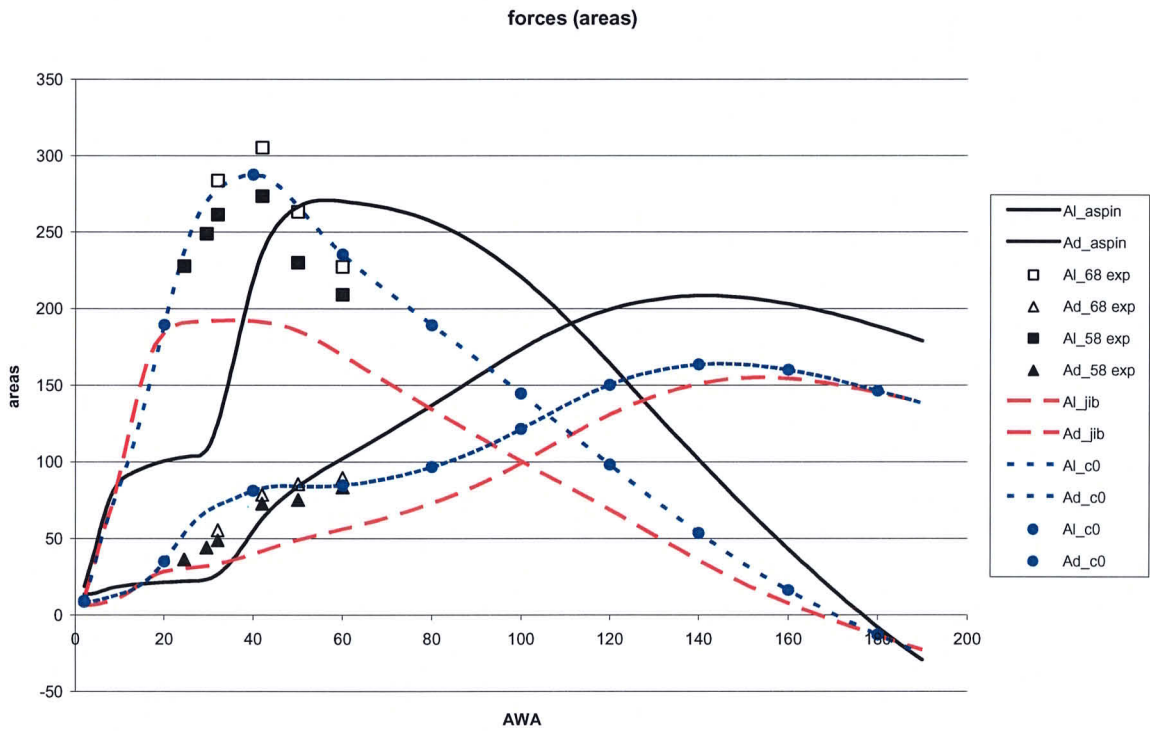


Figure 3.3

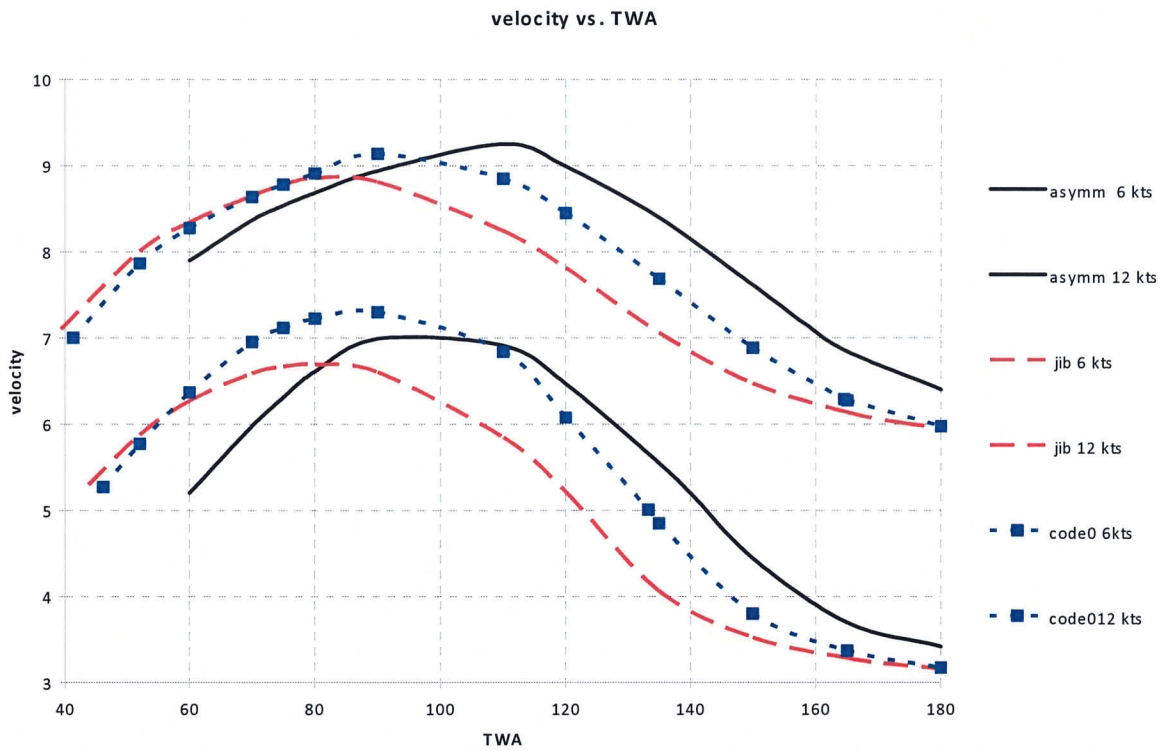


Figure 3.4

Figure 3.4 shows the final performances of one of the test boats, the COMET 45, with the three sailsets, at 6 and 12 knots of TWS. There is a double crossover, between jib and code0 upwind, and between code0 and asymmetric spinnaker at larger angles. The “fine tuning” of the aerodynamic coefficients was done analyzing similar figures for the other two boats (TP52 and Maxi).

3.2 De-powering scheme concept

Thanks to the experimental results obtained from wind tunnel tests a better codification of the effects of overlap, fractionality and mainsail planform (roach profile) on the sailplan aerodynamics is now available at different apparent wind angles for a significant range of sailplan parameters.

Then in principle a more realistic sail de-powering process could be assessed based on a two stage reefing process, first a jib reduction from maximum to minimum area followed by a mainsail area reduction.

This reefing process implies variations in sailplan geometry which are related to changes in aerodynamic behaviour: then for each de-powered configuration it's possible to consider relevant aerodynamic information which can be extracted from the experimental database, in particular in terms of effective rig height and centre of pressure.

The basic idea underlying this new de-powering process is that aerodynamic parasite drag and lift coefficients, effective height (and then the induced drag) as well as the centre of effort height can be modeled as *Bezier curves* depending on the apparent wind angle where the Bezier curve vertices are functions of sail plan parameters roach, overlap and fractionality. The choice of the proper order of the Bezier curves has been carefully considered.

The upgraded de-powering process will be described in detail in paragraph 3.4.2, while the Bezier curves approach will be outlined below.

3.3 Surfaces approach

With reference to rig effective height, for each of the sail plan configuration tested in the wind tunnel we can evaluate effective height as a function of the apparent wind angle by means of a Bezier curve which can be considered an approximating function of the available experimental values. For the present quantities 6th order Bezier Curves prove to be a good choice.

As an example in figure 3.5 experimental data (red points), Bezier control points (green points) and a 6th order Bezier curve fitting effective height values (continuous line) are reported versus apparent wind angle with reference to the high mainsail roach + non-overlapping jib for the 92% fractionality rig.

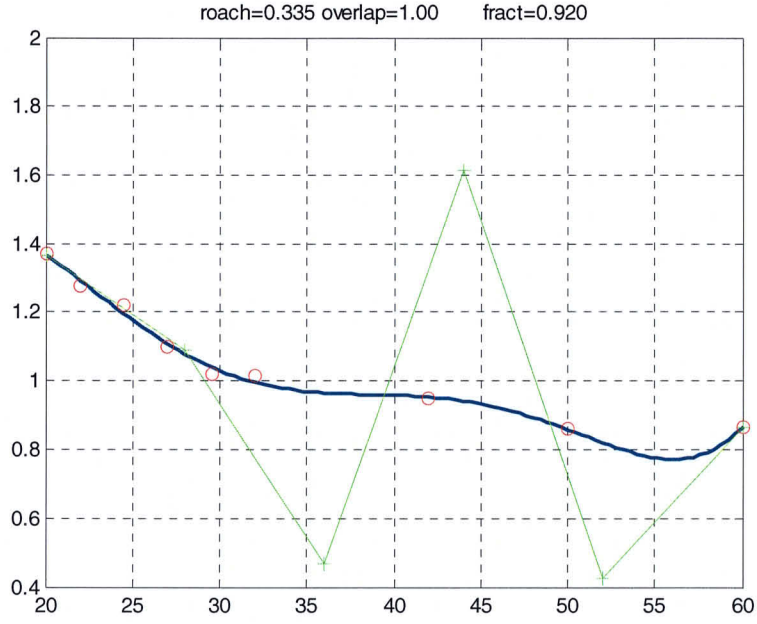


Figure 3.5

The available experimental database provided the opportunity to investigate the dependence of the Bezier Control Points on the sail plan parameters: final conclusion, with reference to the 6th order case, was that each of the effective height Bezier curve control point $H_{eff} p_i$ corresponding to given roach (ro), overlap (ov) and fractionality (fr) values can be expressed by means of the following equation:

$$\begin{aligned}
H_{eff} p_i = & a_{1i} * ro^2 + a_{2i} * ov^2 + a_{3i} * fr^2 + a_{4i} * ro * ov + \\
& + a_{5i} * ro * fr + a_{6i} * fr * ov + a_{7i} * ro + a_{8i} * ov + a_{9i} * fr + \\
& + a_{10i} + a_{11i} * ro^3 + a_{12i} * ov^3 + a_{13i} * ro^2 * ov + a_{14i} * ov^2 * ro + \\
& + a_{15i} * ro^2 * fr + a_{16i} * fr^3 + a_{17i} * fr^2 * ro + a_{18i} * ov^2 * fr + \\
& + a_{19i} * fr^2 * ov + a_{20i} * ro * ov * fr
\end{aligned}
\quad \text{for } i=1,6$$

where, for each (i^{th}) vertex, coefficients $a_{1i}, a_{2i}, \dots, a_{20i}$ can be previously evaluated by means of a least square fit of the experimental data available from the tests.

In the same way we can evaluate vertices C_{EHP_i} of the 6th order Bezier curve for centre of effort height (non-dimensionalised with respect to mast height) corresponding to the given roach (ro), overlap (ov) and fractionality (fr) values using the following equation:

$$\begin{aligned}
CEH p_i = & b_{1i} * ro^2 + b_{2i} * ov^2 + b_{3i} * fr^2 + b_{4i} * ro * ov + \\
& + b_{5i} * ro * fr + b_{6i} * fr * ov + b_{7i} * ro + b_{8i} * ov + b_{9i} * fr + \\
& + b_{10i} + b_{11i} * ro^3 + b_{12i} * ov^3 + b_{13i} * ro^2 * ov + b_{14i} * ov^2 * ro + \\
& + b_{15i} * ro^2 * fr + b_{16i} * fr^3 + b_{17i} * fr^2 * ro + b_{18i} * ov^2 * fr + \\
& + b_{19i} * fr^2 * ov + b_{20i} * ro * ov * fr
\end{aligned}
\quad \text{for } i=1,6$$

where, for each (i^{th}) vertex, coefficients $b_{1i}, b_{2i}, \dots, b_{20i}$ can be previously evaluated by means of a least square fit of the experimental data available from the tests.

As an example figure 3.6 shows the surface fitting the 6th control point $H_{eff} p_6$ variation at different overlap and roach values considering 92% rig fractionality. In the same figure experimental obtained values are reported too with blue dots.

This surfacing approach inspired the abovementioned more realistic de-powering approach where at each stage in the VPP optimization process the current sail area, fractionality and overlap are calculated and the previously defined surfaces interrogated to provide the Effective rig height and vertical centre of pressure position. The de-powering procedure is described in detail in the following paragraph.

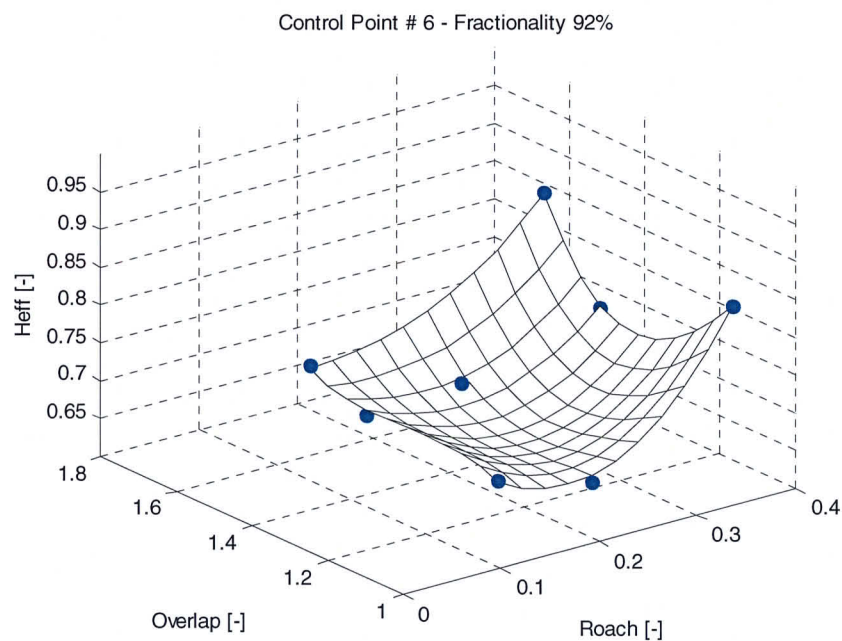


Figure 3.6 – Bezier Control Point #6 versus overlap and roach variations

3.4 VPP Scheme

Current Code

The current IMS VPP de-powering scheme has been in existence for over twenty years and it relies on a 2 parameter scheme based on the *Reef* and *Flat* parameters. Details of the scheme are given in [6] and [7]. It is a simple and elegant solution.

$$\begin{aligned}
C_L &= flat * reef^2 C_{Lmax}(AWA) \\
C_D &= reef^2 (C_{D0}(AWA) + k * flat^2 C_{Lmax}^2) \\
k &= k_{pp} + \frac{1}{\pi H_{eff}^2}
\end{aligned}
\tag{5}$$

As the apparent wind speed rises the sails are de-powered by finding an optimum Flat value which operates on the maximum lift coefficient. The corresponding reduction in induced drag is calculated based on the effective rig height calculated from the basis rig geometry. Eventually heeling moment can no longer be reduced sufficiently by a reduction in Lift coefficient alone and the sail area must be reduced by the application of the Reef parameter. As sail area is reduced the centre of effort is lowered and the effective rig height reduced, and the extra drag of the mast without an attached sail is calculated.

Two shortcomings are apparent when this “stylised” approach is compared to real life.

- The Flat parameter can fall as low as 0.4 before the Reef parameter is called into play. This is probably due in part to the “Twist” function that was introduced to lower CE with reducing Flat. This was done to help low stability boats and was a reasonable codification of trends from various wind tunnel tests. In real life it is unrealistic to expect to be able to shed more than 60% - 50% (i.e. Flat = 0.6 - 0.5) of the lift force by sail trim. Flat values of 0.4 imply a change of moulded sail shape.
- The Reef parameter reduces the sail plan by multiplying I, J, P, and E by the Reef parameter, which gives rise to the sail area reduction pattern shown in Figure 3.7. This is clearly not what happens in real life, most often it is just the headsail that’s reduced in area and then mainly by a reduction in foot length.

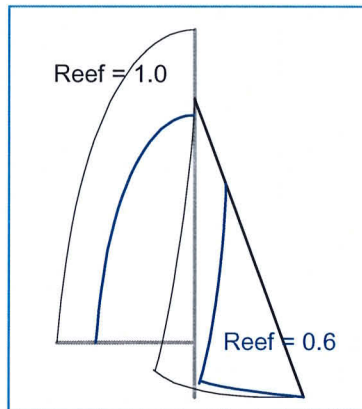


Figure 3.7 - Current IMS sail area reduction strategy.

Despite these effects the scheme worked well as a way of generating a set of aerodynamic forces that could be used to propel the boat in the VPP, it was robust and quick to use in finding optimum performance, and was sensitive to the main performance drivers.

Updated Scheme.

Thanks to the data generated by the Milan wind tunnel tests we can upgrade the quality of our aerodynamic force predictions to provide:

- A better codification of the effects of overlap, fractionality and mainsail planform (roach profile) on the effective rig height and centre of pressure.
- A more realistic sail reduction process based on the application of realistic minimum Flat value; a two stage reefing process, first a jib reduction from maximum to minimum area followed by a mainsail area reduction. The Jib reduction is to the default minimum area which is defined by some minimum values of jib luff and luff perpendicular. Those minima are established as reasonable values that give rise to the smallest headsail a racing yacht may sail with in 20 knots of breeze (i.e the max true wind speed used in the VPP predictions).

The new scheme is based on some new VPP variables “jib foot parameter” ftj , and “mainsail reduction factor” rfm working with a new optimisation parameter RED that replaces the current $Reef$ and $Flat$ parameters.

ftj is jib foot parameter ($ftj=1$ full size jib, $ftj=0$ minimum jib)

rfm is the main reduction factor, it works like the old Reef function but on the main only ($rfm=1$ full main, $rfm=0$ no main).

RED is a combination of these 2 factors into a single optimisation parameter.

$RED = 2$ then $ftj=rfm=1$, i.e. full sail

$RED=1$ then $ftj=0$, $rfm=1$, i.e. jib at minimum size

$RED < 1$ then $ftj=0$ and $rfm < 1$.

The progressive de-powering scheme is shown graphically in Figure 3.8 below. At each stage in the process the current sail area, fractionality and overlap are calculated and the surfaces interrogated to provide the Effective rig height and vertical centre of pressure position.

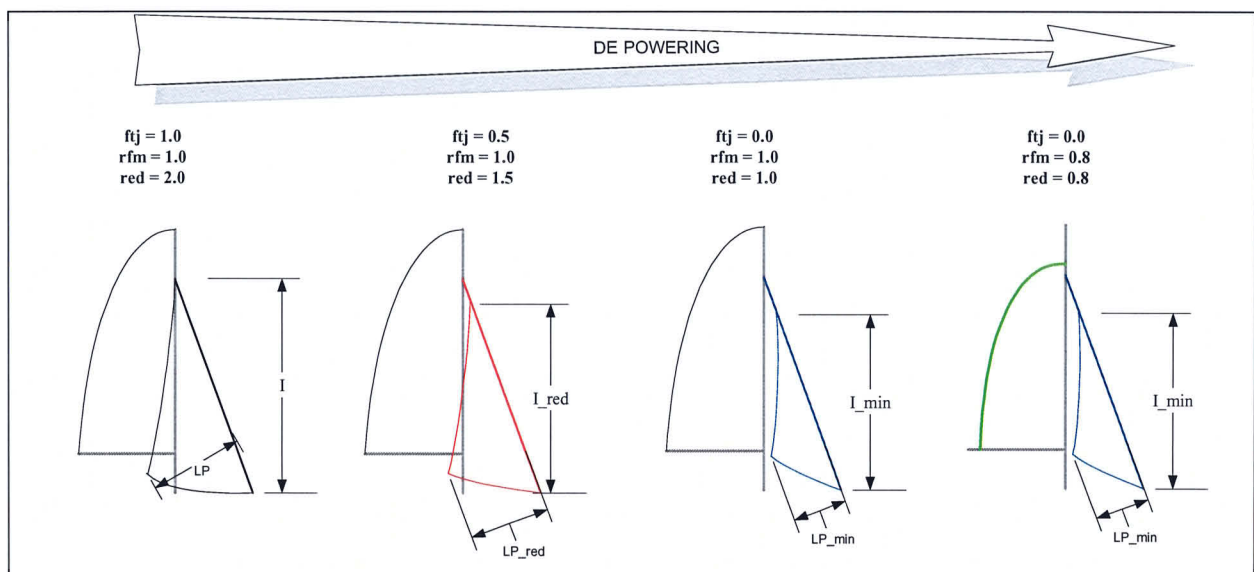


Figure 3.8 - New de-powering scheme.

The calculation of the sail forces is now calculated during each VPP iteration rather than adopting the “RIGANAL” approach of the old VPP code where as much of the aero model as possible was pre-calculated before the VPP itself was run. The current approach would not have been possible even 10 years ago due to the extra burden of calculation making the VPP too slow to run routinely. The extracts from the relevant computer code are shown in Figure 3.9.

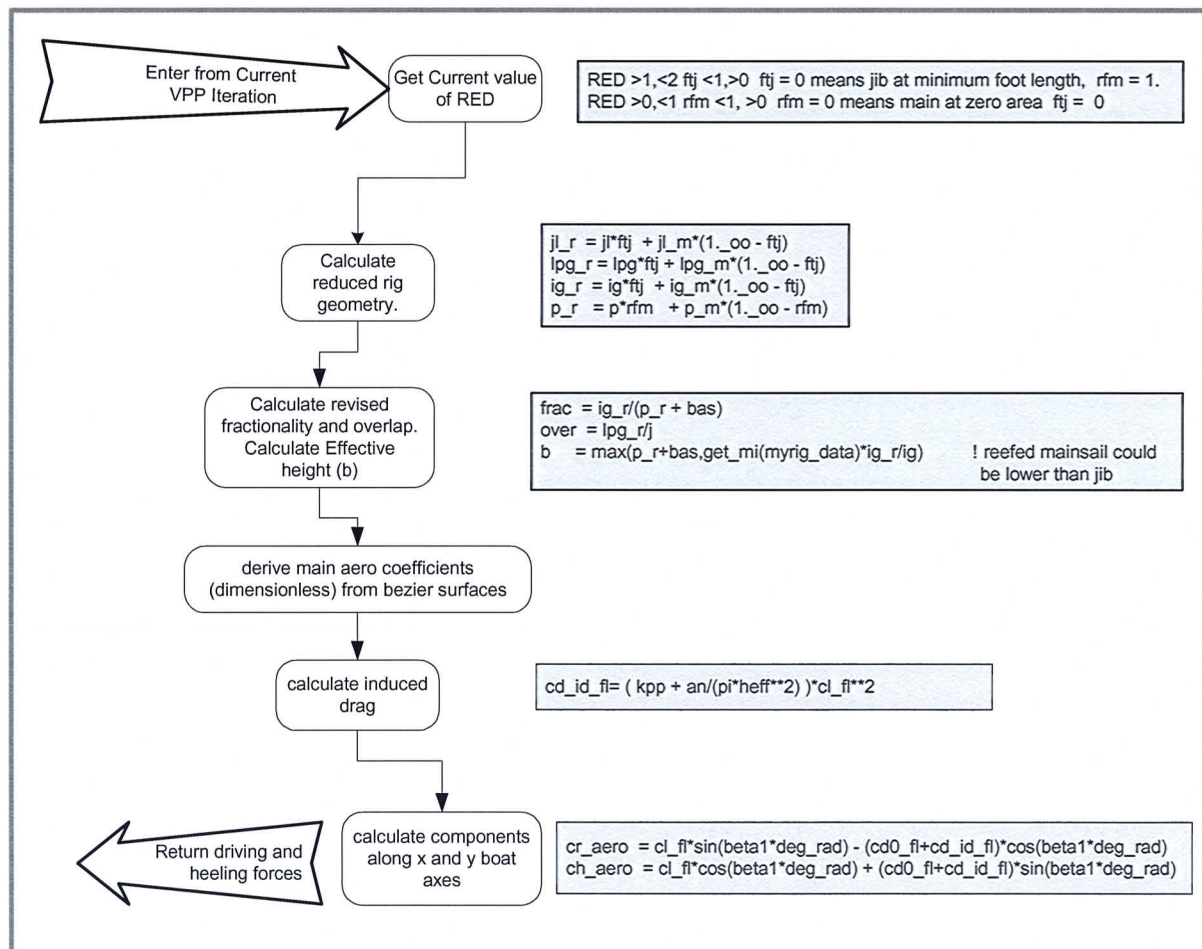


Figure 3.9 - New de-powering VPP code procedure.

4 RESULTS

To demonstrate the effects of the code revisions some parametric sail plan variations were made based around a Comet 45 racing sloop (Winner of the inaugural ORC International World Championship in 2008)

These variations consisted of variations of overlap (90% - 150%) and fractionality (100% (masthead rig) – 85%), each carried out with 3 different roach profiles, (Triangular, IMS limit and high roach), and at 3 different righting moments. It is obviously beyond the scope of this paper to present all this data, but a few key effects have been examined, namely:

- Effect of stability on de-powering behaviour (figures 4.1-4.2)

- Effect of changing fractionality (figure 4.3)
- Effect of changing overlap (figure 4.4)
- Effect of changing roach profile (figure 4.5)

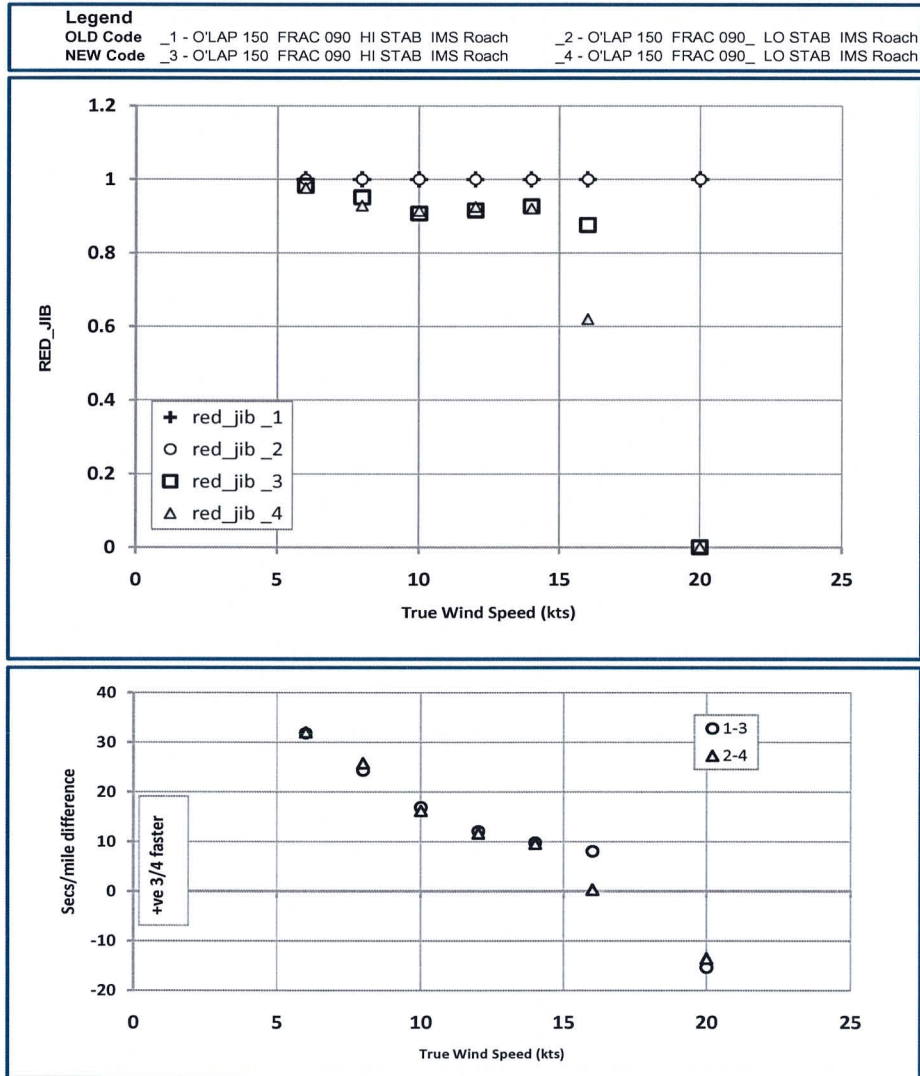


Figure 4.1 - Jib reduction factor and seconds per mile speed differences, varying stability.

Figure 4.1 shows that with the new code the jib reduction factor is brought into play at quite low wind speeds, but does not significantly call for a reduction in jib area until the wind speed has risen above 15 knots. In terms of handicapping the new code speeds up the boats (i.e. new code s/m < old code s/m) in light airs and slows them down in heavy airs. The s/m differences are based on the optimum upwind VMG.

This is explained by the new code predicting higher effective rig heights than the old code, as shown in Figure 4.2, where CHEFF, the effective rig height factor is plotted against true wind speed.

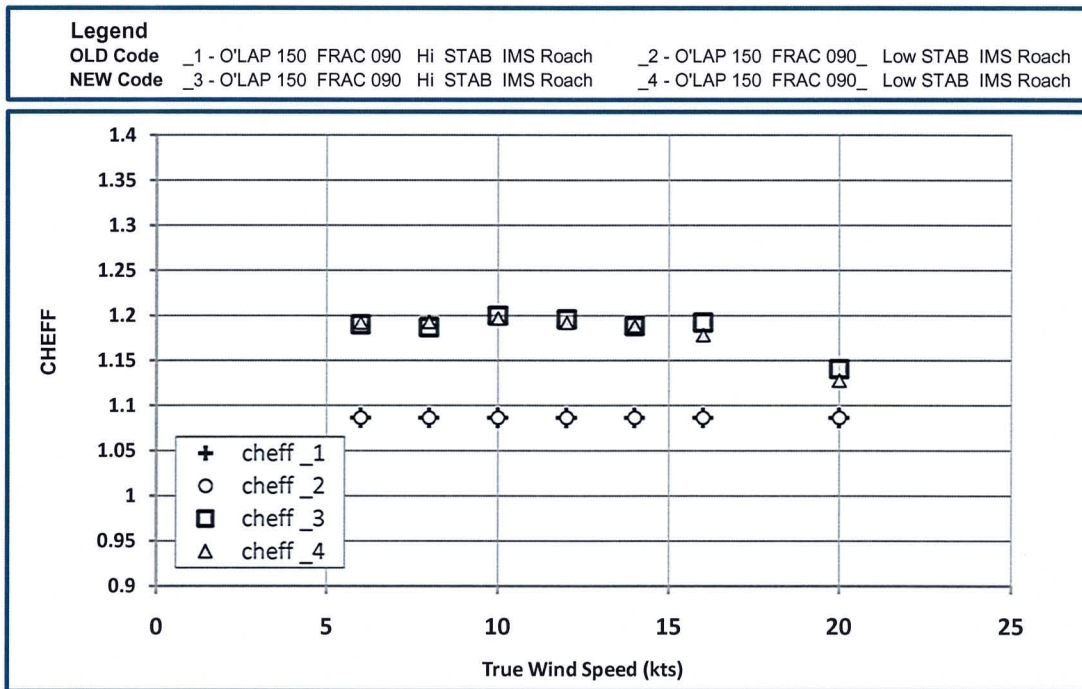


Figure 4.2 - Effective rig height factor vs. true wind speed.

Figure 4.3 shows the variation in Effective Rig height factor and the s/m differences for fractionalities of 0.85 and 1. The upper part of the figure shows that the effective height for the new code is greater for the mast head rig boat (Frac.=100%), and also the difference between CHEFF for the different fractionalities is much greater.

This gives rise to a speeding up of the mast head boats using the new code, which is most pronounced in light airs.

Legend
 OLD Code _1 - O'LAP 100 FRAC 085 Norm STAB IMS Roach _2 - O'LAP 100 FRAC 100. Norm STAB IMS Roach
 NEW Code _3 - O'LAP 100 FRAC 085 Norm STAB IMS Roach _4 - O'LAP 100 FRAC 100. Norm STAB IMS Roach

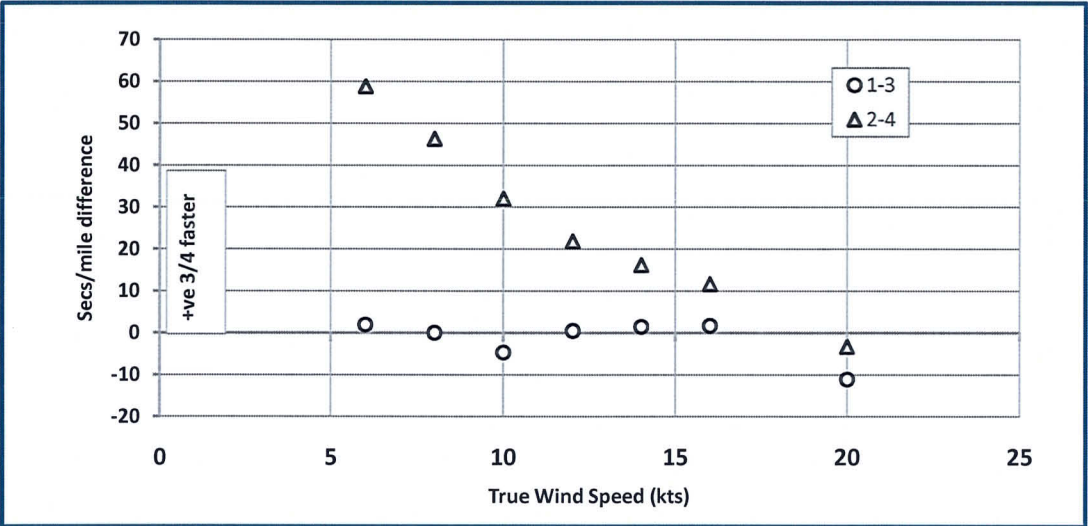
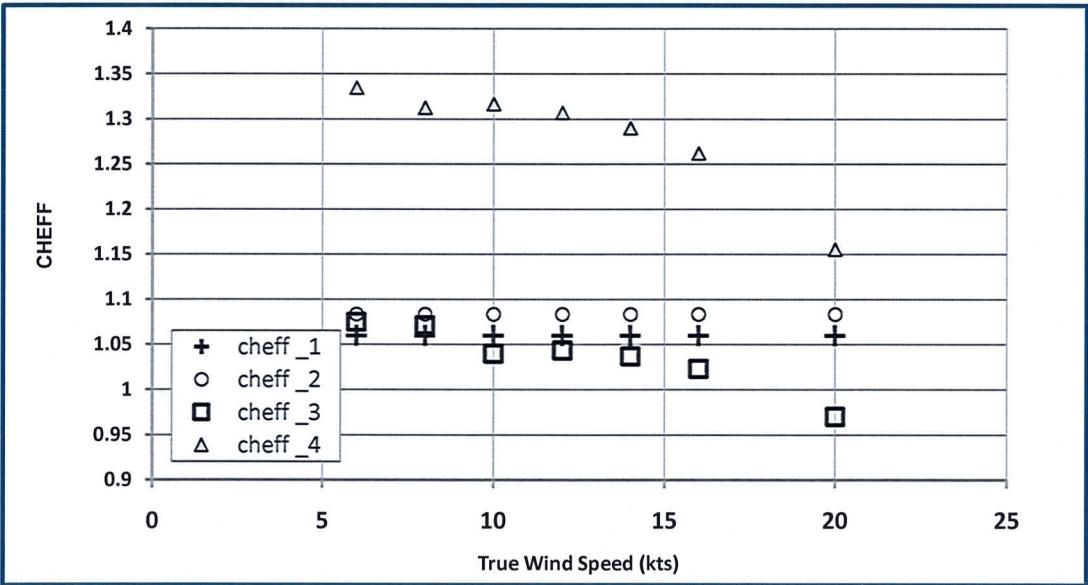


Figure 4.3 – Effective rig height factor vs. True wind speed for 85% and 100% fractionality.

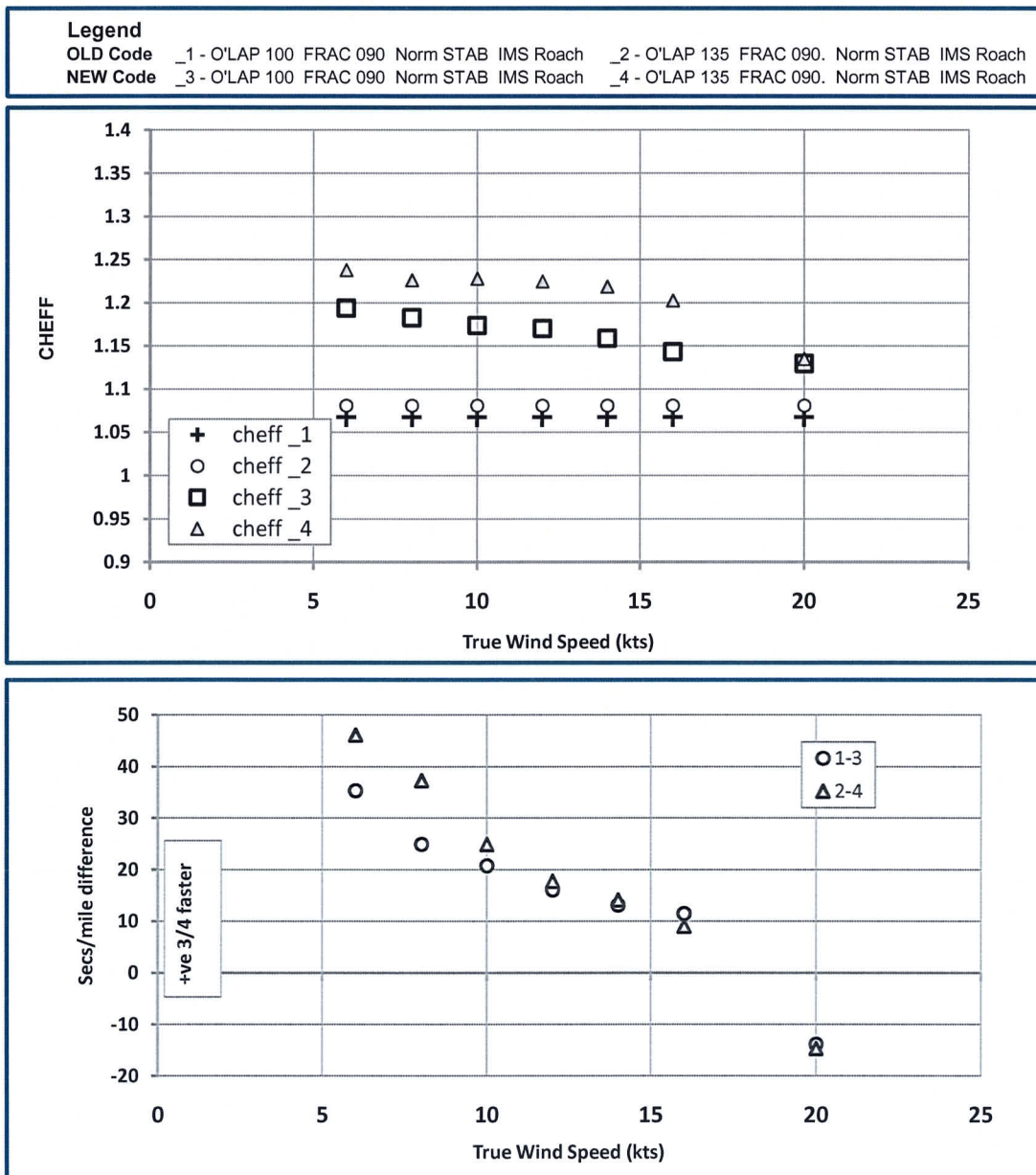


Figure 4.4 - Effective rig height factor vs. true wind speed for different Overlap (100% & 135%).

Figure 4.4 shows the variation of effective rig height factor for different overlaps (100% & 135 %) at 90% fractionality. Here again the effective rig height is higher for the new code and the differences between overlaps are more pronounced for the new code. This results in the new code speeding up the boats in light airs, with the 135% overlap yachts being sped up most.

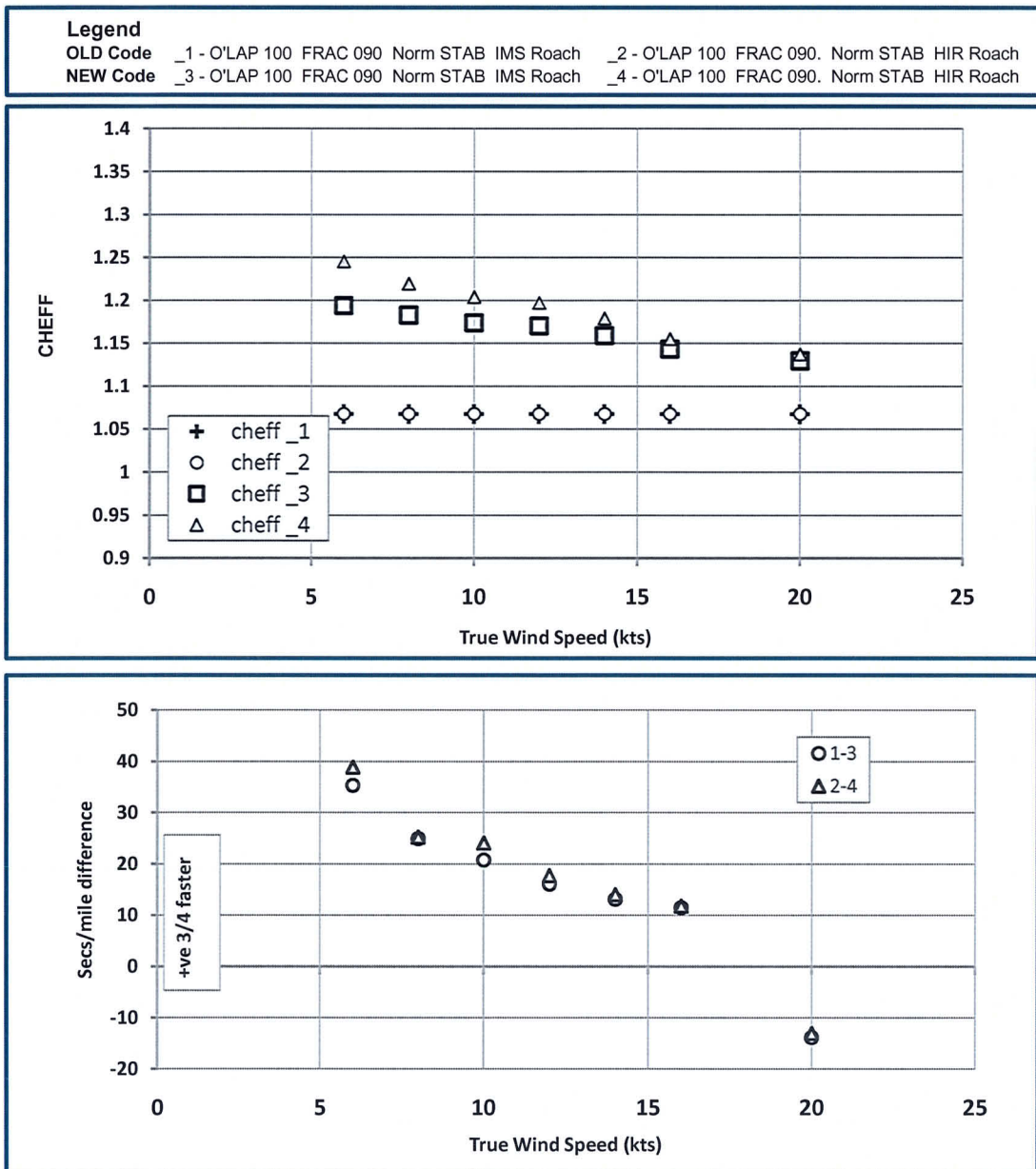


Figure 4.5 - Effective rig height factor vs. true wind speed for different Roach Profile

Figure 4.5 shows the effect of increasing mainsail roach. As expected the new code predicts higher effective rig heights for both the mainsails, and the high roach mainsail has a higher CHEFF than the IMS girth mainsail. This results in slightly higher predicted speeds for the high roach mainsail

5 CONCLUSIONS

This paper describes part of a more comprehensive general research program started in 2005 with partial funding from the ORC with the aim to investigate a series of rig planform variations in mainsail roach, jib overlap and rig fractionalities in order to overcome some perceived inequities in the ratings of boats of various rig design racing under the International Measurement System (IMS).

Moreover activities carried out in order to address new sail configurations in the rating process and in particular Code0 have been described.

The results of this investigation are used to assist the International Technical Committee (ITC) in changing the formulations in the ORC INTERNATIONAL VPP sail aerodynamic model. In particular a new progressive de-powering approach has been included in the VPP code leading to a more realistic sail reduction process based on the application of a two stage reefing process (first a jib reduction from maximum to minimum area followed by a mainsail area reduction).

REFERENCES

- [1] Kerwin, J.E. *A velocity Prediction Program for Ocean racing yachts, Rep 78-11 MIT*, July 1978
- [2] Poor C.L., Sironi N., *The International ,measurement system: a description of the new international rating system*, 11th HISWA Symposium, Amsterdam, 1990
- [3] Fossati F., Muggiasca S., Viola I. : *An investigation of aerodynamic force modeling for IMS Rule using wind tunnel techniques* – 19th HISWA Symposium, Amsterdam, 2006
- [4] Campbell I.M.C.. *Optimisation of a sailing yacht rig using wind tunnel data*. The Thirteenth Chesapeake Sailing Yacht Symposium, Annapolis, 1997
- [5] Edited by Cloughton, Wellicome, & Sheno, *Sailing Yacht Design Theory* Longman 1998
ISBN 0-582-36856-1
- [6] Cloughton, A, *Developments in the IMS VPP Formulations*, The 14th Chesapeake Sailing yacht symposium, Annapolis, USA, 1999
- [7] Teeters J, Ranzenbach R, Prince M, *Changes to Sail Aerodynamics in the IMS Rule*. The 16th Chesapeake Sailing yacht symposium, Annapolis, USA, 2003

Session 12

Bart Verwerft & Jan Alexander Keuning

“The Modification and Application of a Time Dependent Performance Prediction Model on the Dynamic Behaviour of a Sailing Yacht”

by

Bart Verwerft ¹

Alexander (J A) Keuning²

Notations:

α	angle of attack	C_{hull}	hull influence coefficient
β	leeway angle	C_{heel}	heel influence coefficient
β_0	zero lift drift angle	C_L	lift coefficient
δ_r	rudder angle	Fn	Froude Number
Φ	down wash angle	q	dynamic pressure
Λ	sweep back angle of the foil	Sc	wetter surface of the canoe body
φ	heel angle	Tc	draft of the canoe body
ψ	yaw angle	Vs	speed through the water of the yacht
AR_e	effective aspect ratio of the foil	$\frac{dC_L}{d\alpha}$	lift curve slope
b_k	span of the keel		
B_{wl}	waterline beam		

1. Introduction

The introduction by Keuning, Vermeulen and De Ridder in 2005 Ref [1] of a time domain simulation model, for the maneuvering behavior of a sailing yacht with the calculations of all the necessary coefficients in the equations of motions based solely on the results obtained from the Delft Systematic Yacht Hull Series (DSYHS), introduced the opportunity to formulate a time dependent solution of the equations of motion describing the equilibrium of an arbitrary sailing yacht or simulate the reaction of an arbitrary sailing yacht in changing environmental conditions. The development of such a simulation tool is often referred to as the development of a “dynamic VPP”, this in contrast to the “stationary” VPP.

In 2007 Keuning and Katgert Ref [2] already showed the possible beneficial application of this simulation model for the improvement of the tacking procedure of an IACC sailing yacht and Battistin and Ledri showed in a similar application the results for an IMS racing yacht in Ref [3].

This development now opens the opportunity to compare the results of the Velocity Prediction Program (VPP), with either a “stationary” or “steady state” true wind input with, using the same set of equations of motions, the (more) dynamic input of a varying true wind. The implicit assumption being that the later corresponds more to the realistic conditions found in the real sailing environment.

If the performance of all yachts is affected by the changing environmental conditions in the exactly the same way and to exactly the same amount, this is only of academic interest. If however it turns out that yachts, different by their prime design parameters, behave different in and react differently to changing conditions it becomes of more practical interest.

So the aim of the present study was to investigate some of these possible differences by comparing the results for stationary and the dynamic inputs in the dynamic VPP for a variety of changing conditions and a variety of yachts.

To be able to do this some of the formulations in the dynamic VPP, as originally formulated by Keuning e.a. in Ref [1], had to be reformulated to better suite the present applications in mind. In addition an entirely new approach to the side force formulation of the hull and its appendages has been derived. This new formulation overcomes the somewhat inconsistent approach as it was

¹ MSc student Delft Shiphysics Department, Delft University of Technology

² Associate Professor Delft Shiphysics Department, Delft University of Technology

used in the original model between the upright (no heel) and the heeled conditions and yields a better result in particular to the yaw moment developed by the hull and appendages, which is of prime interest in the maneuvering behavior of the yachts. The results of this development and some results of the applications will be presented in this paper.

2. Further development of the model

2-1 Modifications of the model to suite the present project.

Most modifications to the original model are in the aerodynamic formulations, used to calculate the sail forces.

In the original model as formulated by Keuning and Vermeulen Ref [1] no provisions were made for a varying true wind speed and a varying true wind direction. For the present study the provision to do it was considered essential to be able to introduce time dependent true wind speed and true wind direction. Also the possibility to simulate the behaviour of the yachts in a broad range of true wind directions was considered essential. The original model could only handle upwind scenarios. The primary aim of the original research by Keuning and Vermeulen was to formulate a model for the upwind sail balance of a wide variety of (mega) ships. So their main interest was in upwind conditions. Also in the later extension by Keuning and Katgert as presented in Ref [2] for the IACC yacht the primary focus was still on upwind sailing conditions and the associated tacking manoeuvres.

For the present study however it was considered to be important to be able to include a wider range of true wind angles and a varying true wind, both in speed and direction, to be able to compare the results of the static versus dynamic VPP's in a wide range of conditions, because the differences between the two solutions could very well be dependent on this.

So these adaptations to the code have been made. In general the formulations of the IMS sail force model have been used for the calculations and the in frame of this report for the sake of available space, reference is made to the more recent associated reports on this subject by various authors, amongst others, Claughton Ref [10], Cambell Ref [11], Ranzenbach Ref [12] and Fossati Ref [13] and documentations released by the ORC. It should be noted however that at present the model only accounts for the use of a mainsail and a jib.

In addition the possibility is introduced to use a true wind history as obtained from full scale measurements as an input file for the simulations.

In the hydrodynamic model no significant changes have been made. It should be noted however, that the new possibility to sail the boat at broader true wind angles, introduces the possibility of much higher boat speeds to be attained. Special attention therefore has been paid to the validity of the used expressions at these higher forward velocities. Also the yaw moment introduced by the off-centrelines position of the trust force generates a very large yaw moment in the broad reach and downwind conditions, when no spinnaker or poled out jib is taken into account. In the aero model at present only the offset due to heel is used and no attempt has been made to formulate the additional yaw moment due to slacking of the main sheet.

Another modification is the inclusion of different auto pilots to sail the ship in the simulations. In the original model only pre-described rudder scenarios have been used. Because true wind changes and scenarios may now be introduced a simple straight course keeping algorithm with constant helm does no longer suffice. The model was therefore extended with different auto pilot controls, keeping the yacht either at a constant course, constant apparent wind angle or true wind angle.

The autopilots in the model all have a similar structure, in which the input is the instantaneous course difference and course difference velocity. According to:

$$\delta_r^{n+1} = \delta_r^n + c_1 * (\Psi^{n+1} - \Psi_{set}) + c_2 * (\dot{\Psi}^{n+1})$$

where:

- δ_r^{n+1} : new rudder angle
- δ_r^n : rudder angle of the previous time step
- Ψ^{n+1} : heading of the yacht
- $\dot{\Psi}^{n+1}$: yaw velocity of the yacht

The coefficients c_1 and c_2 are determined considering the application in mind.

2-2 New side force model for the hull and appendages

In the original model the total side force of the hull and appendages and the separate contributions of hull, keel and rudder, are assessed differently in the upright and the heeled conditions:

In the upright condition the so called Extended Keel Method, as derived by Gerritsma Ref [4], is used to calculate the side force on keel and rudder, in which the side force generated by the hull is accounted for by the virtually extended keel inside the canoe body to the waterline. The downwash angle on the rudder is approximated as 50% of the leeway angle and the water velocity over the rudder reduced by 10% to account for the wake of the keel.

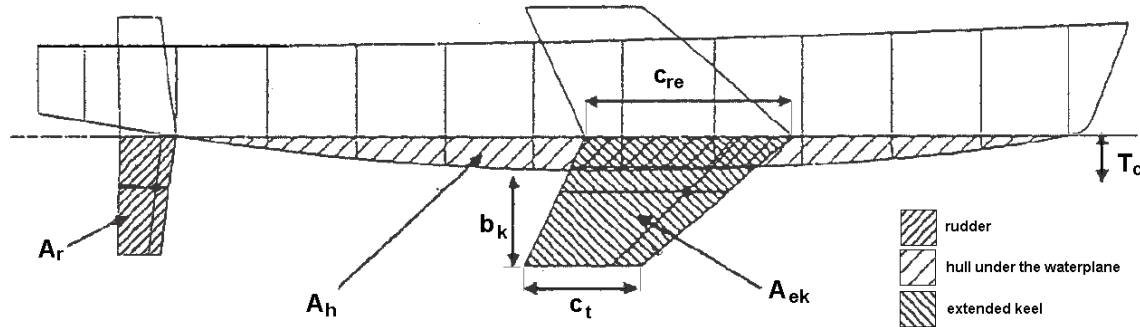


Figure 1: Definitions in the extended keel method

The total side force is calculated as the sum of the force on extended keel and rudder according to:

$$Y_{total} = Y_{ek} + Y_r$$

$$Y_{ek} = \frac{1}{2} \rho V_s^2 A_{ek} \left(\left(\frac{\partial C_L}{\partial \alpha} \right)_{ek} \beta \right)$$

$$Y_r = \frac{1}{2} \rho (0,9 V_s)^2 A_r \left(\left(\frac{\partial C_L}{\partial \alpha} \right)_r 0,4 \beta \right)$$

In which:

Y_{total} :	<i>the total side force in the horizontal plane</i>	[N]
Y_{ek} :	<i>the side force generated by the extended keel</i>	[N]
Y_r :	<i>the side force generated by the rudder</i>	[N]
A :	<i>The lateral area of the foil</i>	[m ²]
$\left(\frac{\partial C_L}{\partial \alpha}\right)$:	<i>the lift curve slope of the foil</i>	[deg ⁻¹]

The full yaw moment in this upright condition is calculated using the side force on keel and rudder with their respective separations to the centre of gravity of the ship and adding the yaw moment on the hull originating from the so called Munk moment. This procedure is fully developed and described by Keuning and Vermeulen in Ref [5].

Under heel this procedure does not work. Therefore in these conditions the results of the side force polynomial as derived from the results of the DSYHS by Keuning and Sonnenberg Ref [6] are used. This polynomial accounts for effects of heel angle and forward speed on the total side force production.

$$Fh \cos(\phi) = \left(b_1 \frac{T^2}{Sc} + b_2 \left(\frac{T^2}{Sc} \right)^2 + b_3 \frac{Tc}{T} + b_4 \frac{Tc}{T} \frac{T^2}{Sc} \right) \frac{1}{2} \rho V s^2 Sc (\beta - \beta_{Fh:0})$$

$$\beta_{Fh:0} = B_3 \phi^2 Fn$$

in which:

$Fh \cos(\phi)$:	<i>the side force in the horizontal plane</i>	[N]
$\beta_{Fh:0}$:	<i>the zero lift drift angle</i>	[deg]
T :	<i>the total draft of hull with keel</i>	[m]
T_c :	<i>the draft of the canoe body</i>	[m]
Sc :	<i>the wetted surface of the canoe body</i>	[m]
Fn :	<i>the Froude Number</i>	[-]

and:

$$B_3 = 0,0092 * \left(\frac{Bwl}{Tc} \right) \left(\frac{Tc}{T} \right)$$

The coefficients b_1 to b_4 are presented as functions of the heeling angle between 0 and 30 degrees of heel.

The use of this expression yields however no information on the contribution of the three different components, i.e. hull, keel and rudder and therefore no result for the yaw moment can be found. To overcome this problem the distribution over keel and rudder as found in the upright condition is used in the heeled condition also. The Munk moment on the hull is calculated taking the geometry of the heeled hull in account. This procedure is also described in Ref [5]. Keuning, Katgert and Vermeulen Ref [7] improved the prediction of the side force production for higher aspect ratio keels and the yaw moment under heel by taking the newly derived formulation for the influence of the downwash of the keel on the rudder into the calculations.

This situation of using two different approaches was considered undesirable and inconsistent. So in the framework of the present study a new method has been developed.

In this new method the side force generated by keel and rudder is calculated using the expression derived by Whicker and Fehlner (W&F) for thin airfoils Ref [8]. This expression reads

$$\frac{d C_L}{d \alpha} = \frac{a_0 AR_e}{\cos \Lambda \sqrt{\frac{AR_e^2}{\cos^4 \Lambda} + 4 + \frac{57,3 a_0}{\pi}}}$$

In which:

$$\begin{aligned} AR_e &: \text{the effective aspect ratio} & [m] \\ \Lambda &: \text{the sweepback of quarter - chord line} & [rad] \\ \alpha &: \text{angle of attack} & [deg] \\ a_0 &: \text{the corrected section lift curve slope} & [-] \\ & a_0 = 0,9 \left(\frac{2\pi}{57,3} \right) \text{ per degree} \end{aligned}$$

In the present calculation the foils are not extended to the free surface, but taken at their actual size. The effect of the hull on the side force generation is formulated separately.

The end plate effect of the hull on the keel is generally taken into account by taken for the effective aspect ratio of the wing the double value of the geometrical aspect ratio of the wing, according to:

$$AR_e = 2 AR_{geo} = 2 \frac{b}{c_{mean}}$$

In which:

$$\begin{aligned} AR_e &: \text{the effective aspect ratio} & [-] \\ AR_{geo} &: \text{the geometric aspect ratio} & [-] \\ c_{mean} &: \text{mean geometric chord} & [m] \\ b &: \text{span of the foil} & [m] \end{aligned}$$

This is not the only effect of the presence of the hull. There is also the “lift carry over” from keel to the hull. From earlier measurements it was already found that the lift generated by the bare hull of a sailing yacht is generally small, so the main effect must be in the lift carry over from keel to hull. In an attempt to capture this lift carry over the ratio between the entire lift of the appended hull and the lift generated by the keel and rudder as calculated by using W&F expression is determined for the DSYHS. This ratio is further referred to as **hull influence coefficient** c_{hull} i.e.:

$$c_{hull} = \frac{L_t}{(L_k + L_r)}$$

In which:

$$\begin{aligned} c_{hull} &: \text{the hull influence coefficient} & [-] \\ L_t &: \text{the total measured hydrodynamic lift of the yacht} & [N] \\ L_r &: \text{the calculated lift of the rudder (with end plate)} & [N] \\ L_k &: \text{the calculated lift of the keel (with end plate)} & [N] \end{aligned}$$

This c_{hull} is now determined for the hulls of the DSYHS for the upright condition and this looks like the result depicted in Figure 2.

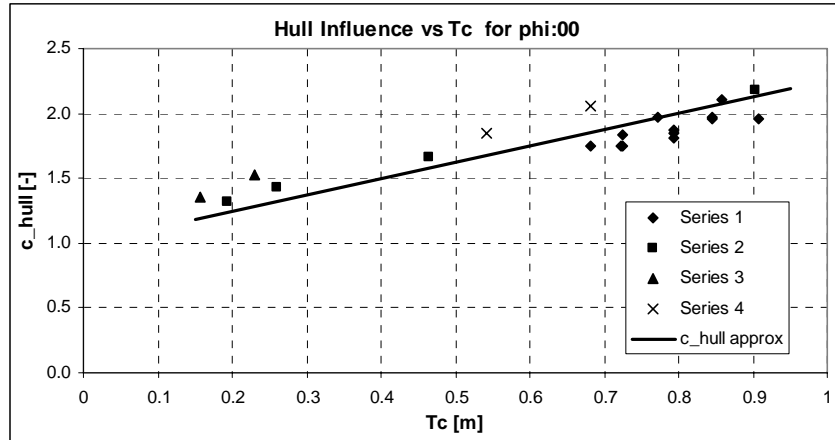


Figure 2: Hull influence coefficients vs. canoe body draft

The relation following for this approach for the keels and hulls in the DSYHS yields the following expression:

$$c_{hull} = a_0 Tc + 1 \quad \text{with: } a_0 = 1.25$$

To extend the range of application of this expression to keels with other plan forms (i.e. aspect ratios) the results of the Delft Various Keel Series (DVKS) and the Delft Systematic Keel Series (DSKS), as previously described by Keuning and Binkhorst in Ref [9] and Keuning and Sonnenberg in Ref [6], are used.

This yields the following dependency and formulation for the hull influence coefficient in the upright condition (Figure 3):

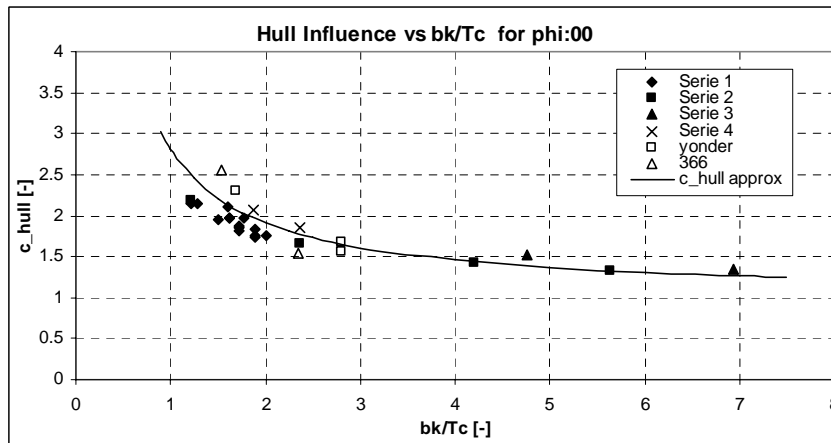


Figure 3: Hull influence coefficient vs. b_k/Tc ratio

With:

$$c_{hull} = 1,8 \frac{Tc}{bk} + 1$$

Now the influence of the heeling angle on the lift has to be taken into account. The influence of the heel angle on the lift production is captured by two mechanisms: one is the lift curve slope reduction due to the fact that the foils are brought closer to the free surface expressed as **heel influence coefficient** c_{heel} , the second one is the **zero lift drift angle** β_0 , which originates from the asymmetry of the hull when heeled. This asymmetry introduces a “negative” angle of attack on the appendages, which increases with heel angle and the beam to draft ratio in particular. This implies that the effective angle of attack on the appendages is reduced with this β_0

At first based on the results of the DSYHS, the DVKS and the DSKS a linear relation between the reduction of the lift curve slope and the heel angle due to the free surface effect is assumed. The results also show a moderate dependency on B/T ratio and forward speed, but for the time being this effect is neglected and shifted to future research. So in the present study for this effect of heel the following expression is used:

$$c_{heel} = 1 - b_0 \phi \quad \text{with: } b_0 = 0.382 \text{ for } \phi: [rad]$$

Also using the results of the above mentioned series an expression has been found for the zero lift drift angle, which shows reasonable agreement with the measured results. This expression reads:

$$\beta_0 = \left(c_0 \frac{B_{wl}}{Tc} \phi \right)^2 \quad \text{with: } c_0 = 0.405 \text{ for } \phi: [rad]$$

For the present research the forward speed influence on the lift curve slope has been neglected.

Finally the downwash angle of the keel on the rudder is approximated using the expression as formulated by Keuning, Katgert and Vermeulen in Ref [7].

$$\Phi = a_0 \sqrt{\frac{C_{Lk}}{AR_{e_k}}}$$

In which:

- Φ : the downwash angle at the rudder [rad]
- AR_e : the effective aspect ratio of the keel [-]
- C_{Lk} : the lift coefficient of the keel [-]

phi	0°	15°
a ₀	0,136	0,137

The lift production of the keel is now calculated as follows:

$$Lc_{keel} = Lk_{W \& F} c_{hull} c_{heel}$$

$$Lk_{W \& F} = \left(\frac{dC_L}{d\alpha} \right)_{(W \& F)} \alpha_{e_{keel}} \frac{1}{2} \rho V_{e_{keel}}^2 A_{lat_{keel}}$$

In which:

$$V_{e_{keel}} = \sqrt{(-v - x_k \dot{\Psi} + (0,43 b_k + T_c) \dot{\phi})^2 + u^2}$$

$$\alpha_{e_{keel}} = \text{atan} \left(\frac{(-v - x_k \dot{\Psi} + (0,43 b_k + T_c) \dot{\phi})}{u} \right) - \beta_0$$

Along the same lines the lift production on the rudder is calculated using the following formula, now including the effect of the downwash of the keel:

$$Lc_{rudder} = Lr_{W\&F} c_{hull} c_{heel}$$

$$Lr_{W\&F} = \left(\frac{dC_L}{d\alpha} \right)_{(W\&F)} \alpha_{e_{rudder}} \frac{1}{2} \rho V_{e_{rudder}}^2 A_{lat_{rudder}}$$

in which:

$$V_{e_{rudder}} = \sqrt{(-v - x_r \dot{\Psi} + (0,43 b_r) \dot{\phi})^2 + u^2}$$

$$\alpha_{e_{rudder}} = \text{atan} \left(\frac{(-v - x_r \dot{\Psi} + (0,43 b_r) \dot{\phi})}{u} \right) - \beta_0 - \Phi - \delta_r$$

The yaw moment is calculated using the side forces generated by the individual components and multiplying it with the distance of the corresponding centre of effort to the centre of gravity of the yacht. The yaw moment of the hull is calculated by taking the Munk moment over the entire length of the hull both upright and heeled as described by Keuning and Vermeulen in Ref [5].

The results of the new approach for the side force and the yaw moment calculation of the hull have been compared with the results of the previous method by Keuning and Vermeulen. In general it was found that the results of the new method show comparable correlation with the measurements as the results obtained with the old method.

This implies however that the new method is preferred due to its higher consistency over the heel angle. An important improvement is also found in the fact that now in both the upright and the heeled condition the actual area of the keel and rudder is taken into the side force calculations, while in the earlier expression only the effective draft of the keel was considered. Changes in the chord were not considered. Also improvements in the method may be expected when more of the available data is taken into account then in the present project. This extension is foreseen in the future.

Some typical results of the different approaches are depicted in Figure 4 to Figure 7.

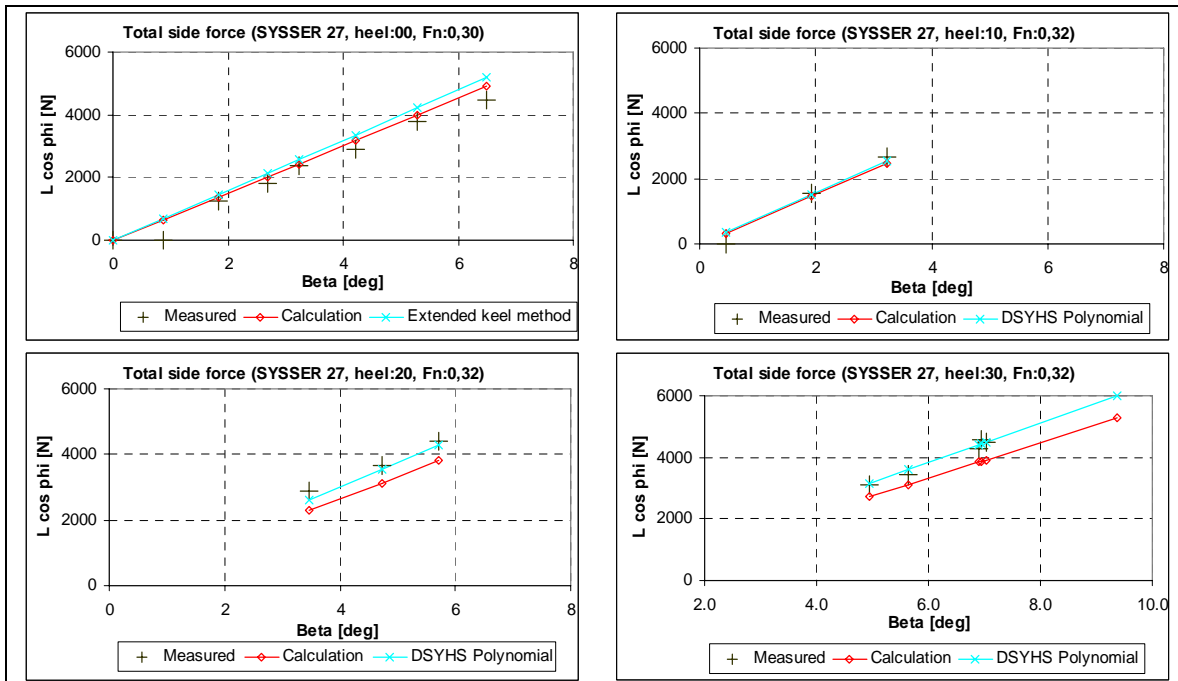


Figure 4: Measured and calculated total hydrodynamic side forces vs. leeway for SYSSER 27

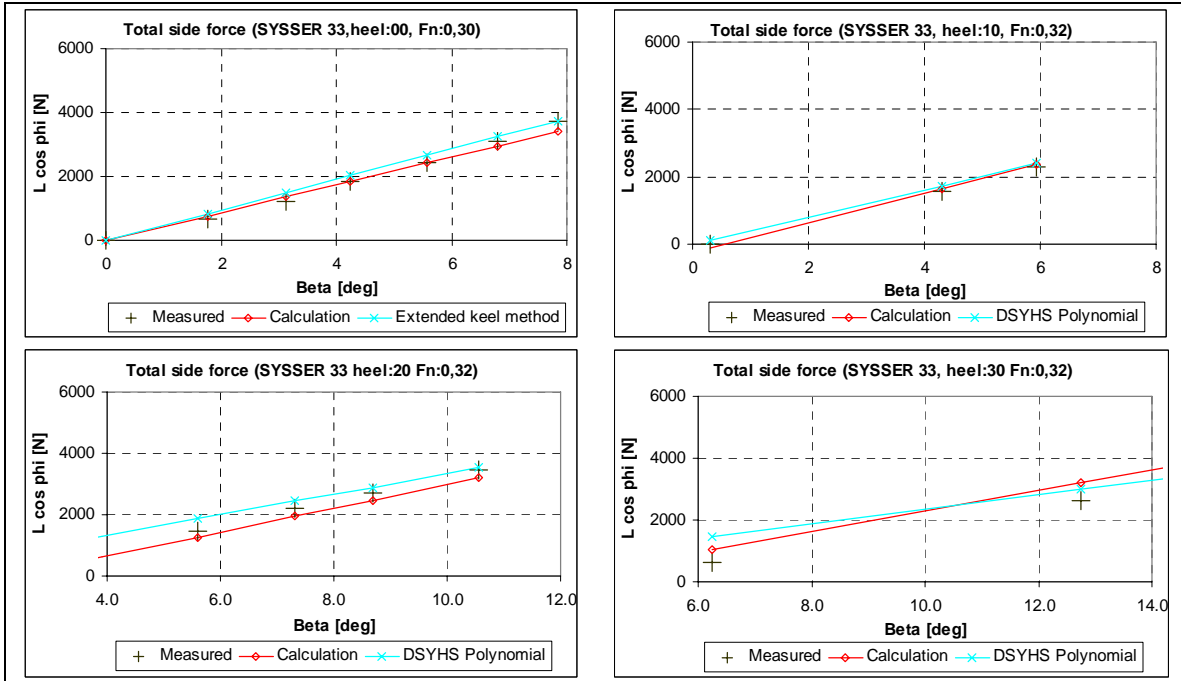


Figure 5: Measured and calculated total hydrodynamic side force vs. leeway for SYSSER 33

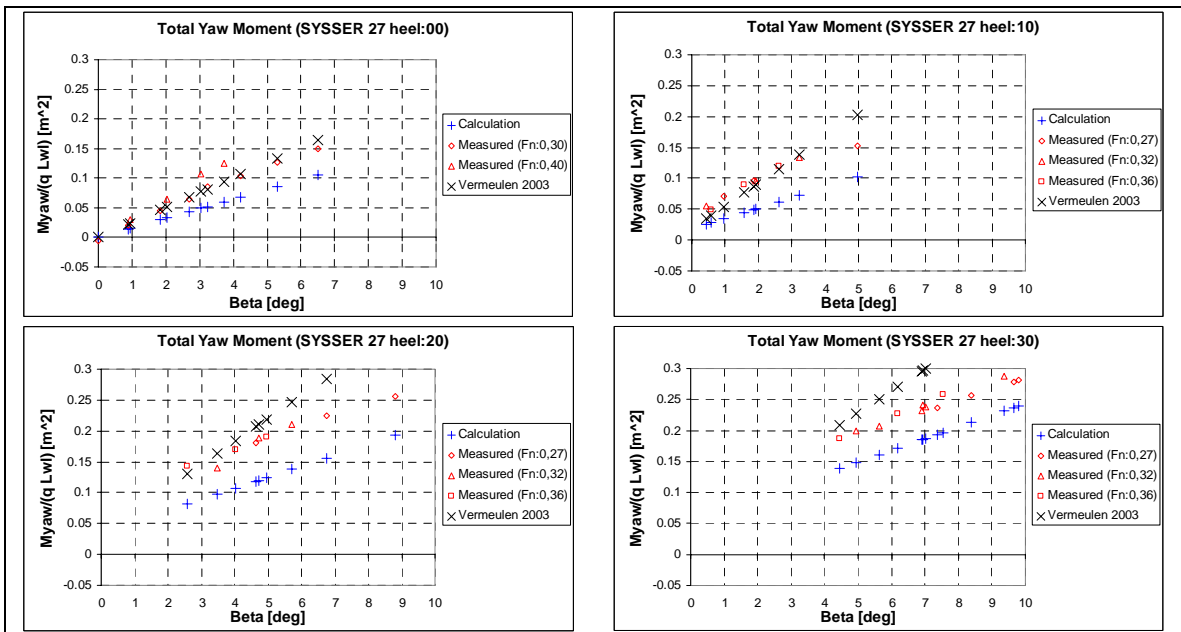


Figure 6: Measured and calculated total hydrodynamic yaw moment vs. leeway for SYSSER 27

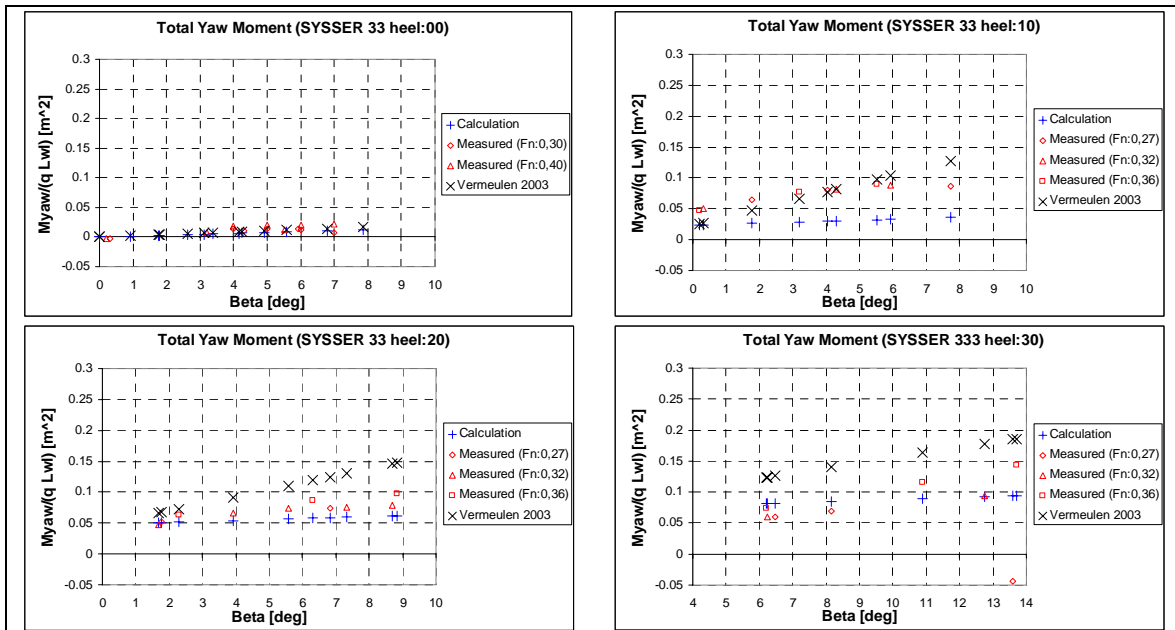


Figure 7: Measured and calculated total hydrodynamic yaw moment vs. leeway for SYSSER 33

3. The Applications

With the dynamic VPP it now becomes possible to investigate the influence of some dynamic phenomena on the performance of sailing boat. These dynamic phenomena may be at present be restricted to fluctuations in true wind strength and true wind direction. The differences between the dynamic solution and the static solution are determined by using the same dynamic VPP but with either a stationary or a fluctuating input. This was done in order to evade possible differences between the customary VPP and the dynamic VPP for the same input. Although by comparison these differences showed to be small some still do exist in particular due to differences in the aerodynamic model. In the following sections all results are presented as differences in distance lost over the distance travelled, presented in percentages, plus meaning distance lost so the boat is slower and minus vice versa.

First it was considered to be of interest to investigate if and how one particular boat is affected by fluctuating true wind strength.

Analyzing some true wind records as obtained from a series of full scale measurements in two different conditions, i.e. close hauled and broad reaching, it appears that a 2 meters per second fluctuation at an average wind speed of around 12-16 knots is not unrealistic. Therefore such an amplitude of the true wind oscillation was selected for this study.

From the same analysis it showed that the “period” of the oscillation depends on the true wind angle: in close hauled condition this period is somewhere around 60 – 70 seconds, in broad reaching condition this is around 200 seconds. This difference between the two conditions can be explained by the fact that broad reaching the gust is followed by the boat so it stays with it for a longer time, while in the upwind condition the opposite holds true. A typical result of such an onboard measurement may be seen in Figure 8 and Figure 9.

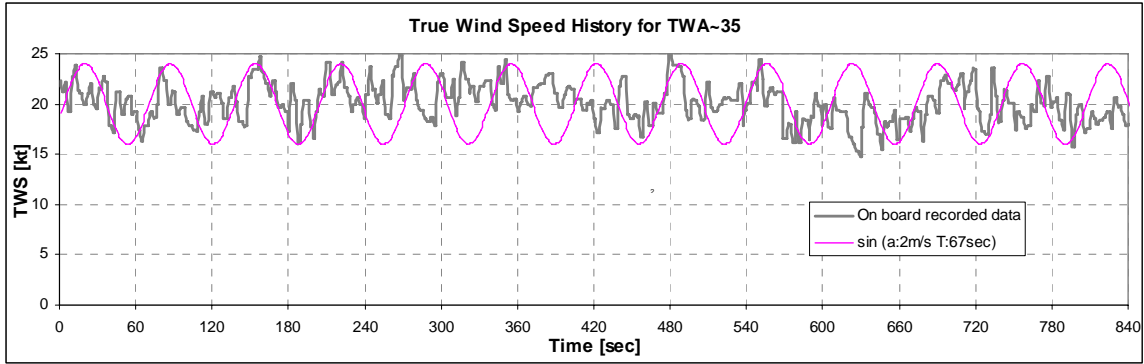


Figure 8: Wind history recorded on board while sailing upwind

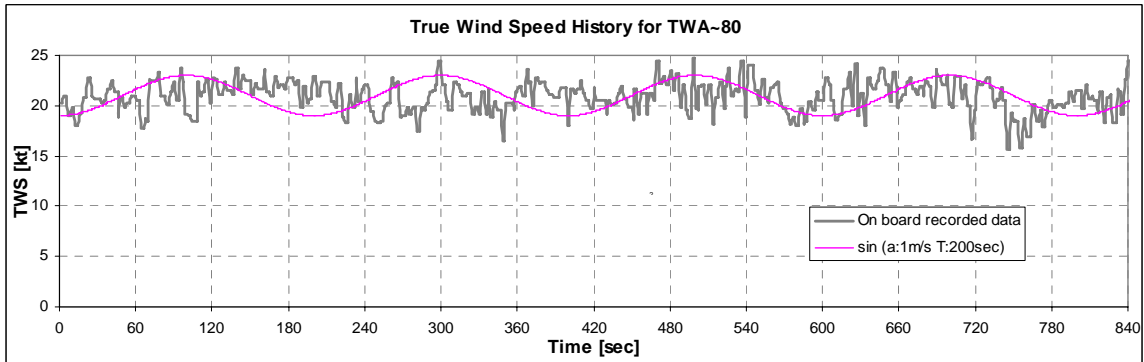


Figure 9: Wind history recorded on board while reaching

What also may be concluded from these records is that there appears a long(er) period fluctuation in the true wind speed, as denoted above, but super imposed on this is a (number of) fluctuations with a significantly shorter period, for these particular records somewhere around 10 seconds and some even shorter. The ultimate approach would be to determine a true wind spectrum, containing all relevant frequencies and amplitudes. In the present study such an attempt has not been made, but instead a simplified approach using a double frequency true wind input signal just to show the effect.

The effort has been made to simulate all these possible scenarios in a more or less systematic way for one particular boat. The main particulars of this boat chosen are presented in Table 1, yacht “b1”. It is supposed to represent a typical contemporary racing boat.

yacht:		b1	b3	b4
		parent	heavy	light
Lwl	[m]	10	10	10
Bwl	[m]	2.5	2.5	2.5
Displ	[m ³]	4.62	10	2.9
Tc	[m]	0.46	0.46	0.46
Sail Area	[m ²]	62.6	62.6	62.6
L/Displ ^{1/3}	[-]	6.00	4.64	7.01
SA/Displ ^{2/3}	[-]	22.57	13.49	30.78

Table 1: Dimensions of the yachts used for the assessment

The different wind scenarios that have been used in the simulations are depicted in Figure 10.

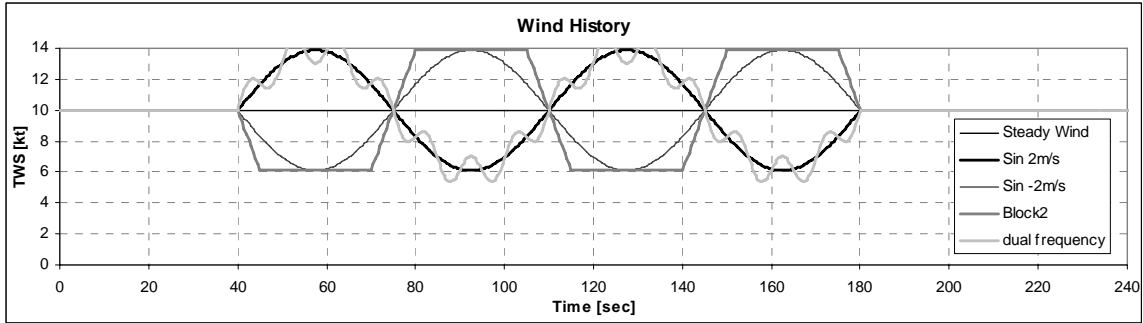


Figure 10: Different true wind scenarios applied

As may be seen here the average wind speed is 10 kts. The amplitude of the fluctuation is 2 m/s. Five different true wind speed scenarios have been used, i.e.:

1. the stationary wind (no change over time)
2. sinusoidal change with amplitude 2 m/s and 70 sec period, starting with an increase
3. sinusoidal change with amplitude 2 m/s and 70 sec period, starting with a decrease
4. a block shaped variation with the same amplitude and period
5. a double frequency harmonic signal with period 1 equal to 70 sec and period 2 equal to 10 sec.

The simulations have been carried out with a true wind angle of 35 and 140 degrees. The autopilot used was the constant true wind angle variant. The respective results of these simulations presented as distance lost using these scenarios are depicted in Figure 11.

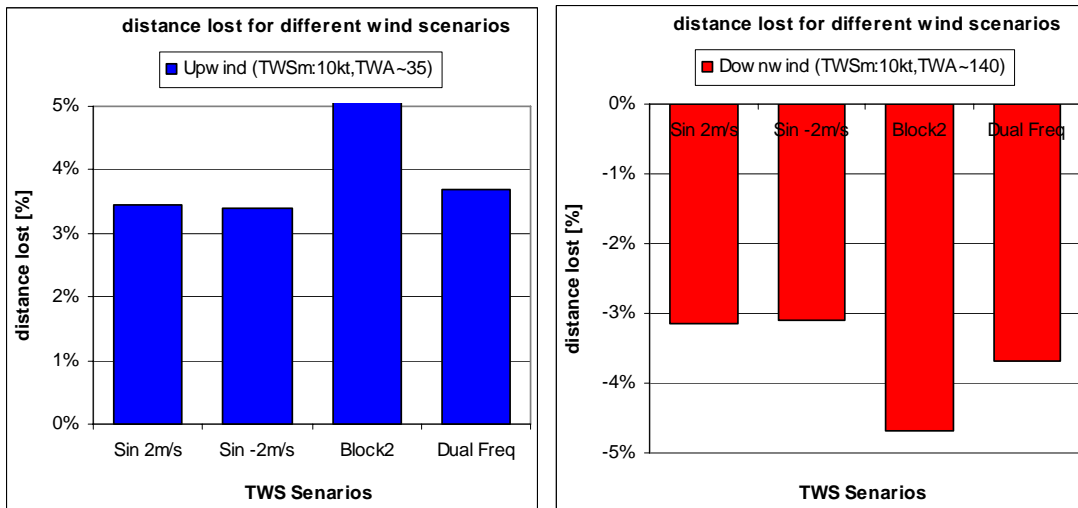


Figure 11: Distance lost in respect to the steady wind scenario for up and downwind course

As may be seen from these results the loss in distance is quite significant, i.e. on average more than 3% of the distance travelled. The biggest loss is with the block shaped gust scenario and amounts some 5%. Apparently the steep flanks of this scenario cause the largest differences. The dual frequency scenario has a larger loss than the pure sinusoidal one, as is to be expected for the same reason. The inclusion of more and / or different periods and amplitudes may lead to further deviations of the purely sinusoidal scenario, but have in the present study not been investigated. Similar results have been found for the condition with 140 degrees true wind angle.

From these results in general it may therefore be concluded that there is a significant difference between the outcome for a steady state true wind and a fluctuating true wind under the given restrictions of autopilot etc. It should be noted however that these differences are of no real interest if all boats are affected in the same way.

This is the reason that the simulations have been extended to three different designs with significantly different weights of displacement. This was considered of interest because a long lasting debate about the difference between heavy and light displacement in this respect has been going on for a long time.

So three different “designs” have been generated and it should be noted that no serious attempt has been made to make it realistic designs. The emphasis was on having boats with very different length displacement ratios. For the sake of simplicity no changes have been made to either sail plan or stability, which makes them from a sailors point of view un realistic designs. The effect of the selected parameters may so be overemphasized. The main particulars of the designs are depicted in Table 1.

To gain more insight in how these different boats are affected by the changing wind speed the following figures have been prepared. In these figures the changing true wind speed, the boat speed, the changing apparent wind angle and the changing driving force for the cyclic wind variation have been plotted for the three different boats.

The first set of graphs (Figure 12) deals with the situation close hauled at 8 knots average true wind speed.

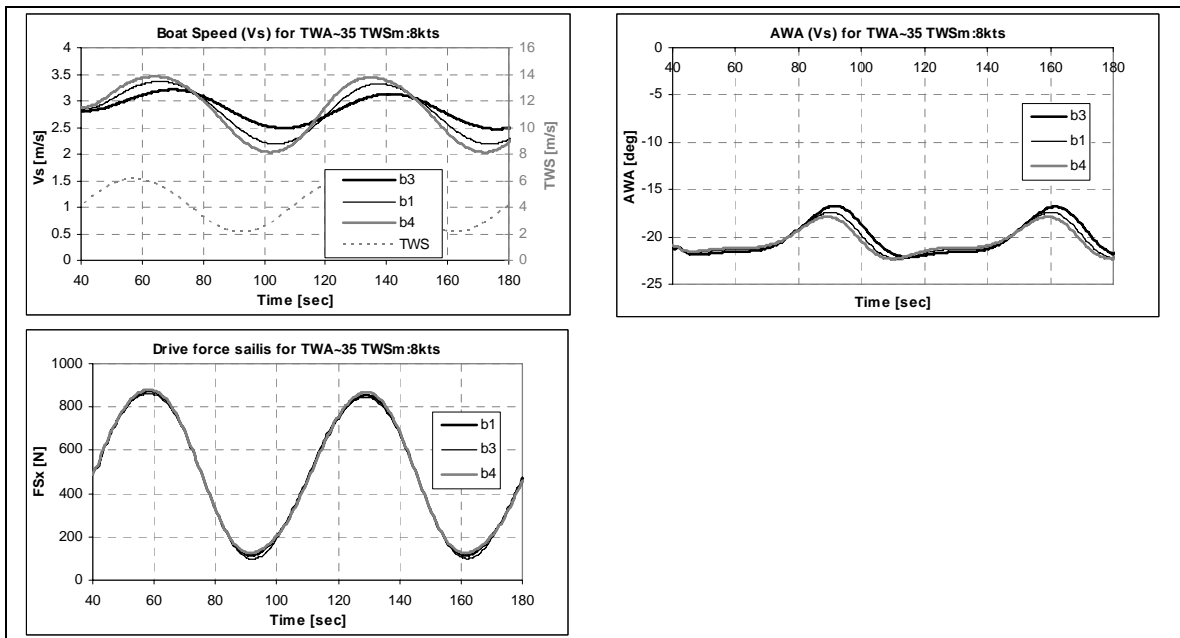


Figure 12: data for close hauled at 8kts average TWS

As may be seen the heavier boat gets a much larger phase shift with respect to the true wind fluctuation than the light boat, meaning she decelerates slower and accelerates slower also, although slightly less. This works out also in the change in apparent wind angle. Due to the large scale the differences between the three designs in the driving force are somewhat masked but the overall change in driving force due to the true wind variations is considerable.

The overall effect of all this is that the lighter boat upwind in light conditions loses more than the heavy boat under the same conditions. The results for downwind in the same wind speed are depicted in Figure 13.

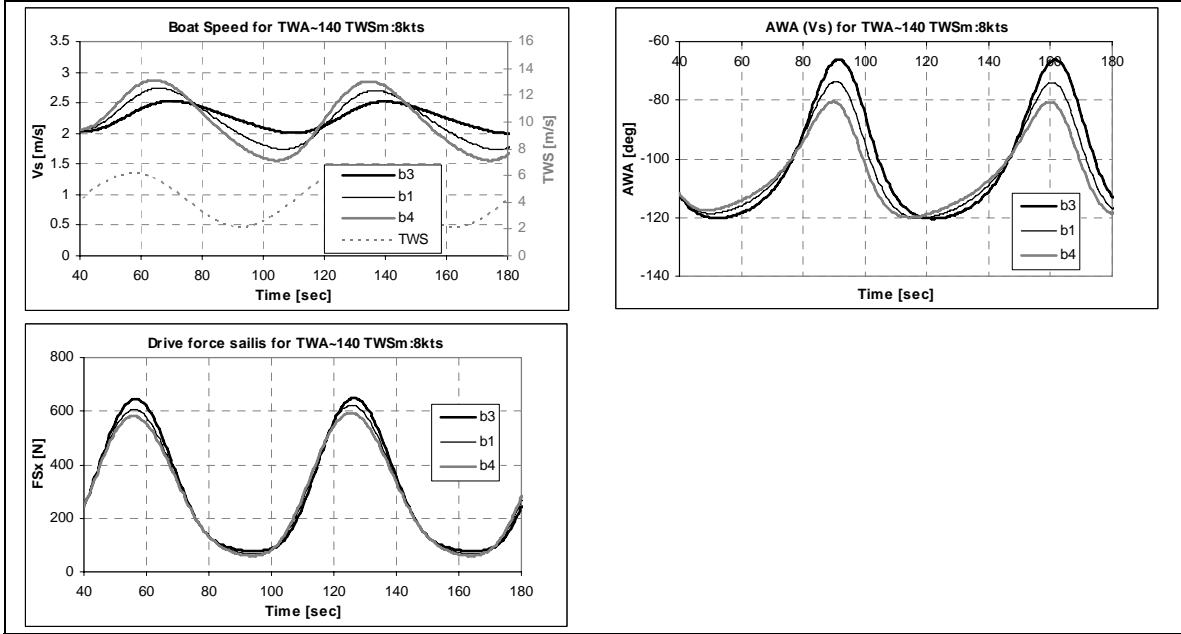


Figure 13: data for downwind at 8kts average TWS

Here the change in apparent wind angle is striking, it amounts almost 60 degrees. Some of the same effects are seen here as mentioned for the upwind case, but in particular the change in the driving force between the designs is significant. Once again the change in apparent wind angle is large in the slow down situation of the boats.

The results for the three different boats in various conditions are shown in the following figures. The first set shows the differences in distance lost for upwind and downwind at relatively low true wind speeds. These results have been reviewed earlier. It shows that the light boat loses more upwind than the heavier boat. In the downwind condition the heavy boat actually gains some distance, while the light boat still loses distance.

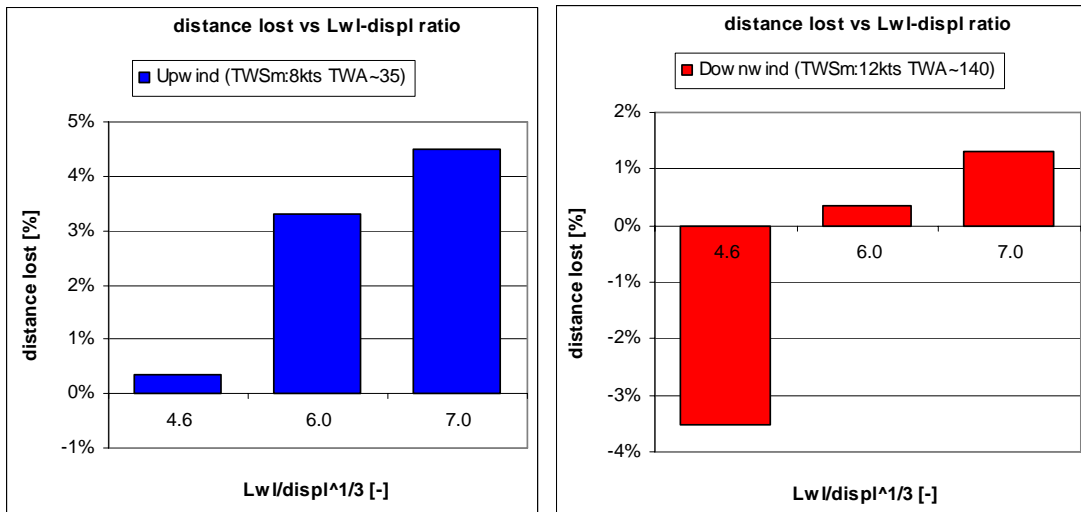


Figure 14: Distance lost for different length-displacement ratios in light winds

In medium range wind conditions (Figure 15) all boats lose: upwind the differences are small, but still the light boat has a disadvantage. Downwind the trend is reversed and shows the light boat a small advantage over the heavier ones.

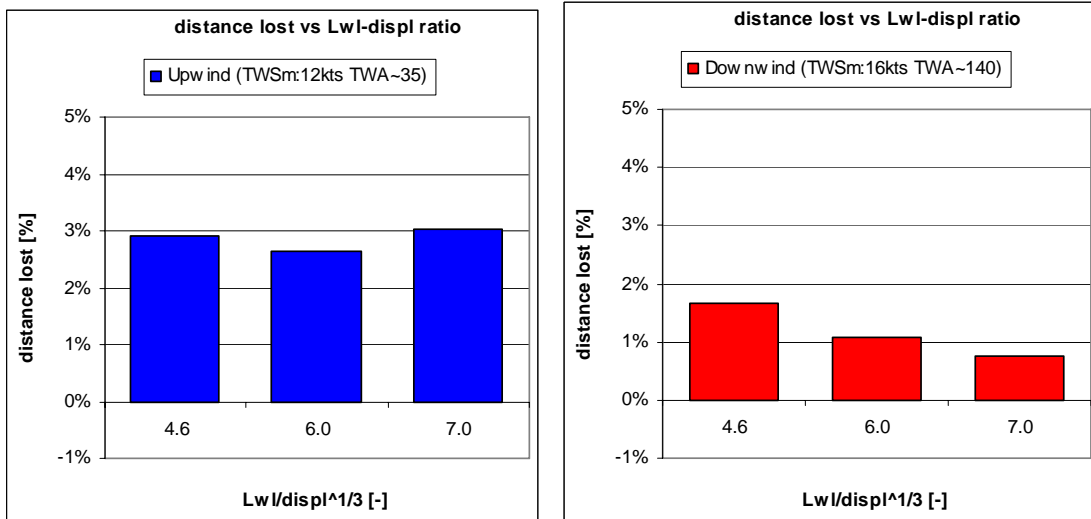


Figure 15: Distance lost for different length-displacement ratios in medium winds

In heavier upwind wind conditions the advantage still is with the heavier boat while downwind the differences are minute, as can be seen in Figure 16.

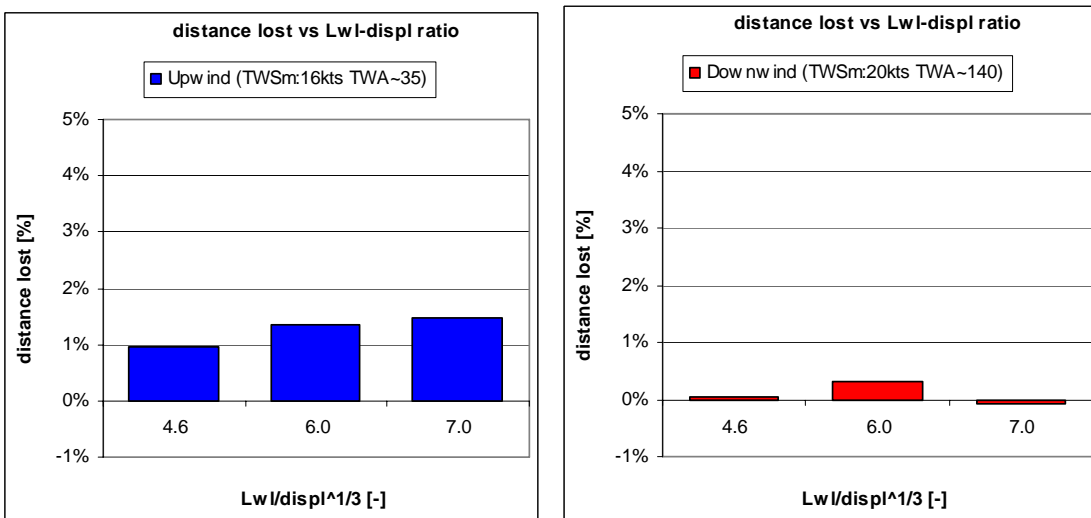


Figure 16: Distance lost for different length-displacement ratios in heavier winds

A few things reviewing these results should be noted here:

First the small difference found in some of the tested conditions may be well within the accuracy band of the calculations and should therefore be considered with some care.

Second in general the effects of waves have not been taken into account. This is one of the foreseen extensions of the dynamic VPP in the future. This holds true for both upwind and downwind conditions. Downwind this implies that no effect of wave surfing has been taken in account. This may lead to much larger differences in downwind conditions in the heavier winds than follows from the present results.

4. Conclusions

The paper shows some results for simulations of sailing yachts under varying conditions. The time domain simulation model that has been derived originally for assessing the maneuvering characteristics of sailing boats offers some attractive alternative applications in this respect.

So it has been used to investigate some of the possible differences between a stationary and a dynamic VPP. Therefore at first approach only a limited number of true wind speed variation scenarios have been used. Although the scope of the present project was restricted and therefore the number of simulations still rather limited some interesting phenomena have been found:

- The actual speed attained under varying more realistic true wind conditions is lower than found in the stationary VPP
- The actual shape of the true wind scenario is of importance
- Different boats are affected differently.
- In general under the conditions tested it was found that heavy boats have the advantage over lighter boats.

In future research further development of the different autopilots is foreseen. Also the adaptation of the aero model in the present model to suite the dynamic behavior more adequately is foreseen. Finally the effect of wind waves should be incorporated, both upwind and downwind.

References

[1]

Keuning, J.A. , Vermeulen, K.J. and de Ridder, E.J.

A generic mathematical model for the manoeuvring and tacking of a sailing yacht.

Chesapeake Sailing Yacht Symposium, 2005

[2]

Keuning, J.A. , Katgert, M. and Mohnhaupt, A.

The use of a maneuvering model for the optimization of the tacking procedure of an IACC sailing yacht.

RINA International conference: The modern Yacht, 2007

[3]

Battistin, D. and Lendri, M.

A tool for time dependent performance prediction and optimisation of sailing yachts.

Chesapeake Sailing Yacht Symposium, 2007

[4]

Gerritsma, J. , Onnink, R. and Versluis, A.

Geometry, resistance and stability of the delft systematic yacht hull series.

HISWA Symposium on Yacht Design and Construction, 1981

[5]

Keuning, J.A. and Vermeulen, K.J.

The yaw balance of sailing yachts upright and heeled.

Chesapeake Sailing yacht Symposium, 2003

[6]

Keuning, J.A. and Sonnenberg, U.B.

Approximation of the Hydrodynamic forces on a sailing yacht based on the Delft Systematic yacht Hull Series.

HISWA Symposium on Yacht Design and Construction, 1998

[7]

Keuning, J.A. , Katgert, M. and Vermeulen, K.J.
Further analysis of the forces on keel and rudder of a sailing yacht.
Chesapeake Sailing Yacht Symposium, 2007

[8]

Whicker, L.F. and Fehlner, L.F.
Free-stream characteristics of a family of low-aspect-ratio, all-movable control surfaces for application to ship design.
Technical report 933, David Taylor Model Basin, 1958

[9]

Keuning, J.A. and Binkhorst, B.J.
Appendage resistance of a sailing yacht hull.
Chesapeake Sailing Yacht Symposium, 1997

[10]

Claughton, A.
Developments in the IMS VPP formulations.
Chesapeake Sailing Yacht Symposium, 1999

[11]

Cambell, I.M.C.
Wind tunnel testing of sailing yacht rigs.
HISWA Symposium on Yacht Design and Construction, 1994

[12]

Ranzenbach, R. and Mairs, C.
Wind Tunnel Testing of Offwind Sails
Chesapeake Sailing Yacht Symposium, 1999

[13]

Fossati, F. , Muggiasca, S. and Viola, I.M.
An investigation of aerodynamic force modeling for IMS rule using wind tunnel techniques.
HISWA Symposium on Yacht Design and Construction, 2006

